# Investigations of elevated aerosols over the Indian region and their radiative impacts

*Thesis submitted to*

**Cochin University of Science and Technology**

*in partial fulfilment for the award of the Degree of*

***Doctor of Philosophy***

***in***

***Physics***

UNDER THE FACULTY OF SCIENCE

by


## Lakshmi N B

**SPACE PHYSICS LABORATORY**

**VIKRAM SARABHAI SPACE CENTRE**

**THIRUVANANTHAPURAM-695 022**

**KERALA, INDIA**


**DECEMBER 2018**

# Investigations of elevated aerosols over the Indian region and their radiative impacts

*Thesis submitted to*

Cochin University of Science and Technology

*in partial fulfilment for the award of the Degree of*

***Doctor of Philosophy***

***in***

***Physics***

UNDER THE FACULTY OF SCIENCE

by

**Lakshmi N B**

SPACE PHYSICS LABORATORY

VIKRAM SARABHAI SPACE CENTRE

THIRUVANANTHAPURAM-695 022

KERALA, INDIA

DECEMBER 2018

# DECLARATION

I hereby declare that the Ph.D. thesis work titled, ***"Investigations of elevated aerosols over the Indian region and their radiative impacts"*** is based on the original work carried out by me under the supervision of Dr. S Suresh Babu, at Space Physics Laboratory, Vikram Sarabhai Space Centre, Thiruvananthapuram and has not been included in any other thesis submitted previously for the award of any degree.

December 2018

Lakshmi N B

(Author)

भारत सरकार
अंतरिक्ष विभाग
**विक्रम साराभाई अंतरिक्ष केन्द्र**
तिरुवनन्तपुरम-695 022
केरल, भारत
**फोन :** (0471) 2562404
**फैक्स :** (0471) 2706535
Mob: +91 9446980533
Website: http://SPL.GOV.IN


**Government of India**
**Department of Space**
**Vikram Sarabhai Space Centre**
**Thiruvananthapuram-695 022**
**Kerala, INDIA**
Telephone : (0471) 2562404
Fax : (0471) 2706535
Mob: +91 9446980533
e-mail: s_sureshbabu@vssc.gov.in

## अन्तरिक्ष भौतिकी प्रयोगशाला
## SPACE PHYSICS LABORATORY

डॉ. एस सुरेश बाबू/Dr. S Suresh Babu
प्रधान, एआरएफ़एस/Head, ARFS

# CERTIFICATE

Certified that the thesis entitled "**Investigations of elevated aerosols over the Indian region and their radiative impacts**", submitted to the Cochin University of Science and Technology, is a bonafide research work carried out by **Ms. Lakshmi N B** under my supervision at Space Physics Laboratory, Vikram Sarabhai Space Centre, Thiruvananthapuram, for the award of Ph.D degree in Physics. The work presented in this thesis has not been submitted for the award of any other degree or diploma to any other university or institution.

दिसंबर/December, 2018

एस सुरेश बाबू/S Suresh Babu
(Thesis Supervisor)

भारत सरकार
अंतरिक्ष विभाग
**विक्रम साराभाई अंतरिक्ष केन्द्र**
तिरुवनन्तपुरम-695 022
केरल, भारत
फोन : (0471) 2562404
फैक्स : (0471) 2706535
Mob: +91 9446980533
Website: http://SPL.GOV.IN

सत्यमेव जयते

**Government of India**
**Department of Space**
**Vikram Sarabhai Space Centre**
**Thiruvananthapuram-695 022**
**Kerala, INDIA**
Telephone : (0471) 2562404
Fax : (0471) 2706535
Mob: +91 9446980533
e-mail: s_sureshbabu@vssc.gov.in

## अन्तरिक्ष भौतिकी प्रयोगशाला
## SPACE PHYSICS LABORATORY

डॉ. एस सुरेश बाबू/Dr. S Suresh Babu

प्रधान, एआरएफ़एस/Head, ARFS

दिसंबर/December, 2018

# ***CERTIFICATE***

Certified that all the corrections and modifications suggested by the audience and the Doctoral Committee of the candidate during the Pre-synopsis seminar have been incorporated in this thesis.

डॉ. एस सुरेश बाबू/Dr. S Suresh Babu
(Thesis Supervisor)

प्रतिहस्ताक्षरित/Countersigned

डॉ राधिका रामचन्द्रन/Dr. Radhika Ramachandran
निदेशक, एसपीएल/Director, SPL

*Dedicated to……*

*My parents and teachers*

# *Acknowledgement*

*At this time of completion of my doctoral thesis, I would like to thank many people who were a part of this journey and conjointly helped me to realize this dream. First and Foremost let me thank all my teachers for their noble blessings bestowed upon me. Their benevolent influence on different stages of my education has made me reach to this day.*

*I thank my guide Dr. S. Suresh Babu who has not only been a supervisor but an affectionate guardian to me who has been a source of relentless inspiration throughout this journey. He imparted the flavor of aerosol science to me and nurtured the independent researcher in me. I fondly remember him saying "I am not your supervisor, rather a mirror that will reflect what you are now, and you can do more". Sir, it indeed had a great influence on me and it is my privilege to complete this work under your enriching guidance.*

*I would like to thank 'Indian Space Research Organization' for providing me with the research fellowship and opportunity to carry out research with the best research facilities. Let me thank Director, Space Physics laboratory, Dr. Radhika Ramachandran, and former directors Dr. Anil Bharadwaj and Dr. K. Krishna Moorthy for their unremitting support for carrying out research at the Space Physics laboratory. A special note of gratitude to Dr. K. Krishna Moorthy for his meticulous guidance and care given to me throughout the period of my research. Thanks to Dr. S. K. Satheesh for his kind guidance and warm support.*

*My sincere thanks to Dr. Vijayakumar S Nair for his sincere advices and encouragement. Thanks for the very productive scientific discussions which immensely helped me in shaping my Thesis. I have been blessed to have a wonderful scientific group to work with and on this occasion I thank Dr. Mukunda M Gogsoi, Sobhan Kumar Kompalli, Dr. Aditya Vaishya and Mr. Santhosh Kumar Pandey for their heartfelt support. I wholeheartedly thank my fellow labmates, Jayachandran, Usha, Subin, Chandrakala, Arun, Ajith for the stimulating company and emotional support.*

*I would like to mark my special gratitude to members of the Academic Committee, Space Physics laboratory for their insightful comments and encouragement during different phases of development of the thesis. It is my pleasure to extent my deep gratitude to members of my doctoral committee, Dr. Tarun Kumar Pant and Dr. S. V. Sunil Kumar for the timely suggestions and support for the*

*realization of my PhD thesis. I would like to thank Dr. Prabha R Nair, Dr. K Rajeev, Dr. Geetha Ramkumar, Dr. C. Suresh Raju, Dr. Rajkumar Choudhary, Dr. K Kishore Kumar, Dr. D Bala Subrahmanyam, Dr. N V P Kiran Kumar, Dr. Siddharth Shankar Das, and Dr. Satheesh Thampi for their valuable advices and suggestions for the betterment of my research work.*

*I fondly remember all SPL family members at this instance for their loving support. Thanks to Dr. G Manju, Dr. Vipin Yadav, Dr. Sandhya K Nair, Dr. Prashant Hegde, Dr. Smitha V Thampi, Dr. Vineeth. C, Dr. Mridula, Dr. Nizy Mathew, and Dr. Uma K N, Dr. G Manju, Dr. Vipin Yadav, Dr. Sandhya K Nair, Dr. Manoj Kumar Mishra, Dr. Vineeth. C, Dr. Nizy Mathew, Dr. Uma K N, Dr. Dhanya. M. B, Sathosh, Subbu and Imran.*

*I thank my friends for they have lighted up my time at SPL with warm hearted affection. A special thanks to Renju, Aryasree, Manoj, Prijith, Tinu, Ambily, Anu, Sreedevi, Ashok, Muhsin, Ajesh, Megha, Suneeth, Aneesh, Vrinda, Sneha, Freddy, Maria, Lavanya, Ashwathy, Govind, Nalini, Roshny, Edwin, Koushik and many more for their kind support. A special thanks to Dr.Sreelatha, Mr. P. Padeep Kumar, Dr. Dinakar Prasad Vajja, Mr.Ajeesh, Mr. Pramod, Mr. G. S. Pradeep, Mr. Jino, Mr. Samdas and Mrs. Santhi for their kindhearted affection. My sincere thanks to SPL office staff to provide administrative support. I thank Ms. Suseela, Ms. Geetha C., Ms. Sisira, Ms.Shalini, and Ms. Shiji for their sincere efforts.*

*Last but not the least, special thanks to my family. Words cannot express my gratitude towards my Parents who have longed for this achievement and kept faith in me at each and every stage of my life. Thanks to my grandparents for all the blessings and good wishes you have showered on me. Thanks to my adorable sisters and their family for a life time of endless love and affection that keeps the flame alive in me. I thank my parent in-laws and all other loved ones for all the love and faith in me. Thanks to Sreejith for being the best team mate in all good and bad moments that life has presented us with. Last but not least a special thanks to my daughter who made me realize that struggle is not a sign of weakness rather of strength. I owe it all to you.*

***Lakshmi***

# List of Publications

## Peer-Reviewed Journals

1. Prijith, S. S., S. Suresh Babu, **N. B. Lakshmi**, S. K. Satheesh, and K. Krishna Moorthy (2016), Meridional gradients in aerosol vertical distribution over Indian Mainland: Observations and model simulations, **Atmospheric Environment**., 125, 337–345, doi:10.1016/j.atmosenv.2015.10.066.

2. **Lakshmi, N. B**., V. S. Nair, and S. Suresh Babu (2017), Vertical Structure of Aerosols and Mineral Dust Over the Bay of Bengal From Multisatellite Observations, **Journal of Geophysical Research,** Atmos., 122(23)4th December, 12845–12861, doi: 10.1002/2017JD027643.

3. Kompalli, S. K., S. Suresh Babu, **N. B. Lakshmi**, and K. Krishna Moorthy (2016), Spring-time enhancement in aerosol burden over a high-altitude location in western trans-Himalaya: Results from long-term observations, **Current Science**, 111(1), 117–131, doi:10.18520/cs/v111/i1/117-131.

4. Vaishya, A., S. Suresh Babu, V. Jayachandran, M. M. Gogoi, **N. B. Lakshmi**, K. Krishna Moorthy, and S. K. Satheesh (2018), Large contrast in the vertical distribution of aerosol optical properties and radiative effects across the Indo-Gangetic Plain during SWAAMI-RAWEX campaign, **Atmospheric Chemistry and Physics**, 18, 17669-17685, doi.org/10.5194/acp-18-17669-2018.

5. **Lakshmi, N. B**., S. Suresh Babu and V. S. Nair (2018), Recent regime shift in mineral dust trend over South Asia from long term CALIPSO observations, *IEEE Transactions on Geoscience and Remote Sensing* (Under Review)

6. Gogoi, M. M., **N. B. Lakshmi**, V. S. Nair, S. K. Kompalli , Moorthy, K. K., and Babu, S. S (2018), Vertical profiles of aerosol number size distribution across the IGP: Seasonality and enhanced coarse-mode absorption in the lower free-troposphere during spring, *Journal of Earth System Science* (Under review)

## Symposium Presentations

1. Gogoi, M. M., S. S. Babu, K. K. Moorthy, J. P. Chaubey, V. S. Nair, M. R. Manoj , S. K. Kompalli, **Lakshmi. N. B**, Roseline. C. Thakur, Thamban Meloth, S. Rajan: Aerosol Characteristics over Norwegian Arctic: Results From Indian Scientific Expeditions, Presented in ISAR-3, Tokyo, Japan, Jan-2013.
2. **Lakshmi. N. B**, S. S. Babu, S. S. Prijith, K. K. Moorthy, V. S. Nair, 'Vertical structure of aerosols over Bay of Bengal from airborne and space borne observations', Conference of Indian Aerosol Science and Technology Association, 2014 (IASTA2014), Banaras Hindu University, Varanasi, 11th - 13th November, 2014 **(BEST PAPER AWARD)**
3. **Lakshmi, N.B**, S. S. Babu, S. S. Prijith, V. S. Nair and K. K. Moorthy, 'Vertical structure of aerosols and mineral dust transport over Bay of Bengal from multi-year space borne observations', National Climate Science Conference, Indian Institute of Science, Banglore, 2– 3 July 2015.
4. Kompalli, S.K., S. S. Babu, M. M. Gogoi, **Lakshmi. N.B**., and M.R. Manoj, Aerosol climatology over a free-tropospheric location in western trans-Himalayas: Results from multi-year measurements of aerosol physical and optical properties, National Climate Science Conference, Divecha Center for Climate Change, Indian Institute of Science, Bangalore, 2-3 July 2015.
5. **Lakshmi, N.B**, S. S. Babu, Prijith. S, V. S. Nair, K. K. Moorthy, 'Seasonal and spatial variation of vertical structure of mineral dust transport over the Bay of Bengal using multi-satellite observations', National Space Science Symposium, Vikram Sarabhai Space Centre, Trivandrum, 9 - 12 Feb 2016.
6. S. S. Prijith, S. S. Babu, **N.B. Lakshmi**, S. K. Satheesh and K. K. Moorthy, Vertical distribution of aerosols over the Indian region: role of prevailing meteorology', National Space Science Symposium, Vikram Sarabhai Space Centre, Trivandrum, 9 - 12 Feb 2016.
7. Gogoi, M. M., S. S. Babu, **N. B. Lakshmi**, Nair, V.S., and K. K. Moorthy, "Aircraft Measurements of Aerosol Number Size Distribution Over India: Radiative Implications of Elevated Coarse Mode Absorption during spring", AS06-003, 18th Annual Meeting of the Asia Oceania Geosciences Society (AOGS-2017), Singapore, 06-11 August, 2017.

# Contents

# List of frequently used acronyms

| Abbreviation | Expansion |
|---|---|
| AERONET | Aerosol Robotic Network |
| ARMEX | Arabian Sea Monsoon Experiment |
| AOD | Aerosol Optical depth |
| ARF | Aerosol Radiative Forcing |
| ARFINET | Aerosol Radiative Forcing Over India Network |
| AS | The Arabian Sea |
| BC | Black Carbon |
| BoB | The Bay of Bengal |
| CALIPSO | Cloud Aerosol Lidar Infrared Pathfinder satellite Observation |
| CALIOP | Cloud Aerosol Lidar with Orthogonal Polarization |
| GCM | Global Circulation Model |
| GHG | Green House Gases |
| GOCART | Goddard Chemistry Aerosol Radiation and Transport |
| EHP | Elevated Heat Pump |
| HSRL | High Spectral Resolution Lidar |
| HYSPLIT | Hybrid Single Particle Lagrangian Integrated Trajectory |
| ICARB | Integrated Campaign for aerosols, Gases and Radiation Budget |
| IGP | Indo-Gangetic Plain |
| IGBP | ISRO Geosphere Biosphere Programme |
| INDOEX | Indian Ocean Experiment |
| IMD | Indian Meteorological Department |
| IPCC | Inter-governmental Panel for Climate Change |
| IR | InfraRed |
| ITCZ | Inter Tropical Convergence Zone |
| LIDAR/lidar | Light Detection And Ranging |
| LW | Longwave Radiation |
| MABL | Marine Atmospheric Boundary Layer |
| MODIS | Moderate Resolution Imaging Spectroradiometer |
| MPL | Micro-Pulse Lidar |
| MPLNET | Micro-Pulse Lidar Network |
| MWR | Multi-Wavelength solar Radiometer |
| PBL | Planetary Boundary Layer |

| | |
|---|---|
| PDR | Particle Depolarization Ratio |
| RAWEX | Regional Warming Experiment |
| SAMUM | Saharan Mineral Dust Experiment |
| SBDART | Santa Barbara DISORT Atmospheric Radiative Transfer |
| SH | Scale Height |
| SNR | Signal to Noise Ratio |
| SSA | Single Scattering Albedo |
| SW | Shortwave Radiation |
| TOA | Top Of the Atmosphere |
| WICARB | Winter - Integrated Campaign for aerosols, Gases and Radiation Budget |

# List of frequently used Symbols

| Symbol | Expansion |
|---|---|
| $P$ | Backscattered signal power |
| $\beta'$ | Volume attenuated back-scatter coefficient |
| $C$ | Calibration Coefficient |
| $\delta_v$ | Volume depolarization ratio |
| $\delta$ | Particle depolarization ratio |
| F | Radiation flux |
| T | Air temperature |
| λ | Wavelength of radiation |
| ρ | Density of the air |
| $C_p$ | Specific heat capacity of the air at constant pressure |
| g | Acceleration due to gravity |
| z | Altitude |
| τ | Aerosol optical depth |
| α | Ångström exponent |
| σ | Aerosol extinction coefficient |
| $\beta$ | Aerosol back-scattering coefficient |
| $\sigma_{scat}$ | Aerosol scattering coefficient |
| $\sigma_{abs}$ | Aerosol absorption coefficient |
| ω | Single scattering albedo |
| g | Asymmetric parameter |
| ζ | Up scatter fraction |
| b | Hemispheric back-scatter ratio |
| $Q_{ext}$ | Extinction efficiency |
| σ* | Mass extinction efficiency |
| $M_d$ | Mass concentration of dust |
| $R_{eff}$ | Effective radius |
| $C_{ext}$ | Extinction cross-section |
| $\tau_d$ | Dust optical depth |
| $\sigma_d$ | Dust extinction coefficient |
| $\beta_d$ | Dust back-scattering coefficient |
| $f_d$ | Dust fraction |
| $S_a$ | Lidar ratio of aerosols |

# List of Figures

# List of Tables

# Preface

The effect of aerosols are conspicuous in perturbing the Earth's radiation budget and climate through their interactions with solar radiation, modification of cloud properties and their influence on the hydrological cycle. The radiative effects of aerosols are strongly influenced by their altitude distribution. Altitude profile of aerosols is normally assumed to be exponentially decreasing with height with a specific aerosol scale height. However, aerosols generated at the surface are lifted up vertically to free tropospheric altitudes through convective activity or directly injected above the boundary layer by processes like long range transport, volcanic eruptions or by the ever increasing air traffic. These aerosols are transported through different altitude levels in conjunction with the prevailing winds and makes their distribution vertically and horizontally heterogeneous. Thus, the aerosols resides above the well-mixed atmospheric boundary layer are referred to as *'elevated aerosols '*.

Characterization of elevated aerosols assumes greater importance over the Indian region due to their effect on energy budget of the earth-atmosphere system, thermal structure of the atmosphere, regional circulation, and hydrological cycle. Transport of elevated aerosols to the oceanic region and its deposition over ocean surface affects its bio-geo chemical cycle whereas their transport to the Himalayas affect its snow/glacier cover through aerosol – cryosphere interaction. Though there are several studies on the aerosol characterization over the Indian region, most of them are based on near surface or columnar measurements and focussed to a particular region. A comprehensive understanding on the altitude distribution of aerosols and its radiative effects over the Indian subcontinent and surrounding oceanic regions is yet to emerge. This thesis present a comprehensive picture of the elevated aerosols over the Indian region and their radiative impacts based on a synergy of observations from space-borne, airborne and ground based platforms, and radiative transfer model calculations.

Overview of aerosols, their optical and physio-chemical properties, vertical distribution, and their radiative effects, and climate impacts is given in chapter1. Satellite remote sensing of aerosols over the land has inherent uncertainty associated with estimating atmospheric path radiance from surface reflectance. However, Cloud-Aerosol LIDAR with

Orthogonal Polarization (CALIOP) on-board Cloud Aerosol Lidar Infrared Pathfinder satellite Observation (CALIPSO) satellite can provide better estimates of aerosols, even over brighter surfaces as it retrieves information from active observations of back scattered signal from different altitudes of the atmosphere.

Details of the datasets and the methodology used to realize the objective of the thesis is described in chapter2. Present study makes use of vertically resolved space-borne observations of CALIOP during the period from 2006 to 2017. Columnar AOD from the ground based observations by ARFINET (Aerosol Radiative Forcing over India Network) over India and Moderate Resolution Imaging Spectroradiometer (MODIS) observation on-board Aqua satellite over the oceanic regions around India are used to normalize the vertical profiles of aerosol extinction coefficient retrieved by the CALIOP. Altitude resolved measurements of single scattering albedo from the aircraft observations under RAWEX (Regional Aerosol Warming Experiment) are made use for the estimation of radiative effects over the study region. Polarization sensitive measurements of CALIOP enable the classification of mineral dust aerosols. The methodology for the derivation of dust extinction coefficient and associated uncertainty analysis are described in this chapter.

Spatial variation and temporal evolution of the vertical distribution of aerosols over the Indian landmass is presented in chapter 3. A significant enhancement in aerosol at the free tropospheric altitudes and a corresponding reduction within the boundary layer is observed during pre-monsoon season. A distinct meridional variation in the aerosol vertical distribution is observed during pre-monsoon over the Indian landmass with minimum vertical extent over the southern latitudes that increases towards the northern latitudes. The pre-monsoon enhancement in elevated aerosols is significantly contributed by the vertical transport of aerosols due to the intense convection as well as the transported mineral dust by the prevailing westerlies. Combining the observations of depolarization ratio and aerosol back-scattering coefficient, three dimensional distributions of dust optical depth and their regional differences over the Indian region is presented.

Aerosol characteristics as well as its altitude distribution over the Bay of Bengal and the Arabian Sea are strongly influenced by the outflow from the adjacent continental regions.

Vertical distribution of aerosols over the Bay of Bengal and the Arabian Sea are examined using multi-satellite observations that include vertically resolved observations of CALIOP supplemented with columnar AOD from MODIS. The results are presented in chapter 4. Distinct seasonal pattern is observed in the vertical structure of aerosols over the oceanic regions with significant enhancement in aerosols above MABL (marine Atmospheric Boundary Layer) from winter to pre-monsoon. Spatial variation of the columnar and vertical distribution of dust extinction coefficient and its fraction to total aerosol loading are estimated. Long term variation in dust extinction showed a decreasing trend over the Bay of Bengal and the Arabian Sea.

Aerosol characterization over the Great Himalayas assumes vital importance due its potential to interact with the Himalayan cryosphere through both direct and albedo effect. However, observational studies on the vertical distribution of aerosols over the Himalayan region are very limited due to harsh conditions for conducting ground based observations and the large uncertainty in retrieval technique due to the high surface reflectance for passive remote sensing from satellites. Using a combination of CALIOP vertical profiles and available ground based observations, the altitude distribution of aerosols over the Himalayas are explored in Chapter 5. Aerosol vertical distribution shows regionally and seasonally distinct characteristics over the Himalayas. Spatial distribution of dust optical depth over the Himalayan region shows highest loading over the mid-Himalayas, mainly contributed by dust. From the profiles of dust extinction coefficient, dust mass flux deposited over the Himalayas is estimated for the pre-monsoon season.

The chapter 6 presents the radiative effects of elevated aerosols over the Indian region, estimated using a combination of observations from ground based, satellite, and air-borne platforms with radiative transfer models. Aerosol induced heating rate is significantly high above the planetary boundary layer during the pre–monsoon season, over the entire Indian region. Long term trend of dust aerosols over the south Asia during the last decade showed a distinct regime shift after the year 2013.

The summary of findings and future direction of this work are presented in chapter -7.

# Chapter 1

# Introduction

## 1.1 Introduction

Predicting future climate involves significant amount of uncertainty due to the lack of adequate understanding on the science of climate change that involves both natural climate variability and human induced climate impacts. Greenhouse gases (GHG) are the recognized climate forcing agents, and anthropogenically induced changes in GHG are held primarily responsible for global warming and associated climate impacts. Atmospheric aerosols are known to partially mitigate the warming effects of GHG through efficient scattering of solar radiation thereby cooling the surface of Earth *(Charlson et al., 1992).* Eruption of Mount Pinatubo of Philippines in 1991 ejected massive amount of aerosols into the stratosphere that visibly impacted the global temperature of around one whole year *(Hansen et al., 1992)*. This established the importance of aerosols and their effects on climate and marked a turning point in the science of aerosols within the scientific community. The Intergovernmental Panel on Climate Change (IPCC) Fifth Assessment Report (2013) has stated that rate of increasing trend of global surface temperature has reduced over the past 15 years (1998–2012) than over the past 30 to 60 years which is termed as a 'hiatus' in global warming in the scientific community *(Trenberth and Fasullo, 2013)*. Several causative mechanisms are proposed for this slowdown in warming, which include heat uptake of Deep Ocean, internal variability, and dimming effect of aerosols. According to *Kaufmann et al., (2011)*, hiatus in global warming is associated with an increase in the sum of anthropogenic and natural forcings. In this scenario, atmospheric aerosols receive considerable attention owing to its cooling effects at the surface and at top of the atmosphere (TOA) to explain the declined warming during the past two decades. In addition, over South Asia, aerosol loading has been found to have an increasing trend of ~ 2% (of its value in 1985) per year during the last two decades *(Babu et al., 2013).* Effects of aerosols on regional climate is well substantiated through numerous studies based on observational evidences *(Sassen, 2003; Ramanathan et al., 2007; Yu, Chin, Yuan, et al., 2015).* Radiative effects of atmospheric aerosols have to be precisely quantified to reduce the uncertainty they poise in understanding the climate change. However, large variability of aerosols in space and time, and their short lifetime in the atmosphere makes their

quantification difficult, which demands for extensive and detailed measurements at regional and global scales. During last few decades, several efforts were made worldwide for aerosol characterization through regular/campaign mode observations from multi-platform (air-borne, ship-borne, and island-based) field experiments, ground based network of observatories and satellite based, observations. These observations led to many discoveries in the field of aerosol science *(Albrecht, 1989; Charlson et al., 1992; Jacobson, 2001; Ramanathan et al., 2007)* and progressively aided in understanding many underlying mechanisms by which aerosols influence the climate.

### 1.2 Classification of atmospheric aerosols

Aerosols are classified based on several factors such as sources, generating mechanism, and most importantly on the size of the particles. Particles directly emitted into the atmosphere due to combustion or disintegration processes are termed as primary aerosols while those which are newly formed from pre-cursor gases (vapours of sulphuric acid, volatile organic carbon and ammonia) through gas to particle conversion are referred as secondary aerosols. Aerosols are produced by natural or anthropogenic sources. Natural aerosols include dust aerosols emitted from the soil, aerosols ejected via volcanic eruptions, bio-mass burning aerosols through forest fires and marine aerosols produced from ocean surfaces. Mineral dust aerosols are emitted to the atmosphere when soil aggregates are entrained into the atmosphere by the surface winds and disintegrate into finer particles. They constitute the largest part of the natural aerosol system and significantly contribute to the global aerosol load. Anthropogenic aerosols are emitted via combustion of fossil fuels and vehicular/industrial/domestic emissions. Black carbon aerosols are a main component of anthropogenic emissions/ smoke emissions from forest fires. It absorbs over a wide range of solar spectrum and is known as an effective heating agent next to carbon dioxide. Volcanic eruption deposits large amount of aerosols composed of volcanic ash, sulphuric acid droplets and dust particles in to the stratosphere where they are horizontally transported by atmospheric circulation over the globe and produce severe climate effects. While natural aerosols contribute as much as 80% in terms of aerosol mass (1000−2150 $Tgyr^{-1}$), their contribution to optical depth is $\sim$ 40 – 50% *(Satheesh and Moorthy, 2005).*

Aerosols exist as a collection of polydisperse particles in the atmosphere, that consists of particles of different sizes with a distribution that is characterized by different modes namely *nucleation mode*, *accumulation mode* and *coarse mode*. Particles with size ranging from a few nanometres to 100 nm is called nucleation mode aerosols, those ranging from

100 nm to 1 μm is called accumulation mode and those which has diameter greater than 1 μm are termed as coarse mode aerosols *(Prospero et al., 1983)*. Nucleation mode particles are formed through homogeneous (gas to particle conversion) and heterogeneous (condensation of vapours on particles) nucleation processes and they significantly affects the aerosol number size distribution. Nucleation mode particles rapidly coagulate to form accumulation mode particles and hence their life time in the atmosphere is very short. Coarse mode particles are mostly produced by natural aerosols through mechanical fragmentation processes. Due to their larger mass, they undergo gravitational sedimentation, which makes their life time short in the atmosphere. Accumulation mode aerosols are the most stable aerosols with the longest residence time in the atmosphere. They efficiently scatter solar radiation with high scattering efficiency owing to their characteristic size range in the visible regime.

### 1.3 Physical and chemical characteristics

Radiative effects of aerosols are determined by their concentration, size distribution, and chemical composition. The physical and compositional characteristics of aerosols are determined by their sources and generation mechanisms. While natural aerosols are mostly coarse in size and non-spherical in shape, anthropogenically emitted aerosols are finer and spherical particles. Particles formed through gas to particle conversion are generally ultra-fine particles in the range of few nanometres. Particle size distribution is one of the most important characteristic of atmospheric aerosols that decides the radiative properties of aerosols. A simple empirical inverse power law *(Junge, 1963)* and modified Gamma function *(Deirmendjian, 1969)* were widely used earlier to represent the number size distribution. Under realistic atmospheric conditions, aerosol number size distribution is best represented by lognormal distribution as shown by equation (1). Logarithmic scale is convenient to represent the large orders of magnitude of aerosol size distribution ranging from 1 nm to 100 μm. Number concentration of aerosols at a given radius *r* as indicated by *n(r)* is given by

$$n(r) = \left( \frac{N_i}{\sqrt{2\pi}\sigma_{mi} r} \right) \exp\left( \frac{\log(r) - \log(r_{mi})}{2\sigma_{mi}^2} \right) \qquad (1.1)$$

In case of mixed system of aerosols, number size distribution can have more than one mode indicated by the index *i*. $r_{mi}$ and $\sigma_{mi}$ are the mode radius and the standard deviation respectively of the $i^{th}$ mode and $N_i$ is its total number density. Aerosol size distribution is represented in terms of surface, volume, and mass which are relevant in different aspects

of aerosol studies. Aerosols are mostly treated as spherical particles in Mie calculations for retrieving their optical properties. In case of non-spherical aerosols such as mineral dust, this assumption can induce significant uncertainty in determining their radiative properties. Investigations of dust aerosols using discrete dipole approximation technique have shown significant deviation in the scattering phase function, asymmetry parameter, optical depth and single scattering albedo of dust particles from those estimated by volume-equivalent spheres *(Kalashnikova and Sokolik, 2002).* Particle non-sphericity is found to have significant effect on retrieval of aerosol size distribution from observations of angular scattering *(Heintzenberg and Welch, 1982).* The numerical solution to the electromagnetic scattering of non-spherical particles can be obtained for a few specific shapes of particles but it is difficult to account for the diversity of particle shapes in a given natural system of aerosols, which makes the problem largely complicated. Methods like discrete dipole approximation, geometric optic approximation and using ellipsoidal models derived by T-matrix calculations, reduce the uncertainty induced by particle shape to an extent, though computational expense is quite high for the estimation of radiative properties through these methods *(Mishchenko et al., 1996).*

Characterization of chemical composition of aerosols plays an important role in determining their radiative properties and is quite challenging due to different possible sources, mixing of different aerosol species and transformation processes like condensation, coagulation, and heterogeneous reactions, especially during long-range transport. Radiative properties of bulk aerosol volume are controlled by the chemical/physical characteristics of the constituent individual particles. Aerosols can be either externally or internally mixed state in the atmosphere. In external mixing, there exists no physical and chemical interaction between different aerosol types whereas internal mixing induces changes in chemical composition of individual particles through chemical reactions or coating processes. Rather than homogeneous internal mixing (different species mix together to produce an isotropic particle), particles mostly occur as a core-shell structure due to coating by water soluble components *(Jacobson, 2000).* Estimation of refractive index of internally mixed multi-component aerosol particles is complicated due to their complex internal composition. Absorptive properties of aerosols such as BC or mineral dust is observed to be enhanced on mixing with other aerosols *(Martins et al., 1998; Moorthy et al., 2007).* Thus characterization of mixing state of aerosols is important since it induce large uncertainty in the accurate assessment of radiative effects of aerosols in climate forcing *(Andreae and Crutzen, 1997).* By providing surface area for various gases in the atmosphere, aerosols undergo heterogeneous chemical

reactions followed by changes in their composition. Pre-monsoon dust storms over The Indian region acted as a sink for many of the trace gases causing significant changes in tropospheric chemistry *(Kumar et al., 2014).* These processes add to the uncertainty in the characterization of aerosol composition and ultimately in assessing the radiative impacts of aerosols on climate.

### 1.4 Aerosol dynamics: Transport and removal processes

Spatio-temporal distribution of aerosols is determined by source strength, residence time, long-range transport and removal processes. Anthropogenic aerosols are dominated more over the northern Hemisphere where majority of populated land segments are present. Monsoon circulation, associated rainfall and its retreat, plays a crucial role in the distribution and composition of aerosols over The Indian region during different seasons. In the earth's atmosphere, only aerosols with diameter smaller than ~20 μm will remain suspended for sufficient time to produce substantial effects on weather and climate *(Tegen et al., 1996).*

*Stock* and *Einstein* have investigated particle transport in the late nineteenth and early twentieth century as a fundamental physics problem. Stokes Law and Einstein theory of Brownian motion play central roles in understanding aerosol dynamics. Dynamics of atmospheric aerosols are determined by the particle size and surrounding molecular mean free path. A particle in air experience gravitational force that make it to settle down against a viscous (drag) force, which is a resistant force excreted by surrounding fluid medium. Under the influence of these forces the particle moves with a settling velocity, which decides the residence time of that particle in the air. For smaller particles with size approaching mean free path of gases (0.066 μm), drag force will be lesser than that given by the Stokes law where a correction factor (slip correction) is applied for the estimation of actual settling velocity of the particle.

Aerosols are depleted from the atmosphere via dry deposition or wet deposition. Dry deposition involves removal of particles from the atmosphere through gravitational settling of particles and wet deposition is the removal through precipitation mechanism. Dry deposition velocity of particles primarily depends on the size of the particles and other factors like meteorology and underlying terrain. We deposition of aerosols can take place through both in-cloud and below cloud scavenging. Removal of condensation nuclei through precipitation is termed as in cloud scavenging while wash off of aerosols in the atmospheric column through precipitation is termed as below cloud scavenging. For coarse mode aerosols dry deposition is more dominant while accumulation mode aerosols

are mostly removed through wet deposition.Several studies have investigated the patterns of long-range particle transport through satellite observations and direct atmospheric sampling *(Chester et al., 1972; Prospero and Nees, 1977; Windom and Chamberlain, 1978; Takayama and Takashima, 1986)*. However observation based evaluation of aerosol life times are very limited due to the inherent limitations associated with measurements over larger spatial and temporal scales.

### 1.5 Optical properties and aerosol radiative forcing

Aerosols attenuate solar radiation through scattering and absorption and produces cooling of Earth's surface. Scattering aerosols enhances the light scattered back from the atmosphere while light absorbing aerosols like black carbon, diabatically heats the atmosphere by absorbing solar radiation and leads to changes in the stability conditions and cloud formation processes.

#### 1.5.1 Optical properties

In a column of atmosphere, intensity of attenuated solar radiation by aerosols $I$, is given by Beer – Lamberts Law as indicated by equation 1.2.

$$I = I_0 \exp(-\int_0^{\infty} \sigma(\lambda) dz) \qquad (1.2)$$

Here σ is the spectral aerosol extinction coefficient (Dimension Length$^{-1}$), $I_o$ is the intensity of incoming solar radiation at the TOA, and $dz$ is the incremental altitude range. Aerosol extinction coefficient integrated over the column of atmosphere gives aerosol optical depth (τ) at wavelength λ which is the primary parameter used in the estimation of aerosol radiative effects.

$$\tau(\lambda) = \int_0^{\infty} \sigma(\lambda) dz \qquad (1.3)$$

Aerosol spectral extinction coefficient determined by the number of particles per unit volume ($N$) and the extinction cross section ($C_{ext}$).

$$\sigma(\lambda) = NC_{ext} = \int \pi r^2 Q_{ext}(x, m) n(r) dr \qquad (1.4)$$

Ratio of extinction cross section to the geometric cross section of the particle is defined as extinction efficiency factor given by

$$Q_{ext} = \frac{C_{ext}}{\pi r^2} \qquad (1.5)$$

Optical characteristics of a particle is mainly determined by the ratio $x=2\pi r/\lambda$ called size parameter and the complex refractive index represented by m. Thus, information on aerosol size distribution and aerosol composition is critical in assessing the radiative impacts of aerosols. Estimation of extinction efficiency factor is mathematically estimated using Mie theory proposed by Gustav Mie *(Mie, 1908)* with a priori knowledge on the aerosol refractive index and size distribution. It has to be noted that Mie theory is applicable for homogeneous spheres and hence does not account for the changes in the optical parameters due to the non-sphericity of the particles. Physio-chemical characterization of aerosols with light scattering and absorption photometry experiments involves the inverse applicability of Mie theory that involves retrieval of size distribution and refractive index from measured light scattered intensity and absorption parameters.

Information of effective contribution of scattering with respect to total extinction is very important in assessing the radiative effects, which is determined by their chemical composition, particle size distribution, and shape. Probability of a photon to be scattered rather than absorbed when it interacts with a particle is defined as the single scattering albedo (SSA, ω). For a system of particles in the atmosphere, ω is given by

$$\omega = \frac{\sigma_{scat}}{\sigma_{scat} + \sigma_{abs}} \qquad (1.6)$$

where $\sigma_{scat}$ and $\sigma_{abs}$ are scattering and absorption coefficients of the volume of atmosphere under concern at a specific wavelength. It can vary from 0 to 1. While it is 1 for a perfectly scattering particle, it is 0 for purely absorbing species. SSA decreases as relative contribution of absorbing aerosols increase and it determines the sign of aerosol radiative forcing at TOA. The value of SSA at which the sign of TOA radiative forcing changes from negative to positive is called 'critical single scattering albedo', which depends also on the reflectance of the underlying surface.

Another important parameter that affects aerosol radiative effect is phase function, which determines the angular distribution of scattered energy around a particle. It is defined as the ratio of the energy scattered by aerosols per unit solid angle in a given direction *(θ)* with respect to the incident direction *I(θ),* to the average energy scattered per solid angle in all directions as given by

$$P(\theta) = \frac{I(\theta)}{\int_0^{\pi} I(\theta)\sin(\theta)d\theta} \qquad (1.7)$$

In the Rayleigh regime (x<<1), phase function is symmetrical and in the Mie regime (as x approaches 1), phase function becomes more asymmetric with dominant forward lobe and complex side lobs. A number of optical parameters are derived from phase function which is effectively used in radiative transfer models for specific applications. They are asymmetry parameter (*g*), upscatter fraction (ζ) and hemispheric back-scatter ratio (*b*). Asymmetry parameter is the intensity weighted average of the cosine of the scattering angle as given by equation 1.8 and indicated the degree of forward/backward scattering. Value of g is 1 for particles which scatter completely in the forward direction while -1 for that scatter completely in backward direction. For uniform and isotropic scattering, the value of g is 0.

$$g = \frac{1}{2}\int_0^{\pi} \cos(\theta) P(\theta) \sin(\theta) d\theta \qquad (1.8)$$

The upscatter fraction (ζ) is the fraction of light scattered by the particle into the upward hemisphere relative to the local horizon. Hemispheric back-scatter ratio *(b)* is the ratio of light backscattered, *I(180°)*, to the total scattered light intensity. It can be directly measured using integrated nephelometer with a backscatter shutter arrangement. Aerosol optical depth, single scattering albedo, and asymmetry parameter are the primary parameters that are used in global radiative transfer models to address the radiative effects of aerosols.

### 1.5.2 Aerosol direct effect

Scattering of solar radiation by aerosols back to the space produces a loss of energy in the earth- atmosphere system while absorption of radiation by aerosols leads to gain of energy in the atmosphere, which is dissipated through diabatic heating of the atmosphere. This is termed as the *direct effect* of aerosols. In shortwave regime, aerosols produce a net cooling (negative forcing) at the earth's surface and warming (positive forcing) in the atmosphere through absorption of solar radiation. In long wave regime it can produce surface and atmospheric heating (eg. mineral dust). For a plane parallel atmosphere, net flux of radiation reaching a layer of thickness Δz with the mid-altitude at z is given by the difference in the downward flux density $F^{\downarrow}$ and upward flux density $F^{\uparrow}$ as given by

$$F(z) = F^{\downarrow}(z) - F^{\uparrow}(z) \qquad (1.9)$$

The energy absorbed within the layer is given by the loss of flux density within that layer. The absorbed energy is used to heat the layer and produce a change in temperature within the layer as indicated by

$$\Delta F(z) = F(z) - F(z+\Delta z) = -\rho C_p \Delta z \frac{\partial T}{\partial t} \quad (1.10)$$

where $\rho$ is the density of the air, $C_p$ is the specific heat capacity of the air at constant pressure. Thus the rate of change of temperature within the layer is given by

$$\frac{\partial T}{\partial t} = -\frac{1}{\rho C_p}\frac{\Delta F(z)}{\Delta z} \quad (1.11)$$

Equation 1.15 can be expressed in terms of pressure coordinates using equation for hydrostatic equilibrium

$$dp = -\rho g dh \quad (1.12)$$

Thus atmospheric heating rate within a layer is given by

$$\frac{\partial T}{\partial t} = \frac{g}{C_p}\frac{\Delta F(p)}{\Delta p} \quad (1.13)$$

Flux reaching a layer is determined by the amount of solar insolation at TOA, absorption by gases like water vapour, carbon dioxide and ozone, scattering and absorption by aerosols, molecular scattering and radiation reflected from surface and reflection and scattering from clouds in case of cloudy atmosphere. Radiative transfer calculations carry out the estimation of flux at TOA or surface based on the input generated based on observations or models. Annual solar heating rates over the globe shows a maximum solar heating of $\sim$ 0.5 $Kday^{-1}$ is observed at an altitude of 4 to 5 km over the tropical and subtropical regions (solar constant of 1366 $Wm^{-2}$) *(Liou, 1980)*. Among the aerosols, black carbon is known to be the main absorbing species of short wave radiation absorbs light over the entire solar spectrum. Other absorbing aerosols include mineral dust aerosols which absorbs in the long wave regime and some of the organic aerosols which have absorption over UV regime. Although absorptive properties of major molecular species like water vapour, Carbon dioxide, and ozone are well understood, absorption due to aerosols are not completely understood owing to their complex internal composition. Thus it is important to obtain quantitative information on the heating rates of aerosols in both shortwave and long wave regime to understand its effects on climate.

### 1.5.3 Aerosol Indirect effect

Aerosols indirectly affect the radiation balance by altering critical cloud parameters such as cloud effective radius and cloud albedo, by virtue of their role as cloud condensation nuclei. This subsequently leads to changes in convective conditions, which either suppress or enhance the formation of clouds and precipitation. Being cloud condensation nuclei,

physio-chemical properties of aerosols has direct influence on cloud properties, such as cloud life time, cloud droplet concentration, and cloud effective radius. For a fixed cloud liquid water content, increase in the concentration of aerosols leads to reduction in cloud droplet size resulted in a system of more number of cloud particles with small size which offers more effective surface area for reflection of radiation increasing the cloud albedo. This leads to loss of solar energy backscattered to the space and a cooling of the climate system. This phenomena is termed as aerosol *first indirect effect (Twomey effect)(Twomey, 1977).* This has a profound effect in cloud evolution in terms of the ability of clouds to generate droplets that are large enough to initiate precipitation, which will increase the cloud lifetime. This effect is traditionally called the aerosol *second indirect effect (Albrecht, 1989).* Aerosols can also affect the properties of ice clouds or mixed-phase clouds by acting as ice nuclei (eg. mineral dust aerosols). Hygroscopic growth of aerosols in the atmosphere basically depends on their micro-physical properties and concentration. Simultaneous observations of microphysical properties of cloud droplets and aerosols are required to address the problem of aerosol-cloud interaction. However, the inherent limitations in observing aerosol properties within a cloud system in ambient atmospheric conditions causes significant amount of uncertainty in the investigation of aerosol-cloud interaction studies (figure 1.1).

### 1.5.4 Aerosol Semi-direct effect

The absorption of solar radiation by aerosols warms the atmosphere and modifies the vertical temperature profile. This influences the cloud formation due to its effect on atmospheric conditions of relative humidity and atmospheric stability. Modifying cloud properties through absorption of radiation is known as the *aerosol semi-direct effect (Hansen et al., 1997). IPCC (2007)* defines semi-direct effect as follows "Absorption of solar radiation by absorbing aerosols affects static stability and the surface energy budget, and May lead to an evaporation of cloud particles". Extensive warming induced by absorbing particles can dissipate the cloud prematurely by enhancing the cloud evaporation. In addition to aerosol indirect effects, this forms one of the largest uncertainties in assessing the aerosol impacts on climate *(Kaufman and Fraser, 1997; Koren et al., 2004).* Several modelling *(Lohmann and Feichter, 2004)* and observational studies *(Ackerman et al., 2000; Wilcox, 2010; Amiri-Farahani et al., 2017)* have shown the impacts of aerosol absorption on cloud cover especially at higher altitudes. Semi-direct effect of aerosols are found to be dependent on the location of the aerosol layer with respect to clouds *(Choobari et al., 2014)*. When the aerosol layer is located below the clouds, it enhances the convection and

increase cloud cover. But when aerosol layer is present above the cloud top, it can suppress the vertical growth of clouds and enhance the horizontal development by supressing entrainment due to changes in atmospheric stability *(Johnson et al., 2004).* These effects can create either a positive or negative radiative forcing at the top of the atmosphere, which is poorly understood and adds to uncertainty associated with radiative impacts of aerosols due to aerosol-cloud interaction.

### 1.6 Aerosol forcing on climate: uncertainties

The effect of aerosols on the radiation balance of earth-atmosphere system is quantified as 'aerosol radiative forcing'. The term 'Radiative forcing' indicates the effect of an atmospheric component on Earth's climate. It is the change in net radiation reaching the surface/TOA due to the presence of a particular constituent (aerosols, clouds, or gases) in the earth's atmosphere. It is expressed in Watts per square meter, $Wm^{-2}$. Radiative forcing is estimated as the difference between the net radiation reaching the surface/TOA with the perturbation and without the perturbation. Aerosol forcing at TOA is a resultant forcing due to warming in the atmosphere and cooling of the surface. The sign of the aerosol radiative forcing at TOA depends on the relative contribution of absorbing aerosols in the column indicated by single scattering albedo of aerosols in the column. It also depends on the albedo of the underlying surface and presence of clouds. Studies on aerosols radiative forcing started decades back and has improved significantly during the last twenty years *(Coakley and Chylek, 1975; Charlson et al., 1992; Jones et al., 1994; Chylek and Wong, 1995; Alpert et al., 1998; Satheesh and Ramanathan, 2000; Jacobson, 2001; Penner et al., 2004; Bellouin et al., 2005; Lubin and Vogelmann, 2006; Chand et al., 2009; Samset et al., 2014; Tegen et al., 1996; Andersson et al., 2015).* The Fifth assessment report of IPCC (2013) introduces the term '*effective radiative forcing' (ERF)* changing the concept of radiative forcing (RF) that has been used since past many years. In estimating RF, surface and tropospheric conditions are considered to be static, while in ERF calculations of feedback/ response of all physical variables in the earth-atmospheric system to the perturbations are considered, except for those associated with ocean and sea ice. According to *IPCC (2013)* global forcing due to anthropogenic aerosol radiation interaction ($RF_{ari}$) is estimated to be -0.35(-0.85 to 0.15) $Wm^{-2}$ with high confidence. Estimation of $ERF_{ari}$ with rapid adjustments gives a more negative value of -0.45(-0.95 to 0.05) $Wm^{-2}$ with medium confidence. Effective radiative forcing estimation of aerosol-cloud-interaction $ERF_{aci}$ has a value of -0.40 (-1.2 to 0) $Wm^{-2}$ through the uncertainty involved in the estimation is very high. Initial modelling studies on effect of aerosols and greenhouse

gases on atmospheric temperature using one dimensional models have shown that if global background aerosol concentration is increased to 4 times of present concentration, it can diminish the global surface temperature by as much as 3.5° K *(Rasool and Schneider, 1971).*

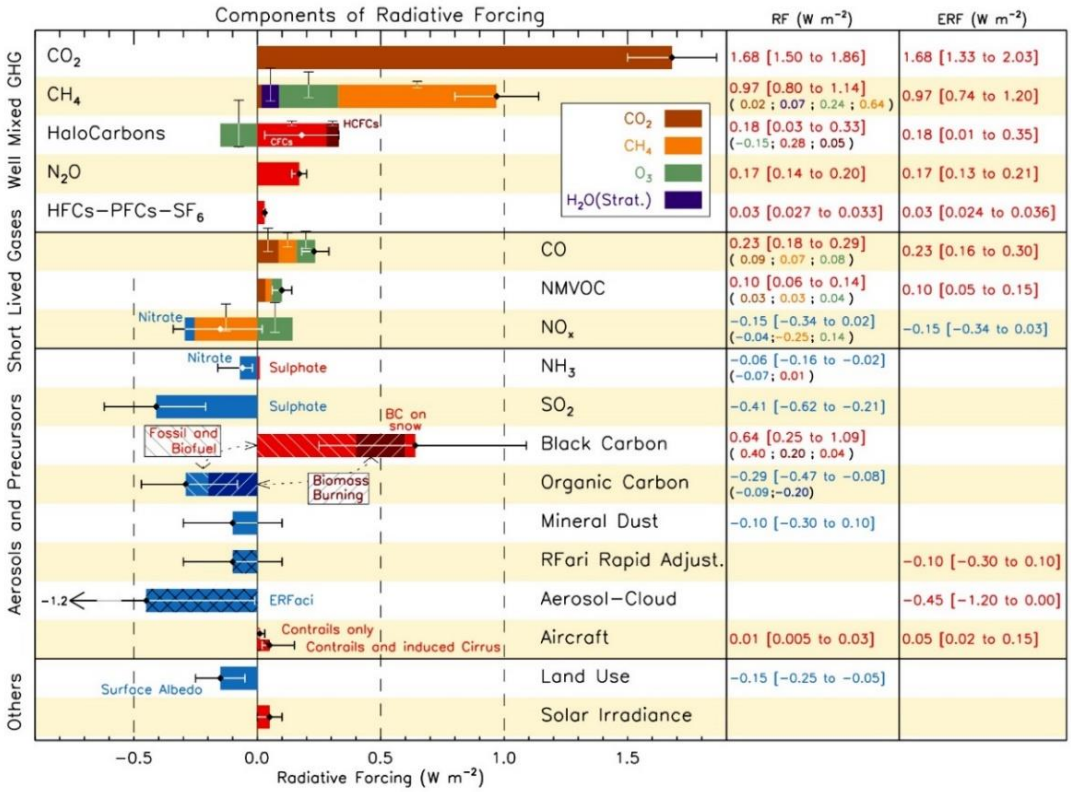


***Figure 1.1*** *- Radiative forcing (RF) of different atmospheric components in 2011 with respect to 1750. Horizontal bar represents the overall uncertainty and vertical bar represents that of individual components. Estimates of ERF are as numbers in the right most column. 'ari' and 'aci' represents aerosol-radiation-interaction and aerosol-cloud-interaction respectively (IPCC., 2013).*

According to *Herman et al., (1975)*, for low surface albedo, the reflected solar flux May either increase or decrease with increasing aerosol loadings, depending upon the complex part of the refractive index of the aerosols, while for high ground albedos (> 0.4), aerosols reduce the reflected flux (warming of the earth-atmosphere system). Studies on aerosol heating rates and its effect on atmospheric temperature profiles were initiated during early 1980s using one-dimensional radiative models mainly focusing on the effects of volcanic eruptions *(Hansen et al., 1978;Hansen et al., 1992; Lacis et al., 1992).* Impacts of huge amount of aerosol emission on atmospheric temperature as a result of high yield nuclear explosions, referred to as '*nuclear winter*' , that has significantly reduced the land

temperature to subfreezing level, were studied during that period *(Turco et al., 1983; Patterson et al., 1991).* Initially, aerosol radiative effects in global climate models were regarded as the scattering effects of sulphate aerosols. But by the end of twentieth century, climate significance of absorbing nature of anthropogenic aerosols and smoke aerosols were revealed through several modelling/observation based studies *(Langner et al., 1992; Charlson et al., 1992; Chylek and Wong, 1995; Kato et al., 1997)*. Later, through satellite/ground based/airborne observations, the effect of anthropogenic aerosol absorption on climate variables were established *(Satheesh & Ramanathan, 2000; Babu, Moorthy, et al., 2011; Ramanathan et al., 2001).*

Global radiative forcing due to BC is found to be ~20% of that by carbon dioxide and it is considered to be the second largest warming agent in the atmosphere after $CO_2$ *(IPCC 2007). Ramanathan et al.,(2007)* reported that, over south Asia, presence of aerosol brown clouds which consist of carbonaceous aerosols containing organic carbon and elemental black carbon, increased the atmospheric solar heating by about 50% and cause as much warming as greenhouse gases, in contrast to the cooling effects of aerosols. Radiative effects of mineral dust aerosols on long wave regime is a subject of concern in the scientific community as it adds to the warming produced by the greenhouse gases in the earth atmosphere system *(Sokolik and Toon, 1996; Liao and Seinfeld, 1998; Dufresne et al., 2002; Zhang and Christopher, 2003; Haywood et al., 2005)*. Long wave radiative effects of mineral dust aerosols during Saharan dust storms have shown significant influence on surface longwave fluxes and outgoing longwave radiation *(Haywood et al., 2005; Yang et al., 2009; Di Sarra et al., 2011)*.

Aerosol cloud-interaction causes significant uncertainty in assessing the climate impacts of aerosols (IPCC, 2013). *Penner et al.,(2004)* presents observational evidence significant effect of aerosol radiative forcing due to indirect effect by concurrent measurements of aerosol and cloud parameters at contrasting aerosol domains. Several studies have made use of satellite/aircraft based measurements to investigate the aerosol cloud interaction and estimation of aerosols forcing due to indirect effect *(Snider and Brenguier, 2000; Krüger and Graßl, 2002; Rosenfeld et al., 2008; Li et al., 2011; Zhang et al., 2011*). Modelling studies showed that aerosols have a significant influence on solar heating of a clear atmosphere while their effect on cloudy sky is relatively smaller *(Liou et al., 1978)*. But lately, many studies have shown the complex influence of clouds on the aerosol radiation interaction *(Satheesh et al., 2008; Chand et al., 2009)*. Warming of elevated aerosols

considerably increases with underlying cloud cover owing to the enhanced radiation encountered by the aerosol layer reflected from the clouds beneath and at a critical cloud fraction it change the sign of aerosol forcing at TOA by producing a net warming effect over the cooling *(Chand et al., 2009).* Aerosol models validated with observations offer effective optical modelling which can greatly aid in the estimation of aerosol radiative effects on climate. To simulate light propagation through the atmosphere precisely, accurate information on aerosol loading, aerosol microphysical properties, and composition is required. While information on loading is available relatively easily through daily based observations from satellite/ground based network, information on microphysical properties and composition is difficult to obtain. Therefore, it is important to have detailed aerosol characterization over global and regional domains. Inadequate characterization of vertical distribution of aerosols is a major cause of uncertainty in the assessment of aerosol radiative forcing because it plays a vital role in determining the residence time, long rage transport, atmospheric processes, and subsequently the radiative effects of aerosols. The parameterization of aerosol vertical distribution in models are not adequate to represent the real atmospheric conditions as the factors that control the vertical distribution of aerosols is still not clear. Thus adequate measurements on vertical distribution of aerosols are necessary for validating the models and to reduce the uncertainty associated with it.

## 1.7 Aerosol characterization

### 1.7.1 Global characterization of aerosols

The history of aerosol science began in eighteenth century with scientific contributions from John Aitken, John Tyndall, and Lord Rayleigh which later on flourished through the pioneering works by *Christian Junge, (1963), Anders Ångström (Ångström, 1964), Sheldon. K. Friedlander, (1957, 1960),* and *Othmar Preining (1966)*. Volcanic eruptions like Pinatubo in 1991, revealed the direct impact of aerosols on the global climate and studies on stratospheric aerosols were initiated. With the industrial revolution, anthropogenic emissions caused intense increase in tropospheric aerosol levels over the Northern Hemisphere causing visibility reduction. Since then there have been multitude of efforts to understand the optical and microphysical properties of atmospheric aerosols, through laboratory based observations, ground based experiments and campaign mode observations. Network based observations provide measurements with high accuracy for long-term duration, that enable the validation of satellite based observations and chemical

transport models. The Aerosol Robotic Network (AERONET) under NASA, carry out ground based remote sensing of aerosols using radiometers with 1145 observatories worldwide *(Holben et al., 1998)*. Multitude of campaigns were conducted to examine the aerosol characteristics and their effects over the globe, such as Tropospheric aerosol radiative forcing experiment (TARFOX) over North Atlantic Ocean *(Russell et al., 1999)*, Smoke, Clouds And Radiation-Brazil (SCAR-B) *(Kaufman et al., 1998)*, The Indian Ocean Experiment (INDOEX) *(Ramanathan et al., 2001)*, South African Aerosol Regional Initiatives (SAFARI) *(Swap et al., 2002),* Aerosol Characterization Experiment (ACE1, ACE2) *(Bates et al., 1998; Raes et al., 2000)*, ACE ASIA *(Huebert, 2003)* and Integrated Campaign for Aerosols Gases and Radiation Budget (ICARB) *(Moorthy et al., 2008)*. However, network based observations or field campaigns suffer from limited spatial coverage. Satellite measurements enable aerosol characterization over the globe by providing continuous observations with better spatial coverage for long span of time. Satellite era of aerosol remote sensing started in late 70's. Observations of Aerosol Index and associated aerosol products from near UV measurements of Total Ozone Mapping Spectrometer (TOM) on board Nimbus-7 (1979–1992), Meteor-3 (1991–1994), ADEOS (1996–1997), Earth Probe (1996–2000) satellites along with observations from Ozone Mapping Instrument (OMI) on board Aqua satellite constitute the longest space-borne observations of aerosols from 1979 *( Herman and Celarier, 1997; Torres et al., 2007)*. The first map of AOD over global oceans was generated using satellite based measurements of Advanced Very High Resolution Radiometer (AVHRR) on board the National Oceanic and Atmospheric Administration (NOAA) satellite at 0.63 μm from 1981 *(Husar et al., 1997)*. Moderate Resolution Imaging Spectroradiometer(MODIS) on board Terra (2000) and Aqua (2002) satellites provide aerosol optical depth data using multiple channel with separate algorithms over oceans *(Tanré et al., 1997)* and land *(Remer et al., 2005; Levy et al., 2013).* Retrieval of AOD using passive remote sensing involves the challenging task of correcting for surface effect, which is the main source of uncertainty in aerosol retrieval over land. MODIS algorithms over land uses 'Deep blue algorithm' over highly bright desert surfaces by using blue channel where the surface effect is relatively less to correct the radiance at other visible channels *(Hsu et al., 2013).* The Multi-angle Imaging Spectroradiometer (MISR) with multiple angle viewing capacity is another important instrument for space-borne measurements of aerosols over ocean and land with minimum surface effect *(Martonchik et al., 1998).* The MISR algorithm discriminates particles based on their size and provides a categorical aerosol-type classification *(Kahn and Gaitley, 2015).* Another good set of space-borne aerosol observations include Sea-viewing Wide

Field-of-view Sensor (SeaWiFS) provide aerosol products in the NIR channels (765 and 865 nm) though the instrument is primarily designed for investigations of ocean colour during the period 1997 – 2010 *(Gordon and Wang, 1994).* Observations from TOMS and OMI aided greatly in understanding the spatio-temporal distribution of dust aerosols around the globe *(Prospero et al., 2002).* Apart from MISR (multi-angle method) and the TOMS (UV absorption), all passive satellite retrievals encounter with the problem of surface reflection especially for relatively bright surfaces such as arid and semi-arid land and desert.

### 1.7.2 Aerosol characterization over the Indian region

Over the Indian region, aerosol characterization began in 1960s with radiative flux measurements using radiometer soundings and estimation of turbidity parameter from measurements of direct solar radiation *(Mani et al., 1965, 1969)*. By 1980s systematic characterization of aerosols were initiated under ISRO with indigenously developed Multi-Wavelength radiometer measurements from Trivandrum *(Moorthy et al., 1988).* Several national programmes were developed to understand the climatology of aerosols, spatio-temporal distribution of aerosol optical properties and their impacts on radiation balance, such as Indian Middle Atmospheric Programme (IMAP), ISRO-GBP, the Indian Ocean Experiment (INDOEX)-India Programme and the Indian Climate Research Programme (ICRP). Under these programmes a multitude of efforts were made to characterise aerosols over the Indian region and surrounding oceanic regions, through regular ground based network observations and coordinated multi-platform field campaigns. Network based aerosol characterization over the Indian region were established by Aerosol Radiative Forcing over India (ARFI) project under ISRO-Geosphere Biosphere Programme (I-GBP) that carry out regular and long term monitoring of aerosols for assessing the climatology of aerosols, which include island based stations over the Bay of Bengal and Indian Ocean, and high altitude stations over the Himalayas. A part from this, India meteorological Department (IMD) maintains a network of 12 sky radiometers over different locations within the country. These observation provide fairly good long term data set on aerosols over the Indian region at reasonable spatial resolution. Long term observations of AOD under ARFI project revealed that, there is a build-up of aerosols over the Indian region as indicated by the increasing AOD (since 1985) *(Moorthy, Babu et al., 2013).* The Major field campaigns carried out over the Indian region and nearby oceanic regions include, the Indian Ocean Experiment (INDOEX) *(Ramanathan, 2001),* Arabian Sea Monsoon Experiment (ARMEX) *(Moorthy, Babu, et al., 2005)* , ISRO-GBP Land Campaign I

*(Moorthy, Sunilkumar, et al., 2005)* and Land Campaign II *(Nair et al., 2007)*, Integrated Campaign for Aerosols gases and Radiation Budget (ICARB 2006 and WICARB 2009) *(Moorthy et al., 2008, Babu et al., 2012)* and Cloud-Aerosol Interaction and Precipitation Enhancement Experiment (CAIPEEX) *(Kulkarni et al., 2012).* Scientific results from these observations indicated the presence of elevated aerosols over the Indian region and that led to the conception of the Regional Warming Experiment (RAWEX) under I-GBP. RAWEX focus on the characterization of elevated aerosols using aircraft based experiments and high-altitude station based observatories.

### 1.7.3 Aerosol modelling

Aerosol impacts on climate are investigated using global/regional climate models. . During nineteen nineties, direct radiative effects of sulphate aerosols were included in several General circulation model (GCM) simulations. By fourth assessment report of IPCC *(IPCC, 2007),* several modelling experiments included the representation of different natural and anthropogenic aerosols such as BC, organic carbon, mineral dust and sea salt aerosols. GCM simulations indicate that aerosol induced radiative forcing make the lower atmosphere inversion stronger, increase stability within PBL and provide conditions favouring a drier troposphere *(Ramanathan and Ramana, 2005).* This can decrease evaporation which could enhance the life times of aerosols, leading to a positive feedback between aerosol concentrations and subsequent forcing on climate. Several modelling studies employing regional climate models and global climate models have brought out many important impacts of aerosols on temperature structure of atmosphere, monsoon circulation and on the cryosphere *(Lau and Kim, 2010; Nair et al., 2012; Vinoj et al., 2014; Solmon et al., 2015)*. Most of the GCMs have now incorporated the effect of aerosols on radiation and hydrological cycle driven by input from simulations of aerosol composition/loading using chemical transport models. They are now evolving with better radiative transfer codes, more refined methods to account for the effects of condensation on hygroscopic aerosols, better parameterization of clouds and better spatial and temporal resolution. Global chemical transport modelling encompasses a wide variety of aerosol species and continues to refine the representation of the aerosol physical and chemical processes. Satellite measurements coupled with ground based observations are used to constrain these models to reduce uncertainty in GCM simulations.

## 1.8 Climate impacts of elevated aerosols

Altitude profile of aerosols is normally assumed to be exponentially decreasing with height with a specific aerosol scale height in climate models and in atmospheric correction

algorithms. However, aerosols generated at the surface are lifted up vertically to free-tropospheric altitudes through convective activity or directly injected above boundary layer by processes like volcanic eruptions and ever increasing air traffic. These aerosols get transported through different altitude levels in conjunction with the prevailing winds and makes their distribution spatially heterogeneous and seasonally distinct. Aerosols resides above the well-mixed boundary layer are referred to as *'elevated aerosols '*. Elevated aerosols causes both surface cooling and atmospheric warming. Their atmospheric warming potential is high due to the higher amount of radiation available at elevated altitudes which is a subject of concern in the changing climate scenario. Elevated layers situated in the free troposphere can produce extensive warming and the stable layers thus created will increase the lifetime of the aerosols in the atmosphere leading to greater absorption and warming *(Babu, Moorthy, et al., 2011).* Theoretical investigations shows that layer height of absorbing aerosols has more influence on the radiation reaching TOA than that of scattering aerosols *(Mishra et al., 2015).*

Aerosol impact on general circulation and hydrological cycle have been investigated using several modelling simulations (*Cooke, 2002; Douville et al., 2002; Ramanathan et al., 2005; Stenchikov et al., 2006; Lau and Kim, 2006; Ming and Ramaswamy, 2011*). *Chung and Ramanathan (2006)*, studied the effect of brown haze heating and associated weakened SST gradient over the northern Indian Ocean, and found that it cause regionally different effects on monsoon circulation. Aerosol induced cooling is found to enhance the strength of the tropical mean circulation using a coupled atmosphere–slab ocean general circulation model *(Ming and Ramaswamy, 2011)*. *Lau et al., (2006)* proposed the 'Elevated Heat Pump Mechanism' induced by extensive heating due to elevated absorbing aerosols over the Indo-Gangetic Plain and the Himalayas (figure 1.2). According to this theory, elevated aerosol heating induces the formation of an upper level warm core anti-cyclonic circulation over Tibetan Plateau during pre-monsoon season that causes an early onset and strengthening of monsoon rain over the Northern India by strengthening the land-sea thermal contrast. The increased rainfall over the Himalayan foothills and Northern India during early monsoon (May - June) is followed by a reduction in rainfall over central India during later part of the monsoon (July - August) *(Lau and Kim, 2010)*. Long term variability of early summer monsoon rainfall over the Indian region shows an increasing trend which is attributed to the increasing pre-monsoon tropospheric temperature that shows a direct association with long term trend in absorbing aerosols over the Himalayas *(Gautam et al., 2009)*. Advanced onset of monsoon was also observed over the Bay of Bengal and Western Pacific during the last few decades *(Kajikawa et al., 2012)*. Simulations on the effect of

anthropogenic aerosols on south-west monsoon showed that thermodynamic changes induced by aerosols facilitated a relative warming of Indian Ocean that drove the observed earlier monsoon onset, resulting in reduced cloudiness and precipitation in May while enhanced precipitation during June over most of India *(Bollasina et al., 2008; 2011; 2013).* Over the Indian region, monsoon deficient years are found to have associated with decrease in cloud droplet size and increase in aerosol abundance while the effect is opposite for heavy monsoon years *(Patil et al., 2017)*.

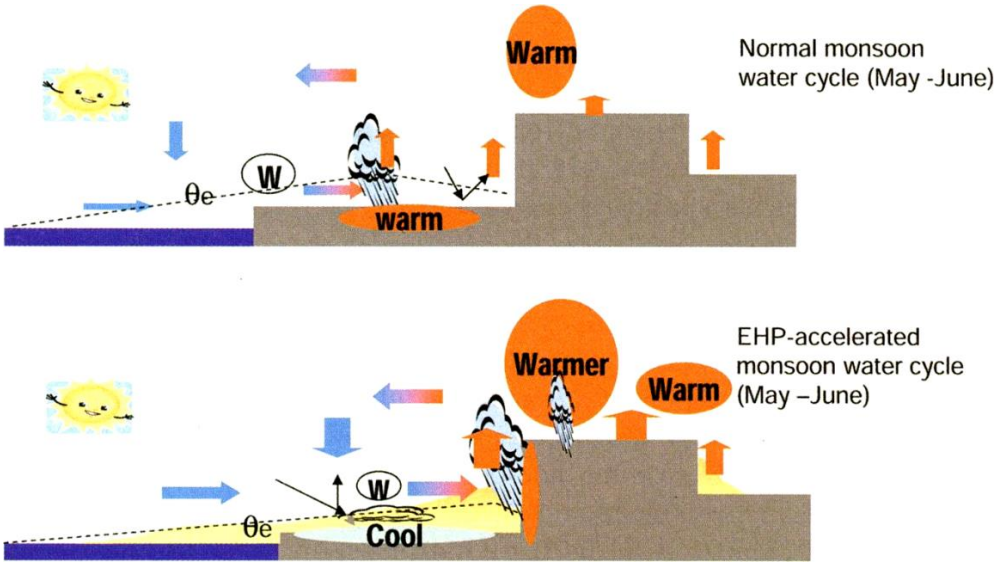


***Figure 1.2*** *- Illustration of 'elevated Heat pump hypothesis (EHP)' (Lau et al., 2008)*

Association of dust aerosols with Asian summer monsoon is being investigated as a topic of interest in the scientific community *(Vinoj et al., 2014; Jin et al., 2015; Solmon et al., 2015).* Role of absorbing aerosols on aerosol monsoon link is studied using different models but observational evidence for the association of aerosols with monsoon is yet to be established. Elevated aerosols are closely associated with aerosol - cloud interaction and subsequent indirect effect on cloud albedo/ lifetime, along with semi-direct effect of aerosols on clouds that causes the evaporation and suppression of the cloud droplets in the atmosphere and even make them termed as "burn off" of clouds. The magnitude of these aerosol induced radiative effects is strongly influenced by the vertical distribution of aerosols especially in the presence of elevated aerosol layers and its position with respect to clouds *(Satheesh et al., 2008).*

### 1.8.1 Characterization of elevated aerosols

Vertical profiling of aerosols is generally carried out using ground based/space based LIDAR or aircraft/Balloon based in situ measurements. Characterization of vertical

distribution of aerosols started way back in 1960s using air-borne sampling techniques. In 1961, *Junge and Chagnon* carried out aerosol profiling at stratosphere using balloon-borne Aitken Nuclei counter and inertial impactor. They found a layer of submicron sulphate particles at the altitude of ozone layer within stratosphere *(Chagnon and Junge, 1961; Junge et al., 1961). Bigg, (1964)* carried out twilight scattering measurements for detecting aerosol layers in the stratosphere. *Elterman et al., (1969)* implemented Searchlight probing techniques to measure aerosol profile up to 50 km altitude which showed a seasonally dependent surface convective dust layer up to 5 km in altitude and a turbidity maximum at the tropopause. *Elterman's* standard model indicated that the aerosols decrease exponentially with height for first few kilometres of altitude with scale heights of 1 – 2 km and the majority of columnar aerosol mass in resides in the lowest few kilometres. However, aircraft based in situ sampling of aerosol scattering measurements using integrated nephalometer combined with ground based lidar measurements, showed distinct variability in the vertical distribution of aerosols in the atmosphere *(Deluisi et al., 1976)*.

Lidar techniques for atmospheric studies started back in early 60s *(Fiocco and Smullin, 1963)*. Detection of stratospheric aerosols layers were carried out using 'optical radar' which is later termed as Light Detection and Ranging (LIDAR) *(Grams and Fiocco, 1967; Fiocco and Grams, 1969; Bartusek et al., 1970; Schuster, 1970; Fox and Grams, 1973; Russell et al., 1976)*. In-situ sampling of vertical distribution of aerosols through air-borne measurements is complex, expensive, and limited in vertical/spatial coverage, while remote sensing of the vertical distribution of aerosols using LIDAR is continuous at the expense of complexity in the retrieval techniques. Lidar is helpful in providing long-term measurements of aerosol vertical distribution over a region with high temporal and vertical resolution though with limited spatial coverage. Various lidar techniques have been used for the characterization of aerosols from the simple elastic back-scatter lidar, that require a priori knowledge of extinction to back-scatter ratio of aerosols to complex Raman lidars or High Spectral Resolution Lidar (HSRL) that enable the direct measurements of aerosol extinction coefficient. Aerosol characterization was carried out along with meteorological parameters using differential absorption lidar (DIAL) system, lidars based on absorption of light by molecules in the atmosphere *(Browell et al., 1983; Higdon et al., 1994)*. In the presence of aerosols, Raman signal deviates from that due to gases like oxygen and nitrogen. With the a priori knowledge on the Raman signal from standard gases, shift in the measured Raman signal is used to directly estimate aerosol extinction profile without assumption on the physical composition of the aerosols

*(Ansmann et al., 1990; Ansmann et al., 1992; Müller et al., 2005)*. Low SNR of Raman lidar compared to elastic lidars limits their application to night time aerosols. HSRL lidar work on the principle of Doppler frequency shift of the scattered radiation from molecules characterized by random motion and from particulates moved by wind and turbulence. Motion of molecules and particles induce deviation in Doppler shift due to their characteristic difference in motion which is used to separate aerosol signal from that of molecules. HSRL uses high resolution spectral bands to filter molecular signal and provides better signal to noise ratio compared to Raman lidar and enable aerosol characterization on diurnal basis. For both Raman and HSRL techniques, two lidar equations are available that separates molecules and aerosols which can be used to directly measure the vertical profile of aerosol extinction coefficient and backscattering coefficient , which is subsequently used to estimate the vertical profile of aerosol lidar ratio *(Liu et al., 2002; Müller et al., 2005; Giannakaki et al., 2016)*. Measurement of lidar ratio provides information on aerosol composition and enables aerosol typing/classification.

The concentration of stratospheric aerosols was almost one order of magnitude greater, compared to earlier observations after the eruption of Mount Agung in March 1963 *(Grams and Fiocco, 1967)*. While most of the lidar measurements were dedicated for stratospheric aerosols and the effect of volcanic eruptions, studies on tropospheric aerosols were limited to a few *(Schuster, 1970 ; Gambling and Bartusek, 1972). Spinhirne et al., (1980)* measured altitude distribution of extinction cross section of aerosol and refractive index in the troposphere using multi-angle lidar systems, assuming horizontally homogeneous atmosphere. This assumption yield poor inversion which is one of the disadvantages with multi-angle lidar profiling. Polarization based lidar technique has also been used to infer information on atmospheric conditions and clouds *(McNeil and Carsweil, 1975; Sassen, 1991)*. Several regional networks have been established for long term lidar measurements. These include European aerosol research lidar network (EARLINET) *(Pappalardo et al., 2014)*, a federation of different European scientific groups, the Asian Dust Network (AD-Net) to obtain self-consistent long term aerosol climatology over the Asian countries established in 1998 *(Sugimoto and Uno, 2009)* and the Micro-pulse lidar network (MPL-Net) by NASA founded in 2000 *(Berkoff et al., 2003)*. Several global campaigns have been conducted using ground based and air-borne lidar observations, and in-situ measurements at regional scales that focused on vertically resolved aerosol microphysical properties, species wise aerosol characterization, and aerosol cloud interaction. These include ship-borne/airborne observations of INDOEX, airborne in situ measurements on the island location at Puerto Rico in Atlantic Ocean (PRIDE) *(Maring, 2003)*, Saharan Dust

Experiment (SHADE) *(Tanré, 2003),* Asian Pacific Regional Aerosol characterization Experiment (ACE-Asia) *(Huebert, 2003),* Mineral dust, and Tropospheric Chemistry (MINATROC) over Europe *(Gobbi et al., 2003),* Unified Aerosol Experiment over United Arab Emirates *(Reid, Piketh, et al., 2008),* African Monsoon Multidisciplinary Analysis (AMMA), and Saharan Mineral dust Experiment (SAMUM) *(Ansmann et al., 2011).*

Significant enhancement in global aerosol characterization has been achieved during the last decade through the observations from Cloud Aerosol Lidar Infrared Pathfinder satellite Observations (CALIPSO) that is intended specifically for the study of vertical distribution of aerosols and clouds. The space-born lidar, Cloud Aerosol LIdar with Orthogonal Polarization (CALIOP), the primary instrument on-board CALIPSO, has marked a new era of space-based lidar measurements over global scale. One of the major disadvantages of aerosol retrievals from space-borne passive remote sensing is the separation of atmospheric radiance from surface radiance. CALIOP is an active sensor that carries out range-resolved measurements and provides the vertical profiles of aerosols with high vertical resolution. CALIOP is best suited for the three dimensional distribution of aerosols over the globe. Numerous studies have been carried out using continuous long term dataset of CALIOP (2007 till present) that significantly improved the knowledge of spatiotemporal distribution of aerosols over the globe *(Uno et al., 2008; Winker et al., 2010; Wu et al., 2012; Liu et al., 2015)*. CALIOP uses 'Cloud Aerosol Discrimination Algorithm (CAD)' for discriminating aerosols from clouds, classify aerosols among seven different pre-defined types of aerosols and accordingly chooses lidar ratio for the retrieval *(Omar et al., 2009).* Being a polarization resolved sensor, CALIOP provide vertical profiles of depolarization ratio of particles in the atmosphere that provide insight on the relative contribution of non-spherical particles in the scattering volume which make it one of the best tool for the characterization of mineral dust over the globe. Previous to CALIOP, the Lidar In-space Technology Experiment (LITE) was flown on-board space shuttle named Discovery during 1994 for a ten day period, to explore the feasibility of space-borne lidar for cloud and aerosol characterization *(Winker et al., 1996).* CALIOP was built from the technical experience provided by the LITE and observations from LITE were used to develop and validate CALIOP algorithms. Recently, NASA has employed a polarization sensitive, multi-wavelength lidar, 'The Cloud Aerosol Transport System' (CATS), on-board International Space Station (January 2015) *(McGill et al., 2015)*. CATS operate at high repetition rate and follow an orbit with an inclination of 51° that enable the observations of diurnal cycle of aerosols and clouds. In the last 50 years lidar observations of the atmospheric aerosols provided a great insight to the spatial and temporal distribution of

aerosols, mixing and compositional properties, generation mechanisms and their interaction with clouds. Inadequate representation of aerosol vertical distribution in climate models causes significant uncertainty in the assessment of radiative effects of aerosols on climate *(Textor et al., 2006; Koffi et al., 2012; Samset et al., 2013).* There have been a few modelling studies which indicate that aerosol vertical distribution is mainly controlled by convective transport and in-cloud scavenging *(Textor et al., 2006; Cui et al., 2006; Ekman et al., 2006; Kipling et al., 2016).* Inter-comparison of aerosol vertical distribution from AeroCom models (Aerosol Comparison between Observations and Models) with CALIOP observations showed significant diversity in the simulated aerosol vertical distribution with observations *(Koffi et al., 2012, 2016).* This demands for the need of sufficient information on vertically resolved aerosols properties.

### 1.8.2 Elevated aerosol characterization over India

The first Lidar based characterization of aerosol vertical profiling over the Indian region was initiated from Thumba in 1981 *(Parameswaran et al., 1984)*. Subsequently, several other groups followed from Pune and Ahmedabad *(Devara and Raj, 1989; Jayaraman et al., 1995)*. Effect of Pinatubo eruption was studied over the Indian region using back-scatter lidar observations which showed a decay of Pinatubo aerosol layer at 17 to 30 km *(Jayaraman et al., 1995)*. Studies on the nocturnal boundary layer and effect of volcanic eruptions on stratospheric aerosols were carried out at Pune, using ground based lidar observations *(Raj et al., 1997; Devara, 1998). Parameswaran et al., (1997)* used a bistatic continuous wave lidar to study the mixed layer properties and derived the altitude distribution of aerosol number density from Thumba. Aerosol characteristics at Upper Troposphere Lower Stratosphere (UTLS) region were studied using lidar observations which showed an increasing trend in aerosol loading at an inland tropical station, Gadanki *(Kulkarni et al., 2008)*. There have been several more attempts over the Indian region to understand the vertical distribution of aerosols with lidar observations *(Rajeev et al., 2000; Satheesh, Vinoj et al., 2006; Badarinath et al., 2010; Mishra et al., 2013)*. Aircraft/balloon borne in situ observations of aerosols carried out over the Indian region provided some of the path breaking observations. *Moorthy et al., (2004)* carried out profiling of black carbon aerosols for the first time over the Indian region, using an instrumental aircraft. Later on BC aerosols were profiled in the free troposphere using high altitude balloon-borne observations, by *(Babu, Moorthy, et al., 2011)* over Hyderabad, an urban site in peninsular India that revealed the presence of remarkably large peaks *(Babu, Moorthy, et al., 2011)*. The observed aerosol peaks were associated with a reduction in the atmospheric lapse

rate and a drastic increase in the atmosphere stability, probably due to BC induced heating in the atmosphere. Aerosol induced regional warming raises serious concern on radiation balance and hydrological cycle especially over the South Asia, as revealed by the observations from INDOEX that took place during 1999 (January - March). Multi-wavelength lidar observations during INDOEX provided one of the first observations of vertically resolved micro-physical properties of aerosol over the oceanic regions of India, which revealed the presence of elevated plumes of anthropogenic pollution over the Indian Ocean *(Ansmann et al., 2000; Franke et al., 2001).* Table 1.1 lists the studies on aerosol vertical distribution carried out over the Indian region through lidar/in-situ measurements.

***Table 1.1 –*** *Reports on altitude distribution of aerosols over the Indian region*

| Location | Method | Reference |
|---|---|---|
| **Thumba** | Ground LIDAR | Parameswaran et al.,(1984, 1995, 1997) |
| **Pune** | Ground LIDAR | Devara, (1998); Devara and Raj, (1989) |
| **Ahmedabad** | Ground LIDAR | Jayaraman et al., (1995) |
| **Indian Ocean** | INDOEX – Ship-borne LIDAR | Welton et al., (2002) |
| **Northern India** | ISR –GBP Land Campaign<br>Aircraft in-situ | Tripathi et al., (2005) |
| **Peninsula** | Ground LIDAR | Satheesh, Vinoj et al., (2006) |
| **Eastern coast** | Ground LIDAR | Niranjan, Madhavan et al., (2007) |
| **Southern India** | Ground LIDAR | Kumar et al., (2006) |
| **Bay of Bengal** | ICARB – Air-borne LIDAR | Satheesh, Moorthy et al., (2009) |
| **Central Himalayas** | Ground LIDAR | Hegde et al., (2009) |
| **Thumba** | Ground LIDAR | Rajeev et al., (2010) |
| **Central India** | RAWEX - High altitude balloon | Babu et al., (2011) |
| **Northern India** | CAIPEX-aircraft in-situ | Padmakumari et al., (2013) |
| **Kanpur** | MPLNET – Ground LIDAR | Sarangi et al., (2016) |
| **Indian landmass** | RAWEX - Aircraft in-situ | Babu et al., (2016) |

Integrated Campaign for aerosols, Gases and Radiation Budget (ICARB) followed by its winter segment, was another major attempt to characterize aerosols over the south Asia with multi-instrument, multi-segment measurements which include air-borne vertical measurements over Indian land mass and adjoining oceans. The results revealed the presence of prominent elevated extinction over the BoB, off the Indian coast with significant loading above 1 km altitude and maximum extinction between 2 km and 4 km

during pre-monsoon *(Satheesh, Moorthy, et al., 2009)*. Over Indian region, aerosol extinction coefficient increased almost three times the surface concentration above 2 km altitude and about 50 -70 % of aerosol optical depth was contributed by aerosols situated above the clouds *(Satheesh et al., 2008).* Subsequent radiative transfer calculations revealed a strong meridional gradient in the atmospheric warming due to aerosols, from 1 K at 2 km altitude near the Indian Ocean to about 5 K at 4 km over the central India *(Satheesh et al., 2008).* A regression analysis between near surface measurements and column values from Winter-ICARB observations, along with simultaneous CALIPSO extinction profiles revealed elevated layer structures and varying vertical heterogeneity over different parts of BoB *(Moorthy et al., 2010).* Over the Arabian Sea, *Welton et al., (2002)* has reported elevated layers of aerosols below 1 km and in the range 2 - 3 km. Over the East coast of India, *Niranjan, Madhavan et al., (2007)* has reported the presence of elevated layers between 2 – 3 km and states that it is associated with the transport of dust from West Asia and North West India.

The efforts of Aerosol Radiative Forcing over India (ARFI) project under Indian Space Research Organization Biosphere Geo-sphere Programme (ISRO-GBP) to understand elevated aerosols and their radiative effects over the Indian region, has led to a multi-year multi-disciplinary, field campaign called Regional Warming Experiment (RAWEX) that focuses on the complete characterization of elevated aerosols over the Indian region. The project aims to quantify the contribution of absorbing aerosols in the regional warming and to delineate the share of long-range transport and local contributions to the warming. Aircraft measurements carried out under RAWEX indicates enhanced absorption during pre-monsoon season which is attributed to the presence of mineral dust loading over the Indian region *(Nair et al., 2016).* The synoptic westerly persistent over the Indian region make it conducive for the long-range transport of mineral dust from the sources of West Asia and Africa. METEOSAT observations of IR brightness temperature has revealed the high absorption efficiency of Asian dust aerosols compared to that of African origin *(Moorthy et al., 2007)*. The following sections elaborate on mineral dust aerosols, their characterization and radiative impacts.

## 1.9 Mineral dust aerosols

Mineral dust is produced by disintegration of soil particles driven by surface winds over the arid areas of the Earth and largely contributes to the mass of tropospheric aerosol. The global dust belt releases large quantity of mineral dust aerosols into the atmosphere that

make it the largest contributor to the global aerosol burden by mass. Dust production is parameterized in aerosol models as a function of the wind speed at the surface, vegetation cover, and soil moisture content. Within the global dust belt, Sahara desert of North and West Africa, deserts over the west Asia, and central Asia are the major dust sources (figure 1.3). Global dust emission rate is estimated to be ~1000 – 5000 Tg/year, as quantified by GCMs *(Huneeus et al., 2011).* Deposition of mineral dust over oceanic surfaces affect ocean biota providing nutrients which in turn affect the emission of carbon dioxide and dimethyl sulphide (DMS) (good precursor of sulphate aerosols over oceans) there by affects the global bio-geo chemical cycles *(Maher et al., 2010; Okin et al., 2004)*. Iron fertilization by mineral dust aerosols over oceanic region is a well-established phenomenon. Transport and deposition of African dust over to the Amazon rainforest provides nutrients to otherwise phosphorous deficient regions of the Amazon. Its effect on the Amazon ecosystem and associated effect on bio-geo-chemical cycles is being investigated in the scientific community with great concern *(Yu, Yuan, et al., 2015)*.

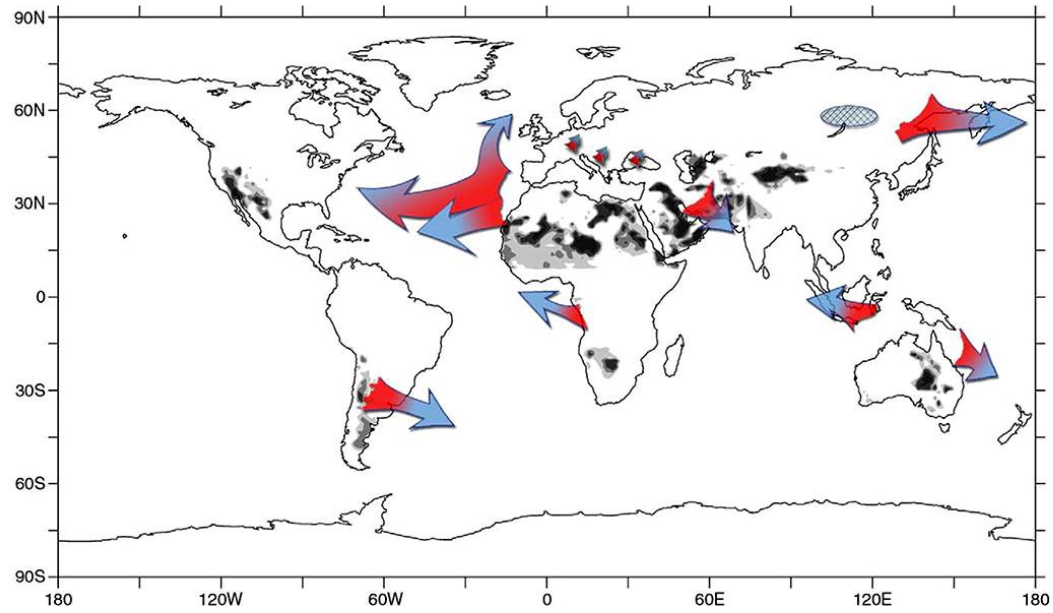


***Figure 1.3*** *- Global dust sources identified using Aerosol index observations of Ozone Monitoring instrument (OMI) (Maher et al., 2010)*

For biogeochemical impacts, the amount of mass deposited is important. Thus deposition of large particles over oceans like mineral dust aerosols assumes importance in the fertilization of ocean biota. Despite of its larger size, mineral dust is greatly transported over long range around the globe and undergoes various chemical reactions that alter its physio-chemical characteristics. Their heterogeneous reactions with trace gases affect the chemical balance of the atmosphere. However, all these processes are yet to be understood

which demands for adequate characterization of physical and chemical properties of the dust particles which includes spatio-temporal distribution of dust aerosols, their mineralogical composition, mixing state, size distribution, and shape.

### 1.9.1 Radiative impacts of mineral dust aerosols

Dust aerosol not only scatters solar radiation but also absorbs and emits outgoing long wave radiation *(Miller and Tegen, 2010)*. Direct effect of aerosols is more significant in shortwave regime (~ 0.2–4 μm) due to its size distribution characteristics. However, particles with sizes of the order of terrestrial (longwave) radiation (>4 μm), such as mineral dust aerosols produce significant longwave radiative effect *(Tegen et al., 1996; Miller et al., 2006).* Mineral dust aerosol draws attention as a recognized warming agent that traps the outgoing long wave radiation and heats the atmosphere alike greenhouse gases, while produces cooling at the surface by scattering the incoming shortwave radiation *(Sokolik and Toon, 1996)*. The long wave effect of dust aerosols on radiation partly compensates their shortwave radiative effects. Being the largest contributor to the total atmospheric aerosol burden along with this multi-effect makes its radiative effects important. While absorption of SW/LW radiation by mineral dust heats the atmosphere, they backscatter the shortwave radiation to the space and cool the atmosphere beneath it and the surface. Dust absorption characteristics depend on its abundance, composition, vertical distribution and it's mixing with other aerosols, which is specific to its source regions. Using multi-sensor observations over the Saharan desert*, Zhang, (2003)* has shown that warming effect of dust aerosols will counteract the shortwave cooling effect of other aerosols. The fifth assessment of IPCC states that mineral dust aerosols exert a radiative forcing in the range of -0.3 to 0.1 $Wm^{-2}$ at the TOA *(IPCC, 2013)*. Model simulations shows that dust originated from anthropogenically disturbed soils termed as 'anthropogenic dust', constitute about 50% of the total dust load and propose that forcing due to anthropogenic dust has to be counted in among the climate forcing factors *(Tegen et al., 1996)*. Dust particles produce indirect aerosol forcing by increasing cloud albedo and by altering cloud life time. Though the multiple effects of dust aerosols on radiation are widely accepted phenomena, they are under characterized in climate models due to limited observations on their physio-chemical properties and, spatial and temporal distributions.

Aerosol monsoon interaction is demonstrated through different hypothesizes. Recently, observational and modelling studies have found that the dust loading over the Middle East can strengthen the monsoon by heating the troposphere over the Iranian Plateau and the

Arabian Sea *(Jin et al., 2015).* Role of mineral dust aerosols in modulating the monsoon over short periods is demonstrated using models and satellite observations *(Jin et al., 2014; Vinoj et al., 2014)*. Using global climate model simulations and satellite observations, it is found that dust induced heating over the North Africa and West Asia has increased the flow of moisture over India and has modulated the Indian summer monsoon rainfall over central India within a short period of one week's time *(Vinoj et al., 2014).* A multivariate empirical orthogonal function analysis using satellite observations and reanalysis datasets found significant correlation of dust aerosols over Middle East region and Arabian Sea with rainfall over central and Eastern India within a time of two weeks *(Jin et al., 2014)*. Investigation using Regional Climate model suggested possible role of west Asian dust forcing in the increasing trend in the monsoon precipitation rate in southern India *(Solmon et al., 2015)*. Inter-comparison study of model simulations with observations indicates that the imaginary part of dust refractive index used in climate models are too low, that results in significantly underestimating dust radiative impacts on the regional climate *(Jin et al., 2016)*. Figure 1.4 shows a schematic of climate impacts of mineral dust aerosols.

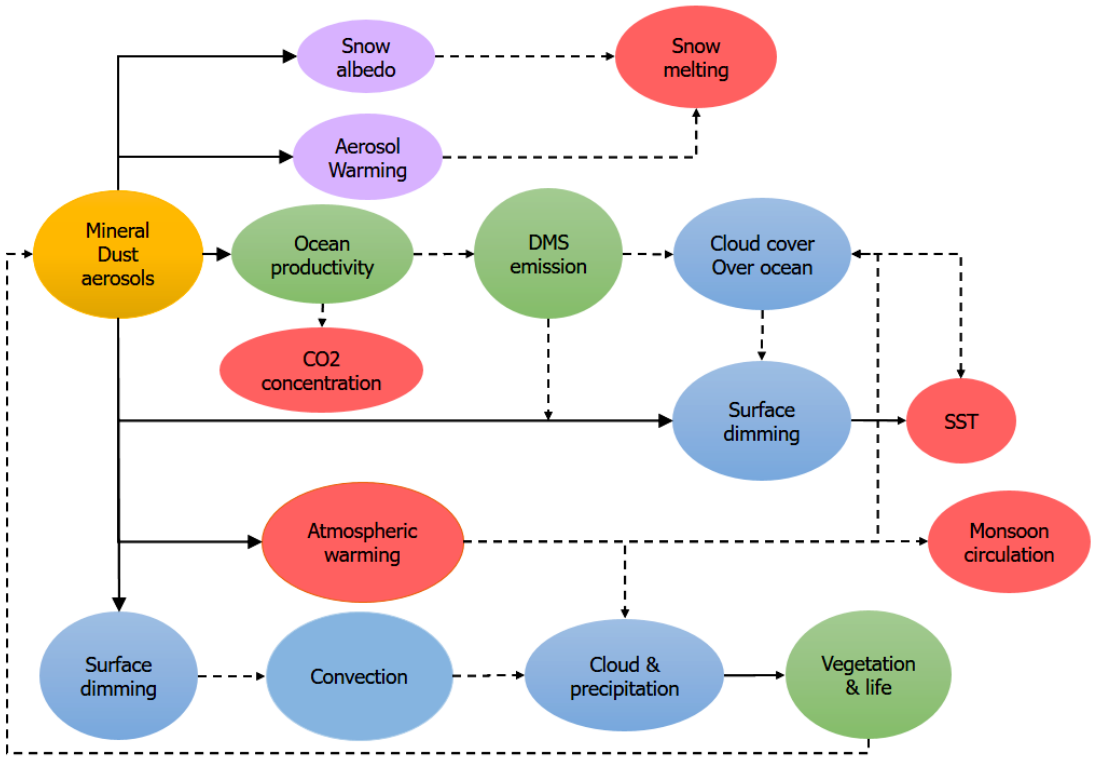


***Figure 1.4 -*** *Impacts of mineral dust aerosols on earth-atmosphere system.*

Deposition of mineral dust over snow causes serious implications by accelerating snow melting and drastic reduction in snow cover over cryosphere *(Painter et al., 2007).* Over the Himalayas, along with global warming, the enhanced surface warming is attributed to

the aerosol induced heating of the atmosphere and reduction of snow albedo by the absorbing aerosols *(Lau et al., 2010)*. Being ice nucleating particles, dust aerosol significantly affect cirrus cloud formation *(DeMott et al., 2003)*. It is shown that Asian dust can influence the global radiation budget by stimulating cirrus cloud formation *(Uno et al., 2009).* Dust induced thermodynamic changes can affect tropical convection and change different atmospheric systems. There are evidence for coupling between dust heating and cyclone activity over tropical Atlantic ocean *(Evan et al., 2006)*. Saharan Air Layer (SAL) present over the Atlantic ocean as a result of dust transport from Africa, is shown to have an effect on tropical cyclone through positive (initial development) and negative (subsequent development) feedback *(Shu and Wu, 2009)*. Recently, effect of dust aerosols on hurricane is also demonstrated using model simulations *(Sun et al., 2008)*.

### 1.9.2 Mineral dust characterization- Global and regional scenario

Radiative effects of dust aerosols have been investigated using ground based/ satellite observations over the desert regions *(Dufresne et al., 2002; Zhang and Christopher, 2003; Markowicz et al., 2003; Haywood et al., 2005; Xia and Zong, 2009; Yang et al., 2009)*. Satellite observations by passive sensors such as the Moderate Resolution Imaging Spectroradiometer (MODIS), the Spinning Enhanced Visible Infrared Imager (SEVIRI), the Multiangle Imaging Spectrometer (MISR), and the Ozone Monitoring Instrument (OMI), enabled the detection of dust plumes. Passive remote sensing measurements rely on measuring the scattering or absorption of light from the particles. However, in case of dust, incomplete information on the non-spherical scattering processes can lead to error in the characterization. MISR algorithm account for particle nonsphericity and uses ellipsoid models derived from T-matrix calculations for aerosol characterization *(Kahn and Gaitley, 2015)*. Based on IR absorption of dust aerosols, METEOSAT observations are made use to study the absorptive characteristics of dust aerosols by estimating the Infra-red difference dust index (IDDI) (*Moorthy et al., 2007*). Though passive sensors can detect the spatial extend of the dust plumes, they are limited in providing information on the multiple layers of aerosols in the atmosphere. Polarization based lidars are one of the best tools to study dust aerosols since polarization of the interacting radiation field is sensitive to the non-sphericity of the particles. Lidar based networks such as EARLINET, AD-Net and MPLNET aids in the long-term characterization of dust aerosols over the globe. The intrusion of dust aerosols from free troposphere into the Planetary Boundary Layer (PBL) and mixing processes of dust with other aerosol species are observed using lidar by *Hara et al., 2009*. Long-range transport of dust can be monitored and tracked by ground-based lidar

networks or space borne lidar *(Uno et al., 2008; Sugimoto and Uno, 2009; Pappalardo et al., 2014).* Being polarization sensitive, CALIOP provide long-term datasets of depolarization ratio that enable the global dust characterization *(Yu, Chin, Bian, et al., 2015)*;

Several field campaigns were carried out over the globe to study the characteristics of mineral dust. Air-borne in situ measurements during Puerto Rico Dust Experiment (PRIDE), showed highly varying elevated layers of dust that extend up to 5 km in altitude and intrusion of transported dust to marine boundary layer *(Reid, 2003)*. Saharan Mineral Dust Experiment (SAMUM) is one of the extensive campaigns for the characterization of Saharan dust aerosols using multiple kinds of lidars including multi-wavelength Raman lidar and HSRL in segments during 2006 and 2008 *(Ansmann et al., 2011)*. SAMUM revealed that Mineral dust layers over Sahara typically lie below 2 km with a typical depth of 1.3 ± 0.4 km with a median effective diameter of 2.5 $\mu$m *(Ansmann et al., 2011; Weinzierl et al., 2011).* African Monsoon Multidisciplinary Analysis (AMMA) is another major campaign that showed the seasonal evolution of Saharan PBL and observed inhomogeneous distribution of dust aerosols within mixed layer over the Saharan region *(Cuesta et al., 2008)*.

Over Indian region, there have been a few efforts to study the dust aerosols through ground based network/ air-borne/satellite observations. Aircraft observations carried out under RAWEX showed enhancement in aerosol absorption during pre-monsoon season and indicated vertical heterogeneity in aerosol distribution within the free troposphere *(Nair et al., 2016).* Over the Bay of Bengal, marine biota is less active as poor vertical mixing and associated shallow mixing layer *(Nair, Moorthy, et al., 2013; Kumar, 2002)*. Transport of mineral dust aerosols to this region can enhance the marine bio-production and generation of aerosols through dimethyl sulphide emission. In this scenario, significant dust transport could affect the size spectrum of aerosols over the Bay of Bengal and subsequently increases the efficiency of processes of coagulation and condensation, which can enhance aerosol heterogeneity over the Bay of Bengal. Inadequate understanding on the emission mechanism, transport processes, physical and chemical development, and removal processes of mineral aerosols is still a source of uncertainty in the assessment of dust impact on the radiation budget.

### 1.10 Relevance/scope of the study: problems to be addressed

Characterization of elevated aerosols assumes greater importance over the South Asia owing to their effect on energy budget of the earth-atmosphere system, thermal structure of the atmosphere, regional circulation and hydrological cycle. Transport of elevated

aerosols to the oceanic region and its deposition over ocean surface affects marine bio-geo chemical cycle where as to the Himalayas, it affects the snow/glacier cover through aerosol–cryosphere interaction. To investigate the impacts of elevated aerosols over the Indian region, the vertical distribution of aerosols needs to be characterized. Though several studies have been carried out on vertical distribution of aerosols using both ground based/space borne observations over different regions of the globe, a comprehensive understanding on the vertical distribution of aerosols over Indian region is yet to emerge. Vertical distribution of aerosols is one of the important parameter for the assessment of radiative effects of aerosols. Most of the model simulations assumed an exponentially decreasing vertical variation for aerosols with specific scale heights. This can impart significant errors in impact assessment when elevated aerosols layers are present in the atmosphere. During pre-monsoon season, prevailing north westerly circulation facilitates the dust transport from the arid/semi-arid regions of north-western India and west Asia to the Indian regions. Mineral dust over Asian region is more absorbing in nature and dust induced atmospheric heating and the surface cooling, are reported to have significant impacts on the Indian summer monsoon. In this context, it is imperative to characterize the spatial and seasonal characterization of the elevated aerosols and quantify their radiative effects over the Indian region. The present thesis focuses on the vertical characterization of aerosols, their spatial and temporal extents, seasonal trends, quantification of mineral dust aerosols and their radiative effect over the Indian land mass, adjoining oceanic regions and the Himalayas.

# Chapter 2

# Details of observations and methodology

Characterization of atmospheric aerosols is challenging owing to their heterogeneous distribution and short life time in the atmosphere. Synergy of observations from satellites, ground based experiments and modelling provides the opportunity to comprehensively study the system of atmospheric aerosols with better accuracy. Over last two decades, there have been numerous efforts to characterize atmospheric aerosols through ground/satellite observations and multi-platform campaigns *(Holben et al., 1998; Satheesh and Ramanathan, 2000; Ramanathan, et al., 2001; Prospero et al., 2002; Moorthy et al., 2008; Chand et al., 2009; Babu et al., 2013)*. These attempts have addressed the surface/column characterization of aerosols while characterization of vertical distribution of aerosols are still limited. To understand the precise nature of radiative effects of aerosols, knowledge on vertical distribution of aerosols is essential. The main objective of this thesis is to characterize the three dimensional distribution of aerosols over the Indian subcontinent and to estimate its radiative effects through a combination of space-borne and ground based observations.

Characterization of atmospheric aerosols is carried out using in situ measurements and remote sensing techniques. In situ observation techniques involve measurement of aerosol properties through direct sampling of ambient air. There are several methods used for the measurement of aerosol properties. Filter based aerosol sampling includes collection of aerosols on quartz filters at a known flow rate which will be subsequently analysed using thermo-optic/chemical methods to retrieve information on aerosol loading and chemistry. Aerosol absorption is estimated by measuring the attenuated light passing through aerosol laden filters (eg. Aethelometer) and aerosol scattering coefficient is estimated from the scattered radiation from aerosols within a cavity (eg. Nephalometer). Optical methods based on optical illumination/light scattering by the particles (Optical Particle Counter) and electrostatic methods based on the differential mobility of particles under electric field (Differential Mobility Analyser) provides size distribution of aerosol number concentration. Since all in situ measurements samples aerosols on to a filter or cavity using external vacuum pump, the bias due to perturbation of aerosol particles and effect of humidity in the sampling process have to be addressed. Though in situ methods

provide real time observations, they are limited over space and time. In situ measurements on-board aircraft/balloon platforms provide information on vertical distribution of aerosols through vertically resolved aerosol measurements at larger spatial scale. While satellite based remote sensing enable effective estimation of aerosol loading, retrieval of aerosol size distribution and composition still have relatively higher uncertainty which has to be carried out through coordinated in-situ measurements. A schematic describing different aerosol measurement techniques is shown in figure 2.1.

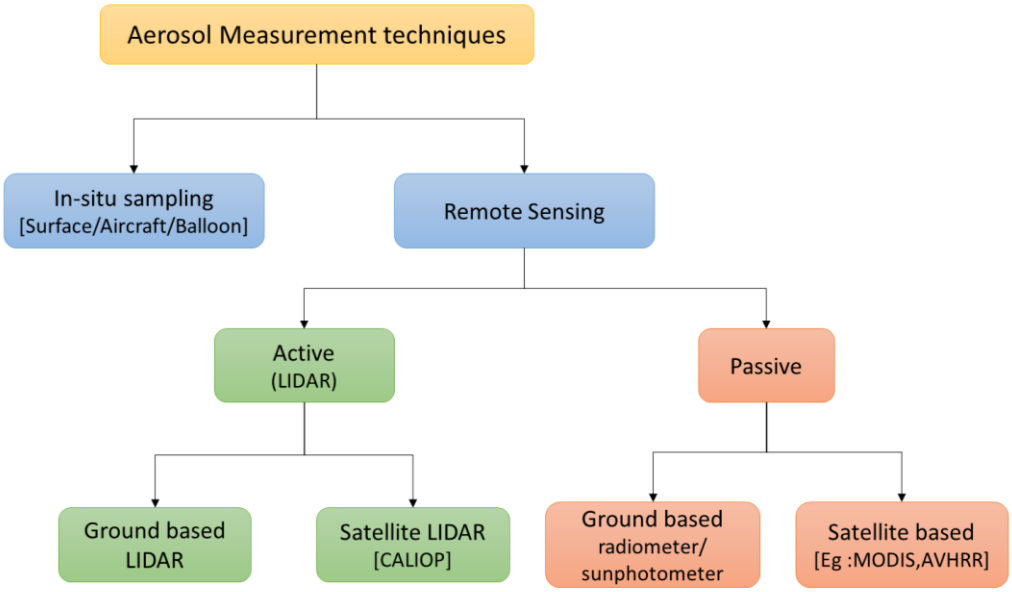


***Figure 2.1*** *- Schematic showing different techniques for aerosol measurement.*

In the remote sensing measurements, the electro-magnetic field that interacts with the scatterers in the atmosphere is measured and the required information will be retrieved without perturbing the interacting particles. Passive sensors (eg. Radiometers) measures ambient light sources that interact with the particles present in the atmosphere while active sensors uses its own electro-magnetic field to interact with the particles (eg: LIght Detection And Ranging (LIDAR)). While ground based remote sensing/in-situ techniques characterize aerosols with better accuracy, satellite based remote sensing provide large scale observations over regional and global scale for longer time scales but at the cost of accuracy and details. The spectral radiance received at passive satellite sensors consists of scattered radiation from the atmosphere and reflected radiation from the surface. The major challenge in satellite based remote sensing of aerosols is to separate the atmospheric component that contain information on the aerosols in the atmospheric column from reflected radiation from the surface. Active sensors overcome this difficulty

by sensing the scattered radiation from different layers of the atmosphere which is probed by an electromagnetic source of its own. Lidars operating in the visible spectrum is the best remote sensing tool to study the vertical distribution of aerosols with high resolution.

Observations on vertical distribution of aerosols are generally carried out using lidar remote sensing or by aircraft/balloon based in situ measurements. In situ observations of vertical distribution of aerosols are limited due to the inherent complexities, costly nature of the experiments involved, and its limited observation capacity over space and time. Remote sensing of aerosols using lidar provides an opportunity to effectively characterize the vertical distribution of aerosols with reasonably high vertical resolution. While observations using ground based lidars are limited with point measurements, space borne lidars provide better spatial coverage with good vertical resolution. Following sections describes various in-situ/remote sensing techniques used in the thesis to carry out the investigation on elevated aerosols over the Indian region and its radiative impacts.

## 2.1 In situ observations

### 2.1.1 Aircraft experiment

Aircraft based aerosol experiments have significantly contributed in the characterization of airborne particles. Aerosol measuring instruments and samplers are mounted in the aircraft to characterize different aerosol properties such as concentration, size distribution, chemical composition, and optical parameters such as absorption/scattering coefficients. Sampling air masses that move relatively slower than the aircraft and operating instruments at ambient low pressure makes the sampling process challenging on-board aircraft. As part of the ICARB and RAWEX campaigns under ISRO-IGBP programme, several aircraft based observations have been carried out over the Indian region which indicated the presence of elevated aerosols over the Indian region *(Moorthy et al., 2004; Satheesh et al., 2008; Babu et al.,2008; 2016; Nair et al; 2016; Vaishya et al., 2018)*. To ensure iso-kinetic sampling of ambient air, a shrouded solid diffuser inlet is used which is fixed under the fuselage of aircraft opening towards the direction of motion of the aircraft. Volumetric flow with a rate of 70 LPM was fixed based on laboratory simulations while the flight speed was maintained at 300 $kmh^{-1}$ during the sampling process. High resolution GPS on-board provides the coordinates of the aircraft. Flight followed a stair case pattern with six altitude levels with 30 minutes of measurement at each altitude level. Data obtained during initial time period when the aircraft rises to desired altitude and that measured between two consecutive altitude levels were discarded while analysing the data to ensure that instruments are stable to the ambient pressure and sampling under

iso-kinetic condition. Vertically resolved measurements of absorption/scattering coefficients were carried out over distinct stations over the Indian region which is used to estimate the aerosol radiative forcing over these regions. Scattering coefficients were measured using integrating nephelometer (TSI 3653, USA) at 450, 550 and 700 nm with an uncertainty of ~±10 % *(Anderson et al., 1996)*. Absorption coefficients were measured using Aethalometer (AE 33, Magee scientific, USA) at seven wavelength channels at 370, 470, 520, 590, 660, 880 and 950 nm with an accuracy of ± 20% with necessary corrections for instrument biases *(Arnott et al., 2005).*

## 2.2 Remote sensing observations

### 2.2.1 LIDAR - CALIOP

Lidar is widely used for studying the vertical distribution of atmospheric constituents due to its high vertical and temporal resolution, and its capacity to make observations in ambient conditions. Lidars are of different kinds that are sensitive to Rayleigh, Mie and Raman scattering in the atmosphere. They enable a wide range of characterization of different atmospheric parameters such as molecular density, atmospheric temperature, vertical profiles of aerosols, clouds and trace gases. The ground based micropulse lidar are operated using eye safe, low energy pulses of micro joules at high repetition rate to probe the atmosphere and receives range resolved backscattered signal which are measured using large telescopes and efficient photo detectors. From the back-scattered signal, profiles of back-scattering coefficient and extinction coefficient are retrieved. Analysis of back scattered lidar signal requires various corrections which include correction for background solar illumination, after pulse correction for the electronic dark noise generated due to laser firing and overlap correction associated with the optics of transmitter-receiver system. With high pulse repetition rate, MPL provides very good temporal resolution which makes it well suited for studying aerosols which are highly variable over time. Though ground based lidars provide high resolution temporal observations, they are spatially restricted and provide only regional information. Space-borne lidars benefits for large scale, continuous, long term observations, but at the expense of temporal resolution and signal to noise ratio. The Cloud-Aerosol Lidar with Orthogonal Polarization (CALIOP) aboard the Cloud-Aerosol Lidar and Infrared Pathfinder Satellite Observations (CALIPSO) is providing continuous and range resolved polarization sensitive observations of global aerosol properties which make it feasible to examine the aerosol vertical structure over large spatial extent with reasonable resolution. The CALIPSO which was launched in April 2006 as one of the A-Train satellites *(Winker and*

*Pelon, 2003; Winker et al., 2006; Winker et al., 2010),* enables the spatial measurements of vertical distribution of aerosols. It is sun-synchronous and positioned at 705 km altitude with an equatorial crossing time at 13:30 hrs and an inclination of 98.22°. It takes 14.55 orbits per day with a separation of 24.7° longitude between consecutive orbits at the equator. Orbit tracks of CALIPSO are shown in figure 2.2.

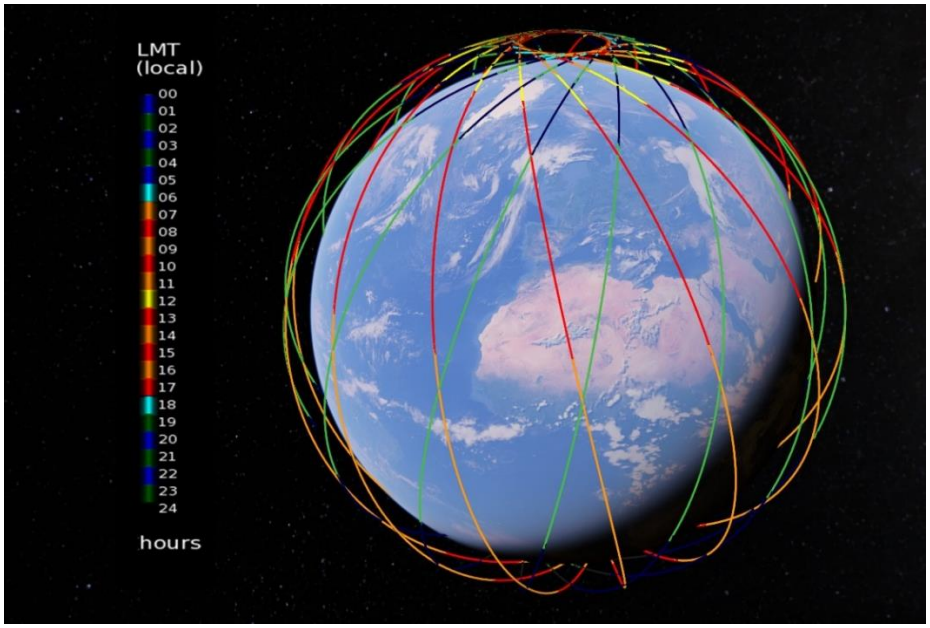


***Figure 2.2*** *- Orbit tracks of CALIOP with local mean time of over pass (courtesy IXION - LMD/CNRS and Google earth)*

The orbit tracks at the equator advances 10.8 degrees westward on subsequent days and over a period of 16 days it completes 233 orbits with a separation of 1.7° between orbits at the equator. With a repeat cycle of 16 days CALIOP carries out aerosol profiling at a resolution of 333 m in the meridional direction and around 1.7° in the zonal direction. Following sections discuss various aspects of CALIOP instrument and data products. Figure 2.3 shows the schematic of CALIOP lidar. CALIOP transmits linearly polarized laser pulses using a solid-state neodymium doped yttrium aluminium garnet (Nd:YAG) laser with a repetition frequency of 20.16 Hz and energy of ~110 mJ through two transmission channels which are at 532 nm and at 1064 nm *(Winker et al., 2007; Hunt et al., 2009).* The range resolved back-scattered energy is collected using a 1m wide telescope and separated into two receiver channels at 532 nm and 1064 nm using a dichroic beam splitter. A combination of etalon and interference filter (pass band ~35pm) is used to reduce the back-ground solar illumination in back-scattered signal at 532 nm. For signal at 1064 nm, interference filter alone is sufficient to eliminate the background signal.

A polarization beam splitter separates the received backscatter signal at 532 nm to parallel and perpendicular components to the plane of the outgoing beam.

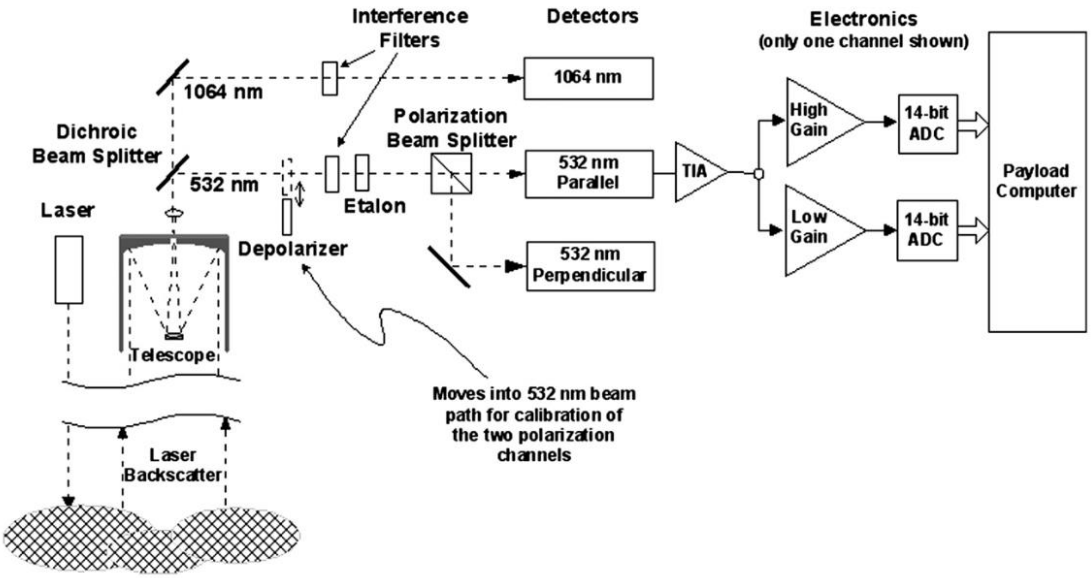


***Figure 2.3*** *- Schematic diagram of CALIOP (Hunt et al., 2009)*

Table 2.1 lists the essential system parameters of CALIOP.

***Table 2.1 -*** *System specifications of CALIOP*

| | |
|---|---|
| **Laser** | **Laser Diode-pumped Nd:YAG** |
| **Pulse Energy** | 110 mJ |
| **Repetition Rate** | 20.16 Hz |
| **Pulse Length** | 20 ns (~6m) |
| **Beam Divergence** | 100 µrad (70m at surface) |
| **Telescope diameter** | 1 m |
| **Telescope FOV** | 130 µrad (~90m at the surface) |
| **Detector** | 532 nm : Photo-multiplier tube<br>1064 nm : Avalanche photo-diode |
| **Detector effective quantum efficiency** | 532 nm : 0.11<br>1064 nm : 0.4 |
| **Detector dark count rate** | 532 nm : 2.3 x $10^3$<br>1064 nm : 2 x $10^7$ |
| **Polarization purity** | 532 nm : >99% (>1000:1) |
| **Digitization rate** | 10 MHz |
| **Vertical sample spacing** | 15 m |

While signal at 532 nm is more sensitive to aerosols, signal at 1064 provides information on the clouds owing to the size spectrum of these atmospheric components. Photo multiplier tubes are used for the detection of relatively weaker back scattered signal at 532 nm, since they have large linear dynamic range and very low dark noise that enable it to measure even single photon events. Signal at 1064 nm is measured using an avalanche photo diode (APD) that has higher quantum efficiency at that wavelength though with higher dark noise (that is suitable for strong cloud signals). Since weaker aerosol signal at 532 nm is sensitive to dark noise, APD is not used for that channel. A pseudo-depolarizer will be introduced in the path of received signal at 532 nm to calibrate the parallel and perpendicular channels of 532 nm signal. Detectors sample the analog signals at a rate of 10 MHz (vertical resolution of 15m) from an altitude of 115 km above mean sea level to 18.5 km below sea level and samples taken between 40 km (for 532 nm) and -2 km are downlinked as profile data. Two analog to digital converters (ADC), one with high gain for weak signal and another one with low gain for strong signals, are used for each receiver channels and their outputs are merged in to a single back-scatter profile.

#### 2.2.1.1 On-board processing and calibration

##### 2.2.1.1.1 Back-ground and offset measurements

DC signal from altitudes between 112 and 97 km is measured to characterize background solar illumination assuming that return signal from atmospheric components is negligible in this altitude range. This DC signal is electronically subtracted from the analog profile before digitization. For weak signals, this May alter the signal to negative values which is prevented by adding a fixed dc offset (mean of 1000 samples acquired in the range 75.3 to 60.3 km) prior to this process. After digitization, this fixed dc is subtracted to obtain the backscatter signals.

##### 2.2.1.1.2 On-board averaging: Vertical and horizontal resolution

The location of the footprint on the ground is determined with an on-board geoid model using data from spacecraft GPS. Geolocation accuracy is about 50 m in the horizontal and 10 m in the vertical directions. Spacecraft moves at a velocity of ~7 km/s with laser pulses shooting at a rate of 20.16 Hz. Lidar foot print covers a distance of ~333 m in collecting a single profile which is the horizontal resolution of sampled profiles. Due to bandwidth limitations for downlinking the data from the satellite, the back-scatter signal profiles are averaged on-board in both horizontal and vertical dimensions. Downlinked profile data includes samples acquired in the range 40 km to 2 km with a vertical resolution of 30 m as determined by the receiver bandwidth.

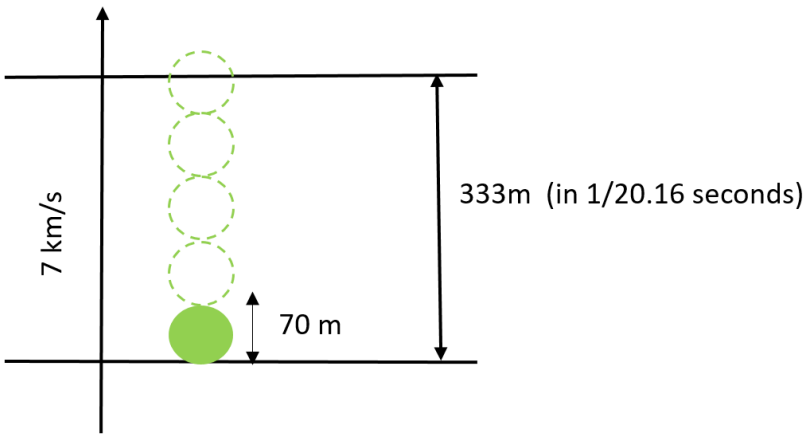


***Figure 2.4 –*** *Spatial resolution of CALIOP.*

Due to low signal to noise ratio characteristic of space-borne lidar, different schemes of averaging is applied to weakly/strongly scattering features. Also at higher altitudes, atmosphere is more homogenous and signal strength is weaker, which requires averaging higher number of profiles at that altitude range. Hence the vertical and horizontal resolution of the downlinked profiles varies with altitude. Minimum averaging is carried out between -0.5 km to 8.2 km where the atmosphere is rather inhomogeneous and dynamic. Table 2.2 shows the horizontal and vertical resolution of the downlinked profile data with respect to altitude above mean sea level.

***Table 2.2*** *- Spatial and vertical resolution of CALIOP signal at 532nm (Winker et al., 2009)*

| Altitude range (km) | Number of shots averaged | Horizontal resolution (km) | Vertical resolution for 532 nm (m) |
|---|---|---|---|
| **-0.5 - 8** | 1 | 0.33 | 30 |
| **8 - 20** | 3 | 1 | 60 |
| **20 - 30** | 5 | 1.667 | 180 |
| **30 - 40** | 15 | 5 | 300 |

#### 2.2.1.1.3 Signal to noise ratio (SNR)

SNR of space-borne lidar is lower than ground based lidars due to large distance between the lidar and the target and the limited laser pulse energy it can have. Lower SNR in CALIOP is compensated by multiple averaging schemes. The degree of averaging at a particular altitude range is determined by the spatial scale of the atmospheric features at that range. To get reliable profile information, it is required that SNR at 532 nm channels at night should be at least 50 for the molecular back-scattering coefficient when averaged

horizontally over 1500 km and vertically by 5 km. SNR during day time for 532 nm signals is greater than 30 % of the required SNR though with time SNR declines due to the degradation of system health and electronics.

#### 2.2.1.2 Calibration: Level 1 data processing

The backscattered signal at r is expressed as given by equation (2.1) after the correction for offset signal, background signal, and system artefacts, the (range of satellite from the scattering volume).

$$P(r,k) = \frac{1}{r^2} E(k) G_A(k) C(k) \beta(r,k) T^2(r,k) \qquad (2.1)$$

where $$T^2(r,k) = \exp(-2\int_0^r \sigma(r,k)dr)\,, \qquad (2.2)$$

*E(k)*= average laser pulse energy for a profile represented by the index 'k',

$G_A(k)$=amplifier gain for profile 'k'. (Amplifier gains are well estimated before launching and taken care in the processing of signal)

*C(k)*=lidar calibration coefficient, (non-ideal instrument effects that includes detector sensitivity and bore sight drift, has to be measured and calibrated during on-orbit processing)

*β(r,k)*=backscattering coefficient of the scattering volume at 'r',

$T^2(r,k)$=two way transmittance from the lidar to the volume of scatterers at 'r'.

CALIOP calibration algorithms provide level 1 lidar data product that contain geolocated attenuated backscatter profiles for the three receiver channels and the information on the product uncertainties *(Powell et al., 2009)*. They are range corrected, energy normalized, gain normalized and calibrated signals that can be written as follows

$$\beta'(z,k) = \frac{r^2 P(r,z)}{E(k) G_A(k) C(k)} = \beta(z,k) T^2(z,\theta,k) \qquad (2.3)$$

*β'* is called the volume attenuated back-scatter coefficient. Calibration algorithm determines the calibration coefficients for the three channels.

i) For 532 nm parallel channel, backscattered signal from 30 - 34 km along with the available a priory information on molecular backscattering coefficients (using standard atmospheric model), and a background aerosol model based on SAGE II aerosol extinction

data. The range corrected normalized back scatter signal at the calibration attitude $z_c$ is given by equation (2.4)

$$X(z_c) = C\beta(z_c)T^2(z_c) \tag{2.4}$$

where, C is the calibration coefficient, $\beta$ is back-scattering coefficient of aerosols and molecules/volume back-scattering coefficient, and $T^2$ is the two way transmittance at the calibration altitude given by

$$T^2(z_c) = \exp(-2\int_{z_c}^{z_{sat}} \sigma_m(z) + \sigma_a(z)dz) \tag{2.5}$$

Where $\sigma_m$ is the molecular extinction coefficient and $\sigma_a$ is the aerosol extinction coefficient. Calibration coefficient C is determined by

$$C = \frac{\beta(z_c)T^2(z_c)}{X(z_c)} \tag{2.6}$$

While $X$ is measured by CALIOP, $\beta$ and $T^2$ are obtained through external models and data sources. Due to high back-ground illumination during daytime, calibration is carried out using the night time samples.

ii) Calibration of 532 nm perpendicular channel cannot be carried out as it is done for parallel channel since the depolarized signal from molecular backscatter is very low (molecular depolarization ~ 0.3 %) *(Powell et al., 2009).* Therefore calibration coefficient of 532 nm parallel channel is used to calibrate the perpendicular channel through Polarization Gain Operation. In this, a pseudo depolarizer is introduced in the path of 532 nm signal before it is resolved into its polarization components. This will produce randomly polarized backscatter signal which results in equal signal levels to both parallel and perpendicular channels, enabling the estimation of relative gain of the channels. Ratio of backscatter signal at these two channels is called Polarization Gain Ratio (PGR) represented by $K_p$ and given by

$$K_p = \frac{C_\perp}{C_{ll}} \tag{2.7}$$

where $C_\perp$ and $C_{ll}$ are calibration coefficients at perpendicular and parallel channels respectively.

iii) Since the signal from stratospheric altitudes at 1064 nm channel is very low, calibration constants of 532 nm channels along with back-scatter from cirrus clouds are used to

calibrate this channel. The ratio of backscatter signal from cirrus clouds at 532 nm and 1064 nm channel will be close to unity due to the large size of cloud particles that is equally sensitive to both the channels. Thus calibration constant at 1064 nm is determined by comparing back scattered signal from 1064 nm to calibrated 532 nm signal from a cirrus cloud layer.

#### 2.2.1.3 Retrieval algorithms: Level 2 processing

Level 2 algorithm retrieve the back-scattering coefficient and extinction coefficient from the calibrated attenuated back-scatter data obtained using level1 algorithm *(Winker et al., 2009).* Figure 2.5 describes how different algorithms are worked together to obtain the final product of extinction coefficient.

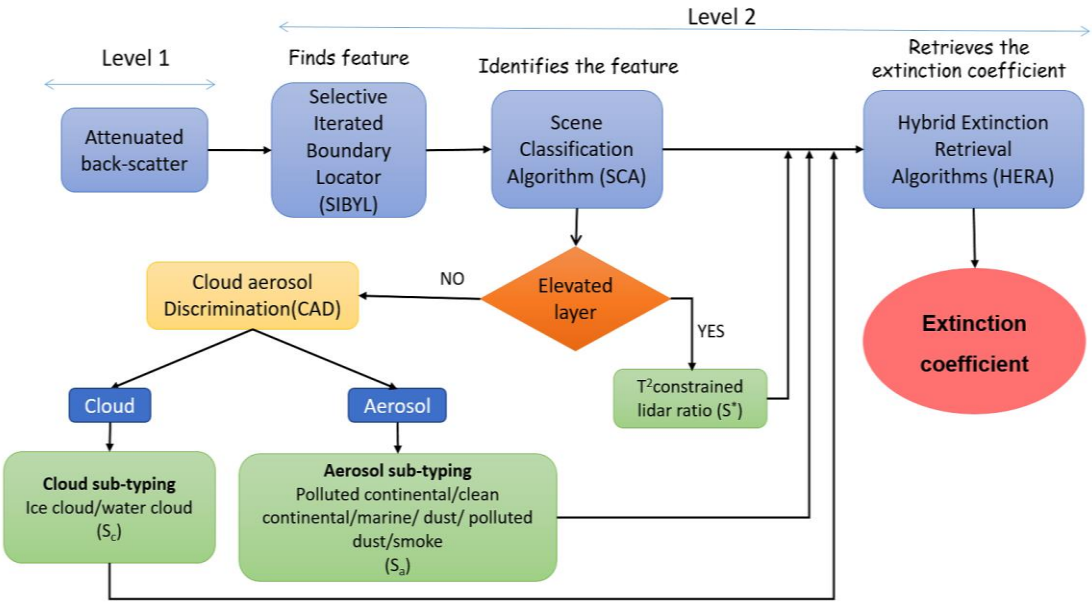


***Figure 2.5 -*** *Basic schematic of different algorithms used in level 2 processing.*

Level 2 analysis consists of different phases that include detection of atmospheric features by a selective, iterated boundary location algorithm (SIBYL) *(Vaughan et al., 2009),* identification of atmospheric features by Scene Classifying Algorithm (SCA) *(Liu et al., 2005)* and retrieval of backscatter and extinction coefficient of those features using a Hybrid Extinction Retrieval Algorithm (HERA) *(Young and Vaughan, 2009).*

##### 2.2.1.3.1 Selective, iterated boundary location algorithm (SIBYL)

SIBYL identify features by observing the enhancement in back-scattered signal from the molecular signal using a parameter called attenuated scattering ratio, which is the ratio of volume attenuated back scatter to molecular attenuated backscatter signal ( obtained

using Goddard Earth Observing System Model). SIBYL employs a threshold method to detect the features in which threshold value of attenuated scattering ratio is adapted according to altitude and profile characteristics. A "feature" describes any extended region of enhanced backscatter signal that rises significantly above the expected molecular (Rayleigh) value *(Vaughan et al., 2009).* With high velocity (7.5 km/s) of the satellite with low shot frequency (20 $s^{-1}$), it is not possible to acquire sufficient number of profiles over atmospheric inhomogeneity in features along the track. To improve SNR, signals has to be averaged without losing information on the inhomogeneity in the atmosphere. Thus SIBYL algorithm takes care to average signals from spatially homogeneous atmospheric features, where the optical properties are homogeneous and signal strength is similar. For aerosols, back-scattered signals are weaker hence more averaging is required to obtain a robust signal with good SNR (mostly > 1 km) while stronger cloud signals can be detected using minimum averaging, even with single shot profiles. SIBYL primarily analyse a segment of 80 km (which is termed as a 'scene' consisting of 240 shots) at a time and scan the profiles of attenuated scattering ratio to identify strong layers. It carry out initial averaging and removes detected layers before further averaging. This enables to carryout different magnitude of averaging (5, 20 and 80 km) to different atmospheric features. SIBYL plays in important role in CALIOP lidar analysis since retrieving extinction coefficient profiles with averaged profiles containing different optical properties (different features) can lead to erroneous results, unrepresentative of the real atmosphere.

#### 2.2.1.3.2 Scene Classifying Algorithms (SCA)

Level 1 processing provides normalized calibrated volume attenuated back scatter signal which is given by equation (2.3). Thus contain the attenuated backscatter due to particulates, and other molecules given by

$$\beta'(z) = \left[\beta_p(z) + \beta_m(z)\right] T_p^2(z) T_m^2(z) \tag{2.8}$$

where β and $T^2$ are the backscattering coefficient and two-way transmittance respectively and subscript 'm' and 'p' represents molecules and particulates respectively.

$$\beta'(z) = \left[\beta_p(z) + \beta_m(z)\right] \exp\left( -2\eta(z) \int_{z1}^{z2} (\sigma_m + \sigma_p) dz \right) \tag{2.9}$$

Here $\sigma$ is the extinction coefficient and $\eta(z)$ is the range dependent multiple scattering parameter characteristic to different cloud and aerosol classes. By the definition of extinction to back scatter ratio (S) or lidar ratio,

$$\sigma = S \times \beta \tag{2.10}$$

Thus, $$\beta'(z) = \left[\beta_p(z) + \beta_m(z)\right] \exp\left( -2\eta(z) \int_{z1}^{z2} (S_m \beta_m + S_p \beta_p) dz \right) \tag{2.11}$$

Molecular backscatter coefficient profile ($\beta_m$) and lidar ratio ($S_m$) is computed theoretically using temperature and pressure distribution from the Global Modelling and Assimilation Office. For the estimation of particulate back-scattering coefficient ($\beta_p$) lidar ratio $S_p$ has to be determined since equation (2.11) contains two unknowns $\beta_p$ and $S_p$.

A group of algorithms called SCA identify and classify the features detected by SIBYL and assign $S_p$ which is required to solve the lidar equation (2.11), and is fed to the retrieval engine (HERA). To estimate the lidar ratio, SCA computes lidar ratio of a detected feature through two methods.

i) For elevated features, SCA will estimate lidar ratio of the feature using transmittance constrained method *(Fernald et al., 1972)* by measuring layer transmittance of clear air above and below the feature, using the following equation that relates optical depth and integrated attenuated backscatter.

$$\gamma' = \int_{layerbase}^{layertop} \beta T^2(z) dz = \frac{2\pi}{\eta S}\left[1 - \exp(-2\eta\tau)\right] \tag{2.12}$$

where γ' is the integrated attenuated backscatter measured within the layer, $\beta$ is the backscattering coefficient, $\eta$ is the multiple scattering parameter, $\tau$ is the optical depth of the layer $S$ is the lidar ratio of the layer and $T^2$ is the measured transmittance within the layer given by

$$T^2 = \exp(-2\eta\tau) \tag{2.13}$$

Taking multiple scattering into account the effective lidar ratio S* is defined as S*=ηS.

Thus, $$S^* = \frac{1 - T^2}{\gamma'} \tag{2.14}$$

The effective two-way transmittance is estimated by fitting the attenuated backscatter both above and below a feature to a reference profile. On measuring $T^2$ and $\gamma'$ effective lidar ratio can be estimated.

ii) If the detected feature is non-elevated, lidar ratio is determined using the aerosol model corresponding to the identified feature type, whether it is a cloud or aerosol using Cloud Aerosol Discrimination (CAD) *(Liu et al., 2009)* . If the feature is non-elevated, SCA will

choose the aerosol/cloud model based on the backscattered intensity, depolarization, and geo-physical location of the measurement. If clouds are detected, SCA computes profile of volume depolarization ratio within the cloud layer and along with auxiliary temperature data, it discriminate the cloud phase (ice/ water clouds) *(Hu et al., 2009)*. If a layer is identified as aerosol, the type of aerosol is identified using depolarization ratio, back-scattered intensity and geophysical location of the measurement *(Liu et al., 2005).* Details of aerosol subtyping and lidar ratio selection are described in the following section (b). The SCA will classify the feature type for both elevated and non-elevated layers, and give a lidar ratio for the feature for extinction retrieval in HERA.

**a) Cloud Aerosol Discrimination algorithm (CAD)**

The cloud-aerosol discrimination (CAD) algorithm separates aerosols and clouds using measured optical parameters and a data base of multi-dimensional probability density functions (PDFs) for aerosols and clouds. Left panel of figure 2.6 shows the scatter plot of the colour ratio (ratio of back-scattering coefficient at 1064 nm to that at 532nm) and back-scattering coefficient at 532 nm to identify cloud and aerosol clusters. While both colour ratio and back-scattering coefficient are high for clouds, they are lower for aerosols except for maritime and desert dust aerosols which lies at different regime in the diagram (figure 2.6). This example shows the capacity of combination of two independent optical parameters in distinguishing cloud and aerosol clusters on a 2D space. But in the real atmosphere there are chances that these two clusters overlap (optically thinner clouds can overlap with aerosols), that makes it difficult to discriminate them. Thus more independent variables May be needed to separate the cloud and aerosol clusters making it better with higher dimensions, reducing the overlap between the probability function. CALIOP being a multi-wavelength, polarization sensitive lidar, provides various optical parameters which are attenuated backscatter ($\beta'$), colour ratio ($\chi'$) and volume depolarization ratio ($\delta'$). These three parameters along with the geo-location information (altitude ($z$) and latitude), a 5D probability function for the two classes, aerosol, and clouds are prepared based on previous measurements of Lidar In-space Technology (LITE) using equation 2.15.

$$P_{aerosol\ /\ cloud}(\beta', \chi', \delta', z, lat) = \frac{n_{aerosol\ /\ cloud}(\beta', \chi', \delta', z, lat)}{N_{aerosol\ /\ cloud}} \qquad (2.15)$$

$n_{aerosol/cloud}$ ($\beta'$, $\chi'$, $\delta'$, $z$, $lat$) is the number of occurrence of aerosol or cloud that satisfy all the 5 attributes and $N_{aerosol/cloud}$ is the total number of events for the two classes. Using the estimated probability a normalized confidence function is estimated using equation 2.16.

$$f_{5D} = \frac{P_{cloud}(\beta', \chi', \delta', z, lat) - P_{aerosol}(\beta', \chi', \delta', z, lat)}{P_{cloud}(\beta', \chi', \delta', z, lat) + P_{aerosol}(\beta', \chi', \delta', z, lat)}$$

(2.16)

For $f_{5D}$ >0 represents clouds and $f_{5D}$<0 represents aerosols with absolute magnitude of $|f_{5D}|$ gives confidence level. $f_{5D}$= 0, indicate no classification can be done. Percentile values of '*f*' is given as CAD score that ranges from -100 to +100. |CAD| = 70 -100 represents high confidence, |CAD| = 70 -100 represents medium confidence, and |CAD| = 70 -100 represents no confidence in the classification *(Liu et al., 2009).*

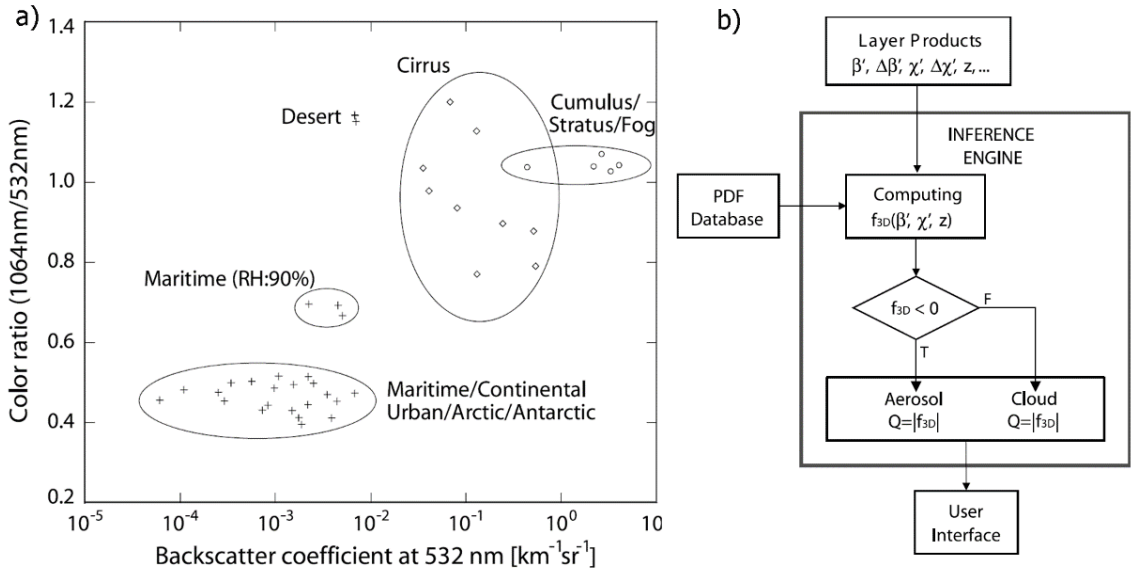


***Figure 2.6*** *- Left panel shows the colour ratio- back-scatter coefficient scatter diagram showing distinct cloud and aerosol clusters simulated using OPAC and right panel shows the schematic flow of CAD algorithm (Liu et al., 2004)*

**b) Aerosol subtyping: Lidar ratio selection algorithm**

Lidar ratio for aerosol, $S_a$, is determined by a Lidar ratio selection algorithm based on the optical (back-scattering coefficient, depolarization ratio, colour ratio), and geophysical characteristics of the aerosol feature. The algorithm identify the type of each aerosol layer (termed as aerosol typing/subtyping) and assign pre-modelled $S_a$ characteristic to the identified type. The value of $S_a$ is determined for each profiles. It depends on the aerosol size distribution and composition. The accuracy of retrieval of aerosol extinction coefficient critically depends on the correct identification of aerosol type. Cluster analysis at AERONET observation sites identify seven aerosol types representative of aerosol systems for level 2 version 4 CALIOP product, which are clean marine, dust, smoke (biomass burning), polluted continental, clean continental, polluted dust, dusty marine

and elevated smoke (Table 2.3). CALIOP aerosol model for these six types of aerosols were developed mainly using AERONET observations and independent observations of $S_a$ *(Young, 1995; Ackermann, 1998; Muller et al., 2000;Anderson et al., 2000; Franke et al., 2001).* AERONET model parameters are constrained to reproduce the independently measured $S_a$ values and lidar ratio corresponding to each aerosol subtype is determined. Look up table of lidar ratios for seven aerosol types are listed in table 2.3.

***Table 2.3*** *- Lidar ratio for six different aerosol types identified (Kim et al., 2018).*

| Aerosol subtype | Version 3 | Version 4 | Version 3 | Version 4 |
|---|---|---|---|---|
| | $S_a$ at 532 nm (sr) | | $S_a$ at 1064 nm (sr) | |
| **Clean marine** | 20 ± 6 | 23 ± 5 | 45 ± 23 | 23 ± 5 |
| **Dust** | 40 ± 20 | 44 ± 9 | 55 ± 17 | 44 ± 13 |
| **Polluted continental/smoke** | 70 ± 25 | 70 ± 25 | 30 ± 14 | 30 ± 14 |
| **Clean continental** | 35 ± 16 | 53 ± 24 | 30 ± 17 | 30 ± 17 |
| **Polluted dust** | 55 ± 22 | 55 ± 22 | 48 ± 24 | 48 ± 24 |
| **Elevated smoke** | 70 ± 28 | 70 ± 16 | 40 ± 24 | 30±18 |
| **Dusty marine** | N/A | 37 ± 15 | N/A | 37 ± 15 |

The algorithm make use of the surface type (International Geosphere-Biosphere Programme(IGBP)), integrated attenuated backscatter (γ'), particulate depolarization ratio (δ) and altitude of the feature, to identify the aerosol subtype. For several aerosol types, color ratio and attenuated backscatter overlap significantly due to which color ratio is not used for subtyping aerosols. Threshold values for γ' and δ are obtained from earlier measurements including LITE observations. Figure 2.7 shows the flow diagram for aerosol classification using CALIOP observations. Main pathways of the algorithm is listed below

1) Before examine other surface types, presence of dust/ polluted dust is checked using depolarization ratio threshold. δ> 0.2 are identified as pure dust (pathway 1) and δ in the range 0.075 to 0.2 are identified as polluted dust(pathways 2 and 3) or dusty marine (pathway 4) based on the surface type. Moderately depolarizing particles within 2.5 km from the ocean surface are characterized as 'dusty marine' system.

3) If the feature has low depolarization ratio (δ<0.075), surface type will be checked (land/ocean). Over land, elevated features with higher attenuated backscatter (γ'>0.0005)

will be classified as elevated smoke (pathway 11). If the feature is not elevated, it will be identified as polluted continental aerosols (pathway 7). If γ'<0.0005 and the surface is desert it will be identified as polluted dust (pathway 5) or if the surface is not desert, it will be classified as clean continental aerosols (pathway 6).

4) Over ocean, if elevated aerosols are present, with low depolarization (δ<0.075), they will be classified as elevated smoke (pathway 12) and non-elevated features with high attenuated backscatter (γ'>0.01) are identified as clean marine aerosols (pathway 10). Non-elevated layers over ocean with lower attenuated backscatter (γ'>0.01) and depolarization ratio (δ< 0.05) are identified as clean marine aerosols (pathway 9) and if γ'<0.01 and δ>0.05 they will be classified as polluted continental aerosols (pathway 8)

Over polar/tundra regions, aerosols are either clean continental or polluted continent (artic haze) which are separated using a threshold value of γ' that's is higher for polluted continental and lower for clean continental. CALIPSO lidar ratio selection algorithm has an uncertainty of 30% for the selected value of lidar ratio.

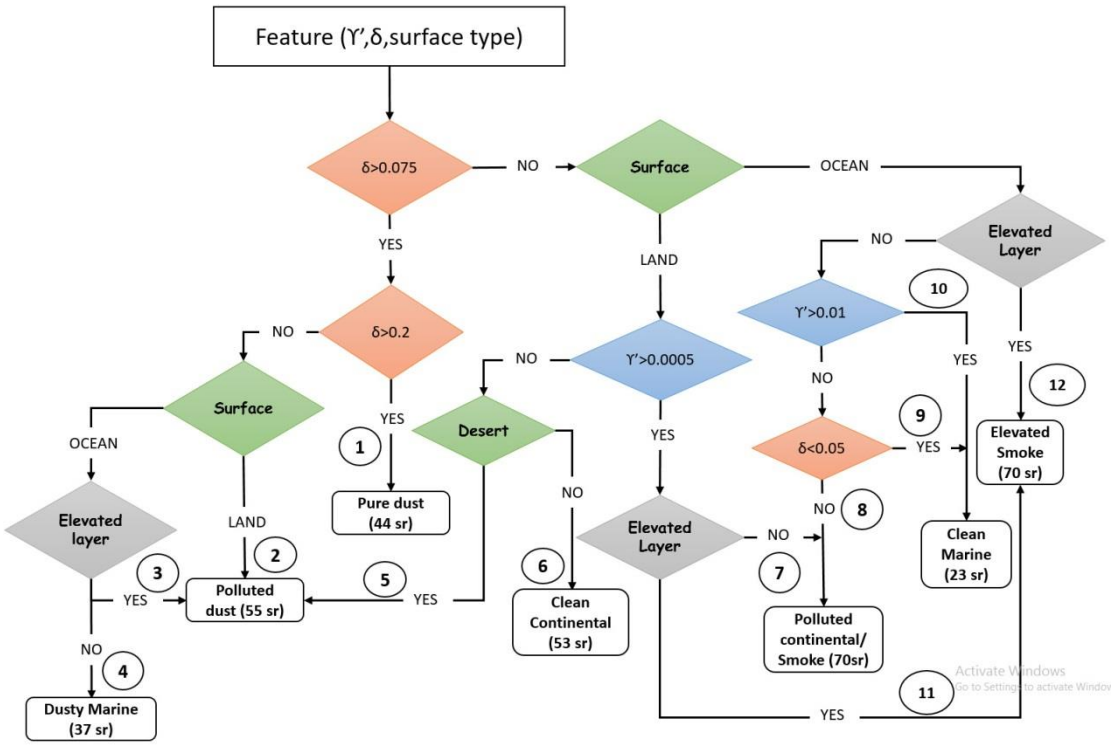


***Figure 2.7 -*** *Schematic of flow diagram of lidar ratio (Sa) selection algorithm for aerosols used in level 2 version 4 (Kim et al., 2018).*

#### 2.2.1.3.3 Hybrid Extinction Retrieval Algorithm (HERA)

Lidar equation for two component atmosphere (molecules and particulates), is generally solved using analytical solutions *(Fernald et al., 1972; Klett, 1985)* or iterative, numerical solutions *(Gambling and Bartusek, 1972; Kovalev, 1993)*. Stable solutions are obtained when the inversion is initialized in the far field (called backward solution), rather than beginning from the near field (forward solution) *(Klett, 1981)*. For ground based lidar, back-ward solutions are best suited since far field boundary (above 30 km or at tropopause) can be assumed as particulate free and close to molecular value. But for space borne lidar, far filed range is (near to the surface of earth) is aerosol loaded and rather inhomogeneous. So, to ensure accurate retrieval, quantitative information on exact boundary values is necessary. Thus CALIOP uses a forward fixed-point iterative method to retrieve the aerosol back-scattering coefficient *(Young and Vaughan, 2009)*.

Attenuated backscatter profiles are renormalized using the difference in attenuation at the top of the atmosphere (at the range $z_N$) and the first analysis point in the profile. Renormalized attenuated back-scatter is given by

$$\beta_N^{'}(z) = \left[\beta_M(z) + \beta_P(z)\right] T_M^2(z_N, z) T_P^2(z_N, z) \tag{2.17}$$

$$\beta_P(z) = \frac{\beta_N^{'}(z)}{\left(T_M^2(z_N, z) T_P^2(z_N, z)\right) - \beta_M(z)} \tag{2.18}$$

Particulate transmittance, $T_P^2(z_N, z)$ is a function of $\beta_P(z)$ given by

$$T_P^2(z_N, z) = \exp\left[-2\eta(z) S_P \int_{z_N}^{Z} \beta_P(z) dz\right] \tag{2.19}$$

Thus equation (2.18) is in the form $\beta_P = f(\beta_P)$ (2.20)

Equations of this form are solved using fixed point iteration method. Initially, particulate back-scatter at $z_N$ is assumed zero where the attenuated back-scatter is due to molecules only (or model value). Using equation (2.18), $\beta_P(z_N)$ is estimated for this condition and it is used to initialize iteration for the next range bin (z). At z, particulate transmittance is obtained using equation (2.19) that is subsequently used in equation (2.18) to estimate $\beta_P(z)$. Iteration begins by using estimated $\beta_P(z)$ in equation (2.19) to estimate $T_P^2(z_N,z)$ that is substitute back in equation (2.18) to estimate $\beta_P(z)$. Iterations are repeated until value of $\beta_P(z)$ from successive iterations become minimum or less than a threshold value. Once particulate back-scattering coefficient is obtained, extinction coefficient is calculated via

equation (2.10), using lidar ratio determined by measuring the clear air transmittance above and below the elevated feature or as selected by the lidar ratio selection algorithm (figure 2.7).

#### 2.2.1.4 CALIPSO –Level 3 LIDAR product

Level 3 CALIOP aerosol products are gridded, 2° along latitude and 5° along longitude. The criteria applied in developing level 3 aerosol products are following. For level 3 aerosol products, CAD scores of -100 to -20 are used. Extinction retrievals are filtered using QC flag values of 0, 1, 16, and 18 and range bins with aerosol extinction uncertainty less than 99.9 $km^{-1}$ are only used for level 3 products. Misclassifying cirrus clouds as aerosol due to weakly scattered signals from their edges is one of the limitations of Cloud Aerosol Discrimination algorithm. Hence aerosol layers near to the clouds are excluded from averaging. Occasionally SIBYL misses aerosol layers at the surface because of attenuation aloft. This causes underestimation in the mean aerosol extinction values near the surface. To rectify this, range bins identified as "clear air" lying under 250 meters that are of poor quality are excluded from level 3 statistics. Bias due to signal from the surface can give huge negative values for range bins near to the surface. To remove the influence of surface contamination in level 3 data, all level 2 aerosol extinction samples near to the surface with aerosol extinction coefficient less than -0.2 $km^{-1}$ are excluded and not used in the computation of level 3 computation.

#### 2.2.1.5 CALIOP - Uncertainties and correction

While total attenuated backscatter agrees better with the independent observations *(Rogers et al., 2011)*, the retrieved aerosol extinction coefficients have higher uncertainty due to the errors and approximations in the retrieval method. Validation of ground based/air borne lidar measurements with column observations, shows that CALIOP aerosol optical depth is biased towards lower values *(Mamouri et al., 2009; Pappalardo et al., 2010; Kittaka et al., 2011; Lopes et al., 2013; Omar et al., 2013)*. *Kacenelenbogen et al., (2011)* carried out a case study to validate CALIPSO aerosol extinction coefficient product using multi-satellite, multi-platform datasets and concluded that CALIOP AOD is lower by a factor of two compared to MODIS, POLDER, AERONET and ground based High spectral resolution lidar (HSRL) observations. Comparison of CALIOP AOD values with AERONET observations shows an underestimation in CALIOP AOD, especially at low optical depths (<0.1) with a median difference of 25%. This is attributed to several factors including cloud contamination, heterogeneity of features within the scene, instrument errors, retrieval

errors, and errors in detection *(Omar et al., 2013)*. The CALIOP detection algorithm will miss features with signal below the instrument sensitivity of $2\times 10^{-4}$ to $4 \times 10^{-4}$km$^{-1}$sr$^{-1}$ in the troposphere *(Winker et al., 2009)*. Several studies attribute the low bias to the inability of CALIOP to detect thin aerosol layers in the atmosphere *(Kim et al., 2013, 2017; Rogers et al., 2014).* It is observed that while CALIOP column AODs are underestimated, CALIOP layer AODs are agreeable with HSRL observations. This implies the presence of weakly backscattering aerosols in the free atmosphere that are not detected by CALIOP. Since CALIOP used pre-defined fixed aerosol types and lidar ratio, in case of prevalence of complex mixtures of aerosols selection of lidar ratio by CALIOP algorithm can result in misclassification and errors in the retrieved extinction coefficient *(Wandinger et al., 2010; Josset et al., 2011; Oo and Holz, 2011; Schuster et al., 2012). Schuster et al., (2012)* showed that for AOD of dust aerosols, are underestimated by CALIOP when compared to AERONET (Aerosol Robotic Network). It is suggested that the assumed lidar ratio for dust aerosols (40 sr) by CALIOP is too low to retrieve dust optical depth accurately. *Oo and Holz (2011)* found that the lidar ratios used for CALIOP retrieval over oceans are lower and demonstrated the advantage of integrated colour ratio in constraining lidar ratio in CALIOP retrievals. . Other inter-comparison studies carried out to validate the lidar ratios used in CALIOP algorithm, include, lidar observations from European Aerosol Research Lidar Network (EARLINET) and also using the Saharan Mineral Dust Experiment observations (SAMUM) *(Pappalardo et al., 2010; Tesche et al., 2013)*. EARINET observations showed that lidar ratio of dust aerosols transported over to the Europe during Saharan outbreaks is around 56 ± 7 sr at 532nm which is higher than the typical value of 40 sr used for dust aerosols in CALIOP retrievals *(Pappalardo et al., 2010).* Observations during SAMUM shows that aerosol back-scattering coefficient at 532 nm from CALIOP is in good agreement with ground based lidar observations, however aerosol extinction coefficient is underestimated by up to 30% *(Tesche et al., 2013)*. This is attributed to the use of inaccurate lidar ratio for dust aerosols in CALIOP retrievals. *Koffi et al., (2012)* have compared CALIOP AOD with MODIS AOD observations (Collection 5) and states that, a comparison of regional averages, rather than co-located samples, yield better agreement. Differences between CALIOP and MODIS AOD averaged over regional scale, were found to lie inside the uncertainty limits of MODIS.

Over the oceanic regions, lidar ratio of aerosols are dependent on the surface wind speed since it cause changes in aerosol size distribution by producing coarse mode particles *(Dawson et al., 2015).* While CALIOP AOD was significantly higher than MODIS observations over continental regions and significantly lower over marine regions *(Koffi*

*et al., 2012).* Oceanic regions of India are well characterized through several ship borne observations including ICARB *(Moorthy et al., 2008).* While satellite observations enable effective estimation of aerosol loading, retrieval of aerosol intrinsic parameters like SSA or phase function from space have relatively higher uncertainty, hence it has to be carried out through coordinated in-situ measurements. Present study make use of ICARB measurements to qualitatively examine the lidar ratio ($S_{ICARB}$) over the Bay of Bengal for pre-monsoon and winter seasons, using an aerosol composition model adopted from *Koepke et al., (2015)* (OPAC). The data set of optical properties of mineral components is generated using T-matrix calculations for spheroid particles of different aspect ratios to account for the non-sphericity of dust particles. The number concentration of the aerosol components are iterated in such a way that the modelled aerosol parameters matches well with the measured aerosol parameters *(Moorthy et al., 2009;Nair, Babu, Moorthy, & Prijith, 2013).* The parameters used to constrain the aerosol model are (i) climatological mean spectral AOD from MODIS during 2007 -2017, (ii) single scattering albedo measured at 550 nm during ICARB experiments in pre-monsoon 2006 and winter 2009, (iii) sea salt optical depth ($\tau_{seasalt}$) derived from the surface wind speed following *Kaufman et al., (2005)*, averaged over the period 2007 – 2017 and (iv) Mean dust optical depth ($\tau_{dust}$) derived from depolarization and backscatter coefficient of CALIPSO (Refer section 2.2.2) over the period 2007 - 2017. However it is to be noted that $S_{ICARB}$ can have uncertainties due to (i) errors in MODIS retrieved spectral AOD (ii) limited dataset on single scattering albedo over the study region and (iii) the uncertainty in the retrieved dust optical depth from CALIOP (Refer section 2.2.1.6).

A combination of lidar observations of aerosol back-scattering coefficient and columnar AOD using sunphotometer/radiometer can be used to estimate the lidar ratio of aerosols present in the column. Here, column AOD at 0.55 μm from Aqua-MODIS measurements and CALIOP derived aerosol back-scattering coefficient are used to estimate columnar lidar ratio over the Bay of Bengal. MODIS derived AOD at 550 nm is used to scale the profiles of aerosol extinction coefficient retrieved by CALIOP algorithm in such way that the extinction coefficients estimated using the scaled lidar ratio ($S_{MODIS}$) matches with MODIS AOD over Bay of Bengal. $S_{MODIS}$ is given by

$$S_{MODIS} = \frac{AOD_{MODIS}}{AOD_{CALIPSO}} \; S_{CALIPSO} \qquad (2.21)$$

Lidar ratio from CALIPSO data ($S_{CALIPSO}$) is estimated as the ratio of seasonally averaged integrated extinction to backscatter coefficient. The lidar ratios for total aerosols ($S_{CALIPSO}$,

$S_{MODIS}$, $S_{MODEL}$) estimated from various techniques are shown in figure 2.8. CALIOP systematically underestimate the AOD compared to model constrained and satellite (MODIS) derived AODs over the Bay of Bengal especially during winter, which is attributed to the uncertainties associated with the lidar ratios used in the CALIPSO retrieval algorithm. Compared to pre-monsoon, the $S_{MODIS}$ and $S_{MODEL}$ are significantly higher (2 fold) than the $S_{CALIPSO}$ (~30 sr) during winter. It should be noted that the outflow of anthropogenic aerosols from South Asia to the Bay of Bengal takes place during winter and these anthropogenic aerosols have higher lidar ratio as reported by several investigators through ship-borne and island measurements *(Cattrall et al., 2005; Giannakaki et al., 2016).* The lidar ratio estimated from the semi-empirical approach ($S_{MODEL}$) further support the values estimated using MODIS AOD measurements.

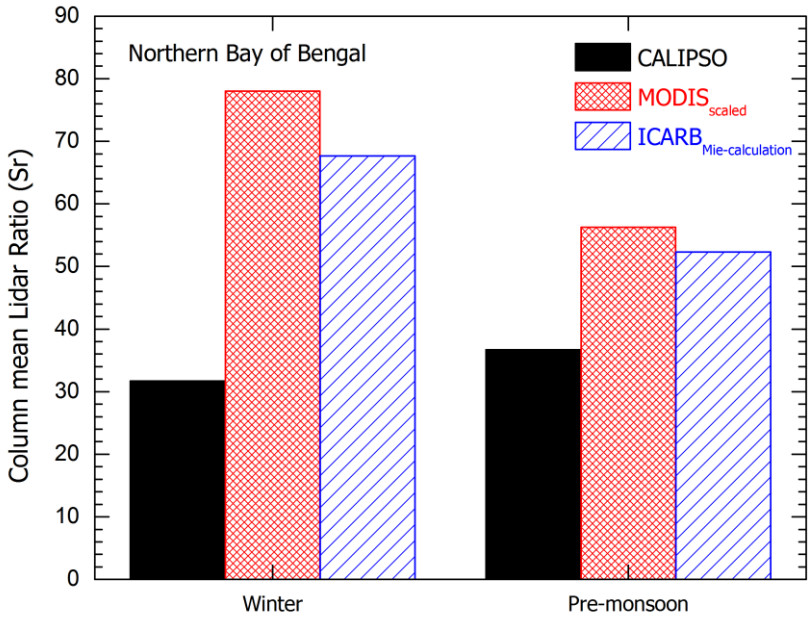


***Figure 2.8*** *- Column lidar ratio for mean CALIPSO measurements over northern Bay of Bengal (22°N – 13°N, 80°E – 100°E) during pre-monsoon and winter seasons. The lidar ratios shown are (i) scaled for MODIS AOD and (ii) retrieved using an aerosol model (adopted from Koepke et al., (2015)) constrained with measured aerosol properties.*

Over the Indian region, ARFINET carry out regular observations of spectral AOD at the stations equipped with MWR/sunphotometer. In the present study, the regional mean CALIOP lidar ratio over distinct regions of Indian land mass is compared with the lidar ratio derived using ground based ARFINET AOD observations using the scaling method . $S_{ARFINET}$ is estimated by constraining the CALIOP profile of aerosol extinction coefficient using ARFINET AOD. $S_{ARFINET}$ is given by

$$S_{ARFINET} = \frac{AOD_{ARFINET}}{AOD_{CALIPSO}} \; S_{CALIPSO} \qquad (2.22)$$

CALIOP lidar ratio is clearly underestimated over the Indian region in comparison with ARFINET derived lidar ratio. It is clear from figure 2.9 that the difference in lidar ratio is large during winter and small during pre-monsoon. Indian region is mostly under the influence of anthropogenic aerosols during winter which changes to naturally occurring transported dust during pre-monsoon *(Pillai and Moorthy, 2001; Babu and Moorthy, 2002).* This indicates that over south Asia, CALIOP algorithm misclassify the anthropogenic aerosols with aerosol species of lower lidar ratio.

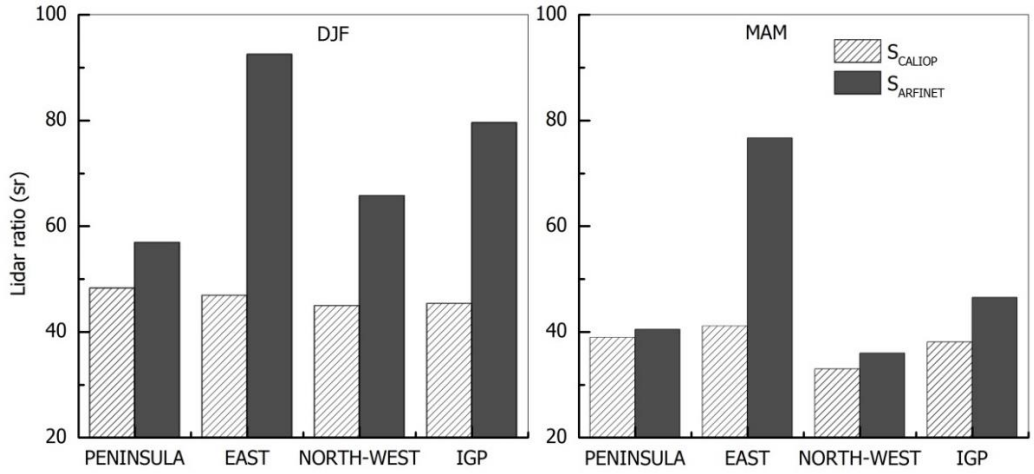


***Figure 2.9*** *- Column lidar ratio of CALIOP ($S_{CALIPSO}$) and that corrected with ARFINET AOD ($S_{ARFINET}$) over distinct regions of Indian land mass during pre-monsoon and winter seasons.*

### 2.2.1.6 Methodology of Dust estimation using depolarization ratio

Characterizing pure dust aerosols through in situ sampling is difficult due to heterogeneous mixing of aerosols in the atmosphere. Lidar based depolarization technique is a good tool to detect and quantify dust particle characteristics. While extinction coefficient gives aerosol abundance over a region, depolarization measurements provides the relative abundance of non-spherical particles. Dust being highly non-spherical, has distinct depolarization ratio that enables us to quantify them using depolarization measurements.

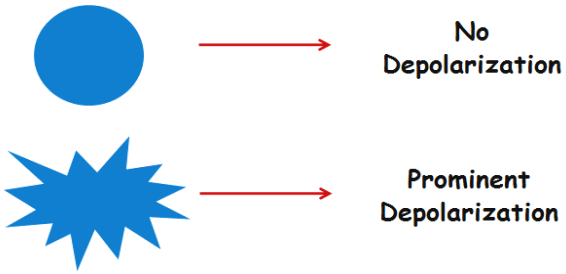


Particle linear depolarization gives an insight about the degree of non-sphericity of the particle and permits the discrimination of different types of aerosols and clouds. While profiles of extinction coefficient provide aerosol abundance at different elevations, PDR (Particulate Depolarization Ratio) indicates relative dominance of non-spherical particles in the aerosol system that can be made use for detecting and quantifying dust aerosols. CALIOP measures the volume depolarization ratio ($\delta_v$), i.e. the ratio of cross polarized attenuated back-scatter ($\beta_{\perp}^{'}$) to co-polarized attenuated back-scatter ($\beta_{ll}^{'}$) with respect to the transmitted signal given by

$$\delta_v = \frac{\beta_{\perp}^{'}}{\beta_{ll}^{'}} \tag{2.23}$$

Depolarization due to particulates (PDR ($\delta$)) is obtained by correcting for the contribution of molecules and is given by

$$\delta = \frac{\delta_v\left[(R-1)(1+\delta_m)\right]-\delta_m}{(R-1)(1+\delta_m)+\delta_m-\delta_v} \tag{2.24}$$

Where R is the attenuated scattering ratio (the ratio of the total attenuated backscatter to the molecular backscatter) and $\delta_m$ is the molecular depolarization ratio (~0.0036 at 532 nm). Thus PDR depends on scattering ratio, R. For high aerosol loading, i.e., for large R, $\delta \sim \delta_v$.

Being highly non-regular in shape, dust causes significant depolarization of 20% to 35% whereas aerosols of anthropogenic sources is comparatively less depolarizing in nature (2% - 5%) *(Freudenthaler et al., 2009; Mamouri et al., 2013; Veselovskii et al., 2016).* Several studies have been carried out using the lidar depolarization ratio technique to differentiate dust extinction from the total extinction *(Shimizu et al., 2004; Sugimoto and Lee, 2006; Tesche et al., 2009).*The Saharan Mineral Dust Experiment (SAMUM) is one of the major campaigns exclusively conducted for studying dust which extensively made use of HSRL and Raman lidar depolarization profiles to examine the spatial distribution and optical properties of desert dust *(Otto et al., 2009; Weinzierl et al., 2009; Ansmann et al.,*

*2009, 2011; Laurent et al., 2010; Müller et al., 2012). Freudenthaler et al., (2009)* has reported a mean linear particle depolarization ratio of 0.31 for pure Saharan dust layers at 532 nm with a mean Angstrom exponent of 0.18 during Saharan Mineral Dust Experiment (SAMUM) and showed a negative correlation of PDR with the Angstrom exponent. Reported values of fine particles depolarization ratio varies from 0.015 to 0.15. Dependence of depolarization ratio on particle size is rather weak while it is strongly sensitive to particle non-sphericity (shape of the particle). However, laboratory experiments shows that when fraction of fine mode dust is varied, PDR values changed from 0.16 to ~ 0.9 *(Sakai et al., 2010)*. Aerosol system over the south Asia is an external mixture of dust and non-dust aerosols in different proportion, due to seasonally varying distinct outflows of continental and marine origin. Considering the heterogeneity of aerosol system (dust and non-dust aerosols) due to mixing, assumption of a single aerosol type and lidar ratio (as used in CALIPSO algorithm) will lead to significant error in the retrieved dust extinction coefficient. PDR measurements of CALIOP enable the separation of dust backscattering coefficient from total backscattering coefficient and quantification of dust extinction coefficient *(Sugimoto and Lee, 2006)*. Here simple two-component model is used to separate dust from a mixture of dust and nondust particles. PDR from a scattering volume containing dust and non-dust aerosols is given by sum of cross-polarized backscatter coefficient from dust ($\beta_d^{\perp}$) and nondust $\beta_{nd}^{\perp}$ to co-polarized backscatter coefficients from dust ($\beta_d^{ll}$) and nondust aerosols ($\beta_{nd}^{ll}$) as shown below.

$$\delta = \frac{\beta_d^{\perp} + \beta_{nd}^{\perp}}{\beta_d^{ll} + \beta_{nd}^{ll}} \tag{2.25}$$

As per definition,

$$\delta = \frac{\beta^{\perp}}{\beta^{ll}} \tag{2.26}$$

For both dust and nondust aerosols,

$$\beta^{\perp} = \beta - \beta^{ll} = \frac{\beta\,\delta}{1+\delta} \tag{2.27}$$

$$\beta^{ll} = \beta - \beta^{\perp} = \frac{\beta}{1+\delta} \tag{2.28}$$

where $\beta$ is the total back-scattering coefficient. Substituting equation (2.26) and (2.27) in (24), $\delta$ can be written as a function of dust backscatter coefficient ($\beta_d$), non-dust back-scatter coefficient ($\beta_{nd}$), depolarization ratio of dust ($\delta_d$) and that of nondust aerosols ($\delta_{nd}$) eliminating parallel and perpendicular components of $\beta_d$ and $\beta_{nd}$.

$$\delta = \frac{\beta_d \delta_d (1+\delta_{nd}) + \beta_{nd} \delta_{nd} (1+\delta_d)}{\beta_{nd}(1+\delta_d) + \beta_d (1+\delta_{nd})} \quad (2.29)$$

Substituting $\beta_{nd} = \beta - \beta_d$ ,

$$\frac{\beta_d}{\beta} = \frac{(\delta - \delta_{nd})(1+\delta_d)}{(1+\delta)(\delta_d - \delta_{nd})} = f_d \quad (2.30)$$

$f_d$ is termed as the dust mixing ratio defined as the back-scatter contribution of dust aerosols in the scattering volume and value of $f_d$ is bounded by $0<f_d<1$. i.e., $f_d = 0$ if $f_d<0$ and $f_d = 1$ if $f_d>1$. The product of $f_d$ and total back-scattering coefficient ($\beta$) gives the dust back-scattering coefficient ($\beta_d$)

$$\beta_d = f_d \times \beta \quad (2.31)$$

The dust extinction coefficient ($\sigma_d$) is obtained as the product of $\beta_d$ and dust lidar ratio ($S_d$), as given below

$$\sigma_d = S_d \times \beta_d \quad (2.32)$$

Since dust extinction coefficient is retrieved from PDR measurements, total backscattering coefficient, and other a priori information ($\delta_d$, $\delta_{nd}$, *and* $S_d$), uncertainty involved in the assumption of a single lidar ratio for a dust-nondust external mixture, is minimized. Radiative effects of dust aerosols have been studied using spheroid models since it cannot be obtained directly by measurements other than lidar based depolarization technique. One of the main advantages of this method is non-requirement of a particle shape model that demands substantial computational requirements.

#### 2.2.1.6.1 Sources of uncertainty

In the present study, a dust lidar ratio ($S_d$) of 44.1 ± 8.8 sr is used for estimating dust extinction coefficient (using equation (31)) as reported by *Liu et al., (2015)* over the dust dominant Atlantic ocean, which is under the influence of Saharan dust transport, by constraining the lidar ratio using AOD above opaque water clouds. This value is close to the lidar ratio of 43.8 sr (67 retrievals) retrieved over Indian region (Kanpur, a region on the dust belt) using AERONET measurements *(Schuster et al., 2012)*. Studies involving direct measurements of dust lidar ratio carried out over Asian region using multi-wavelength Raman lidar indicate dust lidar ratio in similar range of 40 – 47 sr *(Sakai et al., 2002; Murayama et al., 2004).* Using instrumented aircraft observations, *Anderson et al., (2003)* estimated similar value of 45±10 sr for coarse mode dominated outflow over Asian region. *Mamouri et al., (2013)* reported a dust lidar ratio in the range 34 sr to 39 sr during

an Arabian dust outbreak using a new polarization lidar-sunphotometer method. Several experiments with polarization sensitive lidar and High Spectral Resolution lidar (HSRL) and Raman lidar provides the information on the depolarization/lidar ratio of dust aerosols. More documentation on the selected value of dust lidar ratio is available in *Tesche et al., 2007, Wandinger et al., 2010 and Amiridis et al., 2013.* $\delta_d$ and $\delta_{nd}$ can possibly vary around the assumed values due to transport process and dependence on the dust size distribution *(Mamouri and Ansmann, 2014)* that critically depends on the emission and transport mechanism. Figure 2.10 represents variation of dust back-scatter fraction with PDR and for different values assumed for $\delta_d$.

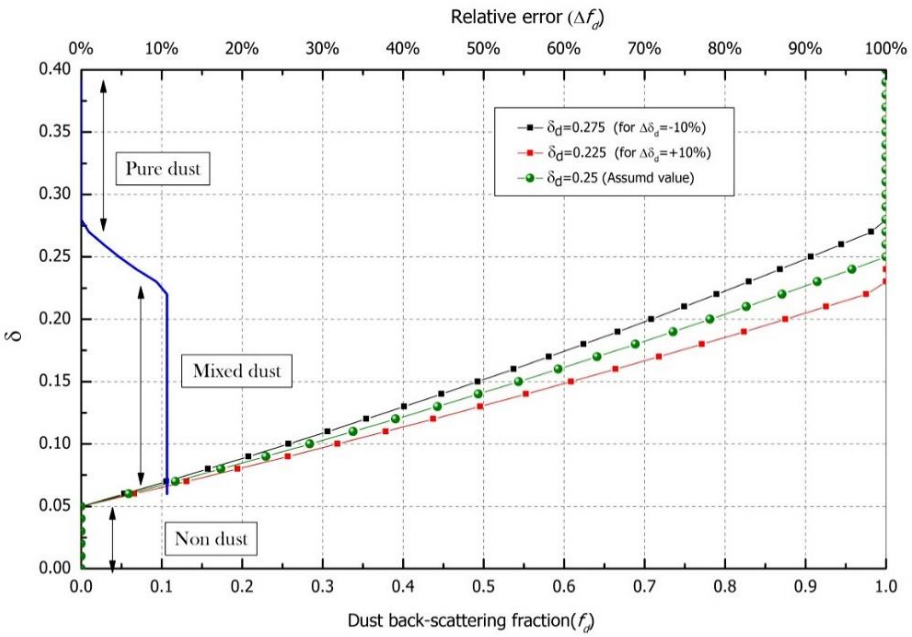


***Figure 2.10*** *- Dependence of dust backscatter fraction to PDR for different assumed values of $\delta_d$ that shows highest and lowest bound of dust backscatter fraction with respect to ±10% in PDR.*

$\delta_d$ represents threshold PDR beyond which dust backscatter fraction becomes one representing scattering volume of pure dust ($\beta=\beta_d$). Dust backscatter fraction is more sensitive to $\delta_d$ rather than $\delta_{nd}$ since it determines the amount of dust mixing in the scattering volume. For 10 % error in $\delta_d$, ($\Delta\delta_d=\pm0.025$), variation of upper and lower bound of values of dust back-scatter fraction with respect to PDR is also shown in figure 2.10. Uncertainty in dust backscatter fraction $f_d$ due to $\Delta\delta_d$ is a function of PDR and it is zero for pure dust while maximum for the mixed dust. For a change of ±10% in $\delta_d$, change in $f_d$ is ±10.6%. To minimize the uncertainty due to the assumption of $\Delta\delta_d$ direct measurements of dust depolarization over the study region is necessary. Table 2.4 lists the measured values of δ for dust and non-dust aerosols over the globe (Table 2.4). Unfortunately

sufficient information on depolarization of dust over Indian region is not available. Following *(Yu, Chin, Bian, et al., 2015)*, it is assumed that $\delta_d$ typically varies from 0.2 - 0.3 and $\delta_{nd}$ from 0.02 - 0.07 to accommodate the all possible variations in the derived dust extinction coefficient due to the possible range of values $\delta_d$ and $\delta_{nd}$ can have. The average of these upper and lower values, $\delta_d$ =0.25 and $\delta_{nd}$=0.045, are used in equation (29) to estimate the dust backscatter fraction ($f_d$) and subsequent dust backscattering coefficient (equation (30)) throughout the study.

***Table 2.4*** *- Reported values of depolarization value and lidar ratio of dust /nondust aerosols.*

| Location | λ (nm) | δ | S (sr) | Feature description | Reference | Technique used |
|---|---|---|---|---|---|---|
| **Tokyo (ACE[a])** | 532 | > 0.3 | 50± 9 | Elevated dust | Murayama, et al (2003) | Raman lidar |
| **Japan** | 532 | 0.2 ± 0.07 | | Dust | Sakai, (2003) | Raman lidar + Aircraft insitu |
| **Beijing** | 532 | 0.15-0.2 | | | Shimizu et al., (2004) | Polarization lidar |
| **Africa/Middle east** | 550 | | 42 ± 4 | Dust | Cattrall et al., (2005) | Sky radiance (AERONET) |
| **Sahara Desert** | 550 | | 59 ± 11 | Dust | Müller et al., (2007) | Raman lidar |
| **Gobi Desert** | | | 35 ± 5 | | | |
| **Arabian desert** | | | 38 ± 5 | | | |
| **Beijing** | 532 | 0.19±0.05 | 38±10 | Dust | Xie et al., (2008) | Raman lidar |
| **Cape Verde** | 532 | 0.31±0.03 | 55±7 | Dust | Tesche et al., (2009) | Raman lidar + HSRL |
| **Morocco (SAMUM)** | 532 | 0.31 ± 0.02 | 55±10 | Dust | Freudenthaler et al., (2009) | Raman lidar + HSRL |
| **Korea** | 532 | 0.27 | | Dust | Shin et al., (2013) | Raman lidar |
| | | 0.16 | | Mixed dust | | |
| **Cyprus** | 532 | 0.28-0.35 | 34-39 | Dust | Mamouri et al., (2013) | Raman lidar + HSRL |
| | | | 38 ± 11 | dust | Rogers et al., (2014) | HSRL |
| | | | 37 ± 11 | Polluted dust | | |
| | | | 27 ± 14 | marine | | |
| | | | 53 ± 11 | Clean continental | | |
| | | | 51 ± 15 | Polluted continental | | |
| **Global** | | | 44 ± 9 | Dust | Liu et al., (2015) | CALIOP |
| **Leipzig** | 532 | 0.02–0.03 | | Smoke (aged) | Müller et al., (2005) | |
| **Sahel (AMMA)[b]** | 355 | 0.03-0.1 | | Smoke | Heese and Wiegner, (2008) | Raman Lidar |
| **Beijing** | 532 | 0.07±0.01 | 44±8 | Heavy pollution | Xie et al., (2008) | Raman lidar |
| | | 0.05± 0.05 | 61±14 | Moderate pollution | | |
| **Cape Verde** | | 0.05 ± 0.01 | 77 | Smoke | Tesche et al., (2009) | Raman lidar + HSRL |

[a] Aerosol Characterization experiment ; [b]African Monsoon Multidisciplinary Analyses.

#### 2.2.1.7 Error estimation

The analysis accounts for the systematic/statistical errors associated with the data products based on the error propagation formula (equation 2.32). CALIOP provides uncertainty estimates for the observed parameters based on SNR, calibration constants and retrieval errors. Profiles of each single pass over the region are averaged to obtain the daily mean profiles. Climatological mean profiles are estimated by averaging the daily mean profiles over different seasons during the period 2007 – 2016. Climatological mean profiles of $f_d$ and $\beta$ is used to obtain profiles of dust back-scattering coefficient $\beta_d$ using equation (30). Thereafter using equation (31) dust extinction coefficient is determined. Along with CALIPSO uncertainty estimates for back-scatter coefficient and assumed errors in $S_{d,}$ $\delta_d$ and $\delta_{nd}$ as $\Delta S_d$=±8.8, $\Delta\delta_d$=±0.05 and $\Delta\delta_{nd}$=±0.025, error in the retrieved dust products are estimated by standard error propagation procedure using the function

$$\Delta q = \sqrt{\left(\frac{\partial f}{\partial x}\Delta x\right)^2 + \left(\frac{\partial f}{\partial y}\Delta y\right)^2 + \left(\frac{\partial f}{\partial z}\Delta z\right)^2} \quad \text{where} \quad q = f(x, y, z) \qquad (2.32)$$

where $\Delta q$ is the relative error and $q$ times $\Delta q$ provides the absolute error.

### 2.2.2 MODIS

Passive satellite sensors have immensely aided in columnar characterization of aerosols over the globe by providing measurements over larger scale on daily basis. The Moderate Resolution Imaging Spectroradiometer (MODIS) on board Aqua (A-train satellite) and Terra provides daily coverage of global land/atmospheric products. It has 36 spectral bands ranging from 0.405 μm to 14.385 μm and acquires data at three different resolutions of 250, 500 and 1000 m. MODIS atmospheric products are provided by MODIS Adaptive Processing System (MODAPS) at different levels. Level 0 denotes observed raw radiance, Level 1 B provides geolocated calibrated radiances, and Level 2 provides orbital track science products and level3 products are the gridded science product at 1° x 1° resolution. Terra passes over the equator at 10:30 hrs local time while descending and 22:30 hrs at night during ascending while Aqua passes over equator at 13:30 hrs at ascending and 1:30 hrs at night while descending mode. Being part of same constellation AQUA and CALIPSO make measurements around ~104s apart. Hence present study make use of Aqua-MODIS observations in conjunction with CALIPSO observations which provides nearly collocated measurements over the globe. MODIS provides column AOD in seven wavelength channels (0.47, 0.55, 0.66, 0.86, 1.24, 1.64 and 2.12 μm) retrieved from cloud free pixels *(Remer et*

*al., 2005).* The MODIS cloud masking algorithm identifies the domain of measurement (land, water, snow/ice, desert, and coast) using information on surface type and solar illumination. The radiances in both shortwave and longwave channels are used to identify the state of the pixel and generate a cloud mask product (MYD35) *(Ackerman et al., 1998)* which is used to eliminate the cloudy pixels before the process of retrieval of aerosols. Details on the retrieval process are given by *Ackermann et al., (1998)* and *Remer et al., (2005)*. Extensive comparison of MODIS level-3 aerosol optical depth (AOD) data (at 0.55 μm) with 171 days of ship-borne sunphotometer measurements over oceanic regions surrounding the Indian peninsula during 2003–2010 showed good agreement with a correlation coefficient of 0.91 and slope of 0.95 *(Nair, Babu, Moorthy, and Prijith, 2013).* Present study, make use of level 3 MODIS collection 6 (MYD08_M3) QA weighted data product over the ocean to obtain aerosol optical depth over the study region *(Levy et al., 2013)*. One of the major challenge with MODIS observations is to separate the contribution of surface reflection in the received radiation from the atmospheric signal. Over land MODIS products have higher uncertainty of ±0.5+0.15τ (τ represents AOD) while over ocean range of uncertainty is lesser ±0.3+0.05τ for MODIS observations. To rectify this, MODIS retrievals adapted the following algorithms i) Dark target algorithms retrieve selectively over dark pixels using correlative analysis between blue (0.47μm), red (0.66 μm) channel where the surface reflectance is minimum and MID-IR channel (2.13 and 3.8 mm) to which aerosols are not sensitive *(Kaufman et al., 1997)* and, ii) Deep blue algorithm corrects radiance received in based on radiance correction on bright channels with respect to radiance measured over the darker, deep Blue band near 0.41 μm *(Hsu et al., 2013)*

## 2.3 Network Observations

### 2.3.1 ARFINET

AOD data from the network stations of Aerosol Radiative Forcing over India (ARFI) project under ISRO Geosphere - Biosphere Program (IGBP), is used in the present thesis for retrieving the aerosol profiles over Indian continent. Figure 2.11 shows the locations of the ARFINET stations over the Indian region. ARFI aims for precise regional aerosol characterization, addressing the heterogeneities in space, time, and spectral domains for periodic estimate of Aerosol Radiative Forcing over India and to estimate aerosol impacts on regional and global climate. ARFINET continuously monitor the aerosol loading over India using in-house developed multi-wavelength radiometers (MWR) and sunphotometers for the measurement of Aerosol Optical Depth (AOD) and Aethelometer for the measurement of black carbon over the entire Indian land mass.

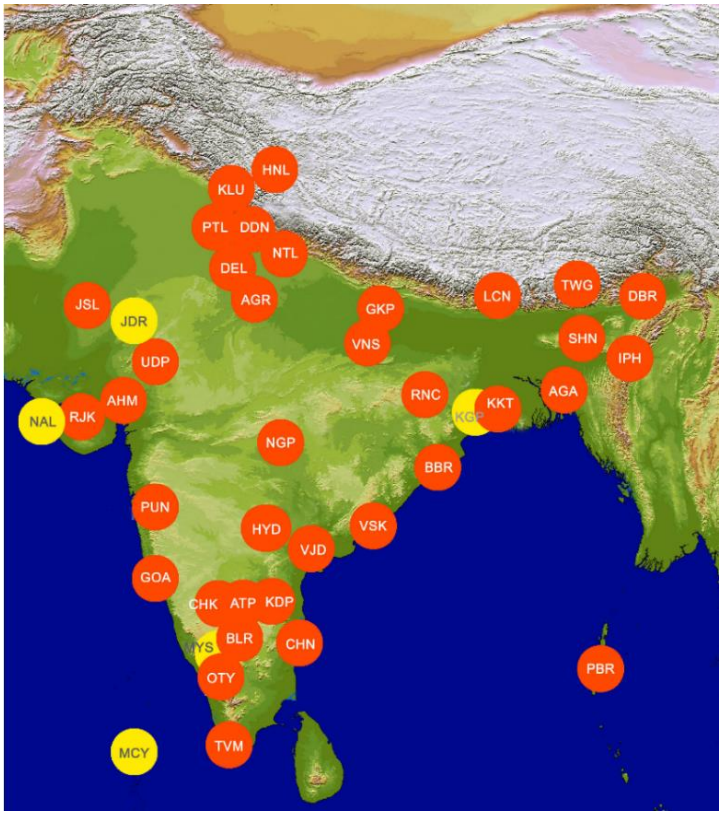


***Figure 2.11*** *- Locations of ARFINET stations over the Indian region as indicated by the circles Red circles indicate operational stations and yellow circles indicate the non-operational stations. Short name of the stations are shown inside them.*

MWR measures aerosol optical depth at ten narrow bands in the spectral range 380 to 1025 nm based on Beer-Lamberts-Bouguer law. The centre wavelengths are 380, 400, 450, 500, 600, 650, 750, 850, 935, and 1025 nm with a narrow band width of 5 nm. The optical filters are mounted on a rotating wheel that is programmed to measure direct sunlight with a field of view of ~ 2° at different solar zenith angles throughout the day. Langley plot method is used estimate AOD from the measurements of direct solar radiation. Observations are mostly carried out during cloud free conditions and collected data will be initially processed for cloud screening before using for the analysis. The uncertainty in the MWR AOD measurements is around ±0.02 at 500 nm *(Satheesh and Moorthy, 1997)*. Some of the stations under ARFINET are equipped with handheld sunphotometer (MICROTOPS manufactured by Solar light company Inc., USA) that measures AOD through instantaneous measurements at five different wavelengths at 340, 440, 500, 675, 870 nm with a bandwidth of ±1.5nm. AOD is estimated based on the pre-determined calibration coefficients. Measurements are carried out under clear sky conditions to avoid cloud

contamination and the in-built GPS receiver provide the position and altitude of measurements. The measurement is carried out by focusing the solar disc on to the sun-centering view window.

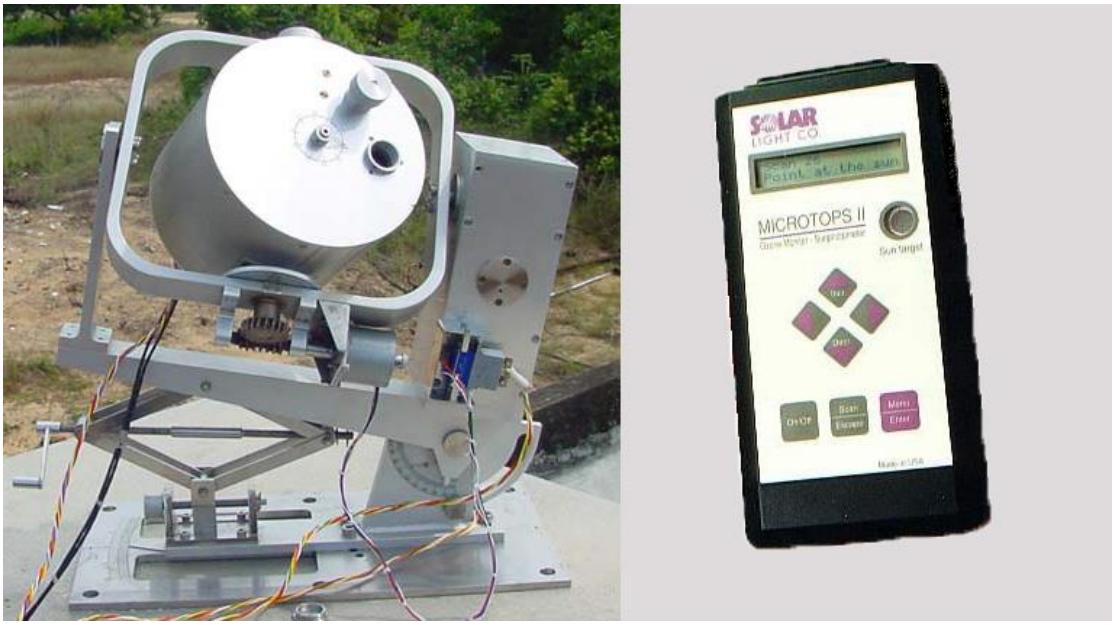


***Figure 2.12-*** *Photograph of MWR (left panel) and sunphotometer (right panel).*

### 2.3.2 AERONET

The Aerosol Robotic Network (AERONET) is a ground based aerosol observatory network under NASA *(Holben et al., 1998)*. Automatic Sun-sky scanning spectral radiometers are used for aerosol characterization at the network station widely distributed more than 1000 measurement sites worldwide. Through sun scanning method, AOD observations are carried out and in addition aerosol single scattering albedo, phase function, particle size distribution and real part of refractive index are retrieved using measurement of angular distribution of sky radiance. Direct solar radiation is measured in eight spectral bands in the range 340 nm to 1020 nm and sky radiance is measured at 440 nm, 670 nm, 870 nm, and 1020 nm.

## 2.4 Auxiliary datasets

In the present study, several data sets commonly used to understand the regional features of background meteorological conditions are used as auxiliary data. The Microwave Sounding Unit (MSU) have been providing the three dimensional distribution of climate variables since 1979 followed by its successor the Advanced MSU (AMSU) from 1998 on-board NOAA polar orbiting satellite series. The temperature of lower troposphere (TLT) is obtained from the combined observations of channel 5 of Advanced Microwave

Sounding Unit (AMSU) and channel 2 of MSU. The vertical extent of this data product is from surface to 8 km but the weighting function of the combined channels peaks below 5 km altitude and can be used with confidence for studying the atmosphere in the lower troposphere *(Mears and Wentz, 2009)*. Rainfall data is obtained from Tropical Rainfall Measuring Mission (TRMM) and IMD. For last 4-5 decades, Indian Meteorological department (IMD) have monitored rainfall series over India by observations from about 300 to 3,000 rain gauges stations spread all over India for the different time duration starting from the year 1841 onwards *(Parthasarathy et al., 1995)*. Surface temperature observations are obtained from Hadley Centre and the Climatic Research Unit (HadCRUT). HadCRUT provides global dataset of monthly average temperatures (gridded datasets) compiling the in situ measurements of surface temperature from weather stations under World Meteorological Organization (WMO) and Global Climate Observation System (GCOS) *(Brohan et al., 2006; Morice et al., 2012)*. Reanalysis datasets uses a synergy of atmospheric data analysis and model forecasting simulations to produce spatio-temporal distribution of various global atmospheric parameters. The Modern-Era Retrospective Analysis for Research and Applications (MERRA) re-analysis provides different climate variable (MERRA300) assimilated standard product to supplement observational datasets at different spatial resolutions *(Rienecker et al., 2008; 2011).* Details of these datasets are listed in table 2.5.

***Table 2.5*** *- Auxiliary datasets used in the study*

| Dataset | Parameter | Reference |
|---|---|---|
| **MSU-AMSU** | Tropospheric Temperature | Mears and Wentz, 2009 |
| **TRMM** | Rainfall rate | Kummerow et al., 1998 |
| **IMD-Rainfall** | Rainfall | Parthasarathy et al., 1995 |
| **HadCRUT** | Surface temperature | Brohan et al., 2006 |
| **MERRA** | Wind fields , Rainfall, Soil moisture | Rienecker et al., 2008; 2011 |

## 2.5 Models

### 2.5.1 SBDART

SBDART (Santa Barbara DISORT Atmospheric Radiative Transfer) is a radiative transfer model that computes radiative fluxes in plane parallel atmosphere and at the surface of the Earth *(Ricchiazzi et al, 1998).* It is developed by the University of California, Santa Barbara, to address different radiative transfer problems associated with satellite remote sensing of atmospheric species and radiation budget calculations over land and ocean over

the wide spectrum of solar radiation. It is based on validated atmospheric models developed over the past couple of decades. It adopts six standard atmospheric models which are tropical, mid-latitude summer, mid-latitude winter, subarctic summer, subarctic winter, and US62. The standard atmosphere model used in the present study is tropical. Basically, five ground reflectance models are incorporated in SBDART which are ocean water, lake water, vegetation, snow, and sand. It is assumed that the angular pattern of reflection from the surface are independent of solar zenith angle and is uniform in all directions (Lambertian reflection). SBDART is capable of computing radiative transfer for both clear sky and cloudy atmospheres. It uses three aerosol models in the lower atmosphere which are typical rural, urban, or maritime conditions, and five for the upper atmosphere. SBDART also allows user defined aerosol properties in addition to the standard aerosol models. It uses DISTORT (Discrete Ordinate Radiative Transfer) method for numerical analysis of plane-parallel radiative transfer in the atmosphere that employs a flat earth reference system. Flat-earth assumption is not valid over large zenith angle, hence compensating corrections are applied using spherical geometry. Radiation flux at different atmospheric layers (up to 50) and in different directions (20 streams) are estimated. It does not contain polarization effects and corrections for refraction, but these effects are small for solar zenith angles less than about 85°.

### 2.5.2 GOCART

Goddard Chemistry Aerosol Radiation and Transport (GOCART) model is a chemical transport model used for studying the time evolution of three-dimensional distributions of atmospheric constituents *(Chin et al., 2009)*. It simulates major aerosols types including sulphate, organic carbon, black carbon, dust and sea salt. The model uses assimilated meteorological data from Goddard Earth Observing System (GEOS-DAS) at a horizontal resolution of grid size 2° × 2.5° at every 6 h time interval. It has different modules for different physical processes in simulating aerosols. These includes surface emission, chemistry, advection, boundary layer turbulent mixing, moist convection, dry deposition, and wet deposition. Model simulates dust sources and distribution, accounts for emission, chemistry, transport, convection, diffusion dry deposition, and wet deposition mechanisms of dust particles, in seven size bins ranging from 0.1 to 6 μm *(Ginoux et al., 2001)*. Validation with network based AOD measurements and satellite observations shows that though the model fairly captures the seasonal variation, absolute magnitude of AOD significantly deviates from the observations *(Chin et al., 2002, 2009; Moorthy, Beegum, et al., 2013).*

# Chapter 3

# Three dimensional distribution of aerosols over the Indian landmass

## 3.1 Introduction

Elevated aerosols over the Indian region are important due to their absorbing nature and the associated atmospheric warming which can affect the thermal structure and stability of atmosphere by absorbing solar radiation *(Babu, Moorthy, et al., 2011)*. The aerosol induced warming depends on the abundance, absorption potential, vertical distribution, presence of clouds *(Chand et al., 2009)*, and on the surface reflectance of the underlying surface *(Haywood and Boucher, 2000)*. Over the Indian region, aerosols are increasing at a steady rate *(Babu et al., 2013)*. Sign of aerosol radiative forcing at the top of the atmosphere (TOA) depends on the abundance of absorbing aerosols that occasionally occur as elevated layers and produce extensive heating in the atmospheric column. Warming potential of aerosols at elevated altitudes is higher due to the availability of more radiation, owing to exponential thinning of the atmosphere. Moreover, the higher residence time of elevated aerosols at these altitudes could magnify their radiative impacts. Aerosol induced diabatic heating can cause changes in the synoptic meteorology and affect regional climate. It assume significance in the context of "elevated heat pump" which explains the role of absorbing aerosols in modifying the south Asian monsoon circulation *(Lau et al., 2006)*. To understand the vertical structure of aerosols over the Indian region, several attempts were carried out using ground/aircraft based lidars and in-situ measurements on-board aircraft/balloons *(Satheesh, Moorthy et al., 2009; Babu, Moorthy, et al., 2011; Nair et al., 2016; Sarangi et al., 2016;)*. However, these measurements were limited in space and time. Present study employs a synergy of satellite observations coupled with ground based measurements to generate a comprehensive synthesis of elevated aerosols over the Indian region. Multiyear measurements (2006 - 2017) of vertically resolved backscatter and extinction coefficients obtained by the space-borne lidar, CALIOP, along with ground based AOD observations from ARFI network (ARFINET) are used to characterize the spatial, seasonal, and vertical variations of elevated aerosols over Indian landmass.

### 3.2 Analysis and Database

Details of different datasets used for the present analysis is given in table 3.1.

***Table 3.1*** *- Details of datasets used in the study*

| Data Source | Product | Period |
|---|---|---|
| **CALIOP** | Aerosol extinction coefficient (0.532 μm) Level 3 – All sky (2° x 5°) | June 2006 – Nov 2016 |
| | Aerosol back-scattering coefficient (0.532 μm) Level 2 - Version 4.1 | June 2006 – May 2017 |
| | Particulate depolarization ratio (0.532 μm) (Level 2, Version 4.1) | June 2006 – May 2017 |
| **ARFINET** | Aerosol optical depth (0.5 μm) | Jan 2006 to Dec 2016 |
| **GOCART** | Aerosol optical depth (0.55 μm) | Jan– Dec 2007 |
| **MODIS (Aqua)** | Normalized Difference in Vegetation Index Collection2 version 5 (MYD13C2v005) | Dec 2006 – Feb 2017 |
| **MERRA-2** | Wind fields (u and v components) (Monthly (1.25° x 1.25°)) (MERRA300.prod.assim.instM_3d_asm_Cp) | Dec 2006 – Feb 2016 |
| | Surface soil wetness (Monthly (0.5° x 0.625°)) (M2TMNXLND V5.12.4) | Mar 2007 – May 2017 |

The aerosol characteristics such as the size distribution and composition, which determines the lidar ratio, over the Indian region changes seasonally with the synoptic changes in airmass type associated with the Indian monsoon system. Thus, the assumption of seasonally and regionally invariant lidar ratio for the vertical characterisation of aerosol over Indian region using lidars can leads to significant errors. This is true for the vertical profiling of aerosol extinction coefficient using CALIOP which has an intrinsic uncertainty in the retrieval technique associated with the assumption of lidar ratio. In the present study, AOD at 500 nm obtained from the long term observations by ARFINET is used to

scale the integrated extinction coefficient retrieved by CALIOP algorithm so that the AOD from CALIOP matches with the ARFINET derived AOD.

CALIOP observations of aerosol extinction coefficient (level2 Version 4.1) are used for examining the spatial variability in aerosols over the Indian region. The CALIOP data is quality checked and screened over Indian region following *Winker et al (2013).* The details of the quality control measures used in the present study are given below.

- Cloud screening is carried out with CAD score in the range -70 to -100 to filter the cloud free pixels with high confidence *(Liu et al., 2009).*
- Extinction quality control flag (QC) of values 0 and 1 are used to obtain extinction retrievals with high-confidence, where 0 corresponds to the constrained retrievals using transmittance measurements and 1 represents unconstrained retrievals where initial lidar ratio remained unchanged in iterations respectively.
- Uncertainty flags of extinction coefficient, back-scattering coefficient and particulate depolarization ratio measurements are used to screen the data. Range bins with an uncertainty flag of value 99.9 $km^{-1}$ are excluded in the study.
- Aerosol extinction coefficient, backscattering coefficient and particulate depolarization ratio (PDR) values are filtered with valid range limits of their magnitude, provided with the data product. Extinction coefficient at 532 nm in the range 0 – 1.25 $km^{-1}$, backscattering coefficient at 532 nm in the range (0 – 0.05 $km^{-1}sr^{-1}$) and PDR at 532 nm in the range 0 – 1, only are used in the averaging.
- Atmospheric volume description flag is used to identify and filter the aerosol pixels. Range bins with "Clear air" flag provided by Atmospheric Volume Description is assumed to be zero and included in the averaging.

## 3.3 Synoptic meteorology over the Indian region

### 3.3.1 Synoptic winds

Synoptic meteorology plays a significant in role in the physical and chemical properties and the spatial distribution of aerosols over Indian region. The seasonal mean wind pattern during winter (DJF), pre-monsoon (MAM), summer monsoon (JJAS) and post monsoon (ON) over the Indian region using MERRA 2 reanalysis dataset (2007 – 2016) with colour variation representing the wind speed at different altitude ranges are shown in figure 3.1 and 3.2.

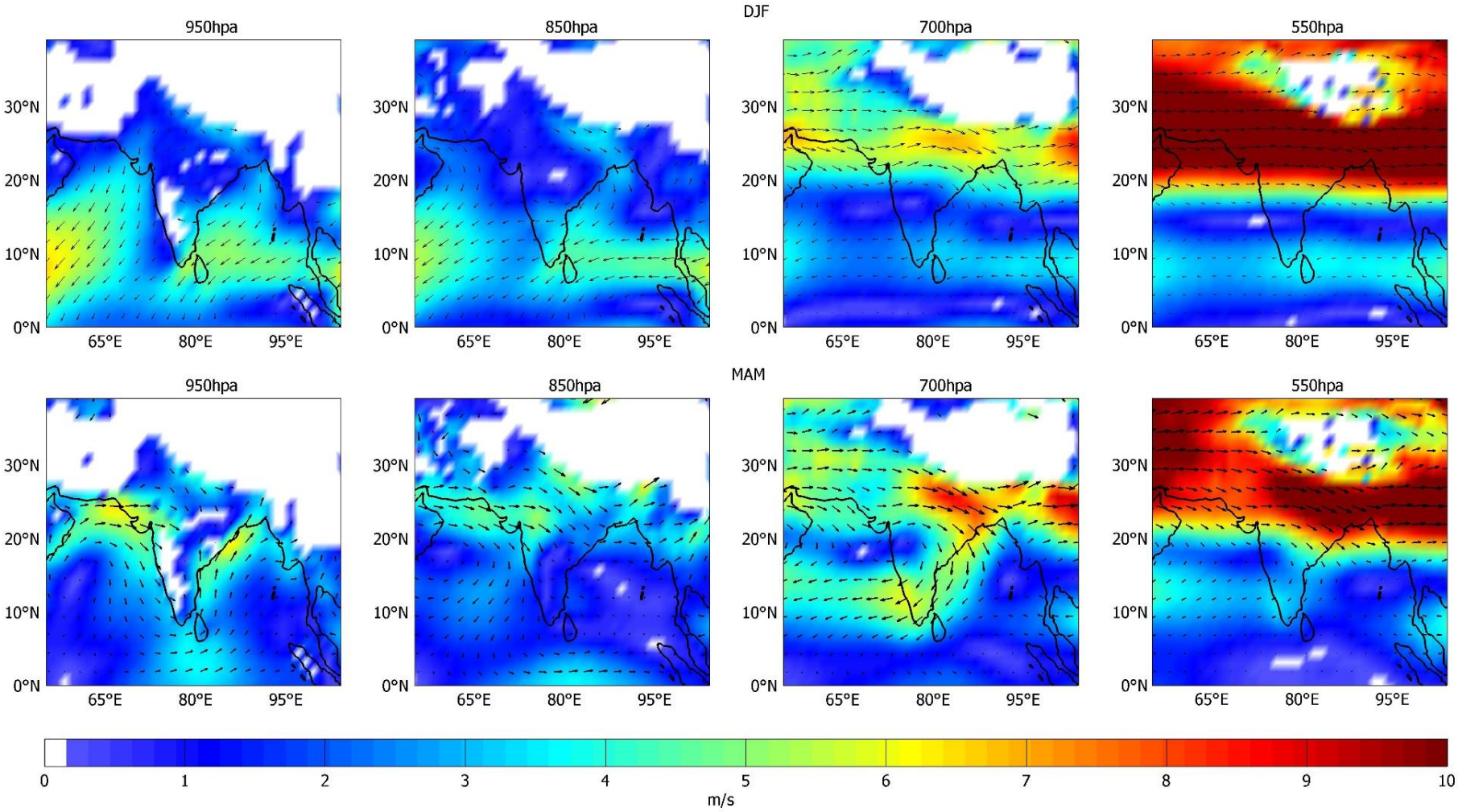


***Figure 3.1*** *- Synoptic Wind fields over Indian region during DJF and MAM at different altitude levels. Colour variation represents the wind speed*

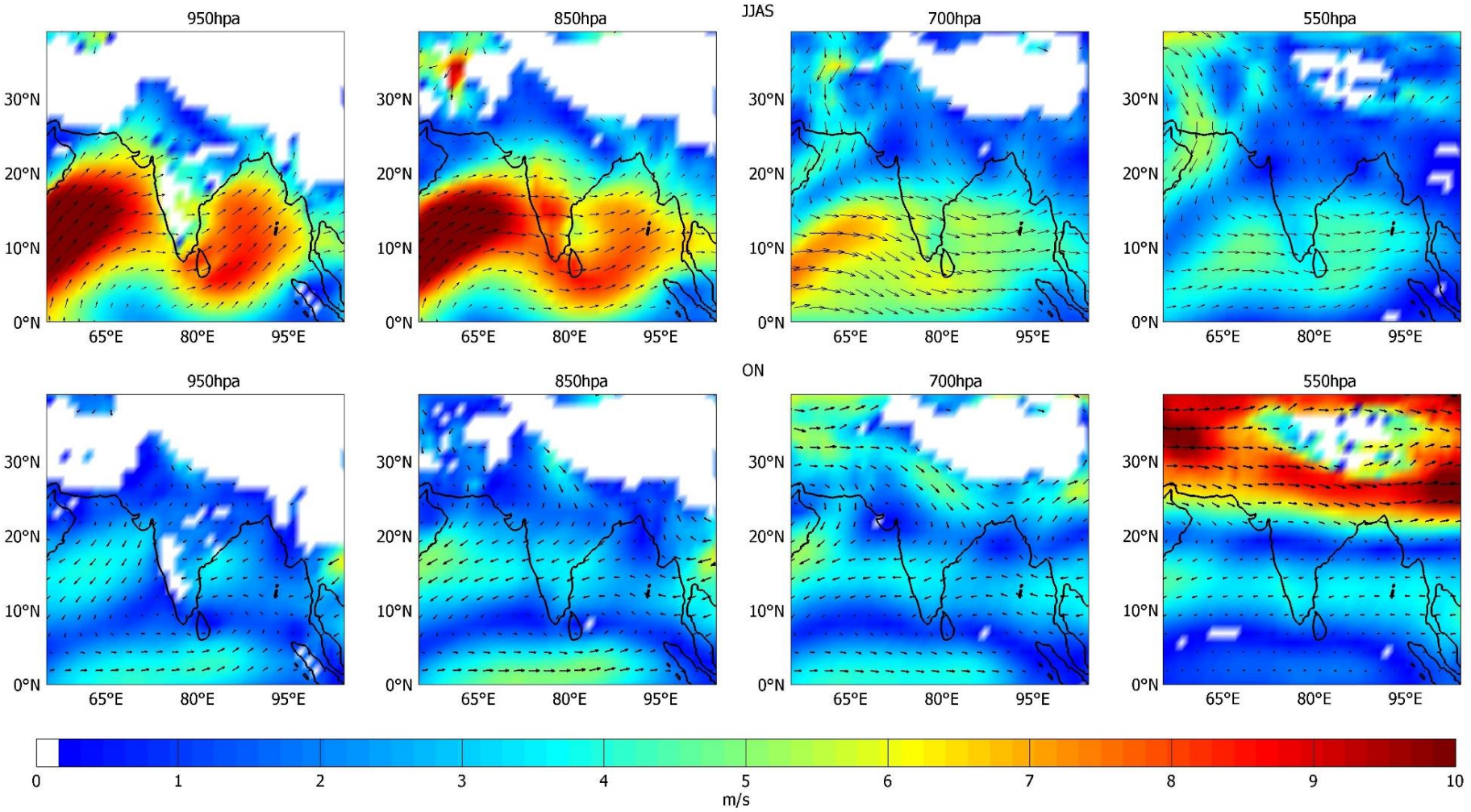


***Figure 3.2*** *- Synoptic Wind fields over Indian region during JJAS and ON at different altitude levels. Colour variation represents the wind speed.*

During winter, northern land mass is cooled and dry wind flows from north-west from the continental region to the oceans. A weak anti-cyclonic circulation prevails over the central India and northern Bay of Bengal during this season from surface up to an altitude of 550 hPa. Pre-monsoon season is a transition period when synoptic winds over the Indian region are in a transition from north-easterly to south-westerly. At higher level (700 hpa) a strong anti-cyclonic circulation is present over the Indian subcontinent with strong north westerly wind with wind speeds reaching up to ~10 m/s. Summer Monsoon season (JJAS) is known as the hot-wet season, characterised by strong south westerly monsoon winds that carry warm moist air from ocean to land with wind speed exceeding 10 m/s that and extensive rainfall occurred over the Indian sub-continent. During post monsoon, winds retreats and sky becomes clear and cloud free over the Indian region. During this season cyclone systems are formed frequently over the Bay of Bengal and the Indian Ocean. Wind pattern is similar to winter season with relatively lesser wind speeds (< 4 m/s).

### 3.3.2 Rainfall

Figure 3.3 shows the mean monthly variability of rainfall over different regions of India. Using rainfall measurements from network of rain gauge stations (306 in number) maintained by Indian meteorological department (IMD) over the period 1871 to 2016. Data have a resolution of up to 0.1 mm/month. Over most of Indian region maximum rainfall is received during July ranging between 2000 – 3000 mm/month.

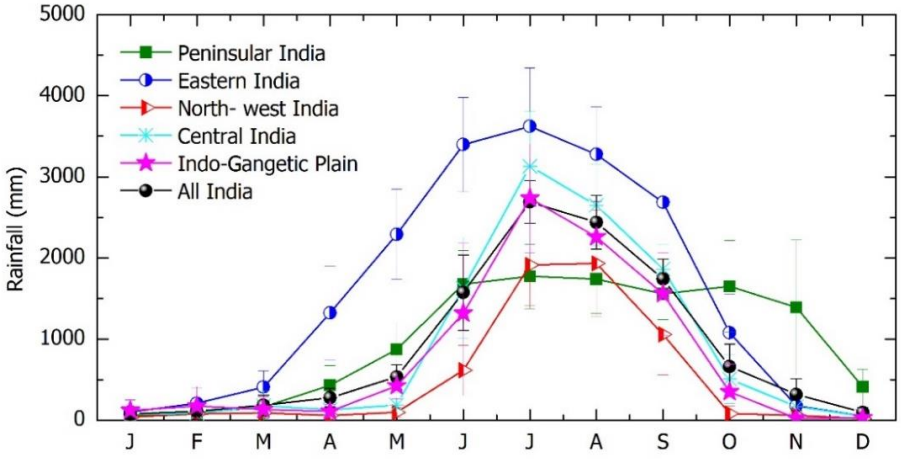


***Figure 3.3*** *- Monthly variation of rainfall pattern over different parts of Indian sub-continent averaged during the period 2006 to 2016.*

Rainfall pattern over the Indian region is determined by monsoon circulation associated with the land-sea thermal gradient. South westerly monsoon causes extensive rainfall over

the Indian sub-continent during June to September which provides three fourth of the annual rainfall over India *(Kumar et al., 1995)*. North easterly winds associated with retreating monsoon travels from cooler northern land of the subcontinent towards Indian Ocean and causes precipitation over parts of peninsula to the east of Western Ghats from December to early March. This regional rainfall influences the life time of aerosols in the atmosphere through wet scavenging and hence modulates the distribution of aerosols in the atmosphere.

### 3.3.3 Surface temperature

Figure 3.4 represents the monthly variation of surface temperature over homogeneous regions of India based on their distinct climatic and geographical settings. These regions include western Himalaya, north-west India, north-central India, northeast India, west coast of India, east coast of India and Interior Peninsula.

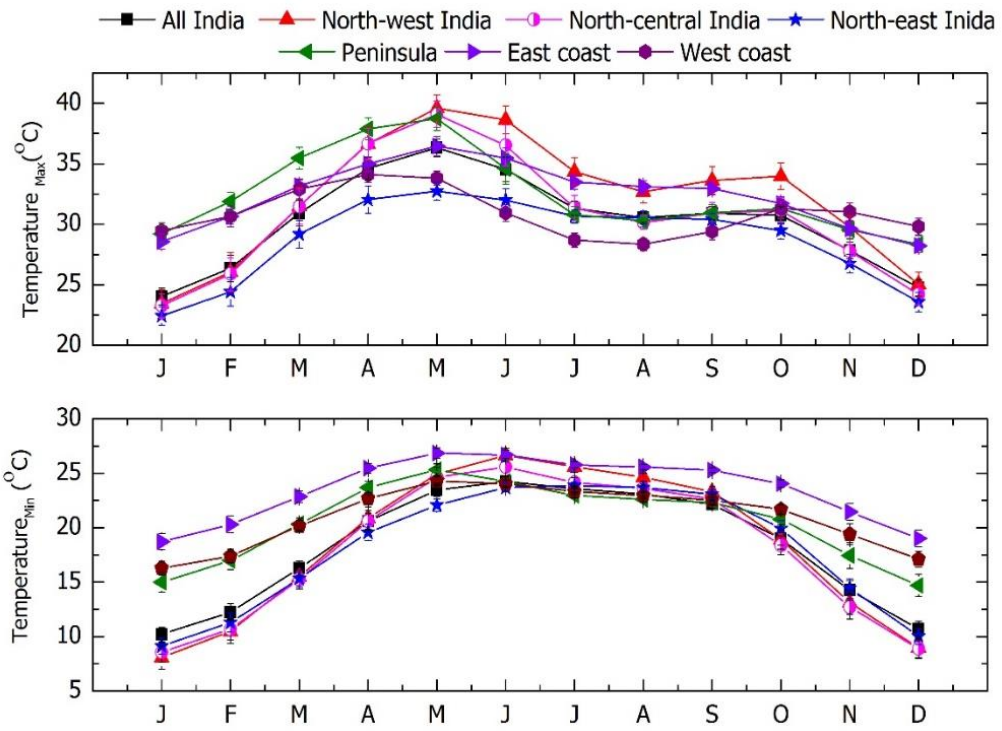


***Figure 3.4*** *- Monthly variation of surface temperature over different parts of Indian sub-continent averaged during the period 1901-2007.*

Observations are obtained over a network of 388 stations for the period 1901-2007 which were sourced from the monthly weather records of the India Meteorological Department (IMD) *(Kothawale and Rupa Kumar, 2005)*. Over Indian region, during the pre-monsoon period, the northern land mass heats up with temperature increasing to maximum mean temperature of ~ 40°C in the month of May. In June and July, extensive rainfall occurs with

the sudden onset of south west monsoon, leading to significant reduction in temperature. From August to October, diminished monsoon rains cause an increase in the surface temperature. During winter months northern land mass become cooler leaving the temperatures to drop. Recent trend in in mean annual temperature over India is observed to have a positive trend of 0.22°C/decade from 1971 to 2003 *(Kothawale and Rupa Kumar, 2005).*

## 3.4 Results and discussion

### 3.4.1 Three dimensional distribution of aerosol over the Indian region.

Aerosol characterization over the Indian region is well recorded by systematic observations from network of multi-instrumented observatories under the Aerosol Radiative Forcing over India (ARFI) project and through extensive field campaigns (ARMEX, INDOEX, and ICARB). These attempts provided a fair closure on surface/columnar characterization of aerosols over the Indian region though vertical characterization of aerosols remains rather unexplored over the region. Present study examines the vertical distribution of aerosols over Indian region during different seasons using multi-year observations of CALIOP observations. Figure 3.5 shows three-dimensional picture of aerosols over Indian region during winter (DJF), pre-monsoon (MAM), Summer-monsoon (JJAS), and post monsoon (ON) seasons using CALIOP level 2 aerosol back-scattering coefficients. Aerosols are confined within PBL during winter over northern and north-eastern regions of India. Reduced aerosol extinction observed over peninsula in all seasons can be attributed to the artefact due to surface elevation of Deccan plateau (~100-1000 m) over the interior of peninsula. Pre-monsoon season is characterized by significant aerosol loading above PBL that is spatially uniform over the entire Indian region. A significant aerosol loading is observed at upper levels (2 – 4 km) over the peninsula, eastern coast, and north eastern India. During summer monsoon, high aerosol loading is observed over Arabian Sea and north-western region with maximum aerosol loading within boundary layer. Higher aerosol loading observed within the PBL can be attributed to the production of sea salt aerosols by strong monsoon winds and transport of dust aerosols from west Asian region. Washout due to monsoon rains is clearly seen over the Indian land mass except over the North-west India. During winter and post-monsoon, significant aerosol loading is observed over IGP. IGP is characterized by high pollution due to anthropogenic emissions that produce thick haze and reduced visibility over this region *(Badarinath et al., 2009; Gautam et al., 2007; Nair et al., 2007)*.

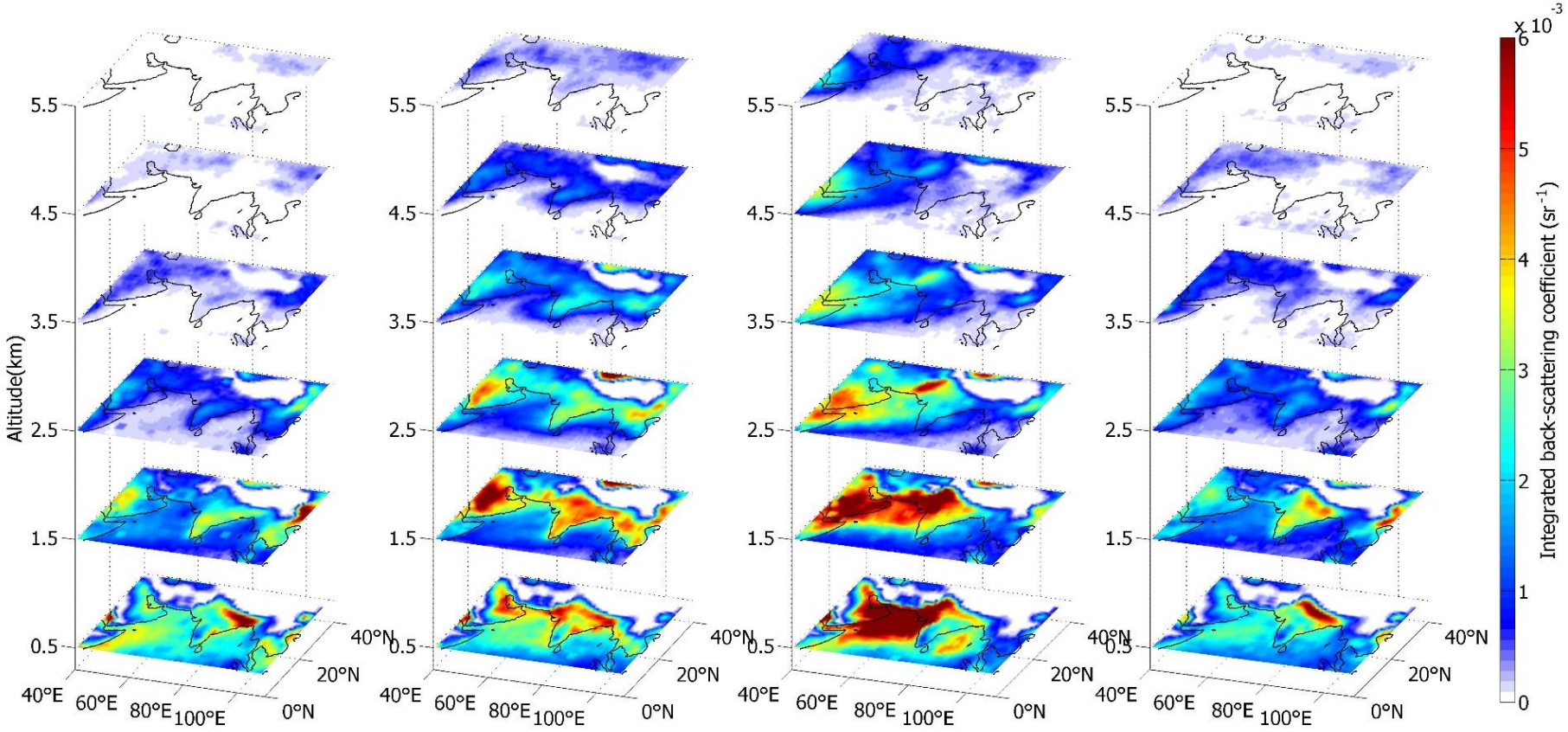


***Figure 3.5 -*** *Three-dimensional distribution layer integrated aerosol back-scattering coefficient during winter (DJF), pre-monsoon (MAM), summer monsoon (JJAS), and post monsoon (ON) seasons. Integrated back-scattering coefficient at each layers of 1km width (for 0 to 1 km, 1 to 2 km, 2 to 3 km , 3 to 4 km, 4 to 5 km, and 5 to 6km are shown at 0.5, 1.5, 2.5, 3.5, 4.5 and 5.5 km respectively.*

### 3.4.2 Meridional variation of elevated aerosols over the Indian subcontinent

Seasonal changes in the tropical atmosphere are highly influenced by the meridional transition of sun over both hemispheres. Influence of this on the aerosol distribution over the Indian region is examined using vertical profiles of aerosol extinction coefficient of CALIPSO Level3 cloud-free dataset, with a grid resolution of 2˚ latitude x 5˚ longitude, during the period June 2006- November 2016. Figure 3.6 shows the meridional cross section of aerosol extinction coefficient over the Indian region, within the longitude band 70°E – 90°E for winter (DJF), Pre-monsoon (MAM), summer monsoon (JJAS) and post-monsoon (ON) seasons.

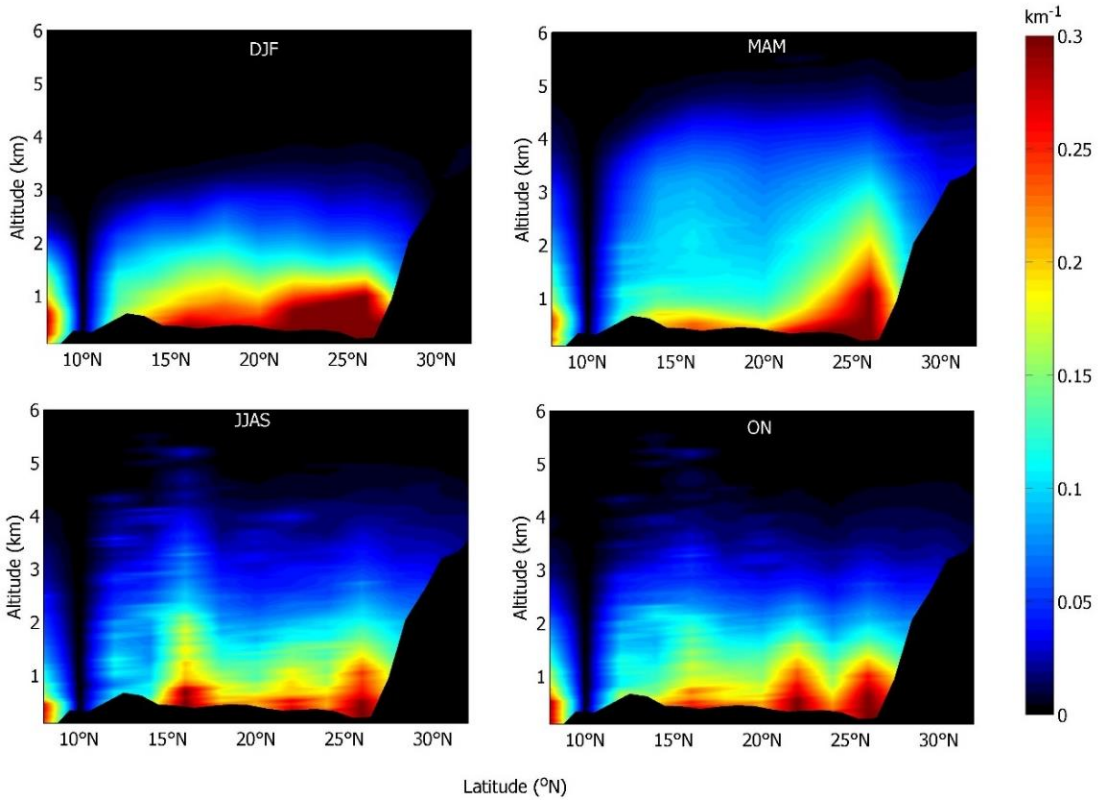


***Figure 3.6*** *- Meridional cross-section of aerosol extinction coefficient averaged over the longitude band 70°E-90°E; (a) for DJF, (b) MAM (c) JJAS seasons and (d) ON seasons. The black shaded area from at the surface represents ground elevation.*

Errors in retrieval due to the uncertainty in lidar ratio is minimized by scaling CALIPSO derived aerosol extinction profiles using measured AOD values from ARFINET during January 2006 to December 2016. Thus, the scaled profiles yielded the same vertical structure as that of CALIPSO derived aerosol extinction coefficient profiles, but with an integrated columnar extinction that matches with seasonal mean AOD values for the

latitude band from ARFINET. Table 3.2 shows different ARFINET observatories in each 2° latitude grid.

***Table 3.2 -*** *Observatories in each latitude grid (2˚ x 5˚) which used for correcting mean aerosol extinction coefficient of CALIOP.*

| **Latitude Range (°N)** | **Location of Observatories** | **DJF** | | **MAM** | | **JJAS** | | **ON** | |
|---|---|---|---|---|---|---|---|---|---|
| | | Mean | SD | Mean | SD | Mean | SD | Mean | SD |
| **7-9** | TVM | 0.372 | 0.000 | 0.41 | 0.00 | 0.31 | 0.000 | 0.38 | 0.00 |
| **9-11** | Nil | | | | | | | | |
| **11-13** | MSR, CHN,BLR | 0.30 | 0.06 | 0.38 | 0.08 | 0.266 | 0.07 | 0.313 | 0.07 |
| **13-15** | ATN | 0.35 | 0.00 | 0.46 | 0.00 | 0.313 | 0.000 | 0.358 | 0.00 |
| **15-17** | GOA | 0.43 | 0.00 | 0.5 | 0.000 | 0.660 | 0.000 | 0.492 | 0.00 |
| **17-19** | HDN, VSK,PUN | 0.42 | 0.02 | 0.45 | 0.018 | 0.390 | 0.051 | 0.385 | 0.05 |
| **19-21** | BBR | 0.42 | 0.00 | 0.44 | 0.000 | 0.361 | 0.000 | 0.376 | 0.00 |
| **21-23** | NGP,KKT | 0.65 | 0.11 | 0.6 | 0.062 | 0.455 | 0.05 | 0.55 | 0.06 |
| **23-25** | AGR,UDP, IPH | 0.42 | 0.12 | 0.53 | 0.087 | 0.409 | 0.10 | 0.35 | 0.07 |
| **25-27** | VNI,SHN,GC,GWT, JDR | 0.56 | 0.15 | 0.61 | 0.219 | 0.564 | 0.09 | 0.55 | 0.13 |
| **27-29** | JPR, DBR,DEL,RTK | 0.42 | 0.06 | 0.55 | 0.109 | 0.384 | 0.06 | 0.38 | 0.08 |
| **29-31** | NTL,RNR,PTL,DDN | 0.29 | 0.10 | 0.38 | 0.088 | 0.320 | 0.08 | 0.38 | 0.17 |
| **31-33** | KLU,HNL | 0.18 | 0.1 | 0.26 | 0.057 | 0.239 | 0.15 | 0.22 | 0.10 |

The vertical extent of significant aerosol concentration (with aerosol extinction coefficient > 0.05 $km^{-1}$) reaches up to ~ 3 km during northern hemispheric winter even though the convection is weaker compared to that in pre-monsoon/Summer seasons. These observations are significant as this feature persists over the years, as evidenced by its presence in a fairly long-term (2006 -2016) averaged data. During pre-monsoon, when convection is significantly high over the Indian landmass, aerosols spread up to ~ 5 km in the free troposphere. During monsoon/post monsoon seasons, vertical distribution of aerosols is rather inhomogeneous in the meridional direction. It is to be noted that aerosol characterization during summer monsoon season is prone to higher uncertainty because of lesser availability of clear sky pixels due to the cloud conditions associated with monsoon circulation over the study region. It is clear from the figure that extinction coefficients are high closer to surface, and decrease to higher altitudes, as would be expected normally. However, the vertical spread of aerosol extinction coefficients increases from south to north in winter and pre-monsoon seasons. A similar meridional

gradient in altitude distribution of extinction coefficient up to central India in pre-monsoon season was reported by *Satheesh et al.,(2008)* based on airborne lidar measurements as part of ICARB campaign in 2006. Over the Himalayan region (27°N – 37°N) aerosol extinction coefficient values are observed to be less than 0.05 $km^{-1}$ during all the three seasons. A discontinuity in the aerosol loading in the latitude range 9°N to 11°N is due to the lack of station based AOD observations over this region.

### 3.4.3 Regional characterization of aerosol vertical distribution

Indian region is characterized by heterogeneous sources of aerosols due to its physical, topographical, and meteorological features. While vast deserts cover the north-west part of the landmass contributes the natural dust aerosols over the Indian region, large amount of anthropogenic aerosols accumulates at the foothills of Himalayas and produce extreme pollution at Indo-Gangetic Plain. The great Himalayas act as barrier to air mass from south and prevailing westerly winds over the northern latitudes of India facilitate the transport of mixed aerosols towards eastern India, which is surrounded by mountain ranges all around. The regional characterization of vertical distribution of aerosols over the Indian region is carried out using CALIOP observations of aerosol extinction coefficient scaled with ARFINET derived AOD. Study regions are shown in figure 3.7.

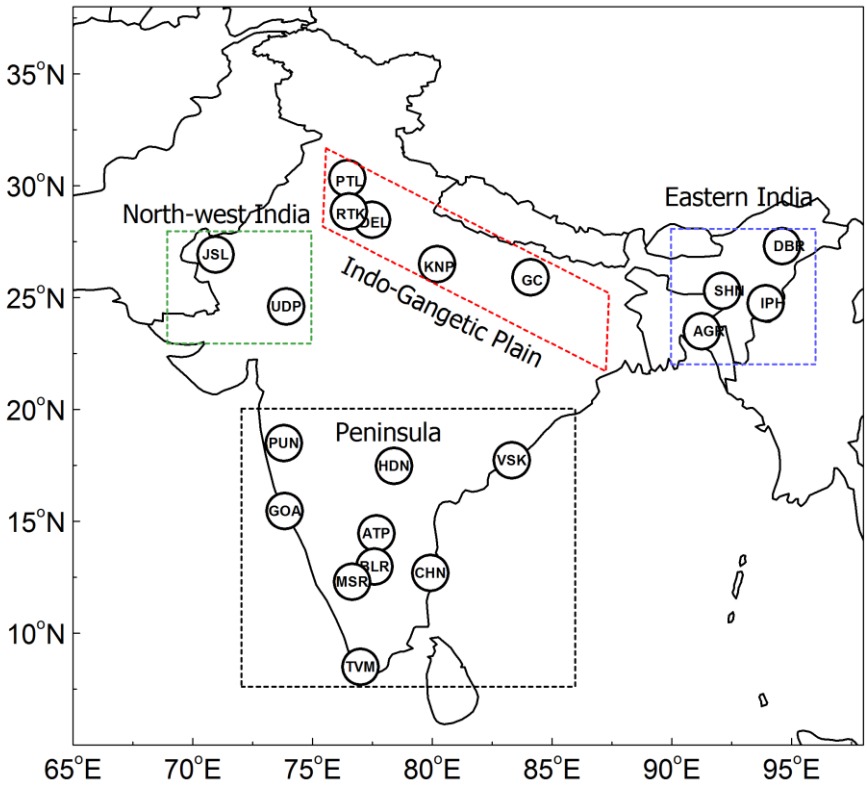


***Figure 3.7*** *- Study regions over the Indian Land mass*

Analysis is carried out over regionally distinct areas of the Indian landmass that includes (i) Peninsular India (8°N - 20°N, 72°E - 85°E), (ii) East India (22°N - 28°N, 90°E - 96°E), a densely vegetated region of distinct topography (iii) north-west India (23°N - 28°N, 69°E - 75°E) which is a dry arid desert region, and (iv) a highly polluted Indo-Gangetic Plain along the foot hills of Himalaya (22°N - 30°N, 76°E - 86°E). Investigation is carried out for winter (December, January, and February (DJF)), pre-monsoon (March, April and May (MAM), summer monsoon (JJAS) and Post-monsoon season (ON)). Upper panel of figure 3.8 shows the climatological mean profile of aerosol extinction coefficient during winter, pre-monsoon, summer monsoon, and post-monsoon seasons (2006-2017) over the study regions, scaled with the seasonal mean AOD from ARFINET. Magnitude of extinction coefficient at higher altitude is lesser compared to that close to surface, yet assumes significance owing to increased heating potential at higher altitudes due to thinning of the atmosphere. Thus to show the variation of extinction coefficient at higher altitudes, the profiles of aerosol extinction coefficient are shown in logarithmic scale in the lower panels. In general, during winter/post monsoon, aerosols are mostly confined to the surface with higher extinction coefficient and lesser vertical extent, while during pre-monsoon and summer monsoon seasons aerosol extinction coefficient is above PBL with greater vertical spread. Vertical spread of aerosols is observed to be highest during pre-monsoon season which extends up to 5 km (aerosol extinction coefficient is negligibly small of magnitude $\sim 0.01\ km^{-1}$), while during winter these aerosols resides within the 3 km to 3.5 km altitude range. Similarly during summer monsoon season vertical spread extend up to and altitude range of 4.5 – 5 km and during post monsoon it is in the range of 3.5 – 4 km. On examining the pattern of vertical distribution above PBL, during the winter/post monsoon periods, aerosols exponentially decreases above PBL, while during pre-monsoon it shows a clear enhancement over all four regions.

Along with seasonal variation, aerosol vertical distribution over the Indian region is found to show distinct variation over the regional domain. Vertical profile of aerosol extinction coefficient shows a convex pattern over Peninsula/eastern India (~ 1.5 – 5 km) during pre-monsoon while over IGP and north-west India, this shows a near-linear decrease. Over Peninsula, similar vertical patterns are observed during winter and post monsoon seasons with aerosol extinction coefficient dominating from surface to ~ 2 km while during convective seasons aerosol extinction coefficient is higher above 2 km. Over eastern India, vertical pattern during summer monsoon, post monsoon and winter shows similar vertical profiles with a clear pre-monsoon enhancement above PBL. The entire eastern India receives heavy rainfall with an earlier onset (compared north-west/IGP) of monsoon and

minimum surface temperature (figure 3.4) during the monsoon months. Over north-west India, similar vertical patterns are observed during pre-monsoon and summer monsoon season with a higher extinction above PBL during post monsoon season. North-west India receives the minimum rainfall during monsoon thereby retains a higher surface temperature compared to other parts of India (Figure 3.3 and 3.4).

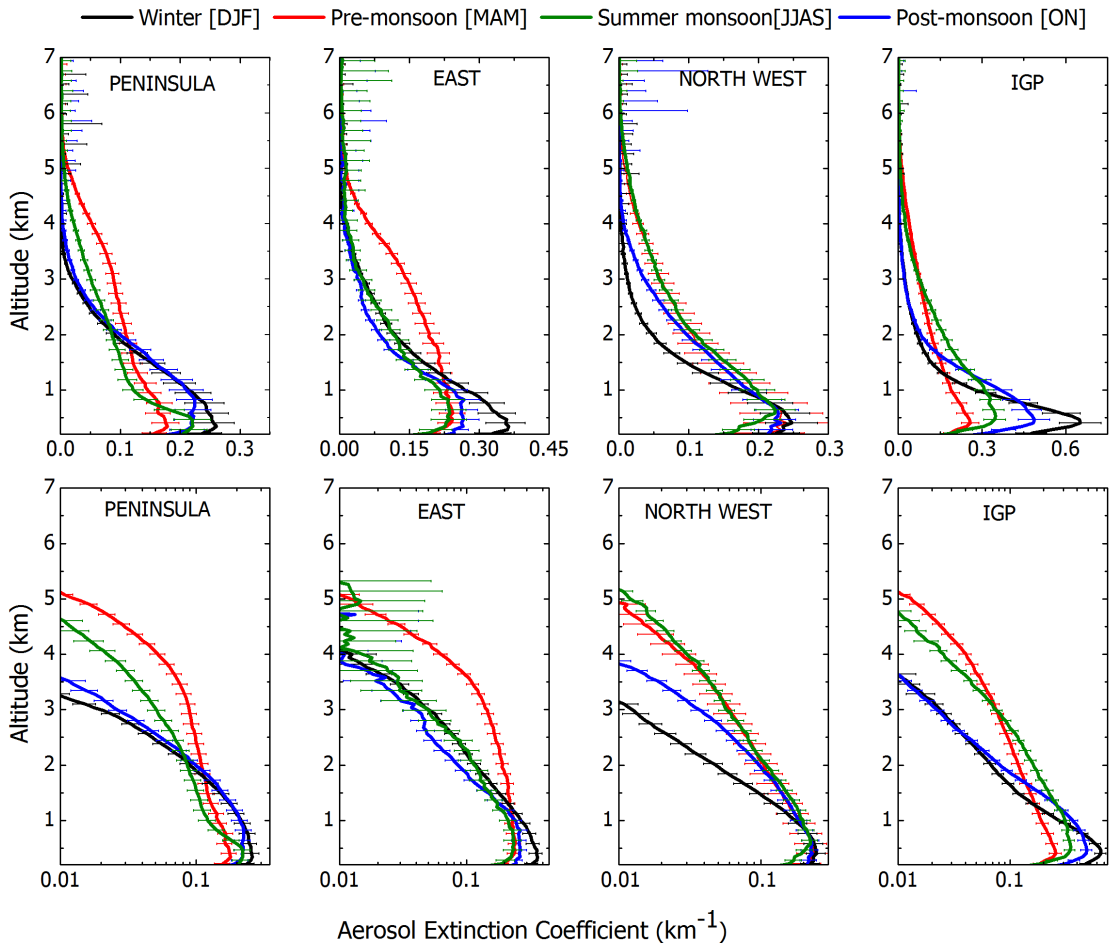


***Figure 3.8*** *- Climatological mean profile of aerosol extinction coefficient during winter (DJF), pre-monsoon (MAM) and post monsoon (ON) (2006 -2017) over the study regions, corrected with ARFINET mean AOD (upper panel). Lower panel shows the variation of aerosol extinction coefficient in logarithmic scale.*

Reduced monsoon rains sustain the connective activity during summer monsoon and post-monsoon seasons over this region. Also long range transport of aerosols through higher altitudes from west Asian regions (where summer is the most dust active period), May also contribute to enhanced aerosol optical depth over this region. Higher aerosol extinction during post monsoon (up to 4 km) over North-west India can be attributed to the transport from west Asia during this season. Over IGP, vertical pattern of aerosol extinction coefficient is clearly higher during convective seasons. After monsoon rains,

aerosols rapidly builds up from surface to 2 km during post monsoon and settle down during winter when solar insolation is reduced due to the passing of ITCZ over to the southern Hemisphere.

On examining the fractional contribution of extinction at different altitude layers to the columnar AOD, it is found that a regional average of ~ 65 % - 69 % of the aerosols reside above 1 km during the pre-monsoon season and summer monsoon while it is ~ 45% - 53 % during winter and post monsoon. Figure 3.9 shows the scale height of aerosols over the study regions during different seasons.

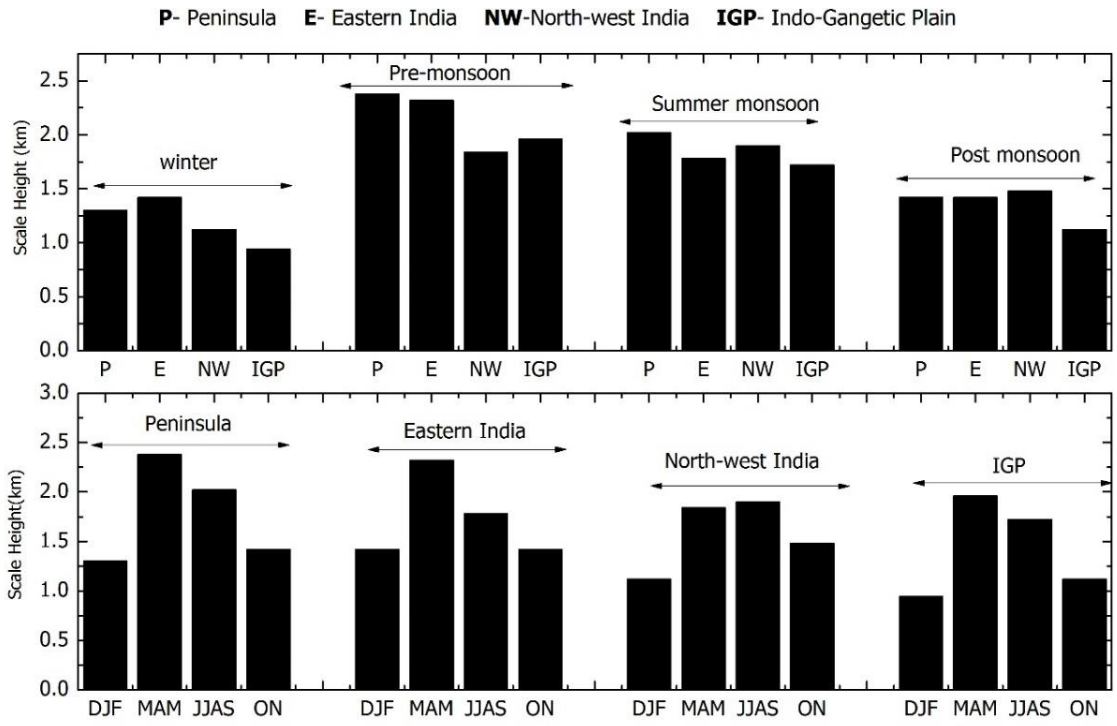


***Figure 3.9-*** *Scale height of aerosols over the study regions. Upper panel shows the seasonal variation and lower panel shows the regional variation of aerosol scale height.*

Aerosol scale height is determined by the vertical distribution of aerosols. Unlike gases, aerosol number density does not exponentially decrease with altitude especially in the presence of elevated layers aloft. Hence, aerosol scale height is estimated as the altitude within which integrated aerosol extinction becomes 1/e of the columnar aerosol optical depth *(Yu et al., 2010).*. Pre-monsoon season is characterized with highest aerosol scale height with highest percentage contribution of aerosols above PBL to the columnar loading, followed by summer monsoon, post monsoon and least aerosol scale height is observed during winter. Regional variation in aerosol scale height shows that, aerosol scale height is generally higher over peninsula (~2.38 km) and eastern India (~2.32 km)

compared to IGP and North-west India. Aerosol scale height is observed highest over Peninsula during pre-monsoon (~2.38 km) and is observed minimum at IGP (~ 0.9 km) during winter, which can be attributed to the increased concentration of anthropogenic aerosols emitted within PBL that reduces the relative fraction of aerosols above boundary layer over IGP.

Several studies have reported the presence of elevated aerosol layers over Indian region during pre-monsoon season *(Babu and Sivaprasad, 2014; Niranjan, Madhavan et al., 2007; Satheesh et al., 2008).* Indian Ocean Experiment (INDOEX) observations have revealed the existence of thick haze of ~ 3 km vertical extent in the lower troposphere, as a result of anthropogenic emissions during winter season *(Ramanathan, et al., 2001)*. Profiling of black carbon aerosols in the free troposphere, revealed the presence of multiple peaks at ~4.5 km, and at 8 km over Hyderabad, an urban centre in the peninsular India *(Babu, Moorthy, et al., 2011)*. Warming due to these BC layers induced changes in the environmental lapse rate and atmospheric stability *(Babu, Moorthy, et al., 2011)*. During pre-monsoon, aerosol layers were found to be present up to altitude as high as 6 km over the Indo-Gangetic Plains and Himalayan foothills with a large increase in absorption coefficients (by two to five times) near the Himalayan foothills *(Devi et al., 2011)*. The ICARB revealed the presence of prominent elevated extinction off the eastern coast of India with 75 % - 85 % of AOD contributed by aerosols above 1 km and maximum extinction between 2 km and 4 km during pre-monsoon *(Satheesh, Vinoj et al., 2009).*

### 3.4.4 Pre-monsoon enhancement in elevated aerosols

The temporal evolution of the vertical distribution of monthly mean aerosol extinction coefficient from December (winter) to May (pre-monsoon) is shown in Figure 3.10. Vertical extent of aerosol extinction coefficient increases consistently from December to May. Aerosols from the lower altitudes get pumped slowly to higher altitudes as season changes from winter (December, January and February) to pre-monsoon (March, April and May), forming a prominent system of elevated aerosol over the Indian landmass. Vertical pumping of aerosols to higher altitudes and associated well developed elevated aerosol system during pre-monsoon is evident over all the regions. As season changes from winter to pre-monsoon, there is a consistent decrease in aerosol within PBL while they get transported to higher heights to form the elevated aerosol layer, with increasing vertical extent up to the month of May. Vertical spread of this pumping reaches up to an altitude of ~ 5.5 km in the month of May. Being a tropical region, Indian landmass receives

large amount of solar radiation during pre-monsoon which lead to intense convection that causes major vertical re-distribution of near-surface emissions. Enhanced convection during northern hemispheric summer leads to increased vertical spread of aerosols and hence a decrease in its surface concentration. Surface/ column observations at high altitude stations at Himalayan range also shows an enhancement in aerosol loading during pre-monsoon which is attributed to the uplift of aerosols from the IGP/foot hills of Himalayas and their accumulation on the high altitude regions of Himalayas *(Babu, Chaubey, et al., 2011; Brun et al., 2011; Kompalli et al., 2013)*.

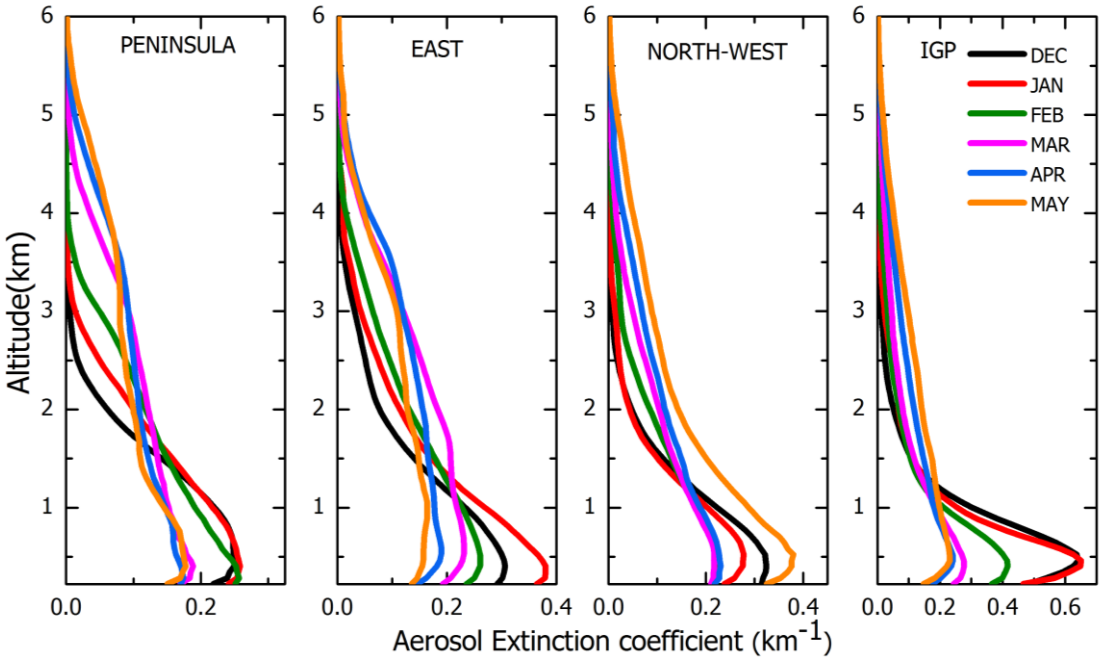


***Figure 3.10 –*** *Monthly variation of aerosol extinction coefficient (December to May) over the study regions averaged during the period 2006-2017, weighted with ARFINET AOD.*

During the winter season, the reduced vertical spread of aerosols over most of the continental India is due to reduction in thermal convection owing to the low surface temperatures. As the convection increases during MAM, aerosols are pumped more into higher elevations, which will lead to less concentration of aerosols near the surface. Aerosols emitted near the surface can be transported to higher altitudes through vertical thermal eddies generated due to increased convection associated with solar heating of the surface or presence of vertical wind shear that will mechanically draws the aerosols upwards. Seasonal study on vertical distribution of aerosols has been carried out at a coastal location on the west coast of India using bi-static lidar measurements *(Parameswaran et al., 1997)*. Above the surface layer (~120 m), aerosol concentration

increases with altitude and reaches a broad peak associated with the PBL cape inversion above which aerosol concentration decreases rapidly. Height of maximum aerosol concentration defines aerosol mixing height and the steady decrease beyond that level is referred to as entrainment region where aerosols move into higher levels in the free troposphere *(Parameswaran et al., 1998*). The maxima in aerosol mixing height during dry months (November and March) is attributed to strong convective mixing, while during summer monsoon season, it is due to the mechanical mixing associated with increased vertical shear in winds *(Parameswaran et al., 1997)*. Strong convection prevailing during spring and summer seasons over the Indian region favours lifting up of aerosols to higher elevations in the atmosphere, even up to upper tropospheric altitudes *(Satheesh et al., 2013)*. Associated with summer monsoon circulation and upward transport of atmospheric constituents, a layer of aerosols is observed at altitudes 13 to 18 km *(Vernier et al., 2011).* Looking at the circulation pattern, an anti-cyclonic circulation (associated with a high pressure) is present over the Indian land region persistently throughout winter and pre-monsoon seasons. During winter this circulation forms at lower altitudes and get stronger upwards that acts as a capping and inhibits the vertical transport of aerosols over peninsular and eastern India, while during pre-monsoon months this circulation is present at upper altitudes, allowing vertical transport of aerosols from the surface. The meridional transition of sun over to the northern hemisphere causes increased convection over the land which primarily causes this enhanced aerosol extinction at higher heights. Also Pre-monsoon season is associated with strong upper level north westerly winds which facilitate the horizontal advection of aerosols from West Asian/North-western Indian regions.

To delineate seasonal difference in the meridional gradient of aerosol vertical distribution, aerosol extinction coefficient during winter time is subtracted from that during pre-monsoon and its meridional variation is shown in figure 3.11. The meridional gradient of difference between the extinction coefficients profiles during winter and pre-monsoon shows an enhancement in aerosol extinction coefficient above PBL at 2 to 4 km altitude during pre-monsoon season over the entire Indian landmass. Positive values indicate regions of aerosol enhancement in pre-monsoon compared to winter while negative values show regions of decrease in aerosol concentration during pre-monsoon. The decrease in extinction values near the surface indicate that this enhancement of aerosols at elevated heights is due to the pumping of PBL aerosols to higher altitudes.

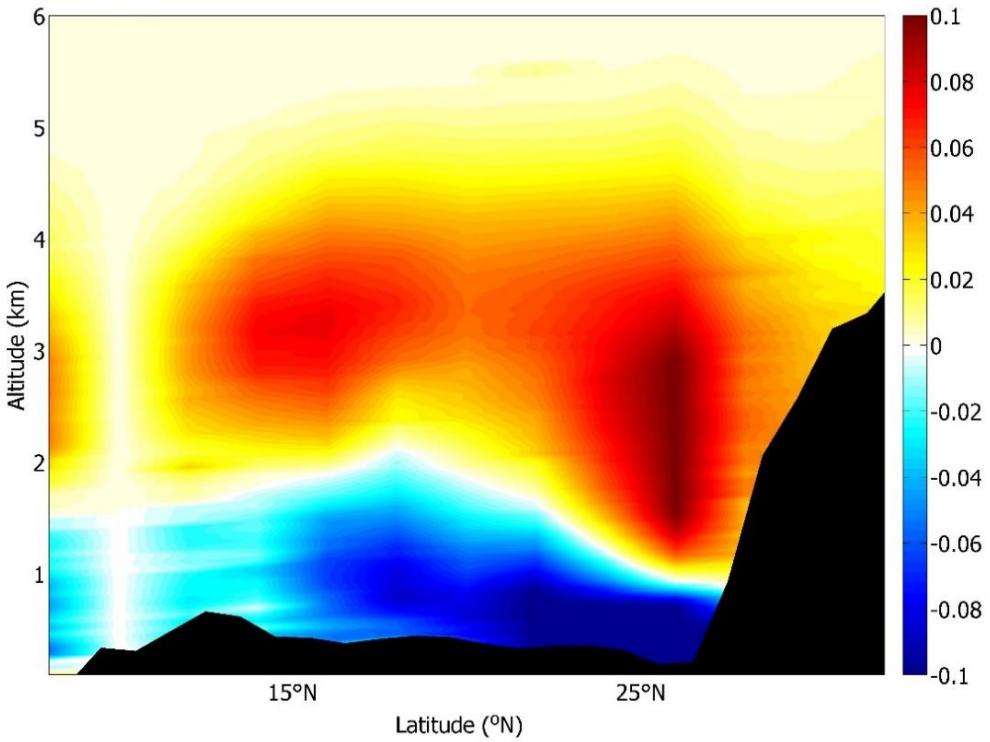


***Figure 3.11*** *- Enhancement in aerosol extinction coefficient over the Indian region from winter (DJF) to pre-monsoon (MAM) using level 3 monthly mean CALIOP profiles of aerosol extinction coefficient (2° x 5°) are scaled with monthly mean ARFINET AOD. The stations used and mean ARFINET AOD. The stations used and mean AOD values over different grid cells are shown in Table 3.2.*

Vertical spread of enhancement in elevated aerosols during pre-monsoon shows a clear meridional gradient. Over the southern latitudes (around 8°N), dominant enhancement in extinction coefficient can be observed at altitudes between 2 and 3.5 km (with a minimum enhancement in aerosol extinction coefficient of 0.05 $km^{-1}$) while it is extending between 2 and 4.5 km over central India around 16 °N, and between 1 and 4.5 km over the northern regions around 25°N. Whereas, the regions of aerosol decrease is observed extending from the surface up to altitudes ~1.5 km at southern, ~2 km at central and ~1 km at northern latitudes. The enhancement in aerosol extinction at higher altitudes (or elevated aerosol extinction) in pre-monsoon months over Indian region is important, as it can alter the meridional temperature and pressure gradients that drive the Indian summer monsoon circulation and in turn May modify the monsoon onset and associated rainfall *(Lau et al., 2006)*. Altitude resolved aerosol characterization; including vertical profiling of aerosol abundance and scattering/absorption efficiencies, over this region is indispensable to understand aerosol impacts on Indian monsoon. Enhancement in vertical distribution of aerosols during summer-monsoon compared to winter season is shown in figure 3.12.

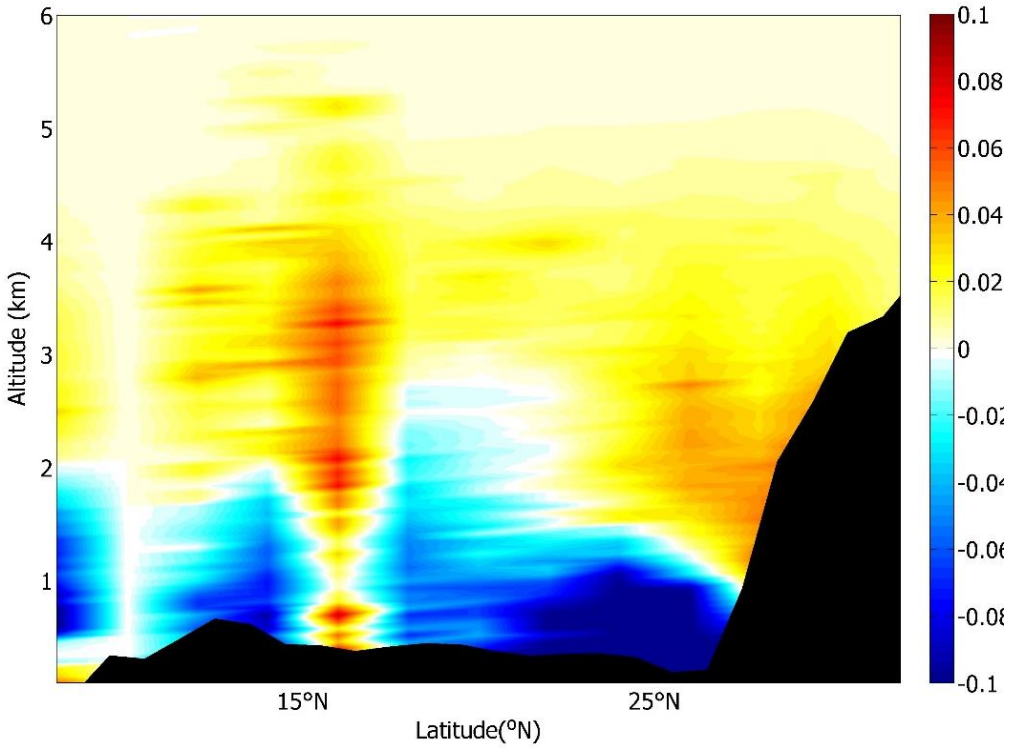


***Figure 3.12*** *- Enhancement in aerosol extinction coefficient over the Indian region from winter (DJF) to summer monsoon (JJAS) season using level 3 monthly mean CALIOP profiles of aerosol extinction coefficient (2° x 5°) are scaled with monthly mean ARFINET AOD.*

A clear deficit of aerosols below 2 km is attributed to wet scavenging by extensive monsoon rains over the Indian landmass. Enhancement in aerosols during summer monsoon above 2 km (~0.02 $km^{-1}$ from winter) is attributed to long-range transport from the west since reduced surface temperature during this season inhibit active convection during this season. Summer season is the most dust active season over the west Asia when large amount of aerosols are transported to Arabian Sea *(Rezazadeh et al., 2013)* and strong monsoon westerly winds associated with this season can bring aerosols to the Indian land mass through upper altitudes.

### 3.4.4.1 Aerosol simulations using GOCART

Chemical transport models can provide information on the optical, physical and chemical information on different aerosol species by carrying out simulations based on physical laws combining available observations and different atmospheric conditions. Goddard Chemistry Aerosol Radiation and Transport (GOCART) simulates major tropospheric aerosol species which are sulphate, dust, Black Carbon (BC), sea-salt and particulate organic matter (pom), by solving the continuity equation involving the processes of

chemistry, emission, advection, convection, diffusion, mixing, dry deposition and wet deposition of each species, using assimilated meteorological fields generated by Goddard Earth Observing System Data Assimilation System (GEOS-DAS) with a horizontal resolution of 2° latitude by 2.5° longitude *(Chin et al., 2009)*. In order to examine seasonal variation of dust aerosols over the Indian region, GOCART simulations are used and are shown in figure 3.13.

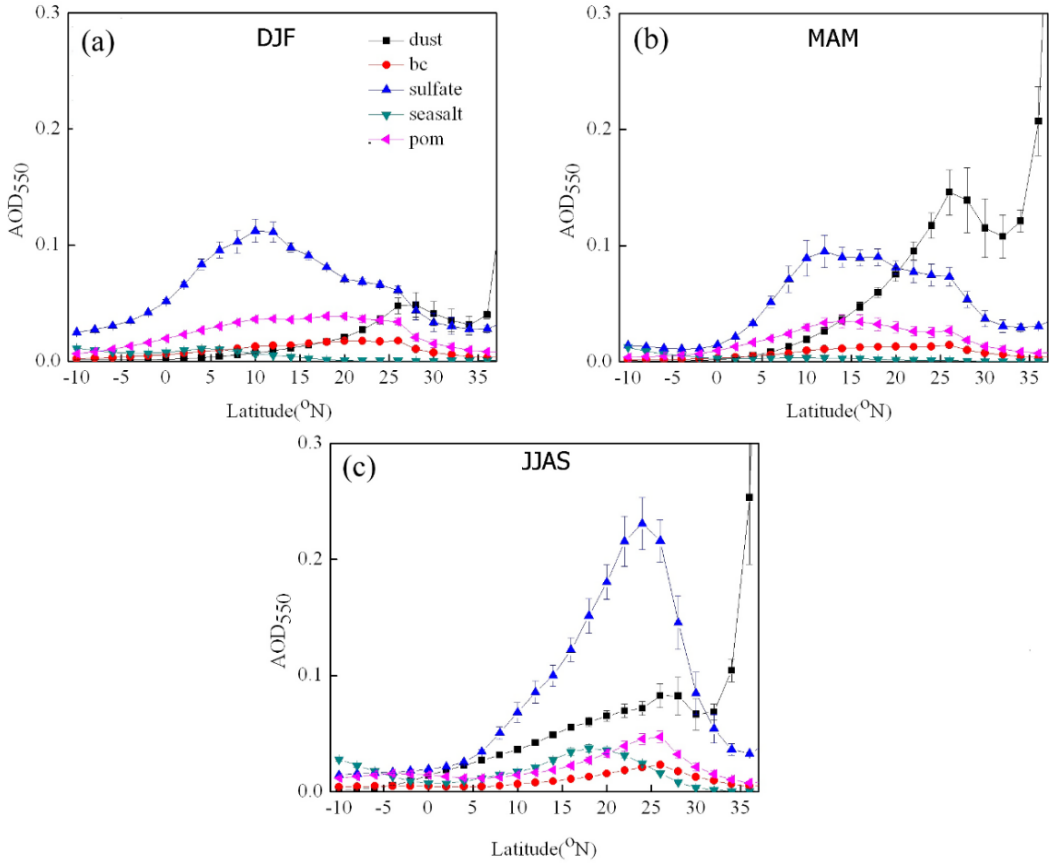


***Figure 3.13 -*** *Latitudinal variation of mean AOD due to different types of aerosols over the Indian region from GOCART simulation for (a) DJF, (b) MAM and (c) JJAS seasons for the year 2007, averaged for the longitudinal band 70°E - 90°E.*

During winter, when the winds over the Indian region are north easterlies , it is shown that the major contribution is from sulphate and organics, which reveals the anthropogenic influence on winter time aerosol system over the Indian region and the role of meteorology in possibly confining them close to the landmass (the prevailing anticyclone does not allow vertical dispersion). *Nair et al.,(2006)* also reported dominance of sulphate in winter time aerosols over peninsular India, from measurements carried out as part of a land campaign conducted in 2004. During this season dust activity would be low as shown by the dust AOD values in figure 3.13, due to low temperatures prevailing over the arid

regions. The contribution of mineral dust becomes significantly large in MAM over the northern latitudes, over the regions at north of 20°N. An inter-comparison study between CALIOP/MODIS observations and GOCART simulations shows that seasonal variations of aerosol optical depth is well reproduced by GACART while magnitude of aerosol extinction by GOCART simulations are underestimated over the Indian sub-continent and aerosol scale-heights simulated by GOCART are consistently higher than the CALIOP observations *(Yu et al., 2010)*. *Moorthy, Beegum, et al., 2013.*, reported that the GOCART simulation of BC aerosols over Indian region captures seasonal/sub-seasonal features but significantly deviates from the absolute magnitude of BC mass-concentration from ground based measurements. Dust loading over India during this period is reported by earlier studies using satellite observations *(Gautam et al., 2009; Moorthy et al., 2007)*. Significant concentration of sea-salt aerosols are observed during JJAS over the regions between 15°N and 25°N along with dust aerosols. Transport of sea-salt aerosols generated at the surface of Arabian Sea by the strong monsoon westerly wind is expected to occur through lower levels. Thus the enhancement in aerosol extinction coefficient during JJAS above 2 km altitude can be attributed to the dust aerosols transported from the Arabian Sea by the monsoon westerly winds.

### 3.4.5 Role of mineral dust aerosols: satellite observations

Being close to the global dust belt, Indian region experiences large number of dust episodes in pre-monsoon and summer seasons under favourable meteorological conditions. The seasonality in dust loading over South Asia is well investigated during the last few decades using various techniques, even though most of the measurements were limited in space and time. A synthesis of AOD over the Indian region using measurements at different ARFINET observatories is presented by *Beegum et al., (2008)* and explains the role of long-range transport of mineral aerosols from west Asia and north-west coastal India in determining the aerosol characteristics over the Indian region. Using aircraft based absorption coefficient measurements during pre-monsoon over the Indo-Gangetic Plain implied vertical heterogeneity in absorbing aerosols and presence of mineral dust aerosols *(Nair et al., 2016)* .

#### 3.4.5.1 Satellite observations of depolarization ratio over Indian region

Depolarization ratio observations by CALIOP is used to examine the role of mineral dust aerosols on the seasonal enhancement in elevated aerosols. Depolarization ratio act as a proxy for dust aerosols by being sensitive to their non-spherical morphology (for dust,

PDR >=0.2). (Refer chapter 2). Figure 3.14 depicts three dimensional distribution of PDR averaged over the Indian region using level 2 PDR data from CALIPSO observations. From figure 3.14, it can be seen that from surface to 1 km, PDR values are around 0.1, indicating that dust aerosols are mixed with spherical particles during all the seasons. Significant mineral dust loading is observed in the free troposphere during pre-monsoon and summer monsoons seasons as indicated by PDR values greater than 0.2. During DJF, the PDR values are low (~0.1) over the Indian landmass indicating the dominance of more spherical particles. The low PDR values during the winter are indicative of the presence of significant anthropogenic sources when the winds in the lower troposphere are from continental landmass. During pre-monsoon, PDR values > 0.2 are seen at altitude above ~1 km, indicating the presence of pure dust over the north-western part of India. Over the eastern and peninsular regions, PDR values are in between ~0.1 – 0.15 due to mixing of dust aerosols with fine-mode/spherical aerosols. PDR observations shows significant dust loading over west Asia and north-west India at 1 to 4 km altitudes. During post monsoon there is signature of dust loading between 1 km to 3 km which eventually depletes during winter when the convective activity becomes dormant in the northern hemisphere. Significant dust transport is observed over the Arabian Sea during pre-monsoon/ summer monsoon seasons in the altitude range 1 km to 4 km. Dust emission basically depends on the surface wind speed, soil moisture and also on the vegetation index. Reason for high dust loading during pre-monsoon season, compared to winter is due to the reduced soil moisture condition, reduction in vegetation and increased surface wind speed during this season as shown in figure 3.15. Based on aircraft based absorption coefficient measurements during pre-monsoon over the Indo-Gangetic Plain, *Nair et al., (2016)* reported the vertical heterogeneity in absorbing aerosols and presence of mineral dust aerosols. But, being campaign based measurements; these studies are limited to cases of certain days in a season. Also vertical characterization of mineral dust aerosols assumes importance due to its semi-direct effect on radiation by impacting the thermodynamic state of clouds *(Huang et al., 2006; Mahowald and Kiehl, 2003).* Over Indian region absorption efficiency of dust aerosols was estimated using thermal Infra-red radiance measured by METEOSAT and it was concluded that dust aerosols over Indian deserts are more absorbing in nature compared with that of African origin *(Deepshikha et al., 2005; Moorthy et al., 2007).* Though numerous studies have been carried out on mineral dust aerosols globally using both ground based lidar and CALIOP observations, dust aerosols over Indian region and their vertical distribution are still under-characterized.

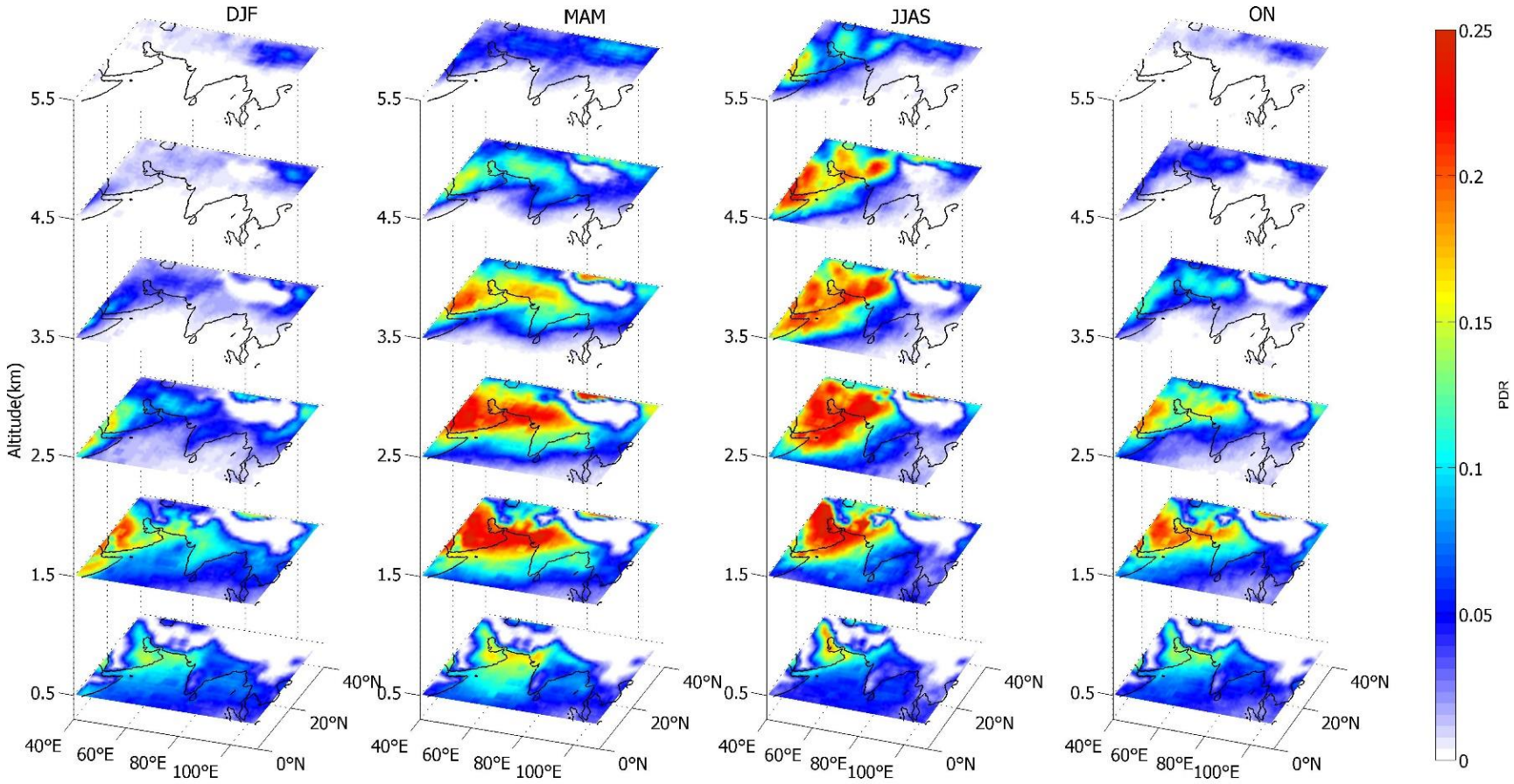


***Figure 3.14*** *- Three-dimensional distribution of PDR during winter (DJF), pre-monsoon (MAM), summer monsoon (JJAS), and post monsoon (ON) seasons. Layer mean PDR represents mean PDR at each layers of 1km width (for 0 to 1 km, 1 to 2 km, 2 to 3 km , 3 to 4 km, 4 to 5 km, and 5 to 6km are shown at 0.5, 1.5, 2.5, 3.5, 4.5 and 5.5 km respectively.*

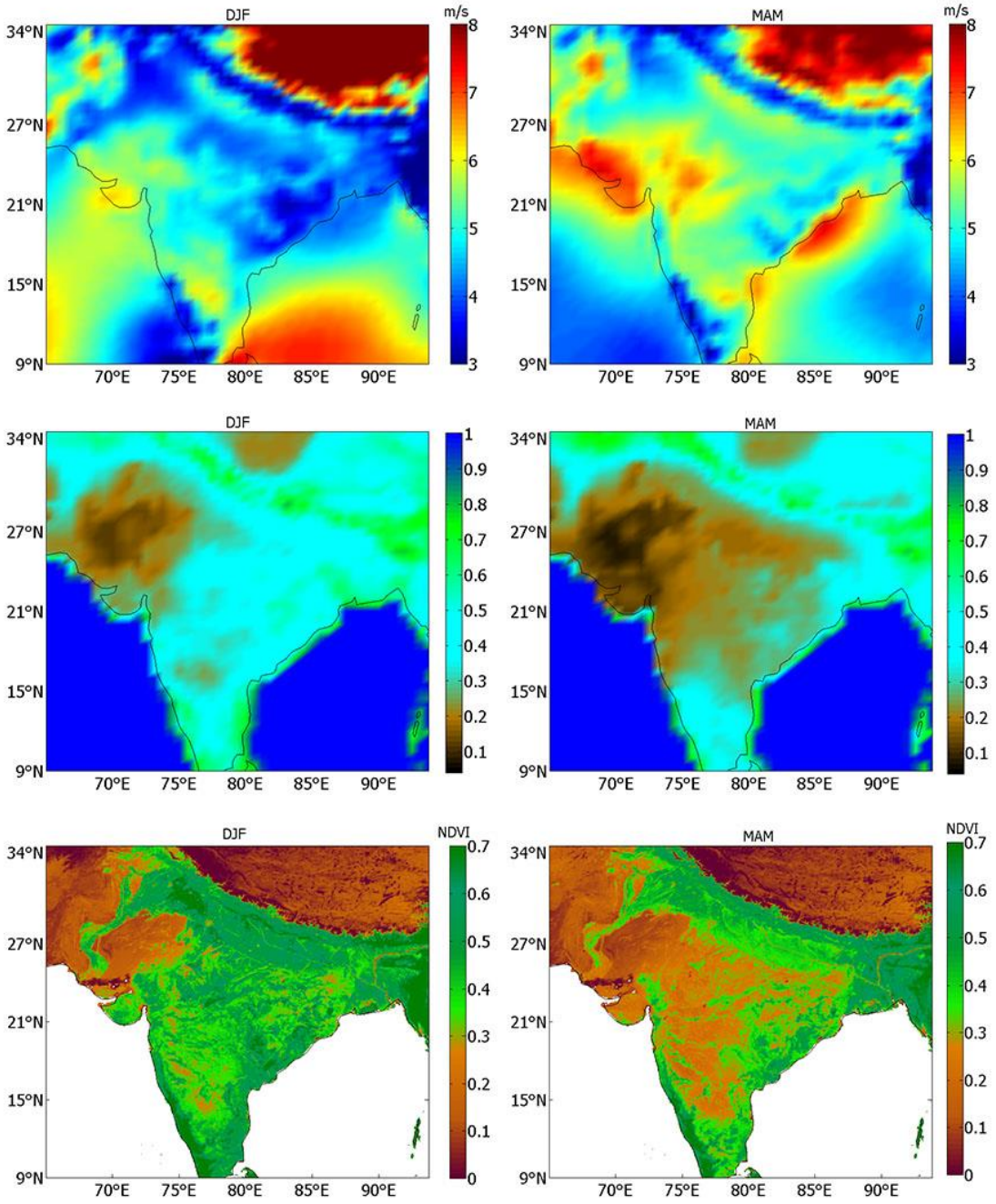


***Figure 3.15*** *- Variation of wind speed at 1000 hpa (MAM) (Upper panel), soil moisture (Middle panel) using MERRA-2 model re-analysis, and Normalized Difference in Vegetation Index (NDVI) from winter (DJF) to pre-monsoon (MAM) averaged over the years 2007 - 2016.*

### 3.4.6 Quantification of mineral dust aerosols in the elevated system

Many studies have shown the importance of integrating the radiative effects of mineral dust in climate models to yield better accuracy in climate predictions *(Haywood et al., 2005)*. Spatial and temporal characterization of dust loading is one of the major requisite in the accurate assessment of dust radiative impacts *(Sokolik et al., 2001).* Vertical

distribution of dust is another major factor that plays an important role in the assessment of dust radiative effects *(Quijano et al., 2000)*. Dust simulations by most of the climate models shows significant deviation from the observations *(Wu et al., 2018).* In this study, a quantitative analysis on vertical distribution of mineral dust aerosols is carried out for the first time over the Indian region using depolarization observations of CALIOP at 532 nm. While profiles of extinction coefficient provide aerosol abundance at different altitudes, PDR gives the relative dominance of non-spherical particles in the aerosol system which is made use for detecting and quantifying dust aerosols. Following the methodology described in section 2.2.1.6 of chapter 2, dust extinction coefficient over Indian region is retrieved using CALIOP observations of PDR. Figure 3.16 shows the three dimensional distribution of dust extinction coefficient over the Indian region. High dust extinction coefficient is observed over west Asia, North West India, and IGP during pre-monsoon season from the surface to up to 4 km. The surface/meteorological conditions favours the aloft of dust particles during pre-monsoon and extensive summer monsoon rainfall decreases the dust loading during summer monsoon period. During summer monsoon season, intense dust loading is observed over west Asia and north-west India, while it is reduced over the remaining parts of India owing to monsoon washout. Low dust levels were reported over the Arabian Sea during summer monsoon season (ship-borne chemical analysis of aerosols) due to the effect of monsoon low level jet that blocks the direct dust transport to Arabian Sea, along with high levels of sea-salt aerosols generated by the strong surface winds *(Tindale and Pease, 1999).* During post monsoon, anomalous dust loading is observed over IGP at the surface due to higher surface temperature after monsoon rains facilitating the dust emission that decreases as the season changes to winter as the surface temperature drops due to the movement of ITCZ to the southern hemisphere. Several studies have been carried out using the lidar depolarization ratio technique to differentiate dust extinction from the total extinction *(Shimizu et al., 2004; Sugimoto and Lee, 2006; Tesche et al., 2009). Yu et al., (2010)* estimated dust fraction from CALIOP measurements using a broad classification, based on threshold PDR and compared with GOCART simulations over regions of distinct aerosol systems. It showed that over the Indian mainland GOCART underestimates CALIOP by 24% to 40%. A similar analysis of estimation of dust deposition over Amazon region shows that CALIOP based dust estimate is more agreeable with in situ measurements than MODIS derived dust deposition while the modelled dust using different climate models clearly underestimated the dust observed using CALIOP, MODIS and in situ measurements *(Yu, Chin, Yuan, et al., 2015).*

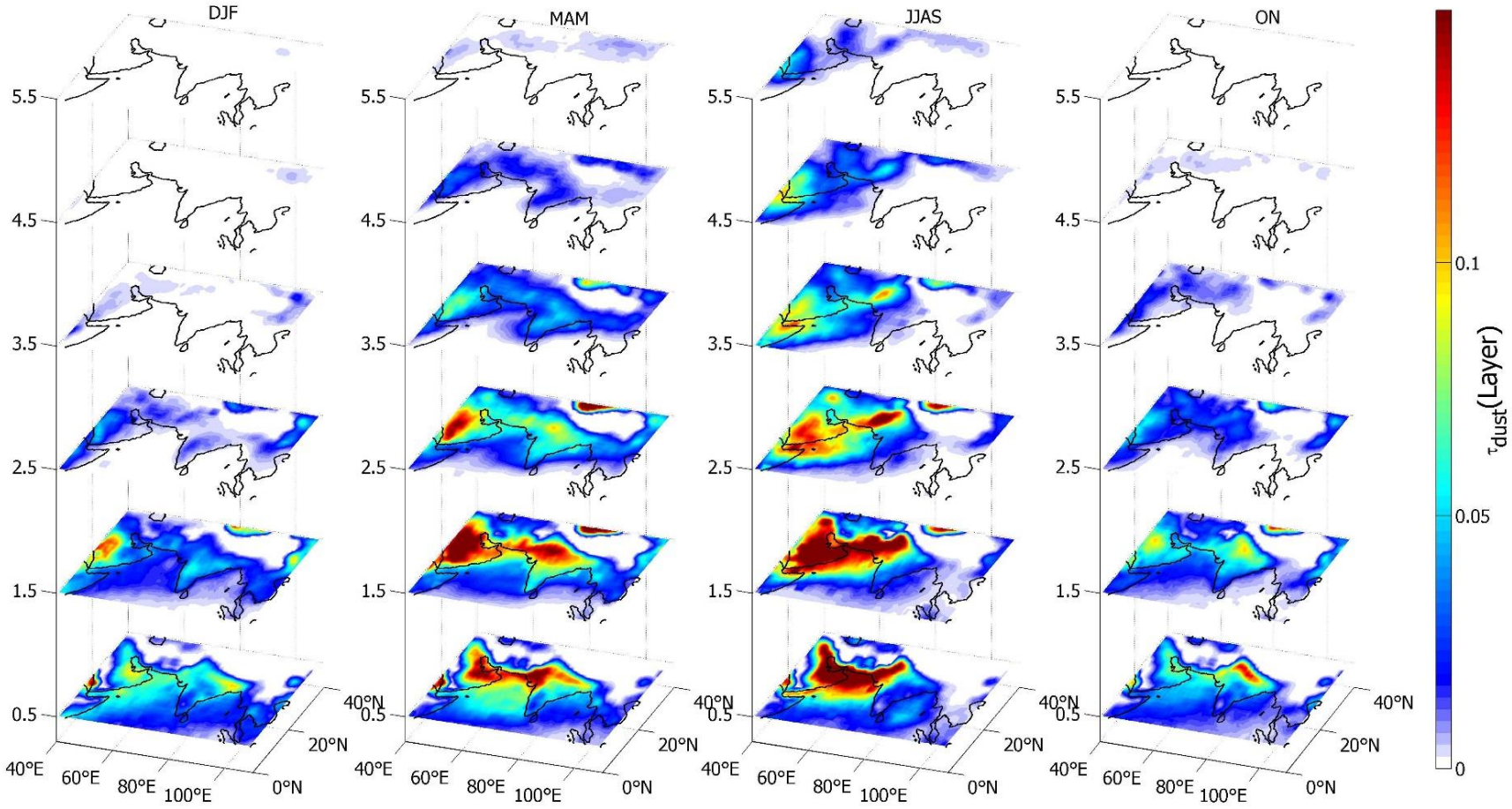


***Figure 3.16 -*** *Three-dimensional distribution of dust extinction coefficient during winter (DJF), pre-monsoon (MAM), summer monsoon (JJAS), and post monsoon (ON) seasons. Layer integrated dust extinction coefficient ($\tau_{dust}$(Layer)) at each layers of 1km width (for 0 to 1 km, 1 to 2 km, 2 to 3 km, 3 to 4 km, 4 to 5 km, and 5 to 6 km are shown at 0.5, 1.5, 2.5, 3.5, 4.5 and 5.5 km respectively.*

Figure 3.17 shows the monthly mean profiles of PDR (Upper panel) and dust extinction coefficient (lower panel) over the years 2006 to 2017 over the distinct regions of Indian landmass.

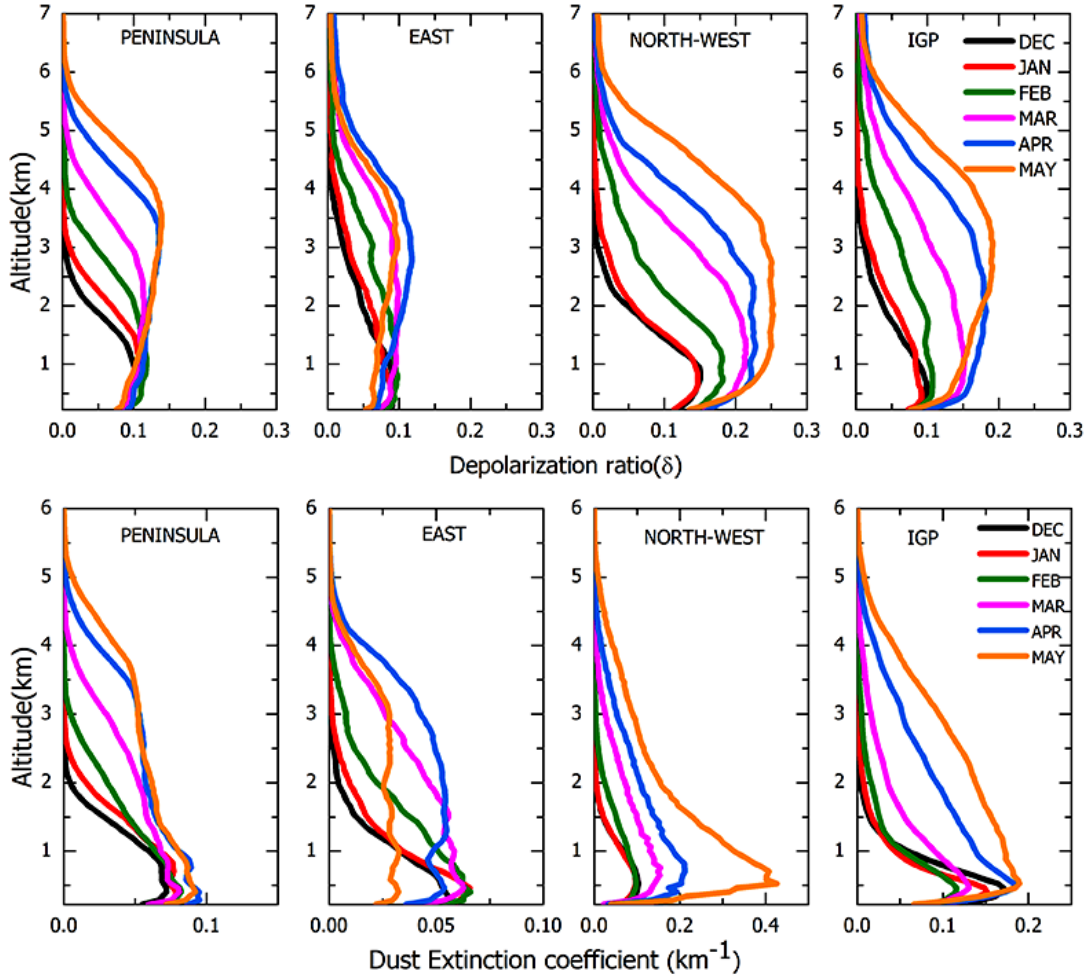


***Figure 3.17-*** *Monthly mean profiles of PDR (upper panels) and dust extinction coefficient (lower panels) over the Indian region (December to May) averaged over the period 2006 – 2017.*

It shows that the magnitude of PDR increases with altitude and peaks within 1 – 4 km over different regions of Indian landmass. It indicates that relative contribution of dust aerosols in the scattering volume is increasing from surface and reaches maximum in this altitude range. In case of convective lifting, increasing concentration of dust at higher altitudes is least expected since along with dust other fine particles will also lift up which will reduce the PDR at higher altitudes. But here PDR is peaking at a specific altitude range (2 – 4 km) indicating that dust particles are additionally contributed by horizontal advection from nearby dust sources. Dust extinction coefficient drastically increases from winter to pre-

monsoon months and peaks in the month of May throughout the vertical column. Magnitude of dust extinction coefficient is higher over IGP/north west compared to peninsular and eastern India. Dust extinction coefficient over IGP/North-west within PBL is significantly higher (~0.1 to 0.2 $km^{-1}$) compared to that at the free troposphere indicating possible dust emission within PBL over this region. . Whereas over peninsula and eastern India, during pre-monsoon months, dust extinction coefficient remains same from surface to up to ~ 4 km indicating the role of horizontal transport in contributing dust aerosols in the free troposphere. Figure 3.18 shows the three dimensional distribution of seasonal enhancement (pre-monsoon minus winter) in PDR and dust optical depth from winter to pre-monsoon over the Indian region.

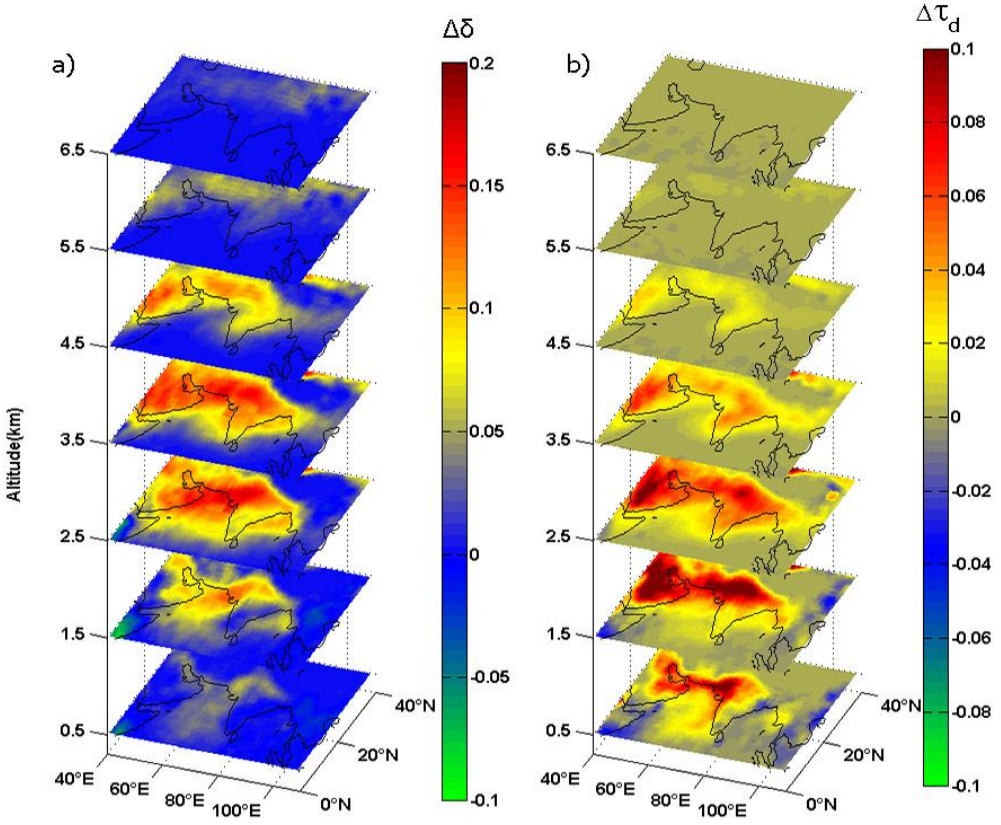


***Figure 3.18 -*** *Three-dimensional distribution of enhancement in a) PDR (Δδ) and b) dust optical depth ($\Delta\tau_d$) from winter to pre-monsoon.*

Figure 3.18 indicate significant enhancement in dust loading in lower troposphere during pre-monsoon compared to winter. Dust loading over Indian region shows at west to east gradient with high loading over the west that gradually reduces towards the east. The enhancement in dust loading is observed from the surface to 5 km altitudes, which is in line with the aircraft measurements during regional aerosol warming experiment *(Babu*

*et al., 2016)*. It should be noted that the absorption potential of pre-monsoon aerosols over India are higher than that of winter despite the severe haze and fog events (resulted from the accumulation of anthropogenic and biomass burning aerosols due to meteorological confinement) during winter. Anti-cyclonic circulation (associated with a high pressure) is persistent over the Indian landmass throughout winter and pre-monsoon. This forms at lower altitudes during winter and inhibits the vertical transport of aerosols during season, while this circulation is shifted to upper altitudes during pre-monsoon, allowing vertical transport of aerosols from the surface to higher height levels.

Figure 3.19 shows the monthly variation of mean dust optical depth (2006 - 2017) along with climatological mean of AOD obtained over the study regions using ARFINET.

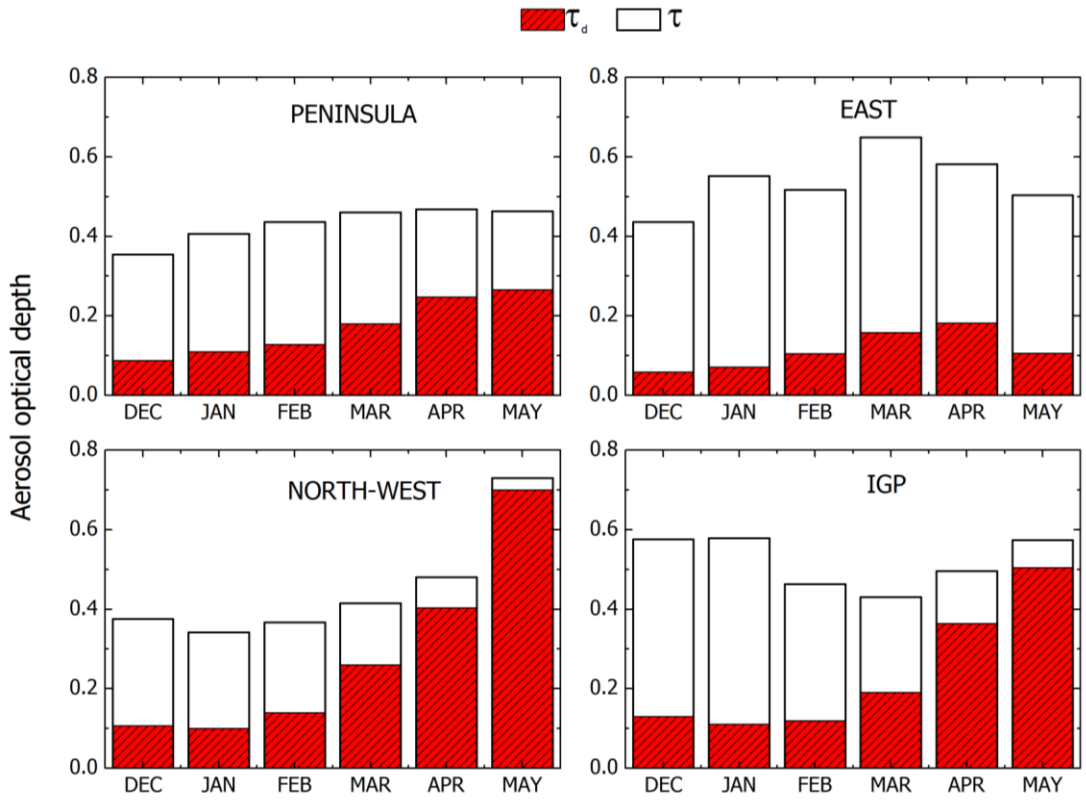


***Figure 3.19 -*** *Monthly variation of AOD (τ) and dust AOD ($\tau_d$) over the study regions using ARFINET and CALIOP observations over the period 2006 – 2017.*

AOD remains more or less constant during pre-monsoon months over peninsula and the dust optical depth consistently increases from December to April/May with a dust contribution of 25% in December and 57 % in May. But the climatological state of AOD remains more or less same during the pre-monsoon months over the Peninsula. Over East though there is significant monthly variation in AOD there is a consistent increase in the

dust AOD from December to April which falls off in the month of May which could be attributed to the characteristic stronger pre-monsoon showers over this region. Over North-west/IGP dust aerosols modulates the AOD indicated by the consistent increase in AOD with dust optical depth during the pre-monsoon months. Using the ARFINET measurements during the pre-monsoon of 2006 (March to May 2006) over the Indian land mass, *Beegum et al., (2008)* observed that over the IGP/northern India, aerosol loading peaked during May while over peninsula, it peaked during April and decreased thereafter, which is attributed to the long range transport of coarse mode particles from the west/north west regions of India. Increasing dust fraction over Indian region during pre-monsoon months indicates subsequent decrease in other emissions during this season. Monthly variation of dust fraction from winter to pre-monsoon over the study regions, shown in figure 3.20, depicted a drastic increase in dust fraction from December to May over northwest India and IGP. Over IGP columnar dust fraction increases from 22% to 87% while over north-west India, it reaches around 99% in the month of May. Over peninsula, columnar dust fraction varies from 24% in December to 57% in May and over eastern India it is from 13% to 21%.

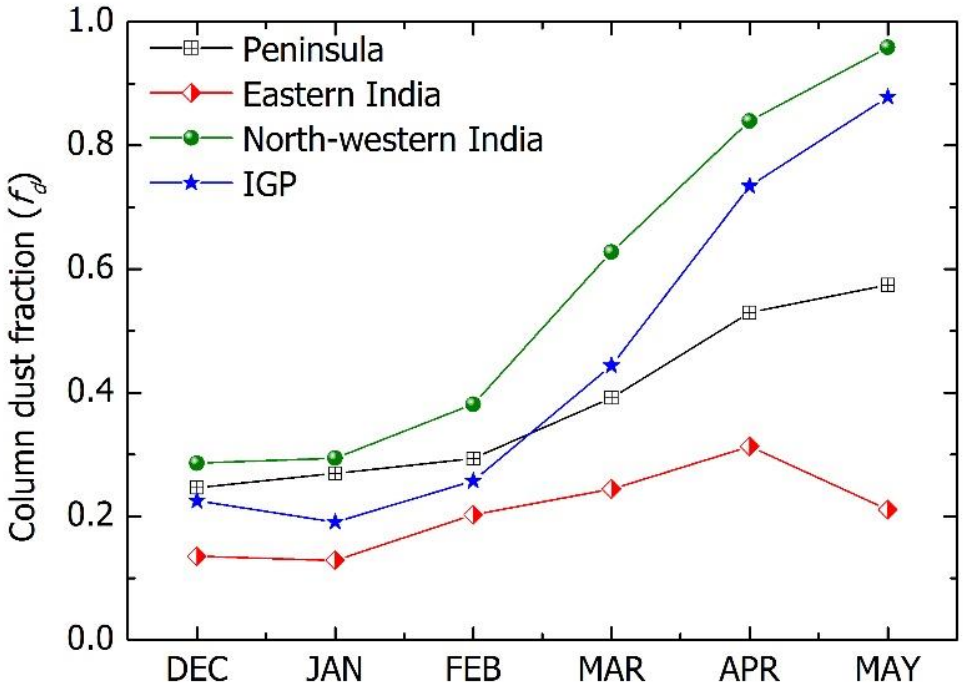


***Figure 3.20*** *- Monthly variation of columnar dust fraction ($f_d$) over the study regions from winter to pre-monsoon.*

Table 3.3 lists the mean values of AOD, dust optical depth, and dust fraction over the Indian region during the period 2006 – 2016.

***Table 3.3 -*** *AOD ($\tau$), dust optical depth ($\tau_d$) and dust fraction ($f_d$) over the study regions on Indian landmass over the period 2006 - 2017.*

| **Region** | $\boldsymbol{\tau}$ | | $\boldsymbol{\tau_d}$ | | $\boldsymbol{f_d}$ | |
|---|---|---|---|---|---|---|
| | **DJF** | **MAM** | **DJF** | **MAM** | **DJF** | **MAM** |
| **Peninsula** | 0.42±0.08 | 0.46 ± 0.08 | 0.1±0.02 | 0.23 ±0.04 | 0.25 ±0.07 | 0.51±0.11 |
| **Eastern India** | 0.59±0.16 | 0.73 ± 0.24 | 0.07±0.02 | 0.15 ±0.04 | 0.12 ± 0.05 | 0.21±0.09 |
| **North-west India** | 0.35±0.05 | 0.48± 0.06 | 0.11±0.02 | 0.43±0.06 | 0.33 ± 0.08 | 0.90±0.16 |
| **IGP** | 0.63±0.27 | 0.53 ± 0.1 | 0.12±0.04 | 0.36±0.05 | 0.13 ± 0.1 | 0.67±0.15 |

Atmospheric dust load is contributed by both natural and anthropogenic sources. Anthropogenic sources of dust include dust emission from disturbed soil (Deforestation, agriculture, urban and industrial practises) and changes in surface water (drying of water bodies) induced by anthropogenic influence. This is termed as "anthropogenic dust " *(Tegen et al., 1996; Huang et al., 2015)*. According to *Tegen et al., (1996)*, half of the modern atmospheric dust load is originated from anthropogenically disturbed soils. Assuming that anthropogenic dust aerosols are confined within PBL, *Huang et al., (2015)* identified a threshold PDR of 0.23 that can be can be used to separate anthropogenic dust from natural dust within the PBL. This indicates that anthropogenic dust aerosols are more spherical (mostly from disturbed lose soil) compared to the natural dust emitted from the soil surface through process like saltation and sand blasting. Characterized by different size and shape anthropogenic dust aerosols May have different scattering characteristics compared to natural dust. Over Indian region 70.2% of that total land area is anthropogenic dust source regions characterized by agriculture and high land use. *Huang et al., (2015)* reported that over the entire Indian landmass ~76% of total dust load is contributed by the anthropogenic dust aerosols.

High aerosol loading over the northern latitudes of Indian subcontinent, with large (~4 km) vertical spread and significant mineral dust fraction, prior to the onset of Indian summer monsoon might have significant impact on the dynamics of Indian monsoon circulation and associated rainfall. Moreover, dust over Indian region is mixed with other species like BC which makes them more absorbing even in visible wavelengths *(Deepshikha et al., 2005; Chinnam et al., 2006; Moorthy et al., 2007).* Absorption of radiation

by these dust dominated aerosol systems and consequent atmospheric heating could be considerably large, especially at higher elevations, so that it can alter the meridional temperature and pressure gradients. In addition, the atmospheric heating due to elevated aerosol absorption can be intense enough to alter the vertical temperature profile, atmospheric stability and hence the processes such as cloud formation. Aerosol absorption over the foothills of Himalaya might strengthen the south Asian monsoon through the hydrological cycle feedback mechanism proposed in the Elevated Heat Pump (EHP) hypothesis *(Lau et al., 2006).*

### 3.5 Summary

The study depicts the three-dimensional state of elevated aerosols and their seasonal evolution over the Indian region using multi-year (2006 - 2017) observations from the space-borne lidar, CALIOP. Since the assumption of lidar ratio in the retrieval of aerosol extinction coefficient from lidar back-scattered signal can causes error in estimations, ground based aerosol measurements from ARFINET are used to correct the CALIOP retrieved extinction values. Using aerosol chemical transport model simulations, plausible implications of pre-monsoon enhancement observed at free tropospheric altitudes over the Indian region is discussed in the chapter. Concluding points are following

- Vertical spread of aerosols is higher during pre-monsoon season which extends up to 4.5 to 5 km, while during winter these aerosols resides within 3 to 3.5 km (below which 98% of aerosols resides)
- Distinct meridional variation is observed in aerosol vertical distribution over the Indian landmass with higher vertical spread at northern latitudes that reduces towards the southern latitudes.
- Over Indian landmass, the enhancement in aerosols at higher altitudes observed as season changes from winter to pre-monsoon followed by a decrease in aerosol loading within PBL. This pre-monsoon enhancement in elevated aerosols have high particle depolarization ratio indicating the prominent role of mineral dust in the elevated aerosol system over the Indian region.
- Using depolarization observations of CALIOP, contribution of mineral dust to the total system of aerosols is quantified and three dimensional distribution of dust optical depth over the Indian region is presented. Dust fraction is highest over the source regions over the north-western India (90%) and is least over the eastern India (21%). During pre-monsoon season, IGP and Peninsular India are characterized by ~ 51% and ~ 67% of dust aerosols respectively.

# Chapter 4

# Altitude distribution of aerosols over oceanic regions around Indian subcontinent

## 4.1 Introduction

Over marine environment continental outflows make the aerosol system more complex. There have been several attempts to characterize aerosols over the oceanic regions of India through ship cruises and long term observations from islands *(Ramanathan et al., 2001; Li and Ramanathan, 2002; Satheesh and Srinivasan, 2002; Moorthy and Babu, 2006; Babu et al., 2008, 2012; Nair et al., 2009; Moorthy et al., 2010).* The Indian Ocean Experiment (INDOEX) carried out extensive aerosol measurements that focused on continental outflow over northern Indian ocean and Arabian Sea during winter period *(Moorthy and Saha, 2000; Ramanathan et al., 2001; Leon et al., 2001; Forêt et al., 2005)*. Arabian Sea Monsoon Experiment (ARMEX) carried out under Indian Climate Research Programme (ICRP) explored the seasonal changes in aerosol properties over the southeastern Arabian Sea and northern Indian Ocean from winter to summer monsoon seasons *(Vinoj and Satheesh, 2003; Babu et al., 2004, 2008; Moorthy, Babu, et al., 2005)*. Integrated Campaign for aerosols, gases and Radiation Budget (ICARB) during pre-monsoon 2006 and winter 2009, inclusively examined oceanic regions adjoining Indian land mass with multi-platform measurements including ship-borne and air-borne measurements *(Moorthy et al., 2008; Babu et al., 2012)*. ICARB provided substantial observations over the Bay of Bengal which was least explored in the previous campaigns. In addition, there have been several efforts to examine the aerosol loading over the oceanic regions of India using satellite observations such as Advanced Very High Resolution Radiometer (AVHRR) *(Rajeev et al., 2000)* and Meteosat *(Leon et al., 2001)* during the period of these experiments *(Rajeev et al., 2000; Satheesh and Ramanathan, 2000; Pelon et al., 2002; Satheesh, Deepshikha, et al., 2006; Krishnamurti et al., 2009).*

Over tropical region and sub-tropical oceans mineral dust radiative effects are particularly large because of their proximity to arid regions that produces mineral dust aerosols *(Prospero, 1979).* Mineral dust transport over to the ocean can affect the thermodynamic

state of the oceanic atmosphere by diabatically heating the atmosphere. Dust induced modulations in Indian summer monsoon over weekly time scale clearly shows the potential of dust aerosols to produce changes in synoptic scale circulations and regional climate *(Jin et al., 2014; ; Vinoj et al., 2014; Solmon et al., 2015).* Its deposition over the ocean surface affects the ocean biota and subsequent bio-geo chemical cycles, especially over the Bay of Bengal (BoB) where marine biota essentially depends on the transport of nutrients from the continental region *(Nair, Moorthy, et al., 2013; Banerjee and Prasanna Kumar, 2014).* Though several studies have reported predominant dust loading over the Arabian Sea (AS) *(Moorthy, Babu, et al., 2005; Satheesh and Srinivasan, 2002)* dust characterization over the BoB is very limited. Though aerosol properties in the atmospheric column and at surface are well characterized over the BoB through ship-borne measurements under ICARB *(Vinoj and Satheesh, 2003; Babu et al., 2004, 2008; Moorthy et al., 2008)* and satellite observations *(Li and Ramanathan, 2002; Rajeev et al., 2000; Satheesh and Ramanathan, 2000),* the vertical distribution of aerosols and contribution of mineral dust aerosols to the columnar aerosol loading are not attempted over the region. In this context, it is imperative to have a comprehensive picture on the spatial and seasonal characterization of the elevated aerosol system over the oceanic regions around India and the transport of dust aerosols over these regions, which are evidently influential on the regional climate and the monsoon system. The chapter focuses on the characterization of vertical distribution of aerosols over Arabian Sea and the Bay of Bengal, quantifies the optical depth of dust aerosols, and examines their recent decadal trend.

## 4.2 Data set

The major datasets used in the present chapter are the vertical profiles of back-scattering coefficient and depolarization ratio derived from the CALIOP (Level 2 data) on board CALIPSO along with AOD at 500 nm from MODIS on board Aqua. CALIOP profiles are averaged over the required spatial and seasonal scales and climatological mean vertical profiles of aerosol extinction coefficients are obtained. The cloud screening and other quality check procedure followed for the CALIOP data is described in chapter 3 (Refer section 3.2). MODIS-AQUA being flown in formation with CALIPSO provides fairly collocated measurements with better spatial resolution and can be used to improve the CALIPSO extinction coefficient profiles by circumventing the AOD bias that is caused by the ambiguity of the assumed lidar ratio (Refer chapter2 Section 2.2.1.5). The AOD is obtained from level 3 MODIS collection 6 (MYD08_M3) QA weighted (AOD is weighted with Quality Assurance (QA) score that indicate the level of reliability of retrieval) data

product over the ocean. Figure 4.1 shows an inter-comparison the scatter plot of AOD from MODIS with simultaneous AOD observations carried during various ship-based campaigns using the Microtops sunphotometer. MODIS derived AOD at 550 nm showed good agreement with the ship-borne measurements with a correlation coefficient of 0.91 and slope of 0.95 *(Nair, Babu, Moorthy, & Prijith, 2013).*

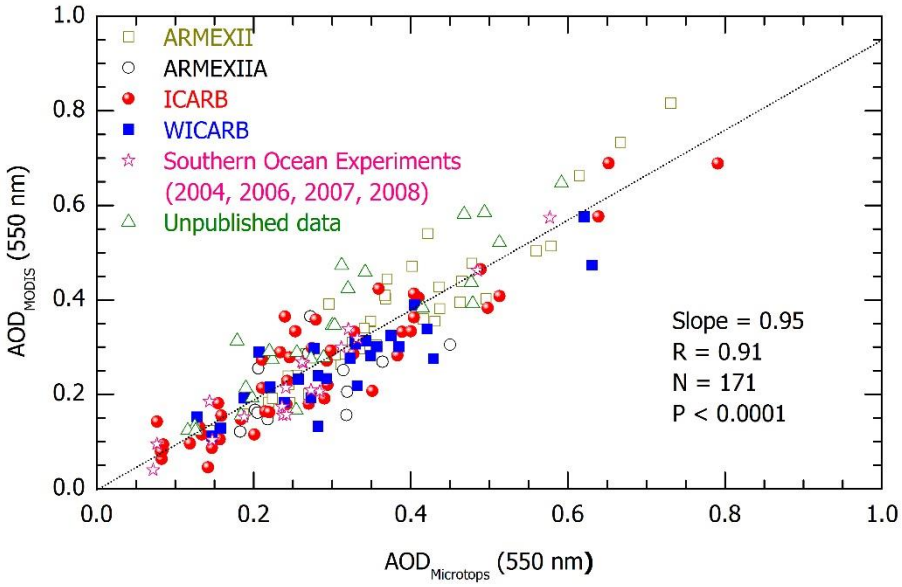


***Figure 4.1 -*** *Scatter plot of MODIS derived AOD and ship-borne AOD observed during various ship-campaigns around the Indian region (Nair, Babu, Moorthy, & Prijith, 2013).*

As discussed in chapter 2 (section 2.2.15), CALIOP observations significantly underestimate the AOD over the globe due to limitations in the assumed lidar ratio and associated uncertainty in the retrieved aerosol extinction coefficient. Thus, to reduce the uncertainty, MODIS derived AOD is used to scale the vertical profile of aerosol extinction coefficient retrieved by the CALIOP *(Takamura et al., 1994)*. In the present study each mean profile include ~1300 daily data, which corresponds to more than 100 thousand individual profiles. Aerosol extinction coefficient shows a relative standard deviation of 50% to 100% in the lower range bins (0 - 1.5 km) and increases at higher altitudes while relative standard deviation for dust extinction coefficient is in the range 100 % - 160 %. From version 3 onwards CALIOP level 2 data product are provided with uncertainty estimates of extinction coefficient, back-scattering coefficient and PDR values based on profile calibration, signal to noise ratios and biases in the lidar ratio assumption. Details of the uncertainty estimation and its propagation in various aerosol parameters are described in *Young et al., (2013)*. Present study make use of uncertainty information provided with CALIOP level 2 version 4.1 data product along with the uncertainty in

various assumed aerosol parameters to calculate the uncertainty propagated in the derived parameters (Refer chapter 2) and is shown as horizontal error bars in the following figures. Details of the datasets is given table 4.1.

***Table 4.1*** *- Details of datasets used in the study*

| Data Source | Parameter | Period |
|---|---|---|
| **CALIOP (Level 2 version 4.1)** | Aerosol back-scattering coefficient (0.532 μm) | 2006 -2007 |
| | Aerosol extinction coefficient (0.532 μm) | 2006 -2007 |
| | Particulate depolarization ratio (0.532 μm) | 2006 - 2017 |
| **MODIS (Level 3 Collection6)** | AOD<br>Fine-mode fraction of AOD | 2006 -2017 |
| **GOCART** | AOD | 2006 -2007 |
| **MERRA (Reanalysis)** | Wind (u and v components) | 2006 - 2016 |

Present chapter focus on the vertical distribution of aerosol over the Arabian Sea and the Bay of Bengal situated over the east and west of Indian peninsula respectively semi enclosed on the north and open to the Indian Ocean at the south. The Bay of Bengal, situated east to the Indian landmass, is confined within a latitude range of 22°N to 5°N and longitude range of 80°E to 100°E, bounded on the west by Peninsular India, on the north by Bangladesh and on the east by Myanmar and, Andaman and Nicobar Islands. Arabian Sea is situated within the latitude range 25°N to 5°N and is bounded on the north by Pakistan/Iran, on the west by the eastern limit of Gulf of Aden /the Arabian Peninsula, and on the east by Indian peninsula. Both these oceanic regions are under the influence of monsoon winds that brings moisture rich airmass from the Indian Ocean during south-west monsoon and polluted continental airmass during northeast monsoon. Convective processes over the Bay of Bengal plays an important role in the onset and progress of Indian monsoon through ocean-atmosphere coupling *(Gadgil, 2000; Bhat et al., 2001)*. Being located on the same latitudinal band, they receive same amount of solar insolation and similarly influenced by the transition of the Inter Tropical Convergence Zone (ITCZ). Annual mean rainfall over the Bay of Bengal is almost three times greater than that over Arabian Sea *(Martin et al., 1993)* and probability of cyclone occurrence is more over the Bay of Bengal owing to higher sea surface temperature compared to Arabian Sea.

Following sections discuss on the spatial characterization of aerosols over the Arabian Sea and the Bay of Bengal.

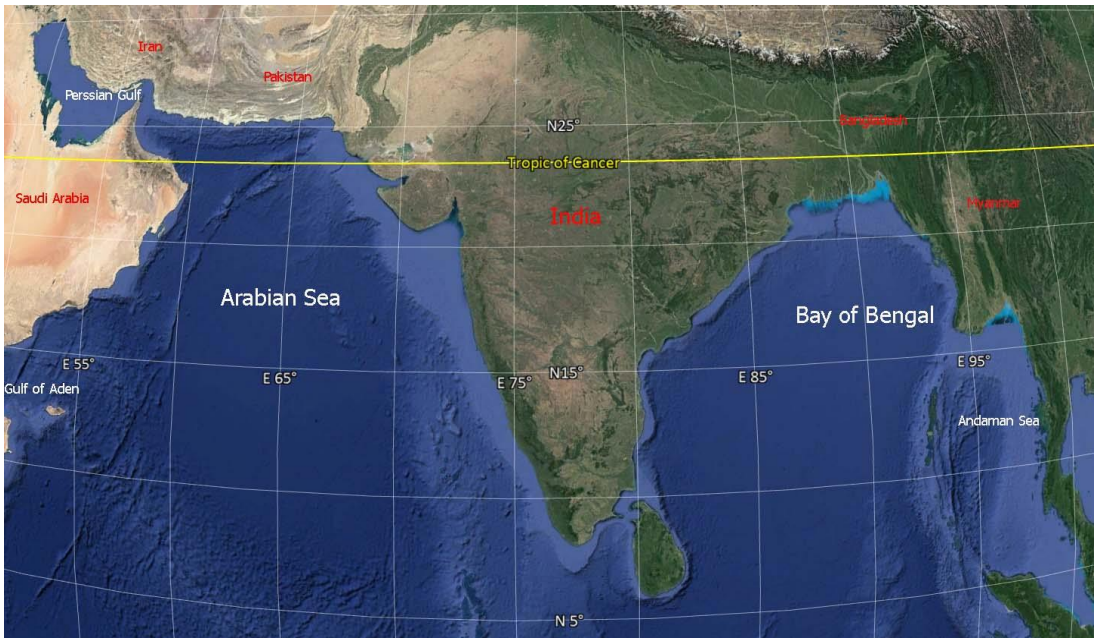


***Figure 4.2*** *- Geographical Map of the Arabian Sea and the Bay of Bengal (Courtesy – Google Earth)*

## 4.3 Results and discussion

### 4.3.1 Climatological state of aerosol optical depth over the oceans

Over the marine environment, though sea-spray constitutes the major source, continental outflows make the aerosol system more complex. Figure 4.3 shows the mean spatial variation of MODIS AOD at 550nm over the AS and BoB during winter season (December, January, and February (DJF)) and pre-monsoon season (March, April and May (MAM)) along with the wind field at 975 hPa from MERRA reanalysis. Aerosol characteristics over the marine environment surrounding Indian region are governed by the seasonally varying circulation pattern which favours the transport of continental aerosols over the oceanic region during winter (Dec – Feb) and pre-monsoon (Mar – May) seasons. Winds are northerly/north easterly during winter which carry polluted air from the continental region to the open ocean which undergo a transition at the lower levels from northerly to westerly during pre-monsoon. During pre-monsoon season, aerosols are more extended towards the open ocean while in winter they are mostly confined close to coastal regions. Figure 4.4 shows the climatological mean value of AOD over northern and southern regions of BoB and AS. AOD during pre-monsoon season is observed to be higher than winter AOD over the entire study region.

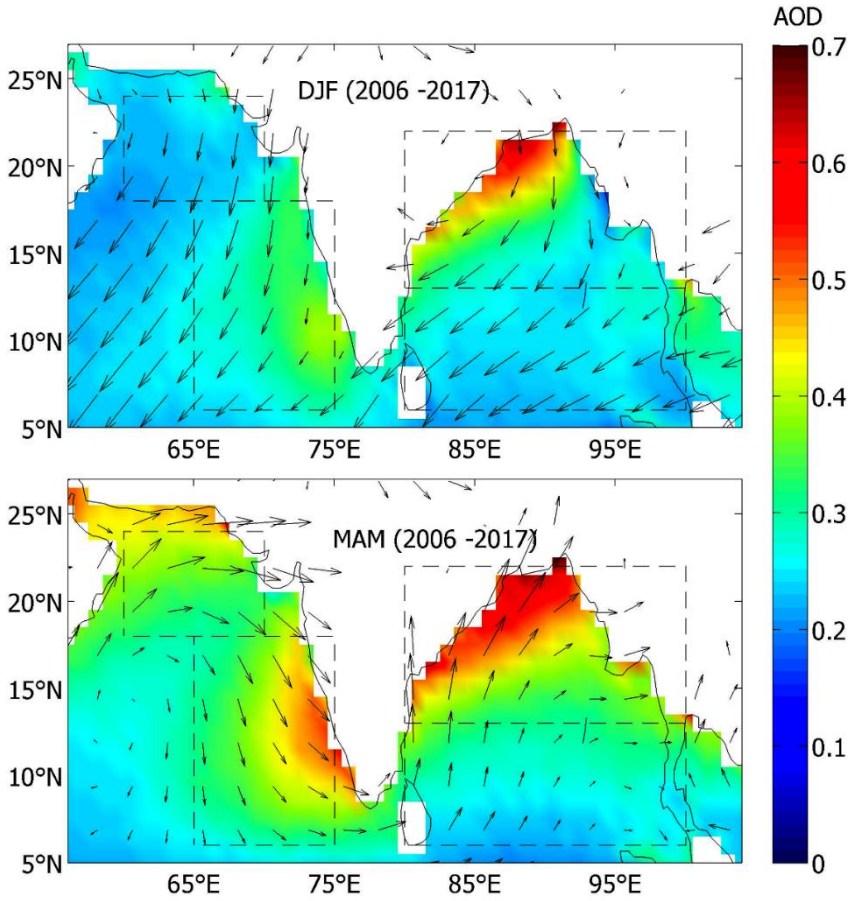


***Figure 4.3*** *- Climatological distribution of AOD over the Arabian Sea(AS) and Bay of Bengal(BoB) using MODIS observations during winter (DJF) and pre-monsoon season (MAM) of (2006-2017). Study regions include northern BoB (13°N - 22°N, 80°E - 100°E), southern BoB(5°N - 13°N, 80°E - 100°E), northern AS (18°N - 24°N, 60°E - 70°E) and southeastern AS(6°N - 18°N, 65°E - 75°E) . Wind pattern at 975 hPa is shown in the figure.*

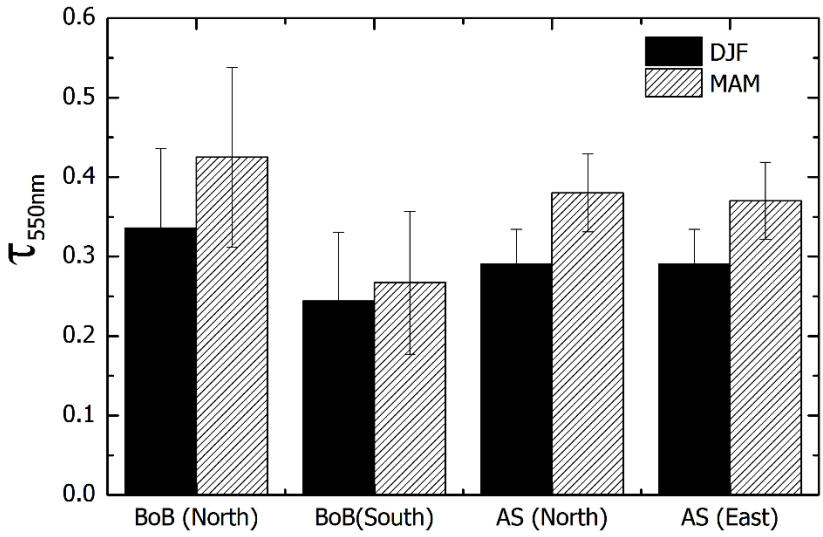


***Figure 4.4*** *– Mean AOD at 550 nm from MODIS over the study regions during the period 2006 – 2017.*

Table 4.2 lists reported values of AOD at mid-visible wavelength (~500 nm) and Ångström exponent (α) over the AS and BoB during the previous experiments.

***Table 4.2*** *- AOD and Ångström exponent (α) reported in the literature over the study regions.*

| Location | Experiment | Period | τ | α | Reference |
|---|---|---|---|---|---|
| **AS NIO** | Pre-INDOEX cruise | Jan-Feb 1996 | 0.2 -0.5 | 0.8 | Jayaraman et al., (1998) |
| **AS NIO** | INDOEX | Jan-Mar 1999 | 0.1 – 0.4 | 0.5 -1.7 | Moorthy and Saha ( 2000) |
| **Eastern AS** | SK-161B | Mar 2001 | 0.35 ± 0.19 | 0.84 ± 0.38 | Satheesh and Sreenivasan., (2002) |
| **AS** | ARMEX | Jul-Aug 2002 | ~0.44 | ~0.35 | Moorthy et al., (2005) |
| **Northern AS** | ICARB | Mar–Apr 2006 | >0.15 | 0.76 ± 0.3 | Moorthy et al., (2009) |
| **Eastern AS** | | | ~0.5 | >1 | |
| **Northern BoB** | SK-161B | Mar 2001 | 0.44 ± 0.19 | 1.23 ± 0.43 | Satheesh (2002) |
| **Northern BoB** | SK-188 | Feb 2003 | 0.41 ± 0.14 | 1.1 ± 0.1 | Vinoj, (2004) |
| **Northern BoB** | ICARB | Mar–Apr 2006 | 0.49 ± 0.01 | ≥1.0 | Moorthy et al., (2009) |
| **Southern BoB** | | | 0.29 | ≥1.0 | Moorthy et al., (2009) |
| **Northern BoB** | WICARB | Jan 2009 | 0.19 ±0.03 | 1.43±0.08 | Moorthy et al., (2010) |
| **Southern BoB** | | | 0.27±0.03 | 0.8±0.17 | Babu et al., (2012) |

#### 4.3.1.1 The Bay of Bengal (BoB)

In general, the atmosphere over the BoB is found to be more turbid compared to the AS and Indian Ocean *(Kedia and Ramachandran, 2008; Moorthy et al., 2009).* Aerosols over the BoB are highly heterogeneous due to the influence of contrasting air masses from heavily inhabited surrounding landmasses *(Satheesh, Srinivasan, et al., 2006).* The spatial distribution of AOD shows significant aerosol loading over the northern and north western regions of the Bay of Bengal. These regions are also characterized by high values of Angstrom exponent and scattering coefficients indicating the presence of fine mode dominated anthropogenic aerosols *(Moorthy et al., 2010; Nair et al., 2009*). Ship-borne and island based measurements during winter showed higher Angstrom exponent over the eastern parts associated with high values of AOD indicating a fine mode outflow from the East Asian region *(Moorthy et al., 2003, 2010*). Aerosol parameters showed a prominent latitudinal gradient with high values over northern BoB that rapidly decreasing beyond

south of 13°N. Ångström exponent of AOD and scattering coefficient almost reduces to half over the southern BoB that clearly indicates a drastic change in the size distribution of aerosols *(Nair et al., 2009).* Based on the distinct signature of aerosol system observed north and south of 13°N over the Bay, aerosol features of northern BoB and southern BoB are investigated separately (as shown by dotted line in figure 4.3).

#### 4.3.1.2 The Arabian Sea (AS)

AS is a region under the influence of transported mineral dust of natural origin from west Asia *(Moorthy, Babu, et al., 2005; Babu et al., 2008)* and anthropogenic aerosols from the Indian sub-continent *(Krishnamurti et al., 1998; Rajeev et al., 2000; Ramanathan et al., 2001)*. These studies reported large spatial heterogeneity in aerosol loading over the Arabian Sea. Over AS, distinct plume of aerosols is observed off to south west coast of India and over the northern AS associated with the west Asian dust plume (as seen in figure 4.3). The region of high AOD over the Northern Arabian is designated as "west Asian High "by *Moorthy and Saha, (2000)* due to its close proximity to west Asian region based on ship-borne observations during INDOEX. Over the southeastern Arabian Sea, INDOEX observations showed the existence of a large distinct aerosol plume during winter months which was present during pre-monsoon *(Moorthy and Saha, 2000; Moorthy et al., 2009)*. *Krishnamurti et al., (2009)* termed this eastern plume to the 'Bombay plume', anthropogenic emission from the cities of Mumbai/Pune during the winter months and carried out simulations to find that a diverging outflow of these pollutants over to the BoB results in the reduction of winter rains over the southeast coast of India. MODIS observations over the Arabian Sea (figure 4.3) clearly showed the plume on the southeastern AS during winter and pre-monsoon seasons and the west Asian plume during pre-monsoon. Aerosol plume over the southeastern Arabian Sea is observed to be stronger during pre-monsoon compared to winter. Based on the spatial heterogeneity in aerosol optical depth over the AS, study regions are chosen over the northern AS (24°N - 16°N, 60°E - 69°E) which is under the influence of transport from the west Asian region, and also over the plume region on the southeastern AS off to the south west coast of India (16°N - 6°N, 65°E - 75°E) as shown in figure 4.3.

### 4.3.2 Vertical distribution of aerosols over the oceans.

Vertical characterization of aerosols over the oceanic regions around India is very limited other than the air borne/ship borne lidar observations carried out as a part of

INDOEX/ICARB. To comprehend on the vertical distribution of aerosol extinction, climatological mean (2006 – 2017) profiles of aerosol extinction coefficient are examined over the study regions for winter and pre-monsoon seasons. Following section elaborates on the seasonal evolution of aerosol vertical distribution over the study regions.

#### 4.3.2.1 The Bay of Bengal

The monthly mean profiles of aerosol extinction coefficient profiles from winter to pre-monsoon over northern and southern BoB is shown in Figure 4.5.

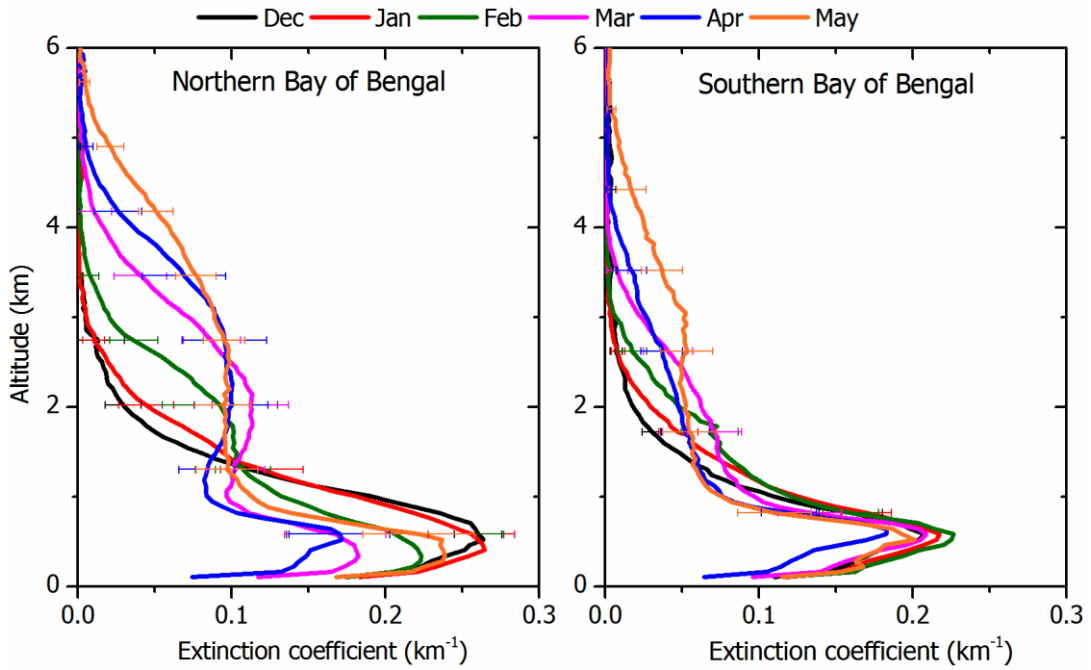


***Figure 4.5 -*** *Monthly mean profiles of aerosol extinction coefficient corrected with MODIS AOD from December to May during the period 2006 - 2017 over the Bay of Bengal.*

Over Northern BoB, from December to May there is a consistent increase in the magnitude and vertical extent of aerosols above ~ 1.5 km with a corresponding reduction below. This exactly resembles the monthly vertical variation of aerosols over the Indian land mass (especially the peninsular region) and clearly indicates that vertical distribution of aerosol over northern BoB is completely modulated by the aerosol transport from the mainland. However, over the southern Bay of Bengal, though the profiles of aerosol extinction coefficient above MABL showed an enhancement, the profiles within the MABL is more or less invariant. This clearly indicates that continental transport modulates the aerosol distribution throughout the entire column over the Northern BoB while it influence only above the MABL over the southern Bay of Bengal.

#### 4.3.2.2 Arabian Sea

Figure 4.6 represents the monthly mean (2006 - 2017) profiles of aerosol extinction coefficient over the Arabian Sea from winter to pre-monsoon (December to May).

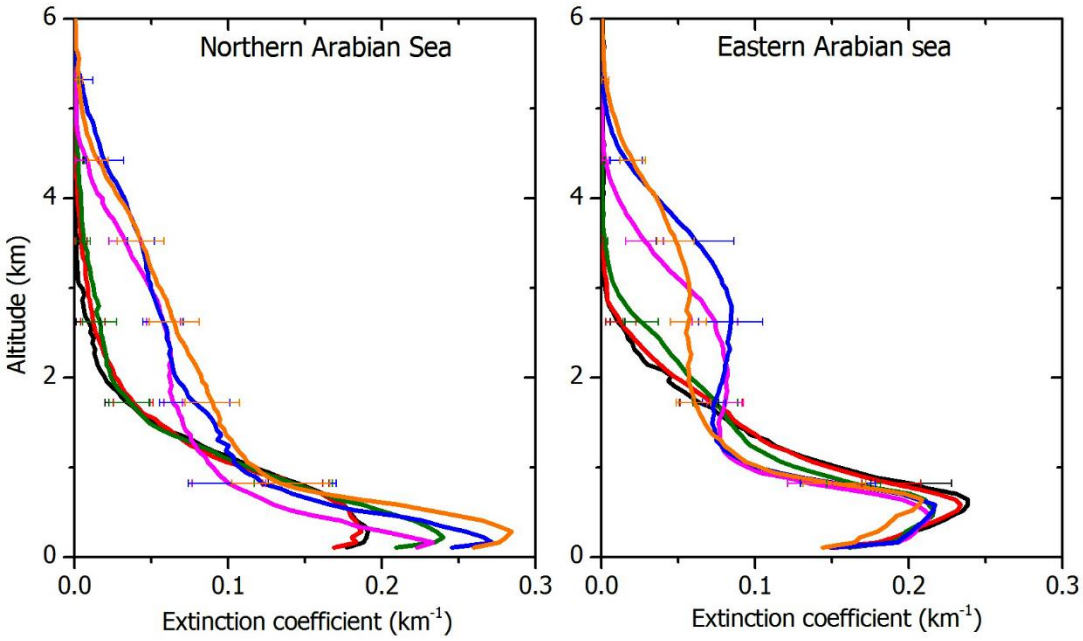


***Figure 4.6*** *- Monthly mean profiles of aerosol extinction coefficient corrected with MODIS AOD from December to May during the period 2006 - 2017 over the Arabian Sea.*

Vertical distribution of aerosols over the southeastern plume region of AS shows a significant enhancement in aerosol loading above ~1.5 km similar to that over Northern BoB, though a drastic reduction in aerosols below 1.5 km is not observed in this region. Over the northern AS, aerosol loading from winter to pre-monsoon is quite different from other regions. Here a consistent increase in aerosol loading is observed throughout the column from December to May contributed by the dust transport from the horn of Africa by the south westerly winds at the lower levels and north westerly from the Arabian Peninsula above MABL as seen in the circulation pattern shown in figure 4.7.

Figure 4.7 shows the circulation pattern above (700 hPa) and within the (975 hPa) MABL with colour variation indicating mean AOD at 550 of MODIS during winter and pre-monsoon. Role of circulation parameters in the transport of aerosols over to the oceanic regions of India has been studied during different campaign periods. Presence of anti-cyclonic vorticity over the central India during winter season has been shown to transport aerosol from the Indian mainland to the Bay of Bengal has been reported during winter

phase of ICARB that leads to an increase in AOD over the north/north-western part of BoB *(Prijith et al., 2012)*. Role of anticyclonic circulation in the generation of elevated aerosol plumes have been demonstrated over the west coast of the India based on satellite observations *(Aloysius et al., 2011).* North-westerly arm of anti-cyclonic circulation during winter and pre-monsoon seasons are favourable for the transport of polluted and dusty continental air mass over to the Bay of Bengal.

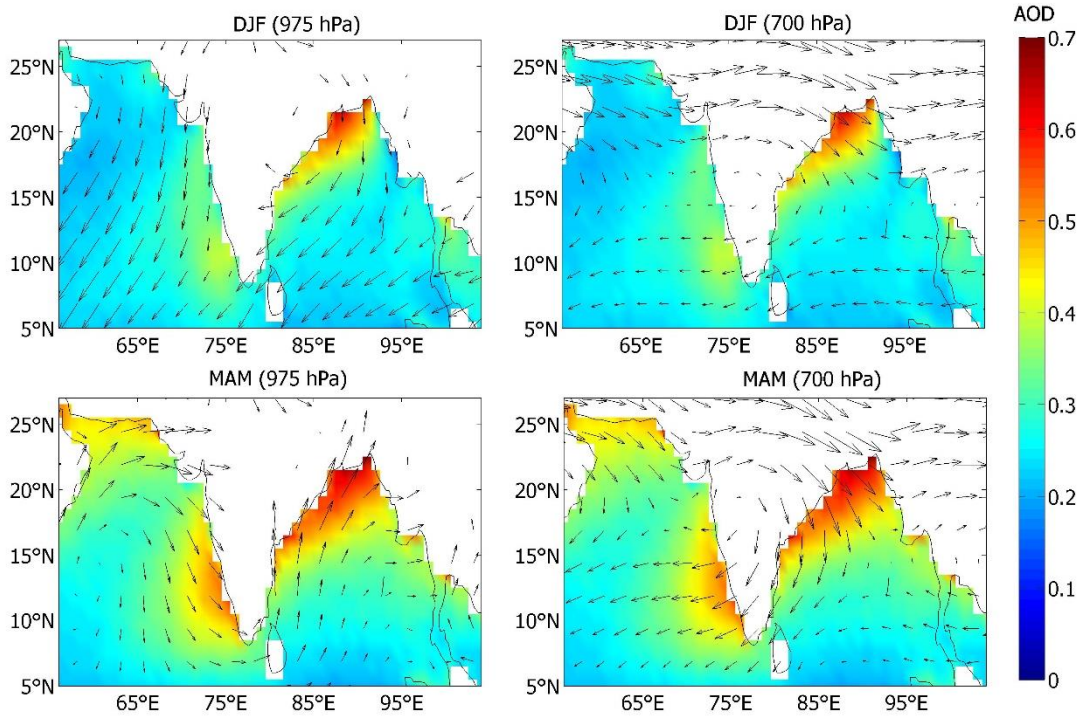


***Figure 4.7 -*** *Mean wind fields within MABL (975 hPa) and above MABL (700 hPa) over the period 2006 - 2017 over the study regions during winter and pre-monsoon using MERRA reanalysis data. Colour variation indicates AOD at 550 nm (MODIS).*

Transport from prominent dust sources of north-western deserts along with contribution from convectively lifted dust aerosols from the mainland make pre-monsoon season the most dust active period over Indian landmass and presence of this dominant upper level north-westerly winds as a part of anti-cyclonic circulation over the Indian landmass extending over the northern/western BoB enhance the possibility of dust transport over the BoB (Refer chapter 3, figure 3.1). Though it is present also during the winter season, reduced solar insolation and associated lesser surface heating makes it a dust dormant period. Hence presence of dust over the BoB during winter season is generally insignificant. However, to assess the impact of dust transport and its seasonal variation, it is important to quantify and estimate its contribution to the total aerosols. Thus, the contribution of dust to the total extinction coefficient is estimated using the depolarization

measurements from CALIOP as discussed in the chapter 2 section 2.2.1.6. Following section discuss on the altitude distribution of dust aerosols over the BoB and AS.

### 4.3.3 Altitude distribution of dust extinction coefficient over BoB and AS

The altitude distribution of extinction coefficient due to total aerosol and dust aerosols, over BoB and AS is shown in Figure 4.8. Aerosols over both the AS and the BoB have a seasonally distinct vertical structure. Winter time aerosols are mostly confined within the boundary layer due to diminished convection characteristic to the season.

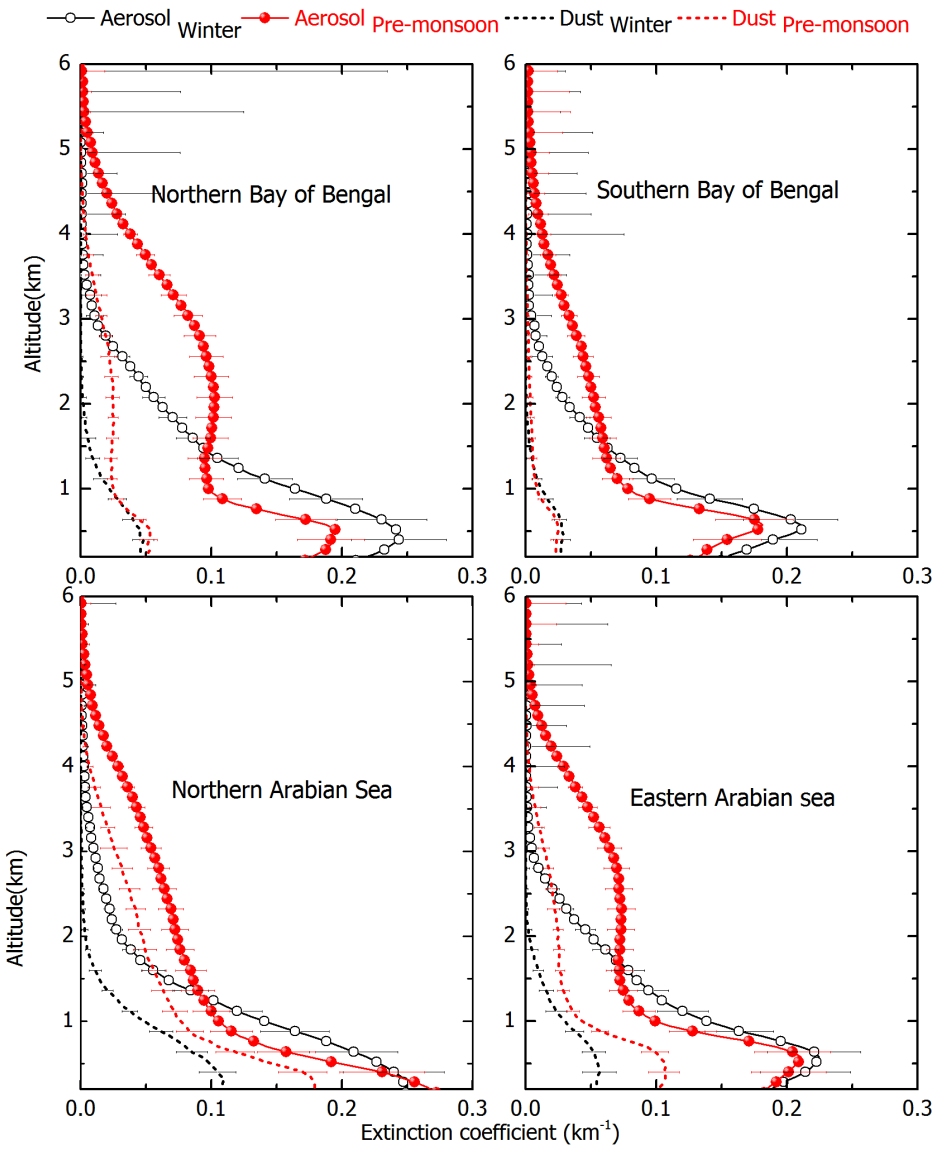


***Figure 4.8*** *- Vertical distribution of total aerosol extinction from CALIOP corrected with AOD from MODIS and dust extinction coefficient, separated using CALIOP depolarization observations over the study regions for winter (black) and pre-monsoon (red) during the period 2006-2017. Error bars represent the measurement uncertainty.*

During winter aerosol loading within the MABL is higher over the Bay of Bengal. As season changes to pre-monsoon, aerosol loading is enhanced above MABL. Vertical distribution of aerosol extinction coefficient shows a layer of enhanced loading in the altitude range of ~ 1.5 km to 5 km over the northern BoB. Dust aerosol extinction is observed to be significant in this altitude range. Over the Bay of Bengal aircraft based lidar measurements as a part of ICARB experiment clearly showed presence of elevated aerosols. Presence of elevated layers above marine atmospheric boundary layer off the coast of the BoB that extended up to ~600 - 800 km revealed the heterogeneous vertical structure persisting over this small, yet highly complex oceanic region *(Satheesh, Moorthy, et al., 2009)*. Over southern Bay of Bengal, aerosol extinction increases from surface to the top of the boundary layer and then falling off with altitude during both the seasons. Rate of reduction of extinction coefficient above marine boundary layer is higher for winter compared to pre-monsoon season. Magnitude of dust extinction coefficient is too low with no distinct seasonal variation. A well-defined boundary layer peak is observed, over the southern Bay of Bengal, at ~ 580 m associated with capping of aerosols and the peak height is found to be independent of the seasons while over the northern BoB a well-mixed boundary layer is observed during pre-monsoon season. A steady value of extinction coefficient ($0.19km^{-1}$) is observed over the northern BoB during pre-monsoon season from surface to ~ 530 m which decreases drastically to ~$0.1km^{-1}$ (marking marine boundary layer height) beyond 500 m up to 2.5 km. Winter time boundary layer over northern Bengal shows a broader peak compared to southern BoB with aerosol extinction coefficient varies in the range ~0.22 to 0.25 $km^{1}$. Vertical distribution of aerosol extinction coefficient over the southeastern AS shows a similar pattern with northern BoB during pre-monsoon season with enhanced aerosol loading within 1.5 to 5 km. Anti-cyclonic circulation over the Indian region strengthens at 700 hPa with a wind speed of 6 - 8 m/s that carries aerosols from the northwest India/ IGP to north/north western BoB and to the plume over the southeastern Arabian Sea (Refer chapter 3, figure 3.1). This explains the higher aerosol loading observed between 1.5 km to 5 km over the northern BoB and southeastern AS during pre-monsoon as shown in figure 4.8. As showed by MODIS observations (figure 4.7), AOD strengthens over these plume regions from winter to pre-monsoon. This could be due to the higher strength of anticyclone circulation during pre-monsoon that effectively transport aerosol from the Indian landmass with high wind speed compared to weaker anti-cyclonic circulation persisting during winter.

Over Northern AS, significant aerosol loading is observed within MABL during both winter and pre-monsoon season. During pre-monsoon it is mostly contributed by dust aerosols.

At surface aerosol extinction coefficient shows a magnitude of ~0.25 $km^{-1}$ that decrease sharply from surface to up to ~ 1 km and almost linearly decrease above 1km at slower rate. Dust loading during winter season is observed to be significant over this region. Using ARMEX observations along with back trajectory analysis, *Moorthy et al., (2005)* showed that over the AS , the aerosols in the lower atmosphere (500 to 1800m) are transported from West Asian regions, western/west coast of India while, at upper levels (above 1800 m), aerosols are transported from North West India, central India and Bay of Bengal via longer trajectories of 4 to 7 days. Island based Lidar observations during INDOEX over the Northern Indian Ocean reported elevated aerosol layer above MABL from 1.5 km to 3.5 km advected from the Indian subcontinent during March 1999 *(Ansmann et al., 2000)*. Using ship-borne micropulse lidar measurements carried out during the INDOEX 1999 field phase (February - March), reported that top heights of elevated aerosol layers were below 4 km for most of the cruise *(Welton et al., 2002).* This is in tune with the vertical extent of CALIOP observations over the study regions. Micro-pulse lidar observations from over Southeast Arabian Sea coast under the influence of southeastern AS plume, indicated the presence of elevated layers between 0-2 km and 2 - 4 km during pre-monsoon season *(Rajeev et al., 2010)*.

To quantify the percentage contribution of aerosols at different altitude regions, cumulative extinction is estimated, starting from surface and is shown in Figure 4.9. Over the northern BoB while 42% of aerosols reside above 1 km altitude during winter, it is 66% in pre-monsoon season. i.e., there is a 24% increase in aerosol extinction from winter to pre-monsoon above 1 km altitude. Over southern Bay of Bengal, a 17% increase in aerosol extinction above 1 km altitude is observed from winter to pre-monsoon. Enhancement in dust extinction above 1 km from winter to pre-monsoon is found to be 40% over northern BoB and 16% over the southern Bay of Bengal. Over northern AS, 20% pre-monsoon enhancement is observed in AOD above 1 km while over southeastern AS it is 17%. Figure 4.10 shows the percentage contribution aerosol extinction above 1 km to the columnar AOD over the study regions. During winter 42% of AOD is contributed by aerosols above 1 km over northern BoB which is caused by the weak anticyclone from 950 to 600 hpa (0.5 km to 4.5 km) (Refer chapter 3, figure 3.1). Strong easterly flow from the East Asia through the lower levels contributes to the aerosol concentrations within 1 km leading to the reduction of the contribution of aerosols from above 1 km (37%) over the southern BoB. Near to the southwest coast of India, frontal convergence of the anticyclonic circulation and northerly flow from the west Asia facilitates vertical uplift of aerosols *(Moorthy et al., 1993)*.

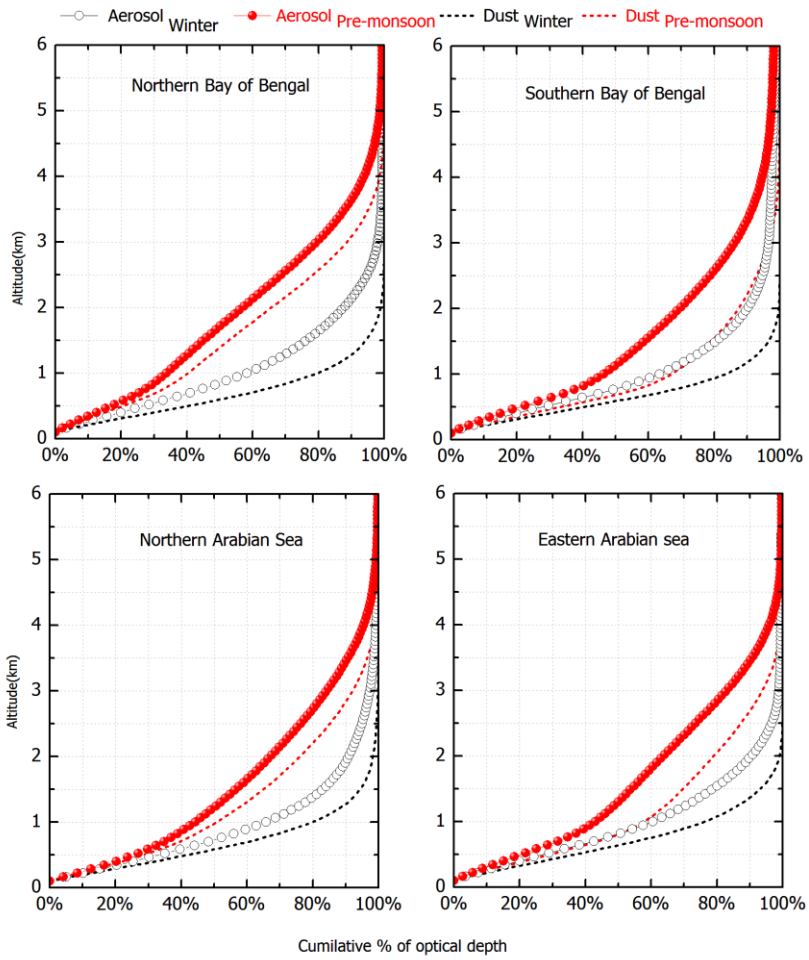


***Figure 4.9 -*** *Cumulative distribution (in percentage) of mean extinction coefficient due to total aerosol and dust aerosol with altitude over the BoB during winter (black) and pre-monsoon seasons (red) over the year from 2006 to 2017.*

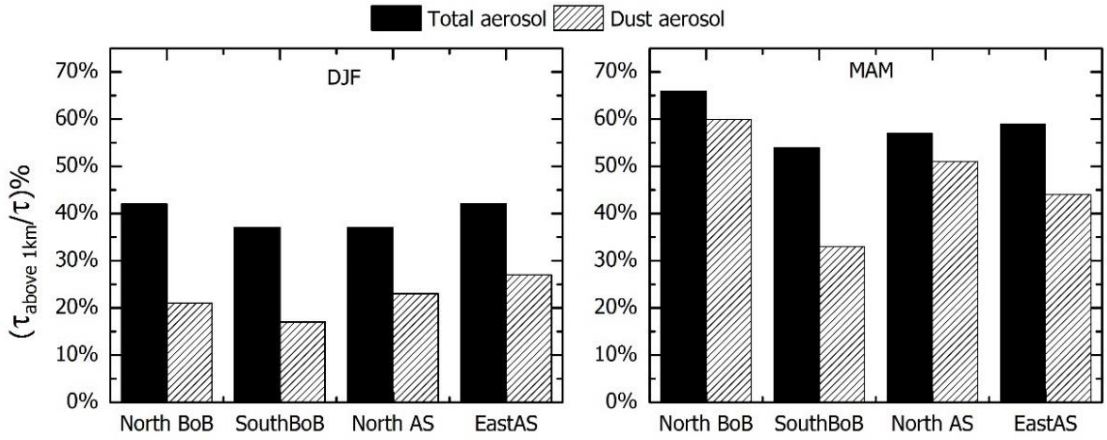


***Figure 4.10 -*** *Percentage contribution of optical depth above 1km altitude due to total aerosols (dust + nondust) and dust aerosols alone.*

Though observed dust fraction during winter is highest during northern AS percentage contribution to dust AOD from above 1 km is observed to be highest over the southeastern AS which might be due to the vertical updraft associated with the frontal effect. During pre-monsoon highest AOD fraction from above 1 km is observed over the northern BoB. The upper level anti-cyclonic circulation is observed to be strongest over the IGP that causes high pollution outflow from north India/Indo-Gangetic Plain which results in high aerosol loading throughout the vertical column up to 4 km over the northern BoB. Due to different circulations at upper (north-westerly as a part of anti-cyclone) and lower levels (south/south westerly), columnar AOD over this region is contributed by different aerosol systems below and above the planetary boundary layer. Studies on circulation parameters over the BoB during ICARB suggests that lower level transport from Indian landmass is inhibited during pre-monsoon while upper level winds that converges over the BoB facilitates the aerosol transport from the central India *(Aloysius et al., 2008)*. They have reported that the aerosols (mostly dust) transported from the west experiences convergence and associated subsidence over the Bay of Bengal. Figure 4.11 shows the climatological value of AOD (MODIS), dust AOD derived using CALIOP and columnar dust extinction fraction during winter and pre-monsoon over southern and northern Bay of Bengal. Average profiles over respective study regions are integrated to get the regional mean dust AOD. Higher dust loading during pre-monsoon is in tune with the results from the Winter-ICARB campaign conducted exclusively over the BoB *(Moorthy et al., 2010)*. Pre-monsoon season is associated with significant dust loading especially over the northern BoB with a dust AOD of ~0.1 and with a dust fraction of 22%, while over the southern BoB dust fraction during Pre-monsoon is ~10% showing a clear latitudinal variation. It is to be noted that while dust loading over Northern BoB shows distinct seasonal pattern, dust loading over south is almost seasonally independent and lesser in magnitude. Average dust fraction during winter is found to be spatially homogenous over the BoB which is ~10% of the total aerosol extinction over the southern BoB and ~13% over the northern Bay of Bengal. Chemical analysis of filter based samples over the BoB in winter period indicate a mineral dust contribution of 11% to the total $PM_{2.5}$while during pre-monsoon it goes up to ~30%, and provides clear evidence for chemical processing of mineral dust aerosols by acidic species despite of its least contribution in this season *(Kumar et al., 2010; Srinivas and Sarin, 2012).* Over Northern AS 62 ± 11 % of total AOD is contributed by dust aerosols during pre-monsoon while over southeastern Arabian plume it is around 37± 6% during this season. During winter, significant dust fraction (34 ± 7%)

is observed over the Northern AS while over the southeastern plume it is decreased to 20 ± 5%.

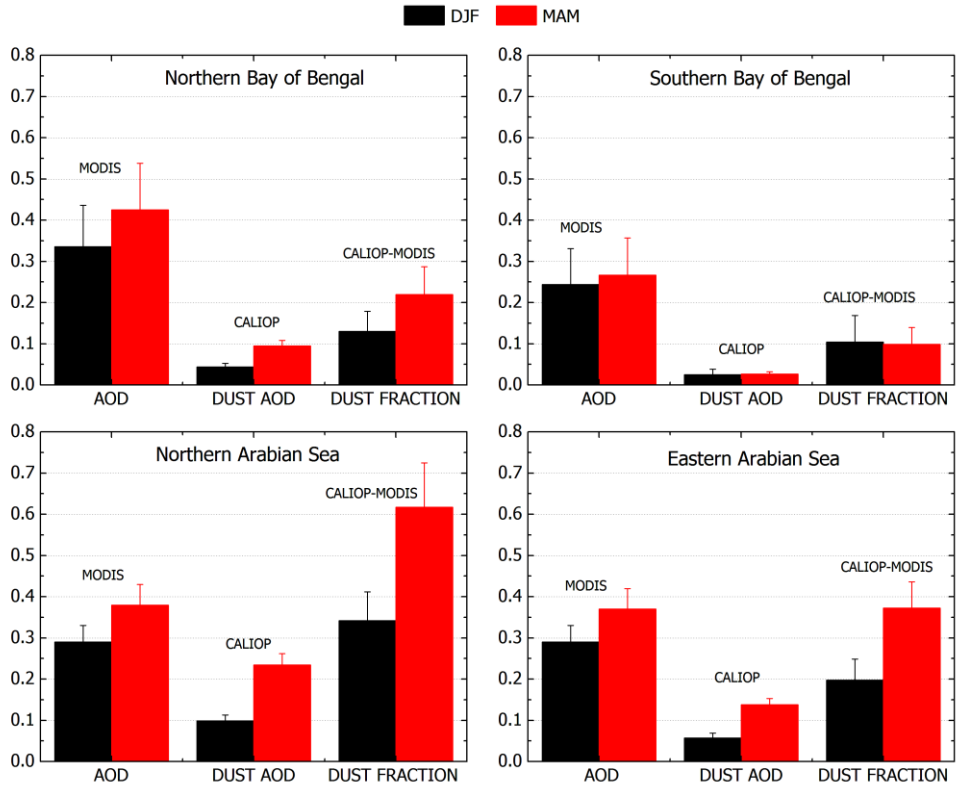


***Figure 4.11*** *- Dust AOD derived using CALIOP depolarization measurements and dust fraction using AOD from MODIS over the BoB for winter (DJF) and pre-monsoon (MAM) (2006 to 2017).*

Table 4.4 tabulates the mean of dust optical depth and dust fraction over the study regions.

***Table 4.3 -*** *Climatological mean values of dust optical depth ($\tau_d$) and dust fraction ($f_d$) over the study regions during the period (2006 - 2017) using CALIOP depolarization observations. Error bars represent the measurement uncertainty over the study regions.*

| **Region** | **Winter (DJF)** | | **Pre-monsoon(MAM)** | |
|---|---|---|---|---|
| | $\tau_d$ | $f_d$ (%) | $\tau_d$ | $f_d$ (%) |
| **BoB(North)** | 0.04 ± 0.01 | 13 ± 4 | 0.09 ± 0.01 | 22 ± 6 |
| **BoB(South)** | 0.02 ± 0.01 | 10 ± 6 | 0.02 ± 0.01 | 10 ± 4 |
| **AS (North)** | 0.1 ± 0.01 | 34 ± 7 | 0.23 ± 0.02 | 62 ± 11 |
| **AS (East)** | 0.06 ± 0.01 | 20 ± 5 | 0.14 ± 0.01 | 37± 6 |

### 4.3.4 Spatial distribution of dust fraction

In the previous section, vertical distribution of dust and its contribution to the total aerosol profiles is quantified using a combination of CALIPSO and MODIS measurements. Spatial distribution of dust AOD and dust fraction is presented in the following section using multi-satellite datasets.

#### 4.3.4.1 CALIOP

Figure 4.12 shows the spatial distribution of dust optical depth ($\tau_d$) and dust fraction ($f_d$) over the BoB and AS during winter (upper panels) and pre-monsoon (lower panels). $\tau_d$ is obtained using depolarization measurements from CALIOP (Refer Chapter 2 Section 2.2.2) and $f_d$ is obtained by weighting $\tau_d$ using concurrent AOD measurements of MODIS. During winter $\tau_d$ is significant over the north/north-western AS with a magnitude of ~0.1 that contributes to ~40% to the total aerosol loading over that region. During pre-monsoon $\tau_d$ is observed to be greater than 0.2 near the continental regions with dust fraction reaching up to 70% to 80% of the total loading. Dust fraction decreases towards central and southern parts of AS. Between 20°N and 10°N dust fraction reduces to ~30% to 50%. Dust fraction over the northern BoB lies in the range of ~20% - 30%. During winter significant dust fraction (~35% to 50 %) is observed over the northern and western part of AS.

#### 4.3.4.2 MODIS

While CALIOP identifies dust aerosols based on depolarization characteristic owing to its non-spherical shape, MODIS make use of the spectral measurements of aerosol optical depth which is sensitive to size of the dust particles. The dust AOD is estimated from MODIS measurements of the AOD($\tau$) at 550 nm, and the fraction of AOD contributed by the fine mode aerosol, fine mode fraction($f$), based on *Kaufman et al.*, (2005*)*. Over marine environments under continental influence, AOD is composed of maritime, ($\tau_{marine}$), dust ($\tau_{dust}$) and anthropogenic ($\tau_{anthro}$) aerosols. The dust aerosol optical depth is given by

$$\tau_{dust} = \frac{\tau(f_{anthro} - f) - \tau_{marine}(f_{anthro} - f_{marine})}{f_{anthro} - f_{dust}} \qquad (4.1)$$

where $f$ is bounded by $f_{anthro} \geq f \geq min\{f_{anthro}, f_{dust}\}$. The $f_{anthro}$, $f_{dust}$ and $f_{marine}$ are the fine mode fraction that corresponds to the anthropogenic, dust and maritime aerosols respectively. We used a priori information on the fine mode fraction of these aerosol types as follows $f_{anthro}$= 0.889, $f_{dust}$= 0.309 and $f_{marine}$= 0.475 provided by *H.Yu* (Personal Communication, 2017). We estimated $\tau_{marine}$ independently using the relationship between the MODIS AOD and sea surface wind speed (1000 mb) from MERRA reanalysis following *(Kaufman et al., 2005).*

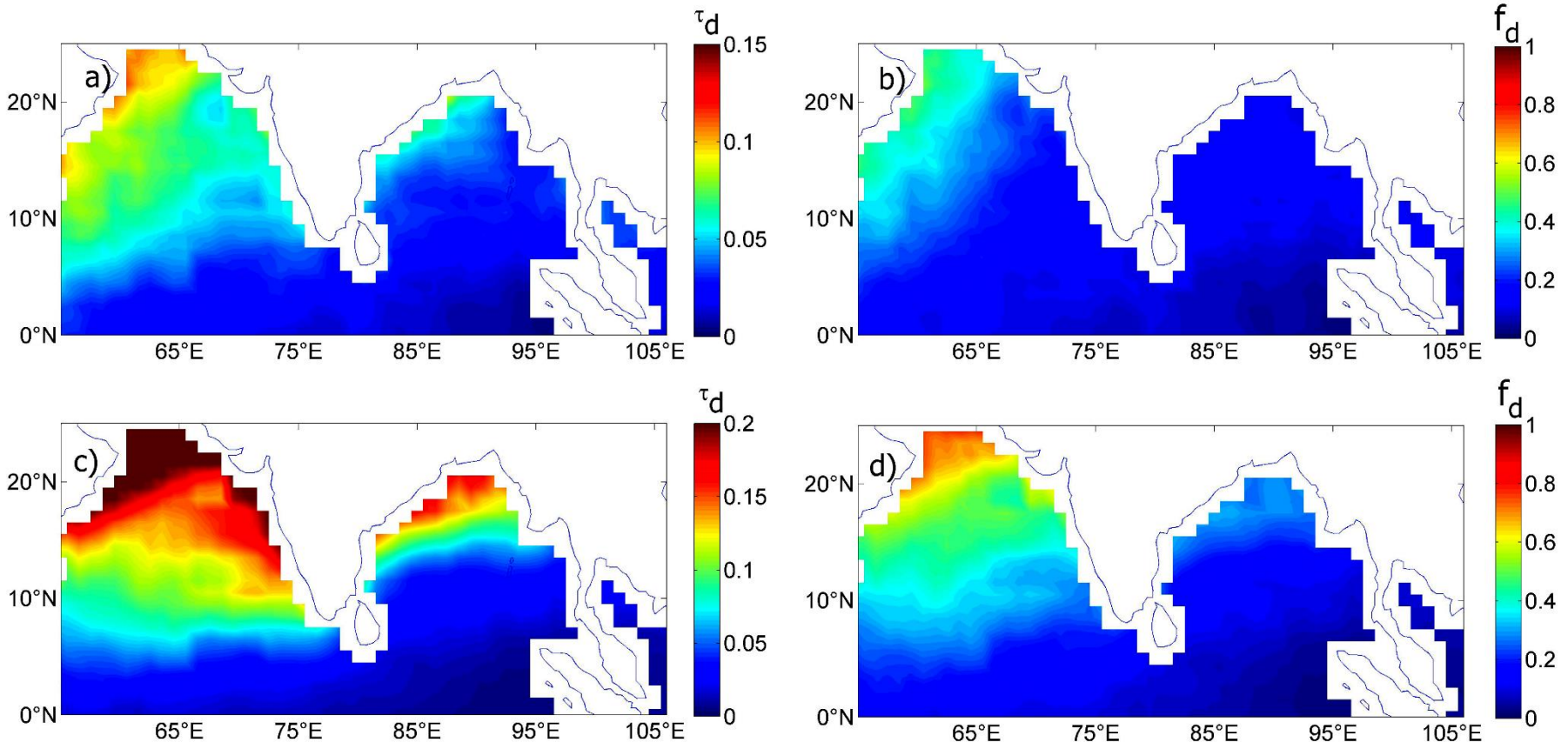


***Figure 4.12*** *- Spatial distribution of dust optical depth ($\tau_d$ in km$^{-1}$) and dust fraction ($f_d$) derived using CALIOP depolarization measurements for winter (a, b) and pre-monsoon (c, d) seasons averaged during the period Dec 2006 to Apr 2017.*

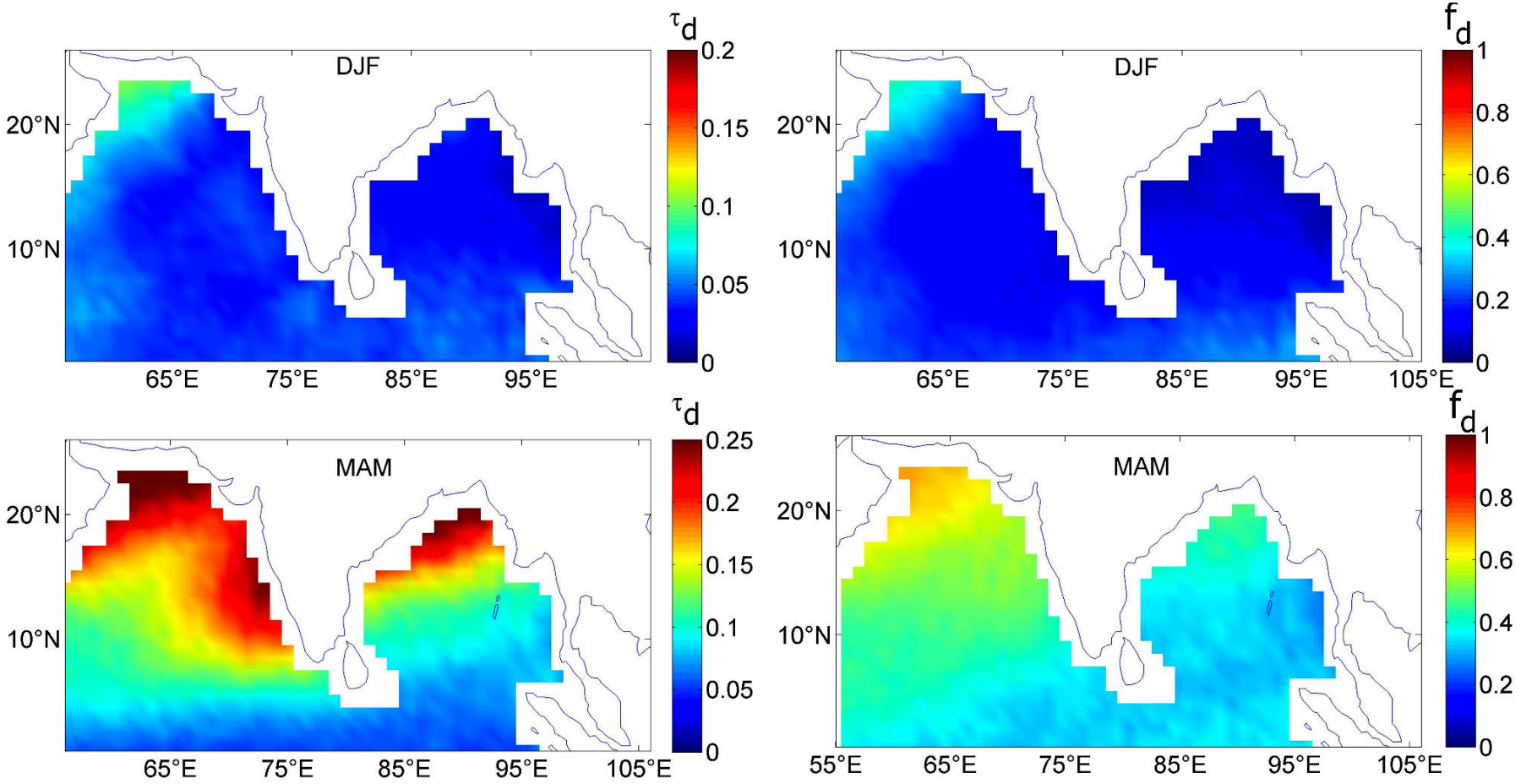


***Figure 4.13*** *- Spatial distribution of averaged dust optical depth ($\tau_d$) and dust fraction ($f_d$) derived using MODIS measurements of fine mode fraction, following Kaufman et al., (2005) for winter (upper panels) and pre-monsoon (lower panels) seasons averaged during the period Dec 2006 to Apr 2017*

The mean value of marine AOD over the BoB yields 0.037during winter and 0.438 during pre-monsoon season. Over AS it is ~0.055 during winter and 0.46 during pre-monsoon. MODIS observations also show the presence of dust aerosols during winter over the Northern AS near to the Oman coast. During pre-monsoon season dust AOD is highest over the northern AS, southeastern AS and north/north west BoB with dusts AOD exceeding 0.2. But the dust fraction is observed highest over the Northern AS with a magnitude around 60%. MODIS derived dust AOD reproduced the AOD plume over the southeastern AS, while CALIOP doesn't show this dust plume over the southeastern AS. Though the seasonal pattern of MODIS derived dust AOD/fraction resembles that derived from CALIOP, they differ quantitatively, and a magnitude wise inter-comparison is carried in the section 4.4.

### 4.3.5 Vertical distribution of dust fraction

A mean picture of vertical distribution of dust fraction over the study region is shown in Figure 4.14 for winter and pre-monsoon seasons.

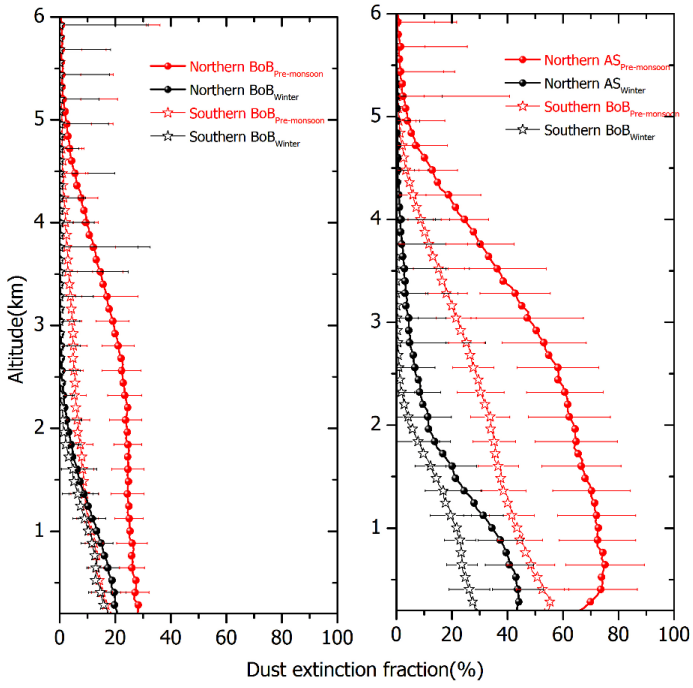


***Figure 4.14 -*** *Vertical profile of dust fraction over the study regions during winter (black curves) and pre-monsoon (red curves) over the northern (solid spheres) and southern BoB (open triangles) over the years 2006 to 2017.*

During pre-monsoon, the vertical distribution of dust fraction is distinctly different over northern and southern BoB whereas during winter both profiles shows only slight variation indicating relatively good spatial homogeneity in vertical distribution. Pre-

monsoon dust fraction over the north shows a steady state (~25%-28%) in the altitude range 0 to ~2.3 km. Vertical extent of dust transport (where dust fraction reduces to 5%) varies from 4 km to 5 km during pre-monsoon whereas during winter it is up to around 2 km over both northern and southern BoB.

Over the northern Arabian Sea, dust fraction during the pre-monsoon is highest in the range from surface to ~ 2.5 km with a value of 60% to 75% which decreases to insignificant values at around 5 km in altitude. Over southeastern AS dust fraction is around 55 % at the surface and decreases linearly upwards with a vertical extent up to 5 km. During winter significant dust fraction of 35% to 45 % is observed from surface to 1 km that rapidly decreases to ~10% at ~2.5 km. Over the southeastern AS, dust fraction ranging from 20% to 30% is observed within MABL during winter that decreased to very small values (<4%) at 2 km.

### 4.3.6 Dust fraction: CALIOP, MODIS and GOCART - Inter-comparison

An inter-comparison of the dust fraction obtained from CALIOP and MODIS satellite observations and GOCART model simulations over the study regions are shown in Figure 4.15.

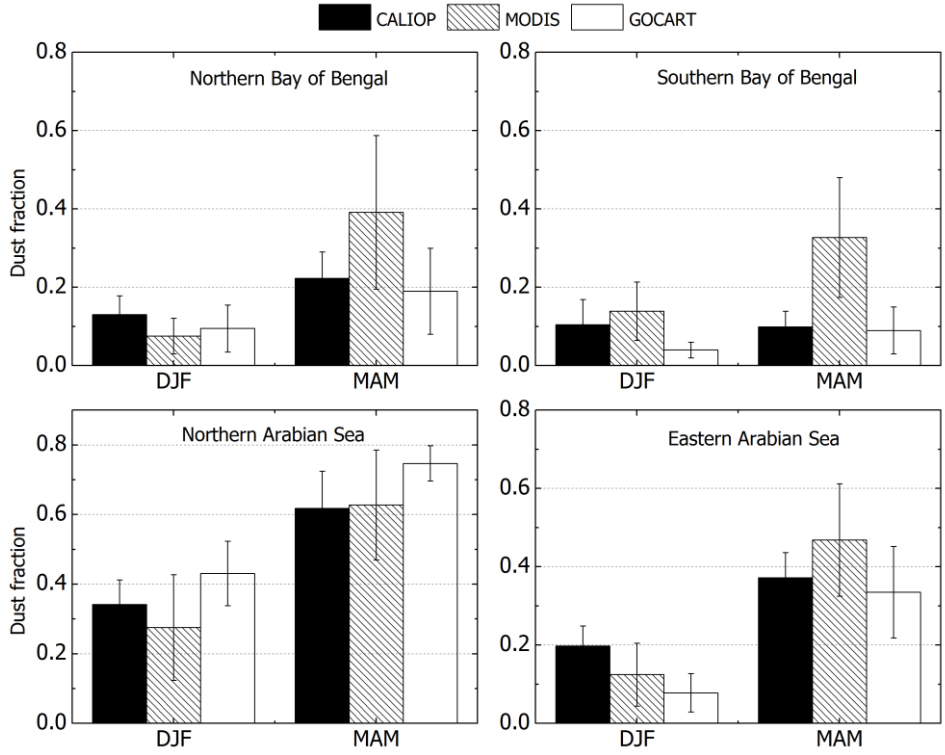


***Figure 4.15*** *- Inter-comparison of dust fraction derived using i) CALIOP depolarization technique ii) MODIS fine mode fraction and iii) GOCART model simulation. Error bar represents the spatial variability of the dust fraction.*

CALIOP dust fraction is estimated as the ratio of CALIOP derived dust AOD to MODIS AOD. MODIS derived dust fraction is higher than CALIOP derived dust fraction except over Northern AS during pre-monsoon (~ 1 fold over north BoB and ~2 fold over southern BoB) and lower during winter. Over the dust dominated northern AS, MODIS dust fraction is comparable to the CALIOP dust fraction and while it is lesser during winter. Fine-mode based separation of MODIS dust does not account for the contribution of fine mode dust particles to the total system which can cause an underestimation in dust aerosols over dust dominated regions. Uncertainties associated with the derivation of dust AOD using MODIS retrieval mainly includes the improper characterization of non-sphericity of dust aerosols, where shape of highly non-spherical dust particles is not taken in to account. Errors associated with the wind speed–AOD relation used in the estimation of marine AOD could also lead to the contamination of size-sensitive dust characterization with coarse mode sea-salt particles. Also, the assumption of seasonally independent fine mode fractions for different aerosol components (as described in section 2.5) while deriving the dust AOD May add error to the dust fraction values *(Yu et al., 2009)*. CALIPSO depolarization technique is advantageous in this aspect as it estimates dust extinction from the direct response of back-scattered radiation to the non-sphericity of the particles though it has limitation due to the assumption of dust and non-dust depolarization ratios in estimating the dust back-scattering fraction. Retrieval uncertainties of aerosol properties from satellites also adds to discrepancy in the estimation of dust fraction *(Kittaka et al., 2011; Kim et al., 2013).* GOCART reproduces the general global scale dust distribution, when emissions are exclusively considered from 'dust hot spots' *(Ginoux et al., 2001)*. It is to be noted that over northern AS, which lie close to the dust source region, GOCART is slightly over estimating the dust fraction compared to satellite derived dust fraction. *Yu et al., (2010)* compared the dust fraction due to CALIOP and GOCART over regions of distinct aerosol systems and have showed that over Indian mainland GOCART underestimates CALIOP by 24% to 40%. Over south Asian region aerosol climate models steadily underestimate the aerosol optical depth (14% - 44%) compared to that retrieved using satellite measurements. Reason for this underestimation during winter is identified as the bias in relative humidity which leads to suppression of aerosol hygroscopic growth and also formation of secondary inorganic aerosols *(Pan et al., 2015)*. A similar analysis of estimation of dust deposition over Amazon region shows that CALIOP based dust estimate is more agreeable with in situ measurements than MODIS derived (*Kaufmann* method) dust deposition while the modelled dust using different climate models clearly underestimated the dust observed using CALIOP, MODIS and in situ measurements *(Yu,*

*Chin, Yuan, et al., 2015)*. Since we have used GOCART simulations over a shorter period (2007 - 2008), a quantitative comparison with the dust fraction derived using CALIOP/MODIS will not be feasible. We have considered GOCART simulations as a representative of the chemical transport models which will provide an independent dataset to compare the dust fraction estimated using CALIOP (depolarization) and MODIS (fine mode) though the inter-annual variability and difference in the length of dataset affect the absolute comparison of various dust fraction estimations.

***Table 4.4*** *- Mean dust fraction ($f_d$) obtained from CALIOP (depolarization method), MODIS (fine-mode method) and GOCART simulations.*

| **Region** | **CALIOP (%)** | **MODIS (%)** | **GOCART (%)** | **CALIOP (%)** | **MODIS (%)** | **GOCART (%)** | **(MODIS-CALIOP) /CALIOP (%)** | |
|---|---|---|---|---|---|---|---|---|
| | DJF | | | MAM | | | DJF | MAM |
| **BoB (North)** | 13 ± 4 | 8±5 | 10±6 | 22 ± 6 | 39±2 | 19±11 | -42 | 75 |
| **BoB (South)** | 10 ± 6 | 14±7 | 4±2 | 10 ± 4 | 33±15 | 9±6 | 33 | 230 |
| **AS (North)** | 34 ± 7 | 27±15 | 43±9 | 62 ± 11 | 62±15 | 74±5 | -19 | 0 |
| **AS (East)** | 20 ± 5 | 12±8 | 8±5 | 37± 6 | 47±14 | 34±12 | -37 | 26 |

### 4.3.7 Aerosol trend over the Bay of Bengal and Arabian Sea

Figure 4.16 shows the long term variation of CALIOP derived dust optical depth and dust fraction along with total AOD from MODIS observations over the northern BoB, northern AS and southeastern AS where dust aerosols contribute significantly of the total aerosols during pre-monsoon season. AOD over southern BoB doesn't show significant trend and observed dust optical depth is too low to examine the trends over this region. Over the AS, linear trend in AOD is positive over the southeastern part (slope = 0.0026 $yr^{-1}$) and negative over the northern part (slope = -0.0016 $yr^{-1}$) during pre-monsoon season of last decade. Over Northern BoB, similar to southeastern AS, AOD shows an increasing trend (0.004 $year^{-1}$). Though AOD shows an increasing trend over these regions, dust AOD

shows a decreasing trend indicating an increasing trend of anthropogenic aerosols that would be much higher than the trend in total AOD during the last decade. Over southeastern AS slope of decreasing dust AOD is much lesser (-0.0008 year-1) compared to other regions but dust fraction shows a significant slope of -0.008 year$^{-1}$. Over the northern AS, dust aerosols are decreasing with a trend (-0.004 year$^{-1}$) which is reflected in the decreasing trend (-0.0016 year$^{-1}$) in total AOD.

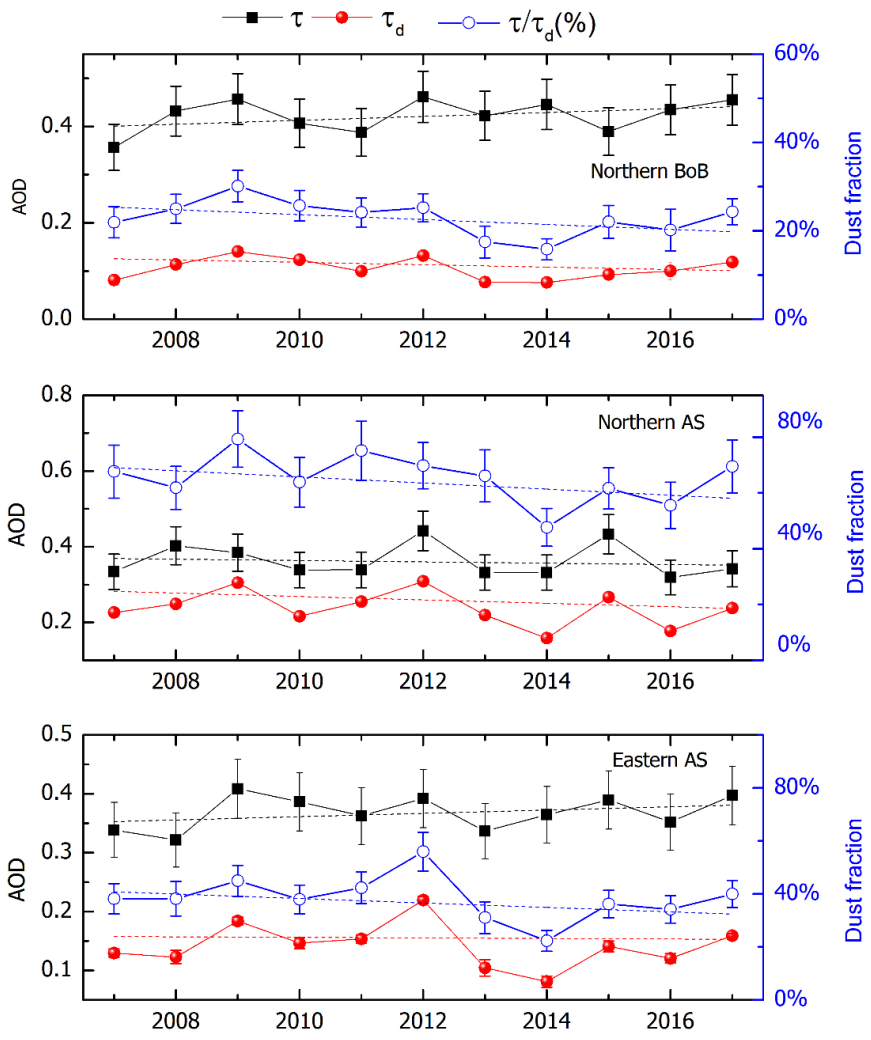


***Figure 4.16*** *- Inter-annual variability in AOD at 550nm , dust AOD at 532nm and dust fraction over the northern BoB, northern AS and southeastern AS during pre-monsoon season using CALIOP depolarization method. Fit lines represent the linear regression lines.*

Study on decadal AOD trend analysis by *Zhang and Reid, (2006)* found statistically significant increasing trend over the BoB using multiple satellite aerosol products. *Babu et al., (2013)* showed statistically significant increasing trend over the Indian region using long term ground based observations of AOD from 35 ARFINET stations (network of

aerosol observatories established under the project of Aerosol Radiative Forcing over India). The authors also showed an increasing AOD trend over the Port Blair, an island location in the central BoB with an annual mean AOD trend of 0.0097year$^{-1}$. Decreasing dust aerosols has implications on climate through direct and indirect effect and by modulating bio-geo chemistry and carbon cycle. There are a few studies that reports on the decreasing dust over regional and global scales using satellite observations and climate models *(Mahowald and Luo, 2003; Shao et al., 2013).* The trends of AOD, dust AOD and dust fraction are found to be significant at 95% confidence level by performing test of significance following *(Weatherhead et al., 1998)*. Inter-annual variability of MODIS derived AOD, dust optical depth and dust fraction using fine-mode observations is examined and shown in figure 4.17.

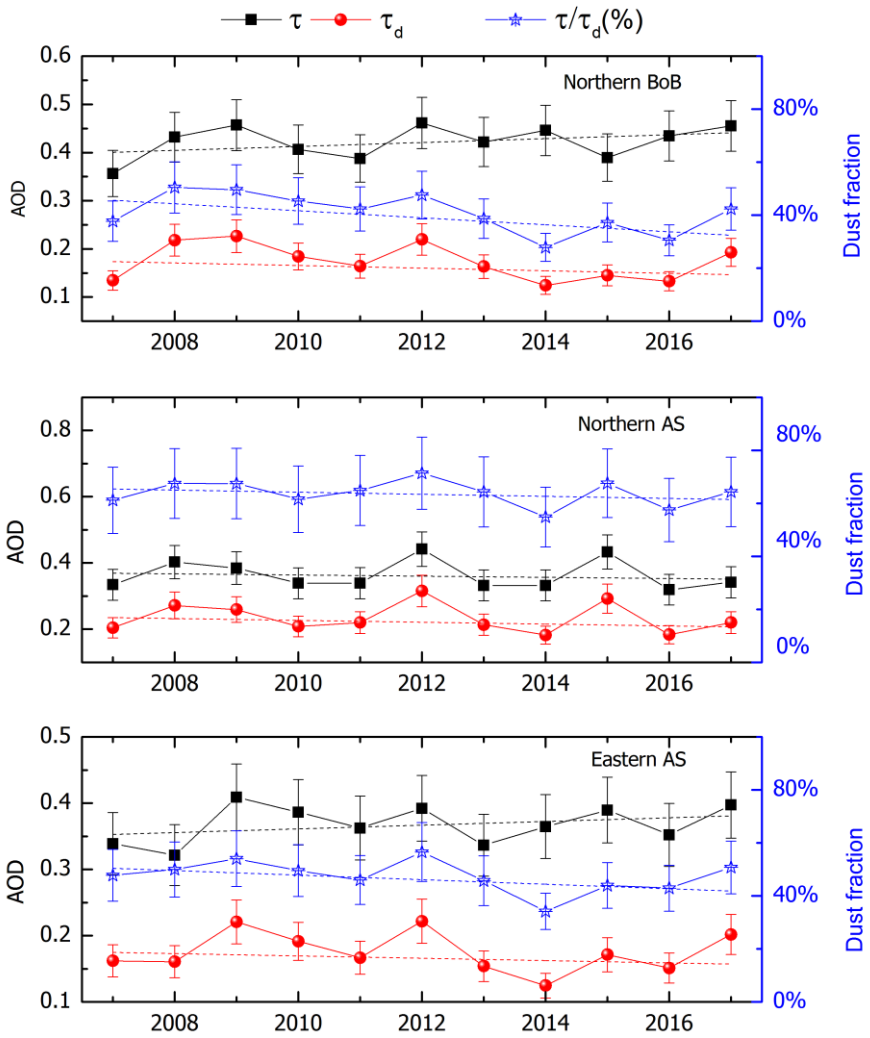


***Figure 4.17*** *- Inter annual variability of AOD at 550nm, dust optical depth at 532nm and dust fraction over northern BoB, northern AS and southeastern AS estimated using MODIS fine-mode observations for pre-monsoon season.*

Over northern BoB and Southeastern AS MODIS derived dust AOD shows slightly higher slopes than CALIOP derived slopes in dust AOD. Over dust dominant northern AS, MODIS derived slope in dust AOD (-0.002 year$^{-1}$) is lesser than CALIOP slope (-0.004 year$^{-1}$) of dust AOD. Details of the trend test are provided in Table 4.6.

***Table 4.5*** *- Details of trend parameters and significance test (Weatherhead et al., 1998).*

| | Parameters | $\tau_{MODIS}$ | $\tau_{d(CALIOP)}$ | $\tau_{d(MODIS)}$ | $f_{d(CALIOP)}$ | $f_{d(MODIS)}$ |
|---|---|---|---|---|---|---|
| **Northern BoB** | Regression Coefficient (R) | 0.39 | -0.21 | -0.26 | -0.41 | -0.54 |
| | Slope($\omega$, year$^{-1}$) | 0.004 | -0.001 | -0.004 | -0.006 | -0.012 |
| | $\lvert\omega/\sigma_\omega\rvert$ | 5.4 | 2.4 | 4.1 | 4.2 | 7.9 |
| | Confidence level | 95% | 95% | 95% | 95% | 95% |
| **Northern AS** | Regression Coefficient (R) | -0.14 | -0.54 | -0.24 | -0.39 | -0.26 |
| | Slope($\omega$, year$^{-1}$) | -0.0016 | -0.004 | -0.002 | -0.01 | -0.003 |
| | $\lvert\omega/\sigma_\omega\rvert$ | 2 | 5.4 | 2.8 | 5.8 | 3.9 |
| | Confidence level | 95% | 95% | 95% | 95% | 95% |
| **South-eastern AS** | Regression Coefficient(R) | 0.32 | -0.05 | -0.2 | -0.32 | -0.41 |
| | Slope($\omega$, year$^{-1}$) | 0.0026 | -0.0008 | -0.001 | -0.008 | -0.007 |
| | $\lvert\omega/\sigma_\omega\rvert$ | 4.3 | 1.6 | 1.6 | 3 | 4.5 |
| | Confidence level | 95% | <95% | <95% | 95% | 95% |

Unlike over land, radiative effects of aerosols over oceans manifest different climatic effects since aerosol induced changes in sea surface temperature would potentially induce changes in circulation and global climate*(Evan et al., 2008, 2009; Foltz and McPhaden, 2008)*. There are evidence for relationship between dust heating and cyclone activity over topical Atlantic, where dry air from the Saharan dust layer that is spread over the marine boundary layer, found to enhance the downdraft and suppresses the cyclone activity *(Evan et al., 2006).* Bay of Bengal is a region of intense cyclone activity during post-monsoon and winter periods. Substantial dust fraction and AOD observed over this oceanic region indicates the need for explicit and detailed quantification of radiative effects caused by aerosols and mineral dust over here.

## 4.4 Summary

The vertical distribution of aerosol and dust extinction coefficient over the BoB and the AS is examined using multi- satellite observations (Cloud Aerosol Lidar with Orthogonal Polarization (CALIOP) and Moderate Resolution Imaging Spectroradiometer (MODIS)) for the period from 2006 to 2017.

- Aerosol loading over the study regions is higher during pre-monsoon compared to winter.
- Distinct seasonal pattern is observed in the vertical structure of both aerosol and dust over the BoB and the Arabian Sea, with a pre-monsoon enhancement in aerosols above MABL. Over BoB, aerosol extinction at the surface is higher during winter with lesser vertical extent while pre-monsoon is characterized by higher aerosol extinction coefficient above MABL. Over AS aerosol extinction coefficient at the surface is almost same for both the season but at elevated heights aerosol extinction coefficient is higher during pre-monsoon.
- Vertical distributions of aerosols are distinctly different over the Northern BoB and Southern BoB. Prominent extinction is observed in the altitude range ~1.5 to 4.5 km over the northern BoB during pre-monsoon while over southern BoB aerosol loading linearly decreases above MABL.
- Over AS, enhanced aerosol loading is observed in the altitude range ~1.5 to 4.5 km over the southeastern AS similar to that observed over Northern BoB during pre-monsoon.
- Prominent dust loading is observed over the northern AS with 34 % of total loading constituted by dust aerosols during winter and 62% during pre-monsoon season. Columnar dust fraction over the southeastern AS is estimated as 20 % during winter and 37 % during pre-monsoon.
- Significant contribution of dust is observed over the northern BoB during pre-monsoon season where 22% of the total aerosol extinction is contributed by dust aerosols transported from the nearby continental regions. During winter, dust transport is found to be less significant with fractional contribution of ~10% - 13% to the total aerosol optical depth over the Bay of Bengal.
- Dust fraction is derived using CALIOP (depolarization technique) and MODIS observations (fine-mode observation based) over the study regions. MODIS derived dust fraction (fine-mode based) shows an overestimation up to 2 fold compared to CALIOP dust fraction (depolarization based). GOCART simulated dust fraction

underestimates the satellite derived dust fractions over the study regions except over northern AS which is a dust dominant region.

- Long term variation (2007- 2017) in AOD shows an increasing trend over the northern Bay of Bengal and southeastern part of AS during pre-monsoon. Over northern AS, AOD is decreasing during the study period. Dust optical depth and dust fraction is showing a decreasing trend over all the study regions indicating the increasing fraction of anthropogenic aerosols over both BoB and AS. Long term trend in dust optical depth derived using both CALIOP (depolarization based) and MODIS (fine-mode based) showed similar results

# Chapter 5

# Elevated aerosols over the Himalayas

## 5.1 Introduction

The Himalayas plays an important role in the distribution of aerosols over south Asia by its topographical characteristics. By obstructing the airflow from the Indian region an aerosol rich domain is created over southern valley of Himalayas and IGP, while it preserves a pristine environment over snow covered regions at high altitudes. Aerosol characterization over Himalayas assumes importance mainly due to two processes, (1) reduction in snow albedo due to the deposition of insoluble light absorbing aerosols (such as black carbon or dust) over the snow surface which accelerates snow melting *(Flanner et al., 2009; Ming et al., 2009)* and (2) the enhanced radiative forcing of absorbing aerosols over highly reflective snow surface *(Lau et al., 2010).* Radiative forcing due to absorbing aerosols critically depend on the underlying surface. High albedo of snow surface strengthens their radiative forcing efficiency in the atmosphere by reflecting more radiation thereby increasing the probability of interaction between aerosols and radiation which leads to enhanced absorption. Over northern India, significant enhancement in elevated aerosol loading is observed during pre-monsoon (refer chapter 3, section 3.4.4), which can produce excessive heating in the atmosphere by absorbing solar radiation. Using climate model simulations, *Lau et al., (2006)* showed that mixture of absorbing aerosols at higher altitude over the IGP/foothills of the Himalayas can act as an elevated heat source in the troposphere and can increase the monsoon intensity over northern India by drawing higher amount of moist air during the pre-monsoon season. *Lau et al., (2010)* discusses the role of elevated aerosols in accelerated snow melt over the western Tibetan Plateau and the Himalayas, during pre-monsoon season and describes the phenomena as one of the manifestations of 'Elevated Heat Pump" (EHP). Model simulations shows that the warming due to snow darkening effect can lead to a warmer and drier boreal summer hydroclimate *(Lau et al., 2018)*. *Nair et al., (2013)* estimated direct radiative forcing and snow-albedo radiative forcing due to deposition of BC over snow, using BC observations from different stations at Himalayas and showed that radiative forcing due to BC induced snow-albedo change was found significantly higher than that due to direct effect. Though the effects of dust/BC on the snow albedo and snow

melting over the Himalayas have been investigated through modelling studies, detailed characterization based on observational datasets are limited over this region *(Lau et al., 2010; Lee et al., 2013).* In this context it is important to have quantitative characterization of the altitude structure of aerosols over the Himalayas in order to address the role of aerosols in enhanced radiative effects and snow melting process over the Himalayas. Aerosol characterization over the Himalayas is initiated under the ARFI Project by establishing a network of stations at Hanle (32.77°N, 78.96°E, 4520 amsl) , Kullu (31.95°N, 77.1°E, 1154m amsl), Nainital (29.38°N, 79.46°E, 1939m amsl), Dehradun (30.31°N, 78.03°E, 700m amsl) and Tawang (32.77°N, 78.96°E, 2916 amsl). Along with regular station based measurements, several field campaigns were conducted over the Himalayas for characterizing aerosols. Under the Regional Aerosol Warming Experiment (RAWEX) of ISRO-GBP, aerosol measurements were carried on-board aircraft from Dehradun over the Himalayan foothills. The Ganges Valley experiment conducted at Nainital have made intense measurements over the central Himalayas using ARM (Atmospheric Radiative Measurement program) mobile facility during June 2011 to March 2012 *(Gogoi et al., 2015; Moorthy et al., 2016).* The present study characterizes the elevated aerosols over the Himalayas using space-borne LIDAR (CALIPSO) observations along with ground based measurements and quantifies the mineral dust aerosols over the Himalayas using vertically resolved depolarization measurements.

### 5.2 Data set

One of the major challenges in the retrieval of aerosols with passive remote sensing over the Himalayas is the highly varying enhanced surface contribution to the radiance received by the satellite from the highly reflecting snow surface. CALIOP overcome this difficulty through the active probing of the atmosphere and retrieves information from the altitude resolved back scattered signal of the atmosphere. However, this method suffers from uncertainty due to the assumed lidar ratio and its inability to detect tenuous layers of aerosols present in the column *(Rogers et al., 2014).* Over cryosphere where atmospheric conditions are pristine, bias in CALIOP derived aerosol extinction coefficient is mainly due to its lower SNR rather than the error in the assumed lidar ratio. Thus the ideal method would be to constrain CALIOP measured aerosol extinction with collocated measurements of AOD. But over the Himalayas, AOD varies significantly with topography due to its complex terrain with steep elevations and valleys. Thus it is not desirable to use regionally limited AOD observations for constraining the CALIOP derived profiles of aerosol extinction coefficient over the entire Himalayas. Hence vertical profiles of aerosol back-

scattering coefficient from CALIOP are used to examine the vertical distribution of aerosols over the Himalayan region rather than the aerosol extinction coefficient. Details of the datasets used in the present study are given in table 5.1.

***Table 5.1 -*** *Data products used for the analysis.*

| Data source | Product | Period |
|---|---|---|
| **CALIPSO** | Aerosol back-scattering coefficient (0.532 μm) (Level 2 - Version 4.1) | Dec 2006 – Apr 2017 |
| | Particulate depolarization ratio (0.532 μm) (Level 2, Version 4.1) | Dec 2006 – Apr 2017 |
| **ARFINET** | Aerosol optical depth (0.5 μm) | Jan 2006 - Dec 2017. |
| **AERONET** | Aerosol optical depth (0.5 μm) | Jan 2006 to Dec2017. |
| **TRMM** | Rainfall rate (TRMM 3A12 V7) (0.5° x 0.5°) | |
| **MERRA** | Snowfall rate (M2TMNXINT – V5.12.4) (0.5° x 0.625°) | Jan2006 – Dec 2017 |
| | Wind fields (u and v components) (1.25° x 1.25°) (M2IMNPASM) | Jan2006 – Dec 2017 |

Station based AOD observations from ARFINET and AERONET are used to study the column loading of aerosols over the Himalayas. Details of the observatories are presented in table 5.2.

***Table 5.2 -*** *Details of the ground based observatories used in the analysis.*

| Number | Station name | Latitude(˚N) | Longitude(˚E) | Altitude amsl(m) | Network |
|---|---|---|---|---|---|
| **1** | Hanle | 32.77 | 78.96 | 4520 | ARFI |
| **2** | Kullu | 31.95 | 77.1 | 1154 | ARFI |
| **3** | Nainital | 29.38 | 79.46 | 1939 | ARFI |
| **4** | Jomsom | 28.77 | 83.77 | 2803 | AERONET |
| **5** | Lumbini | 27.49 | 83.28 | 110 | AERONET |
| **6** | Kathmandu | 27.71 | 85.32 | 1,400 | AERONET |
| **7** | QOMS-CAS* | 28.36 | 86.94 | 4276 | AERONET |
| **8** | Dibrugarh | 27.44 | 94.89 | 111 | ARFI |

*Qomolangma Station for Atmospheric and Environmental Observation and Research, Chinese Academy of Sciences.

### 5.2.1 Study regions

The topography of the Himalayas is highly complex with high mountain ranges and valleys with drastically varying surface elevation. While western part of the Himalayas constitutes high altitude mountains, mid/eastern Himalayas have lower surface elevations. The contour map of the surface elevation above mean sea level (amsl) over the Himalayas is shown in Figure 5.1.

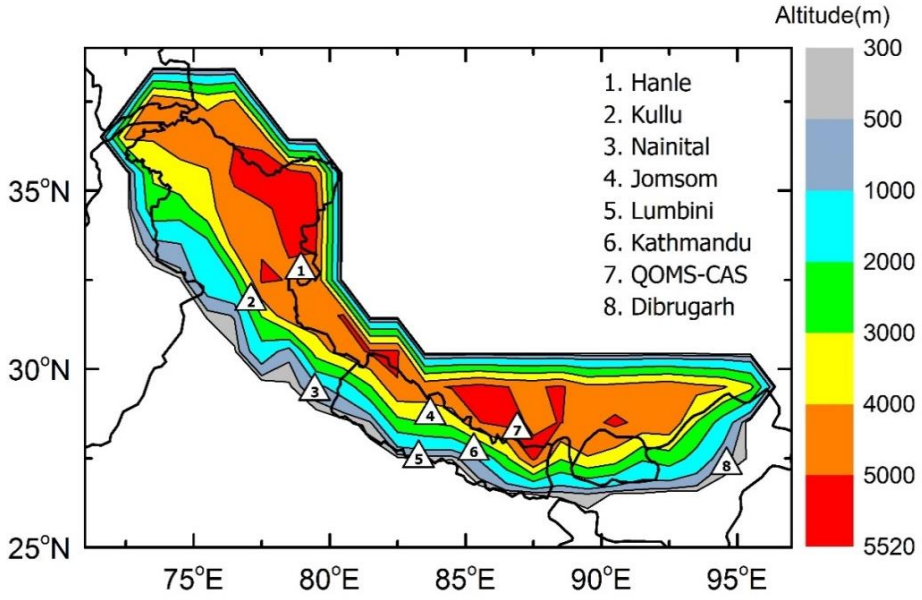


***Figure 5.1 -*** *Contour plot of surface elevation as measured by CALIOP over the Himalayas with locations of aerosol observatories used in the study.*

Aerosol effects on cryosphere significantly depend on the snow cover. Snow coverage and spatial extent of glaciers are regionally distinct over the Himalayas. Glacier melt-water through different rivers recharges the water table over the Indian main land. Himalayan-Karakoram region over the western Himalayas has the largest glacier coverage other than Polar Regions where the snow cover is mainly determined by the westerly circulation during winter. Over central part and eastern region of Himalayas, snow cover depends on the moisture rich monsoon winds *(Anders et al., 2006; Bolch et al., 2012; Copland et al., 2011)*. Glaciers over the western part of Himalayas are rather stable with lowest melting rates while central and eastern parts of Himalayas are characterized by rapid melting of snow cover with a positive trend in snow shrinkage *(Bolch et al., 2012)*. Thus, based on the topography and glacier area the entire Himalayas is divided into three sub-regions of major river basins (Indus, Ganges and Brahmaputra) for the regional characterization of aerosols (following *Bolch et al., (2012)*). They are (1) western Himalayas (including Karakoram), (2) mid-Himalayas, and (3) eastern Himalayas as shown in figure 5.2.

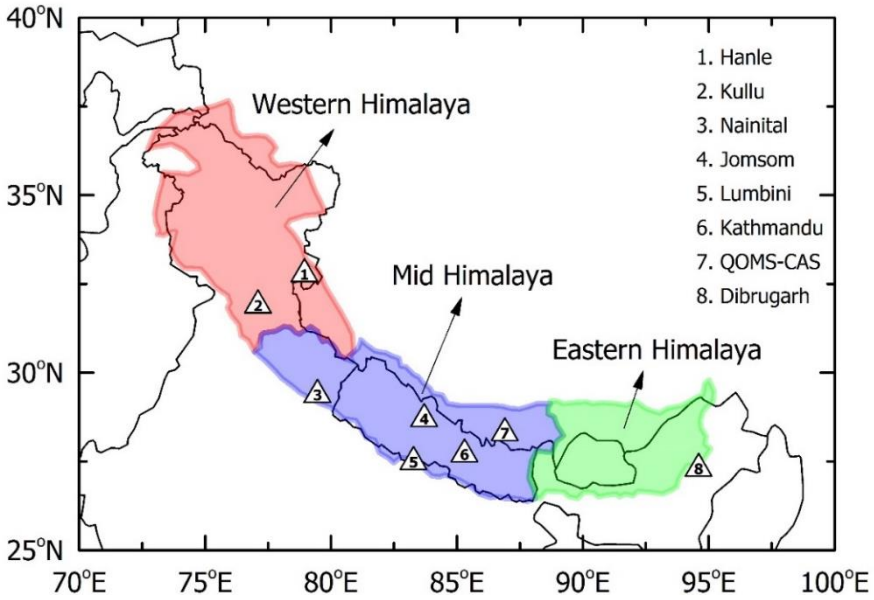


***Figure 5.2*** *- Study regions of Himalaya with locations of aerosol observatories under ARFI network and AERONET. Details of the stations are given in Table 5.2.*

The highly polluted valley regions, relatively clean atmosphere over the high altitude mountain ranges, complex regional meteorology, and highly varying topography demands aerosol characterization with high spatial resolution over the Himalayas.

### 5.2.2 Prevailing meteorology

The Himalayas act as a barrier to atmospheric flows from the Indian mainland and adjacent land areas. During summer monsoon it prevents mixing of warm moist air with dry cold air from the northern latitudes thereby provides heavy rainfall over the Indian region *(Boos and Kuang, 2010).* Figure 5.3 shows wind pattern over the altitude levels 650, 550 and 450 hPa. Wind pattern is mostly westerly during all seasons which is blocked by the mountain ranges up to ~550 hpa altitude that redirect the towards the IGP and eastern India. During monsoon season, the westerly flow is inhibited by the cyclonic circulation over the eastern part of Indian subcontinent. Wind speeds are lowest during monsoon season Wind speed is high during winter with magnitude around 10 m/s. Above 550 hpa westerly prevails throughout the year over the entire Himalayas.

Mean pattern of rain rate during different seasons over the Himalayas is shown in figure 5.4, estimated from Tropical Rainfall Measurement Mission (TRMM) surface rain data product, averaged over the period from 2006 to 2017. Rain rate over regions of surface elevation 2 km amsl are dominated by the Indian summer monsoon season *(Bookhagen et al., 2005; Anders et al., 2006; Bookhagen and Burbank, 2006).*

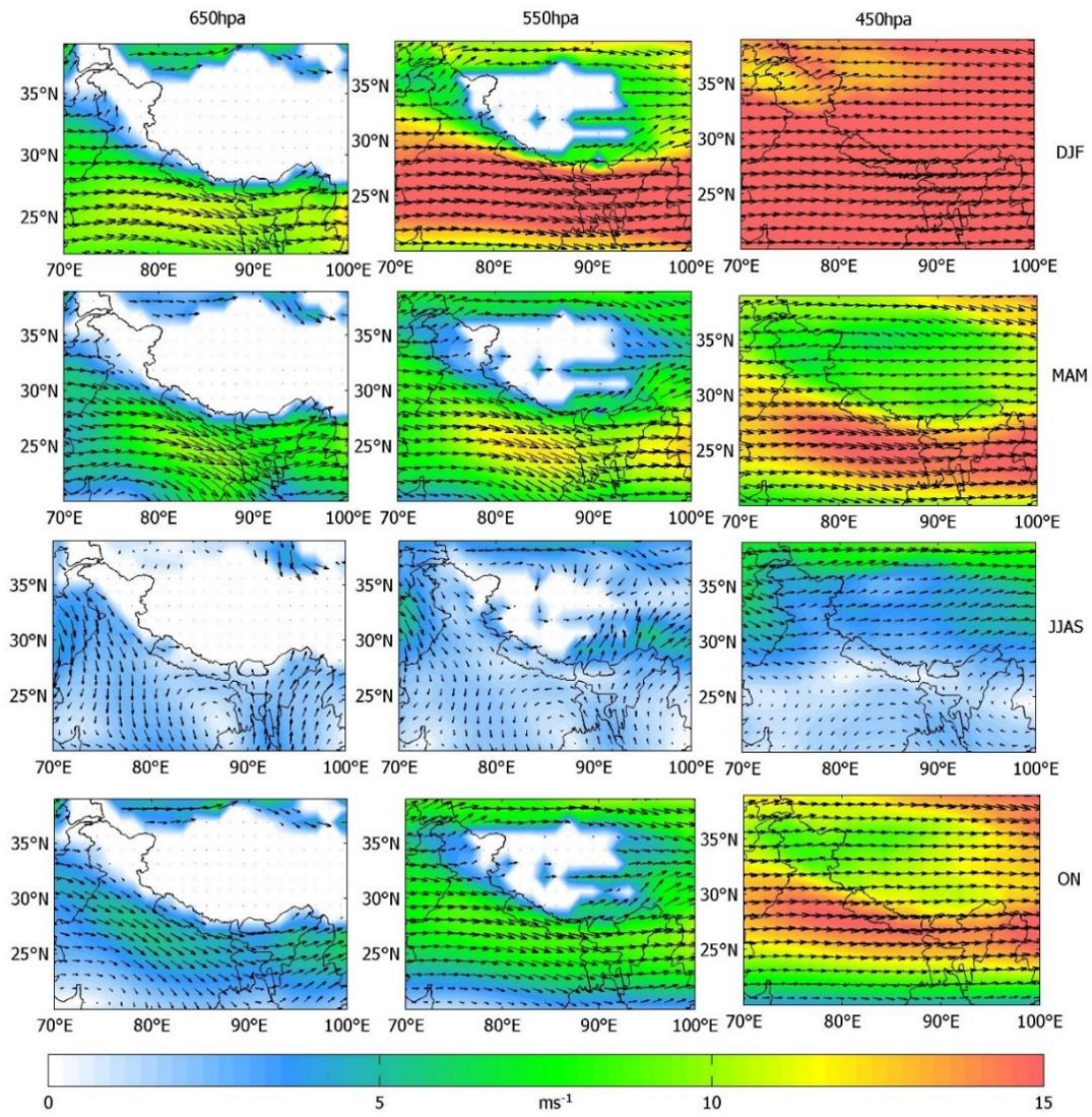


***Figure 5.3*** *- Mean synoptic winds (2006 - 2017) over the Himalayas at three vertical levels (650,550 and 450 hpa) during winter (DJF), pre-monsoon (MAM), summer monsoon (JJAS), and post monsoon (ON). Colour variation indicate wind speed.*

During summer monsoon period, northwest movement of monsoon vortices in the Bay of Bengal provides monsoon rain over eastern and central part of the Himalayas while rainfall over the western Himalayas is caused by the south westerly monsoon winds that carry moist air from the Arabian Sea. Western disturbance is the primary reason for rainfall over Himalayas during winter time (*Barros et al., 2006; Dimri et al., 2015)*. Significant amount of rainfall is observed over the western Himalayas during pre-monsoon season.

Snow fall distribution over the Himalayas plays an important role in the hydrology of south Asia. The precipitation over the Himalayas over high elevation regions occur mainly as

snowfall which increases linearly with altitude over the Himalayas (Singh and Kumar, 1997). Snow coverage over the Himalayas has distinct spatial variation as shown in figure 5.5.

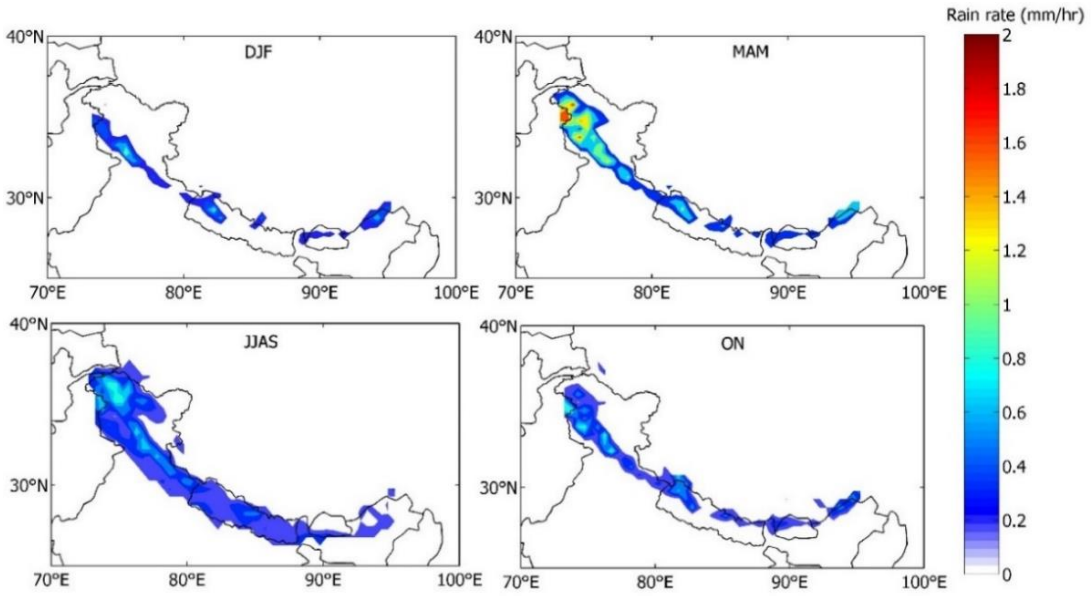


***Figure 5.4*** *- Mean Rainfall rate (2006 - 2017) over the Himalayas during winter (DJF), pre-monsoon (MAM), summer monsoon (JJAS), and post monsoon (ON) using TRMM dataset.*

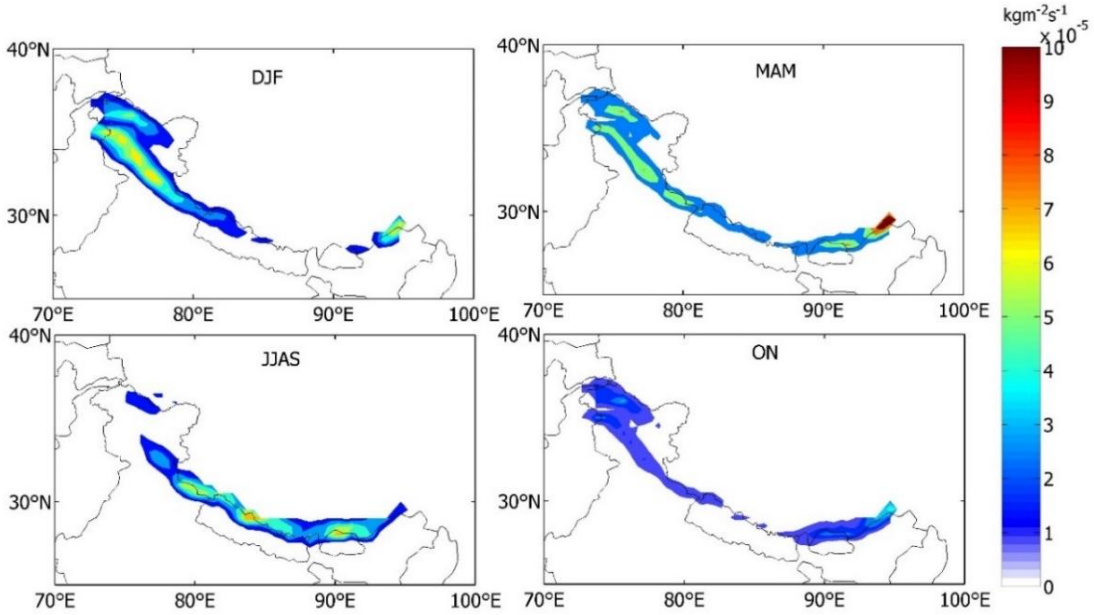


***Figure 5.5 -*** *Mean Snowfall rate (2006 - 2017) over the Himalayas during winter (DJF), pre-monsoon (MAM), summer monsoon (JJAS), and post monsoon (ON) using MERRA reanalysis data.*

There is a clear west to east gradient in snowfall over the Himalayas during winter/pre-monsoon seasons. Higher mean surface elevation towards west of Himalayas and presence

of moisture rich air brought by westerly during winter can be attributed to the higher snow cover over the west. West-east gradient in snow fall weakens during summer monsoon and spread over to central and eastern Himalayas owing to the availability of moisture brought by the monsoon winds. Glaciers over western Himalayas mainly grows during winter snowfall while glacier growth over eastern Himalayas is dominant during summer monsoon snowfall *(Bhambri and Bolch, 2009).*

## 5.3 Results and discussion

### 5.3.1 Aerosol Optical Depth over the Himalayas

Surface topography significantly affects the spatial variability of aerosol loading, especially over regions under the influence of long range transport. Figure 5.6 shows the annual mean AOD at 500 nm over stations (AERONET /ARFINET) located at different surface elevation over the Himalayas.

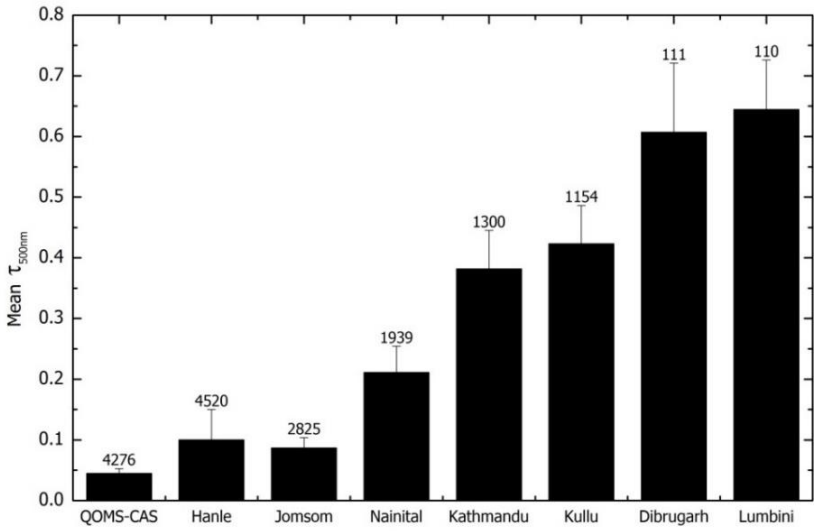


***Figure 5.6*** *- Annual mean AOD at 500nm over stations located at different altitudes over the Himalayas. Numbers above the bars indicate surface elevation in meters. Refer figure 5.2 and table 5.2 for the details of stations.*

Aerosol loading over the Himalayas is evidently dependent on topography and the magnitude of AOD varies drastically with altitude. Over high altitude stations (> 4 km amsl) at Hanle and QOMS-CAS, mean AOD is observed to be ~ 0.05 which systematically increases to ~0.6 at low altitude stations. Low altitude stations at Dibrugarh and Lumibini lies at the foothills of Himalayas where observed AOD is approximately twelve times greater than that observed at Hanle or QOMS-CAS. Presence of strong north-westerly winds that causes intrusion of aerosols from the west over to the Himalayas influence the aerosol loading over Himalayas. IGP being a hot spot of aerosols, can contribute to aerosol

loading over high altitude regions of Himalayas by vertical transport by the mountain valley winds that develop during convectively active months *(Ramanathan and Ramana, 2005; Babu et al., 2011).* Variation in carbonaceous aerosol concentrations measured at Godavari in Kathmandu Valley is observed to be consistent with the annually occurring regional haze over South Asia *(Stone et al., 2010).*Figure 5.7 shows the annual variation of monthly mean AOD at 500 nm at the stations located over the Himalayas.

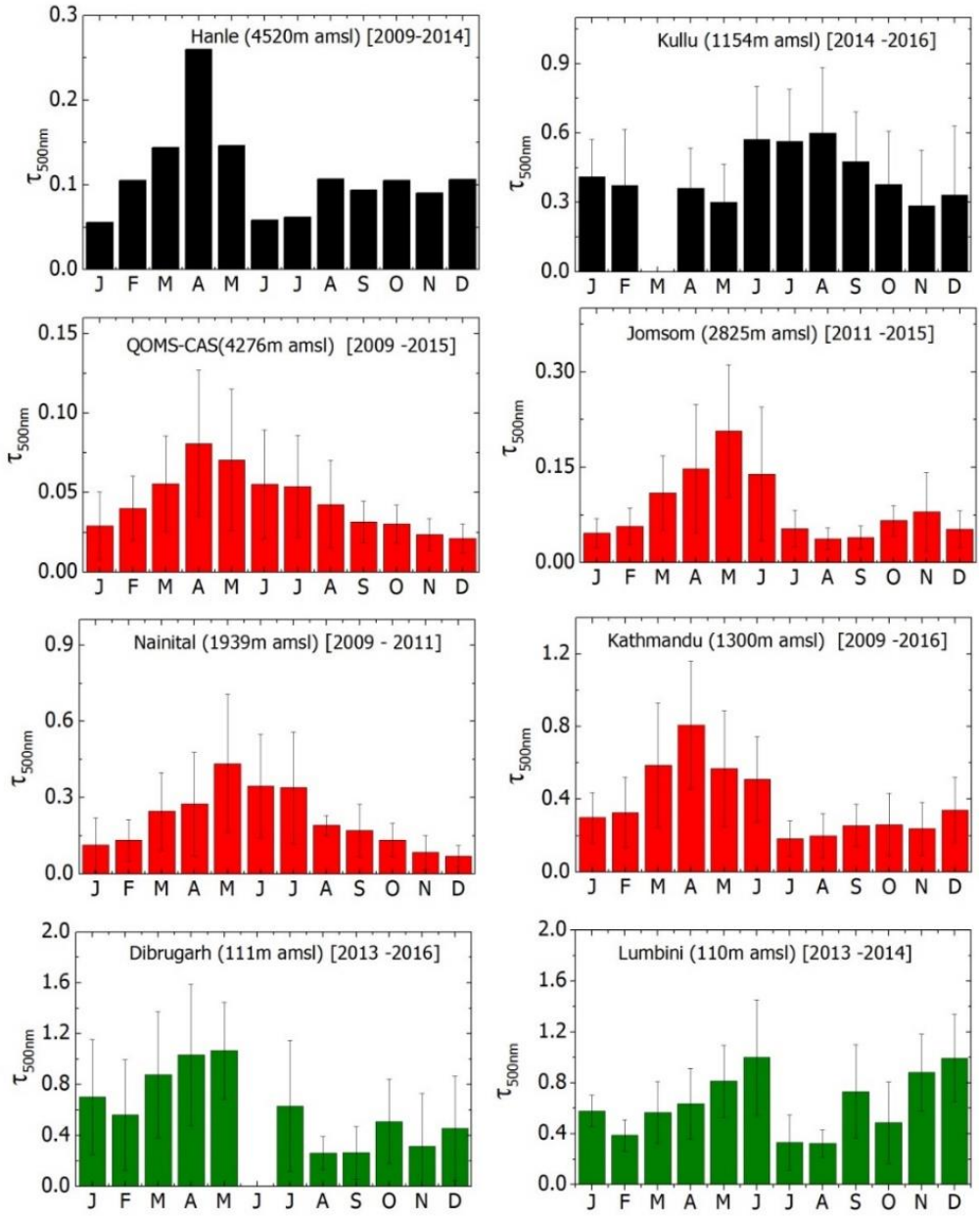


***Figure 5.7*** *- Annual variation of AOD at 500 nm ($\tau_{500nm}$) over regions of different elevations on the Himalayas. Colour of bar represent the study regions where stations are located. Black represents western Himalayas, red represents mid Himalayas and green represent eastern Himalayas.*

Error bar shows the standard deviation in the monthly mean AOD values. An enhancement in AOD is observed over the Himalayan stations during pre-monsoon season. Over Lumbini (110 m amsl), a low lying station over the mid Himalayas, AOD peaks during both pre-monsoon and winter seasons. Enhanced concentration of BC is observed over Hanle (~4520 amsl), a high altitude station at western Himalayas, during pre-monsoon, which is attributed to the uplift of pollutants from the valley regions due to enhanced thermal convection and associated mountain valley breeze during this season *(Babu, Chaubey, et al., 2011).* AERONET observations over high altitude Himalayan station at Nepal Climate Observatory (NCO-P) (5079 m amsl) showed high aerosol loading during pre-monsoon and winter, and lowest during Monsoon season *(Marcq et al., 2010)*. Spectral AOD observations at Dehradun situated over northwest Himalayas (700 m amsl) shows highest AOD during pre-monsoon associated with mineral dust aerosols, moderate loading during monsoon due to mixed type aerosols and lowest values during winter with fine mode aerosol dominance *(Shaik et al., 2017).* Spectral AOD observations at Hanle, shows that monthly variation of Angstrom exponent shows significant variations during different seasons while near surface accumulation mode aerosols remained steady throughout the *(Gogoi et al., 2014)*. This indicates the presence of elevated aerosols at free tropospheric altitudes over the Himalayas region. Several studies have addressed aerosol characterization over the Himalayan regions/foothills using in situ measurements using ground based observatories *(Pant et al., 2006; Babu, Chaubey, et al., 2011; Gogoi et al., 2014; Ningombam et al., 2014; Sarkar et al., 2015; Kompalli et al., 2016).* However, to investigate on the radiative effects of elevated aerosols, vertical characterization is essential. However, detailed studies on the vertical distribution of aerosols over Himalayas are limited. Making use of space borne observations of aerosol profiles, following section discuss on the vertical distribution of aerosol loading over the Himalayas.

### 5.3.2 Vertical distribution of aerosols over the Himalayas.

The study regions, western Himalayas (including Karakoram), mid-Himalayas and eastern Himalayas, are with a mean elevations of 3.7 km, 2.6 km and 2.8 km respectively (Refer figure 5.1). The monthly mean vertical profiles of aerosol back-scattering coefficient measured by CALIOP during 2006 to 2017 over the three different regions of the Himalayas are shown in Figure 5.8. Aerosol vertical distribution shows distinct regional pattern over the Himalayas. Aerosol loading is lowest over the western Himalayas and highest over the Mid Himalayas. Seasonal characteristics of aerosol loading and their vertical spread show distinct regional differences. Over the western Himalayas, the

highest aerosol loading is observed during April to August at ~ 3.7 – 4.5 km amsl with a mean back-scattering coefficient of 0.0009 – 0.002 $km^{-1}sr^{-1}$ that decreases to ~0.00003 $km^{-1}sr^{-1}$ at ~ 7-8 km amsl.

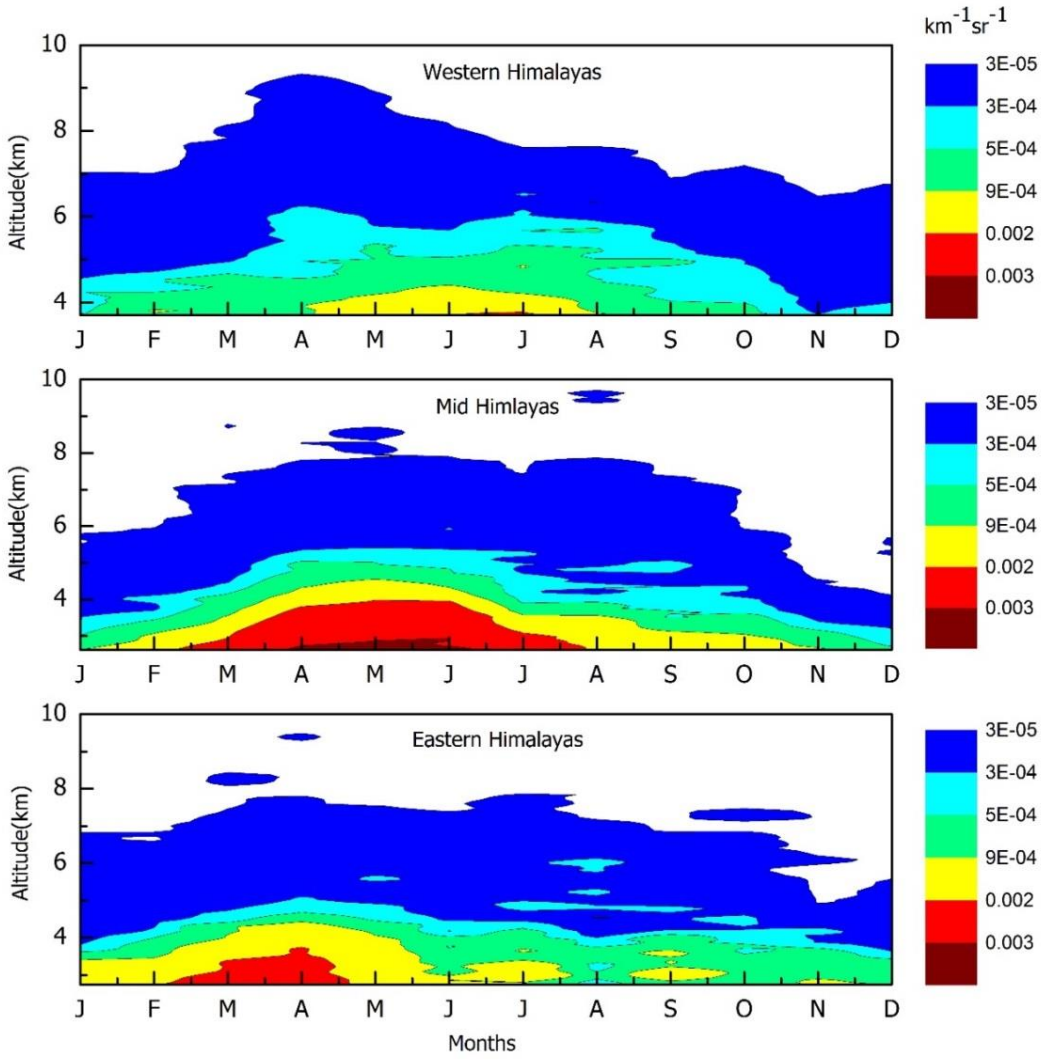


***Figure 5.8*** *- Annual variation of vertically resolved aerosol back-scattering coefficient (CALIOP) over the western, mid and eastern Himalayas averaged for the period 2006– 2017.*

Prevailing westerly facilitate the transport of convectively lifted particles from the regions west of Himalayas during pre-monsoon season. Still aerosol loading is observed over the western Himalayas is low, which can be attributed to its high surface elevation, and enhanced precipitation rate during early pre-monsoon months. During monsoon period, the weak precipitation retains aerosols in the atmosphere (Refer figure 5.9). During April it is observed that vertical spread of aerosols (with backscattering coefficient> 0.00003 $km^{-1}sr^{-1}$) is anomalously high and reaches up to 9 km while aerosol loading at lower levels is lesser compared to following months (May, June and July). Variability in Ångström

exponent over Hanle over the western Himalayas showed that the columnar abundance of fine-mode aerosols varied with season and it is attributed to the presence of elevated aerosol layers over Hanle *(Gogoi et al., 2014; Kompalli et al., 2016).* Over the Mid Himalayas, aerosol loading is found to be highest compared to the west and eastern Himalayas with mean back-scattering coefficient exceeding 0.003 $km^{-1}sr^{-1}$ at ~ 3 km during April – June. As shown in figure 5.9, snowfall rates over the mid Himalayas is lower in magnitude which makes aerosol wet scavenging less effective over this region.

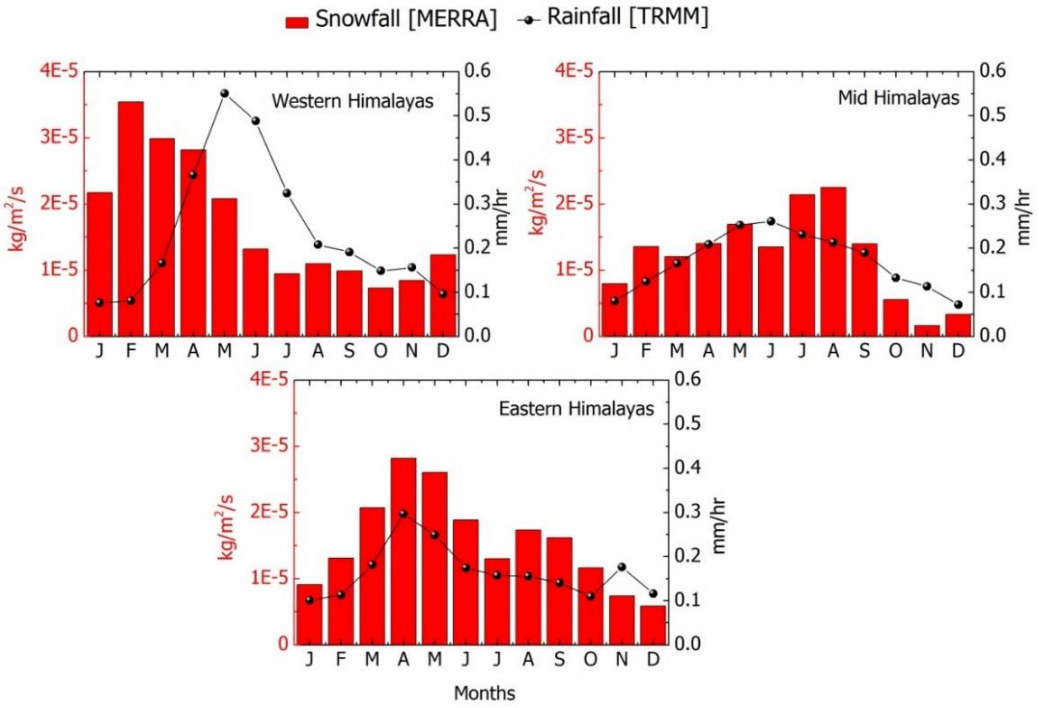


***Figure 5.9 -*** *Annual variation of monthly mean rainfall rate (TRMM) and snowfall rate (MERRA reanalysis) during the period 2006– 2017.*

Aerosol loading builds up from February to June and reduces thereafter with least loading in winter months. Particle mass concentration measurements at Nepal Himalayas (Nagarkot at Kathmandu valley, 2195 m amsl and Langtang Mountain, 3929 amsl) showed increasing aerosol concentration from February to June and decreases from June to September *(Carrico et al., 2003)*. Monsoon washout at Indian mainland can reduce aerosol concentration in convectively lifted up airmass that significantly reduces the aerosol loading during June and the periods after that. Vertical spread of aerosols (with backscattering coefficient > 0.00003 $km^{-1}sr^{-1}$) shows a clear seasonal pattern over the mid Himalayas with an average spread of ~ 7.5 km amsl from March to October that reduces drastically during post monsoon and reach a minimum of ~ 4 km amsl during December. Investigation on seasonal variation of aerosol loading at Nepal Himalaya using station

based observations showed that aerosol build up during pre-monsoon is closely associated with local valley wind systems as well as synoptic circulations by bringing pollutants from southeast Asia during monsoon *(Shrestha et al., 2000).*

Over the eastern Himalayas high aerosol loading with back-scattering coefficient in the range 0.002 – 0.003 $km^{-1}sr^{-1}$ is observed from February, March, and April which decreases in the month of May and following months. Unlike over western Himalayas, snowfall over eastern Himalayas is lowest during winter which increases towards pre-monsoon months and maximizes during May. Pre-monsoon rain /snowfall on the eastern Himalayas could cause wet scavenging of aerosols during this season that significantly depletes aerosols by May and the process get strengthened by enhanced monsoon precipitation (rain and snow) in the following months.

### 5.3.3 Spatial variation of aerosol loading over Himalayas

Figure 5.10 shows the spatial distribution of column integrated aerosol backscattering coefficient over the Himalayas during different seasons. It is interesting to note that the aerosol loading over the Himalayas is lowest during winter when Indian region, especially IGP is affected by high aerosol loading confined within PBL. During this period, the winds are mainly westerly and snowfall rate is significant over western Himalayas. High snow fall rate during this period is mainly associated with the western disturbances that bring moisture rich air over to the Himalayas after passing over the Mediterranean ocean. As the season changes from winter to pre-monsoon, there is a significant enhancement in aerosol loading over the entire Himalayas with high loading over mid and eastern Himalayas compared to western Himalayas. During pre-monsoon, westerly still prevails over Himalayas with an enhancement in rainfall rate and decline in snowfall rate over western Himalayas. Compared to western and eastern Himalayas, mid Himalayas is least affected by precipitation with lower mean snow fall/ rainfall rate around the year. This can be attributed to the high loading of aerosols observed over the Mid Himalayas. Though the region is under the influence of westerly during both winter and pre-monsoon seasons, a 2-fold increase in back-scattering coefficient is observed from winter to pre-monsoon which is attributed to the enhanced convection during pre-monsoon which takes aerosols to the higher altitudes and will be transported horizontally to the Himalayan regions. Over the Indian mainland a clear enhancement in aerosols is observed within 2- 4 km altitude as season change from winter to pre-monsoon (Refer chapter 3, section 3.4.4). During the monsoon and post monsoon season aerosol loading continue to be high with higher loading over the western Himalayas with moderate loading over the mid Himalayas and

least loading over the eastern Himalayas. During monsoon season, snowfall/ rainfall declines over the western Himalayas and aerosol loading is observed to be highest during this season. Over the eastern Himalayas, monsoon and post monsoon season is associated with significant snowfall and moderate rainfall that results in decline in aerosol loading during this period. In general, regional difference in meteorological conditions are observed to have significant influence on the regional differences in the aerosol loading over the Himalayas.

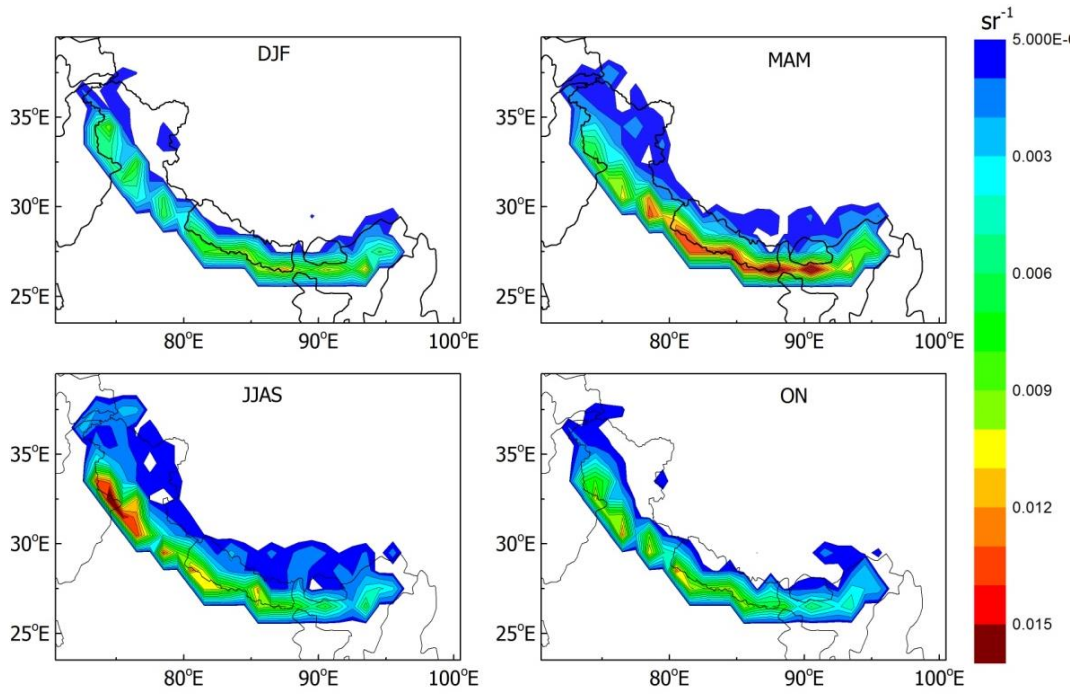


***Figure 5.10*** *- Spatial distribution of column integrated backscattering coefficient of aerosols (CALIOP) over the Himalayas (2006 - 2017).*

### 5.3.4 Vertically resolved spatial variation of aerosols over Himalayas

Figure 5.11 shows the vertically resolved spatial variation of aerosol back scattering coefficient over the Himalayan region from CALIOP observations. Here, integrated back-scattering coefficient over layers of 1 km width is shown at the mid-point altitude level. During winter, aerosols are mostly confined to the lower levels (below 1 km AGL or 5 km amsl) over most of the Himalayan region. However, aerosols are vertically lifted up to ~ 11 km amsl (~7 km AGL) during pre -monsoon season and ~ 9 km amsl (5 km AGL) during summer monsoon over most of the Himalayan region. Ground based LIDAR observations from Nainital (~1960 amsl) in central Himalayas also showed similar seasonal changes in vertical spread of elevated aerosols during pre-monsoon which is attributed to prevailing strong convective conditions *(Hegde et al., 2009).*

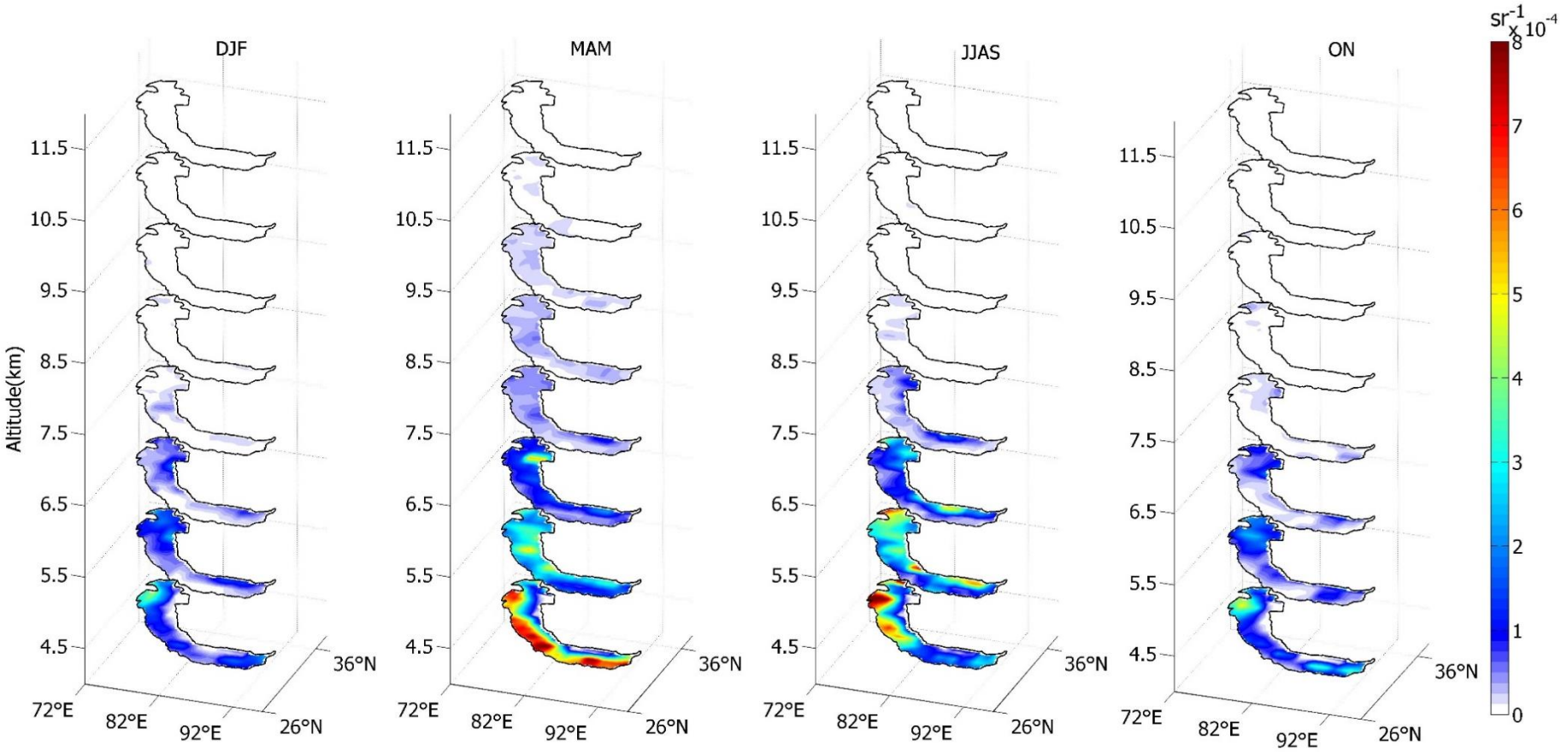


***Figure 5.11*** *- Three-dimensional distribution of aerosol back-scattering coefficient integrated over layers of 1 km width (shown at midpoint of the layer), during winter (DJF), pre-monsoon (MAM), summer monsoon (JJAS) and post monsoon (ON) seasons (2006 – 2017).*

Over the Indian region, enhancement in elevated aerosol loading from winter to pre-monsoon is observed to be associated with increasing mineral dust loading (Refer chapter 3, section 3.4.5). As a part of Cloud Aerosol Interactions and Precipitation Enhancement Experiment (CAIPEEX), vertical distribution of aerosols were measured using instrumented aircraft during 2009, which showed layers of elevated aerosols up to 4 km over the western Himalayas during pre-monsoon period *(Padmakumari, et al., 2013).* In-situ measurements of cloud drop size distribution and concentration showed that clouds observed above the elevated aerosol layers has higher droplet concentrations with small effective radius *(Padmakumari, et al., 2013).* Using back-trajectory analysis, sources are identified as local anthropogenic activities and long range transport of dust aerosols. CALIPSO transects within 200 km from NCO-P showed pollution from the IGP extended up to 4 – 5 km that is carried by the mountain breeze to the station location that contributed to the high surface concentration of BC observed at the station *(Gobbi et al., 2010)*. Aerosol scale heights estimated using ground/column measurements indicated the presence of elevated layers which are attributed to ice particles or mineral particles as well as to cloud-processed aerosols *(Gobbi et al., 2010).*Figure 5.12 shows the percentage contribution of aerosol backscattering coefficient above 1 km from above ground level (AGL) over the study regions.

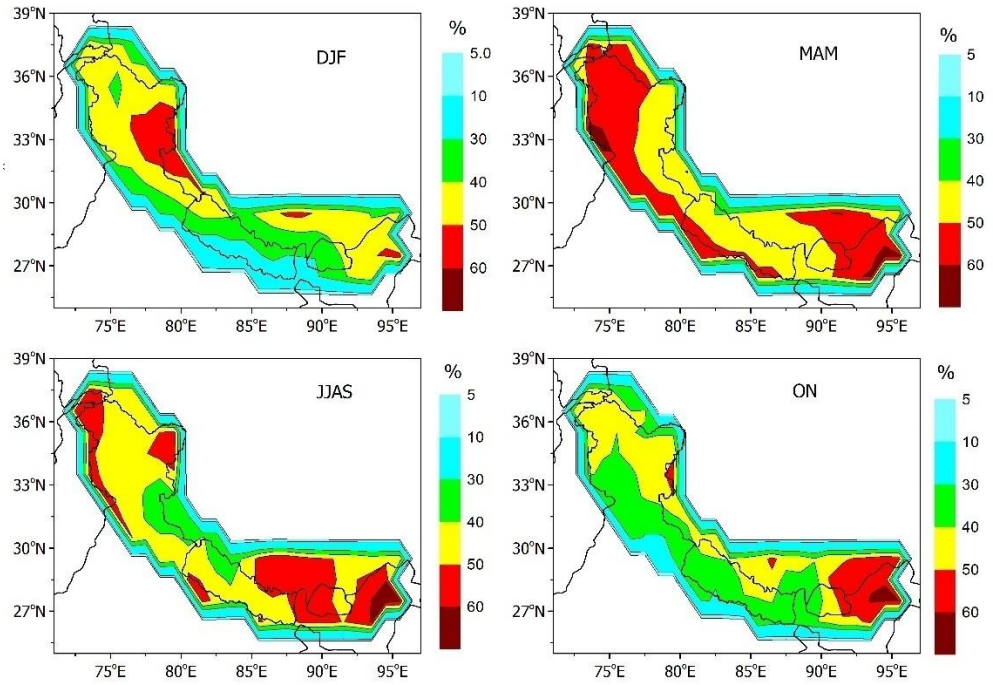


***Figure 5.12*** *- Spatial distribution of percentage fraction of average aerosol back-scattering coefficient (β) above 1 km above ground level to columnar integrated back-scatter coefficient over the Himalayas during the period 2006 - 2017 during pre-monsoon season (MAM).*

CALIOP aerosol backscattering profiles over the period 2006 – 2017 are gridded to 1° x 1° spatial resolution and averaged to estimate the mean columnar fraction of aerosols above 1 km over the study regions. Error bar represent the spatial variability of fraction of aerosols above 1 km within the study regions. More than 35% of aerosols in the column are present above 1 km over the Himalayas. Fraction of elevated aerosols is observed highest during pre-monsoon and summer monsoon seasons with an average of 50±5% and 48±6% respectively, while during winter and post monsoon seasons they are 41±8 % and 42±8%. Elevated aerosol fraction shows distinct regional differences. In general, Western and eastern Himalayas show higher fraction of aerosols above 1 km and mid Himalayas shows the least.

Presence of westerly circulation around the year over the northwest India facilitates the transport of mineral dust aerosols from the arid region of middle-east and northwest towards the Himalayas. Based on satellite based investigations, *Gautam et al., (2013)* reported the role of transported mineral dust on snow darkening and accelerated glacier melting over the Himalayas. Several studies indicate the transport of mineral dust to the Himalayan region using spectral AOD measurements supplemented with back trajectory analysis and satellite images *(Gobbi et al., 2010; Brun et al., 2011; Bucci et al., 2014; Duchi et al., 2014; Ningombam et al., 2014)*. *Gautam et al., (2009)* investigated role of dust aerosols in the widespread warming observed over the Himalayan-Gangetic region using OMI AI (Aerosol Index) and micro-wave remote sensing dataset of temperature. A warming trend of 2.7°C in the 29-year record (1979–2007), is observed over this region when this region is strongly influenced by dust aerosols at elevated altitudes *(Gautam et al., 2009)*. Many studies have observed warming trend over the Himalayas, Tibetan Plateau, and IGP. Absorption characteristics of transported dust enhances in mixed state due to interaction with anthropogenic aerosols *(Deepshikha et al., 2005).* CALIOP observations of depolarization ratio that can be effectively used to categorize aerosols (Refer chapter 2, section2.2.1.6). Depolarization ratio observations along with back-trajectory air mass analysis are used in the following sections to classify dust over the Himalayas.

### 5.3.5 Role of transport on the regional distribution of dust

Being a pristine environment, aerosol sources are limited over the Himalayas. Aerosol loading over the Himalayas is mostly influenced by transport of aerosols through large scale/local circulations. Using surface/column measurements, several studies have indicated the role of long range transport in the distribution of aerosols over the Himalayan region *(Carrico et al., 2003; Babu, Chaubey, et al., 2011; Gogoi et al., 2011).* Apart from long range transport by the prevailing westerly winds, role of mountain-valley

breeze in uplifting aerosols over to the high altitude regions of Himalayas has been reported using station based observations (*Babu, Chaubey, et al., 2011; Decesari et al., 2010*; *Lüthi et al., 2015)*. Still, uncertainty remains in identifying aerosol sources, transportation, and deposition of different aerosol species over the Himalayas. Air mass trajectory analysis is a useful tool to examine the source regions and major advection pathways of aerosols arriving at a location. Hybrid Single Particle Lagrangian Integrated Trajectory (HYSPLIT) *(Draxler and Hess, 1998)* model is used to examine seven day daily back trajectories of isentropic air masses arriving at the study regions of Himalayas at 100 m AGL over the study regions. Analysis is carried out for the representative receptor locations at 35˚N, 75˚E on western Himalaya, 28.8˚N, 83˚E on mid Himalayas and 28˚N, 92˚E on eastern Himalayas. Figure 5.10 (a) shows the mean of 5-day back-trajectories of airmass from west and east of the study regions during MAM of 2007 to 2017.

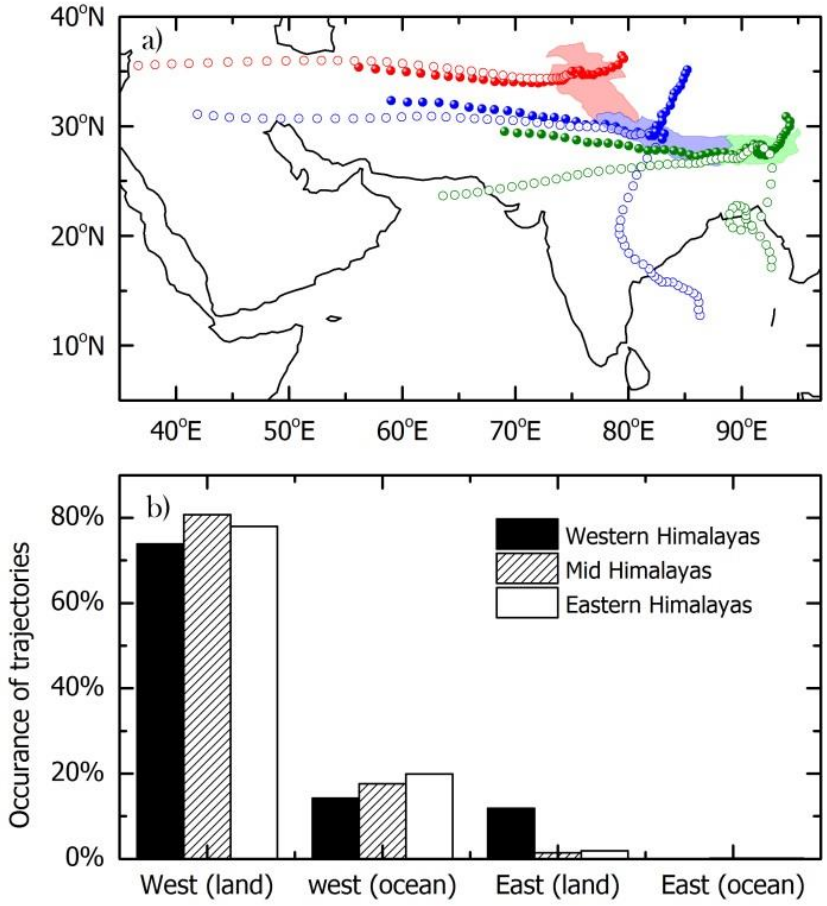


***Figure 5.13 -*** *a) Mean of 5-day back-trajectories of airmass from east and west of the study regions using HYSPLIT trajectory model during MAM of 2007 to 2017. Trajectories from ocean (open circle) and land (solid sphere) are shown separately. Colour of the trajectories represent the receptor locations over the study regions (Western Himalayas – Red, Mid Himalayas – Blue, and Eastern Himalayas -Green) b) Percentage of occurrence of airmass reaching at the study locations at western, mid and eastern Himalayas.*

Trajectories originating from ocean (open circles) and land (solid spheres) are shown separately. Panel (b) shows the percentage of occurrence of 5-day back-trajectories of airmass reaching at the study locations at western, mid and eastern Himalayas during MAM of 2007 to 2017 using HYSPLIT trajectory model. Trajectories reaching at the study locations during pre-monsoon are mostly from the west of the study locations while trajectories from east are negligibly small. 70 to 80 % of the total trajectories are reaching from the western land mass while around 10 to 20% of the airmass are from the oceanic regions in the west. Trajectories from east are less in number over all study regions.

Aerosols advected from the western arid regions can carry aerosols rich in mineral dust. Figure 5.14 shows the frequency distribution of PDR averaged at 10 km latitudinal resolution over the study regions within 3 - 6 km altitude amsl where aerosol concentration is observed to be moderately high. Depolarization criteria is used to segregate the occurrence of pure dust (dust only) ($\delta>0.25$), polluted dust ($0.05>\delta>0.25$) and pure non-dust ($\delta<0.05$) from the PDR spectrum. Over eastern Himalayas, PDR occurrence peaks in the non-dust region while over mid Himalayas it peaks in the polluted dust regime and western Himalayas shows a broad peak in the polluted dust regime. Though PDR spectrum shows distinct signature over study region indicating prevalence of regionally distinct aerosol composition, all three regions are characterized with significant amount of polluted dust.

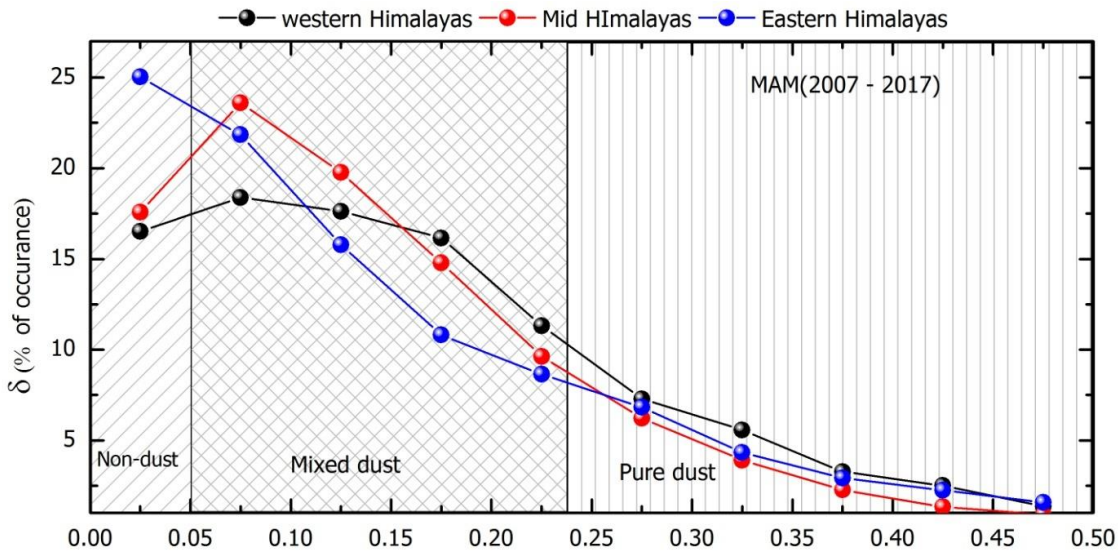


***Figure 5.14*** *- Percentage of occurrence of PDR measured by CALIOP within 3 - 6 km amsl over the study regions during MAM of 2007 to 2017.*

Figure 5.15 shows the percentage occurrence of pure dust, polluted dust, and non-dust over the study regions. About 55% (east) to 65 % (mid) of the aerosols over Himalayas are characterized as polluted dust. In mixed state, absorption characteristics of dust aerosols

can significantly increase. *Deepshikha et al., (2005)* studied the absorption characteristics of dust by estimating dust induced radiance depression in IR measured from space by METOSAT and showed that pure dust over desert regions is less absorbing than that transported to other locations having anthropogenic activities. Here polluted dust represents the case where the dust fraction varying from 1% to 99%. 25% to 35% of the cases are mixed aerosols with more than 50% dust contribution. It is indicated by the grey diagonal pattern in figure 5.15.

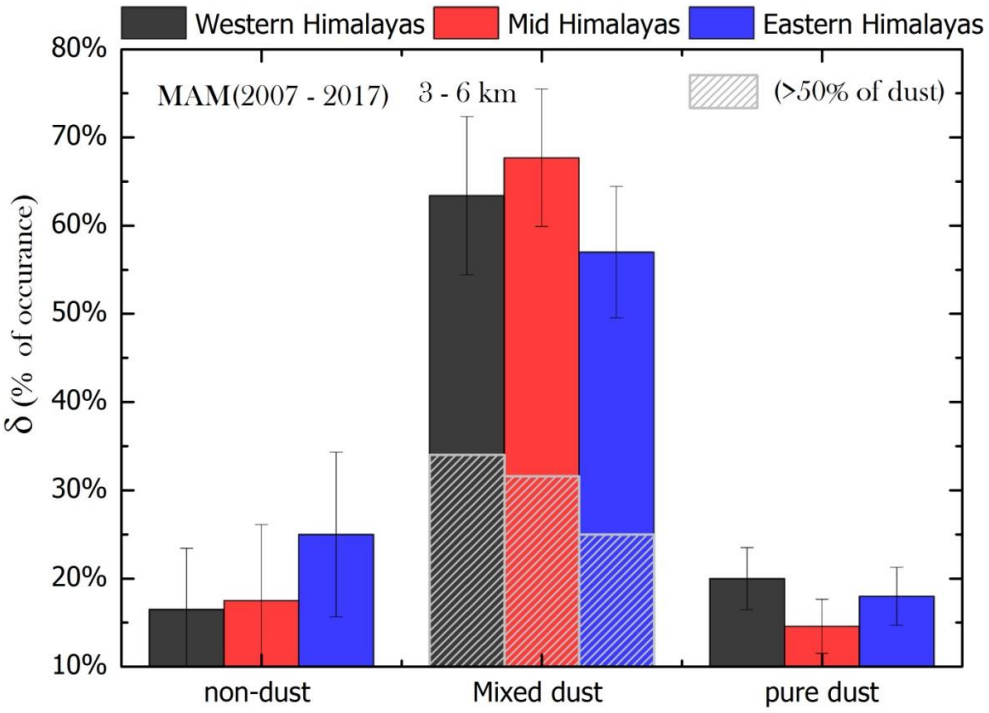


***Figure 5.15*** *- Percentage occurrence of pure dust, polluted dust, and non-dust over the study regions as measured by CALIOP within 3 - 6 km amsl over the study regions during MAM of 2007 to 2017.*

### 5.3.6 Quantification of mineral dust aerosols

Quantitative estimation of mineral dust aerosols over the Himalayas based on observations are very limited though there have been limited attempts using climate modelling simulations *(Ji et al., 2016).* Present study represents the first time quantitative characterization of mineral dust aerosols based on space-borne depolarization observations over the Himalayas. The methodology for estimation of dust extinction coefficient from CALIOP observations of PDR is detailed in Chapter 2. The method is specifically advantageous in estimating extinction coefficient due to dust aerosols in mixed systems *(Sugimoto and Lee, 2006; Tesche et al., 2011).* In the present study, the three dimensional distribution of dust aerosols over Himalayas is generated using CALIOP depolarization observations.

#### 5.3.6.1 Vertical distribution of mineral dust aerosols

Studies on mineral dust effects over Himalayan cryosphere is limited though there are efforts have been made to characterize black carbon aerosols over snow. Using depolarization ratio observations from CALIOP, dust extinction coefficient ($\sigma_d$) is estimated (Refer chapter2 section 2.1.5) and its vertical and spatial variation over the study region is shown in Figure 5.8. Dust extinction coefficient estimated using depolarization ratio solely depends on the particulate depolarization ratio (PDR) observations and a priori knowledge of depolarization ratio of dust / non-dust aerosols and dust lidar ratio. The method is advantageous in separating dust extinction coefficient in a mixed system and avoids the assumption of single lidar ratio for different mixtures as used in CALIOP lidar ratio selection algorithm. The annual variation of the altitude distribution of dust extinction coefficient estimated using CALIOP depolarization observations during 2006 to 2017 over western, mid and eastern regions of the Himalayas is shown in Figure 5.16.

The influence of dust is found to be significant during the period from February to July over western and Mid Himalayas and February to May over eastern Himalayas. The dust extinction coefficient peaks during the month of May over western and mid Himalayan regions where the dust reaches as high as 6 km amsl during this period. Over eastern Himalayas, dust extinction coefficient peaks during the month of April where the dust influence is seen up to ~5 km amsl. Western Himalayas which are close to source regions in the west, shows comparatively less dust loading with dust extinction coefficient ranging from 10 – 20 $Mm^{-1}$ peaking in the month of June. Over Eastern Himalayas dust concentration peaks in the month of April and dust extinction coefficient has a magnitude ranging from 20 – 30 $Mm^{-1}$. Dust loading during winter is negligibly small with dust extinction coefficient less than or equal to 5 $Mm^{-1}$ at the surface. Over mid-Himalayas almost 10 fold increase is observed from winter to pre-monsoon. Seasonal variation in dust loading is similar to total aerosol loading over the Himalayas though effect of wet scavenging associated with the monsoon rainfall is predominantly shown by dust aerosols with a sudden drop in dust concentration during July over mid Himalayas and June over eastern Himalayas. A build up dust aerosols is observed as season changes to post monsoon over mid and western Himalayas, while it is absent over eastern Himalayas. Dust loading spreads up to 5 to 6 km over the Himalayas during pre-monsoon ($\sigma_d$ >1$Mm^{-1}$). Though the magnitude of dust optical depth is smaller at this altitude range, given the high availability of radiation from the bright surface and lower number concentration due to pristine environment along with atmospheric thinning, can lead to higher heating rate at

this altitude range. Effect of dust episodes at Thar desert over Himalayas is reported using micropulse lidar observations at Central Himalayas which showed drastic enhancement in aerosol back-scattering coefficient (~0.03 $km^{-1}sr^{-1}$), during a dust storm at Thar desert, within ~1.3 to 3 km altitude range above ground level with an Ångström exponent of around 0.04 with a heating rate of ~ 0.4 $Kday^{-1}$ *(Srivastava et al., 2011).* Three-dimensional distribution of layer optical depth due to dust aerosols is shown in figure 5.17. Dust extinction coefficient integrated over layers of 1 km width is shown at the mid-point altitude level. Highest dust loading is observed during pre-monsoon season with a vertical extent up to 11 km amsl where a minimum $\sigma_d$ of 2 $Mm^{-1}$ is observed whereas during winter this is confined within 8 km amsl. An east-west gradient is observed in the dust loading with higher dust loading over the western Himalayas during all seasons due to its close proximity to dust sources.

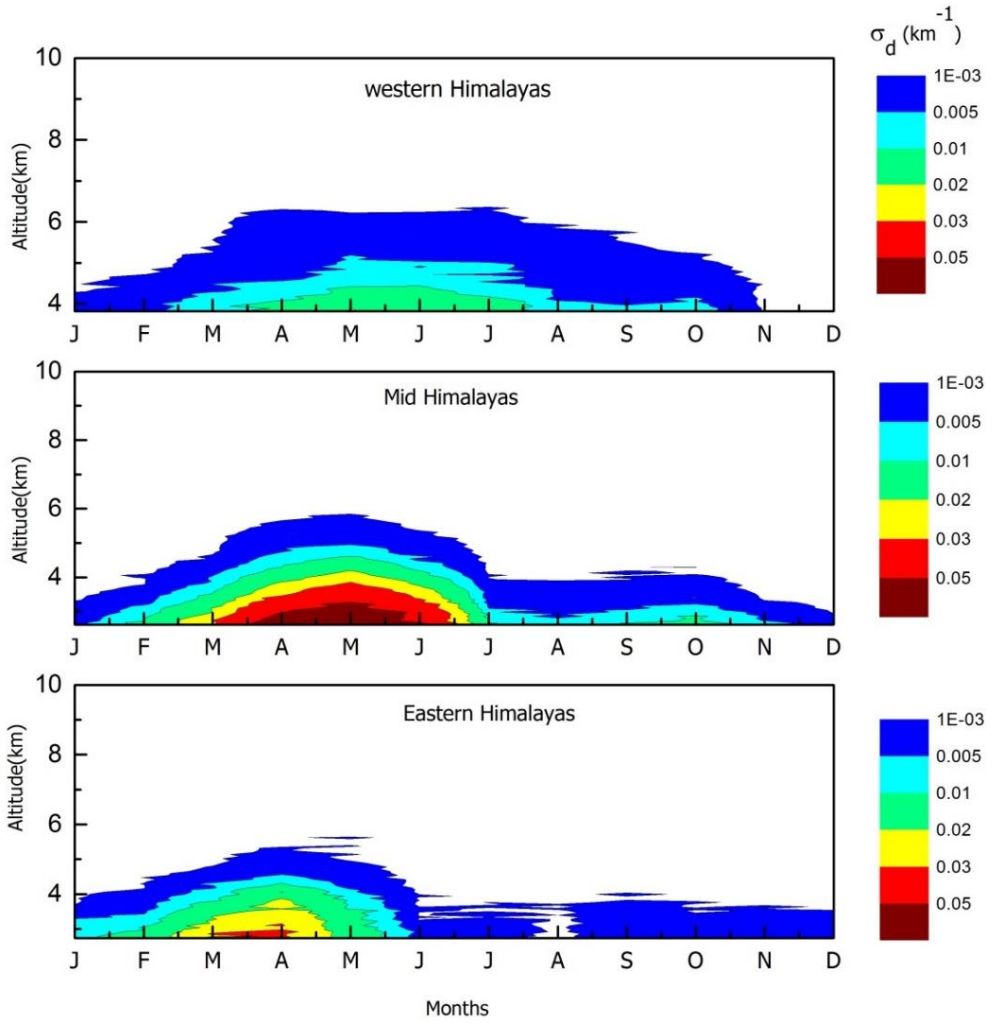


***Figure 5.16*** *- Annual variation of the vertically resolved monthly mean dust extinction coefficient over the western, mid and eastern Himalayas above mean elevation averaged during the period 2006 – 2017.*

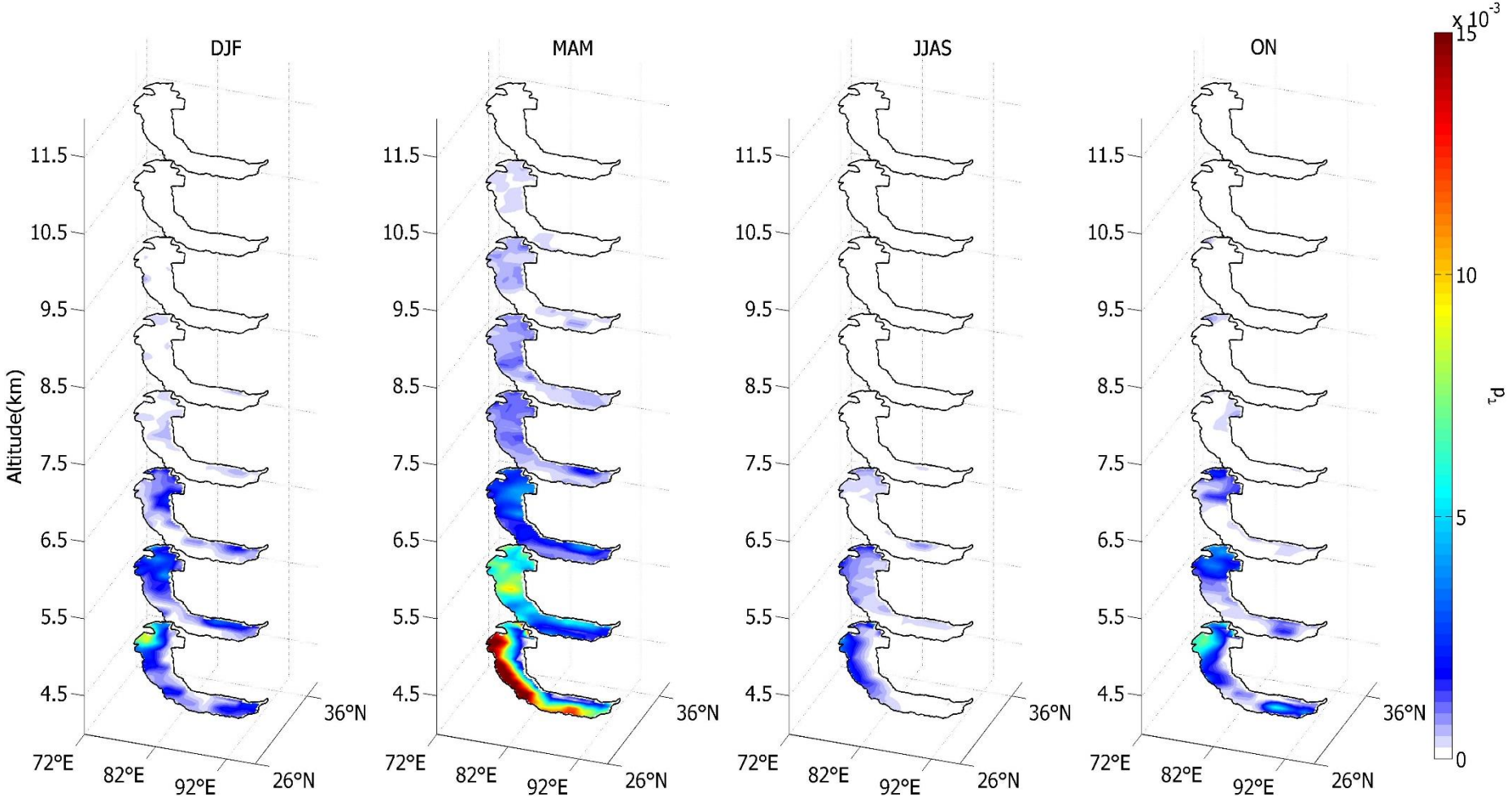


***Figure 5.17*** *- Three-dimensional distribution of dust extinction coefficient integrated over layers of 1km width (shown at midpoint of the layer), during winter (DJF), pre-monsoon (MAM), summer monsoon (JJAS) and post monsoon (ON) season.*

Dust loading is least during summer monsoon though back-scattering coefficient due to composite aerosols is rather high during this season. While westerly circulation dominates during all other seasons, during summer monsoon most of the Himalayas are under the influence of south easterly from the Bay of Bengal branch of monsoon circulation. This change in synoptic circulation pattern can likely be the reason for reduced dust concentration during this season. According to *Duchi et al., (2014)* dust transport frequency over NCO-P was observed the highest during the pre-monsoon and winter seasons (31.8% and21.6% of the season's days respectively) with lower values for the monsoon and post-monsoon seasons (13.9% and 13.2%, respectively) using observations of aerosol size distribution. The spatial pattern of dust loading is found to be similar during post monsoon and winter.

### 5.3.6.2 Dust optical depth

Figure 5.18 The spatial variability in dust optical depth ($\tau_d$) obtained by integrating the profiles of dust extinction coefficient obtained using CALIOP PDR observations (shown in Figure 5.17) over the Himalayas during different seasons is shown in Figure 5.18.

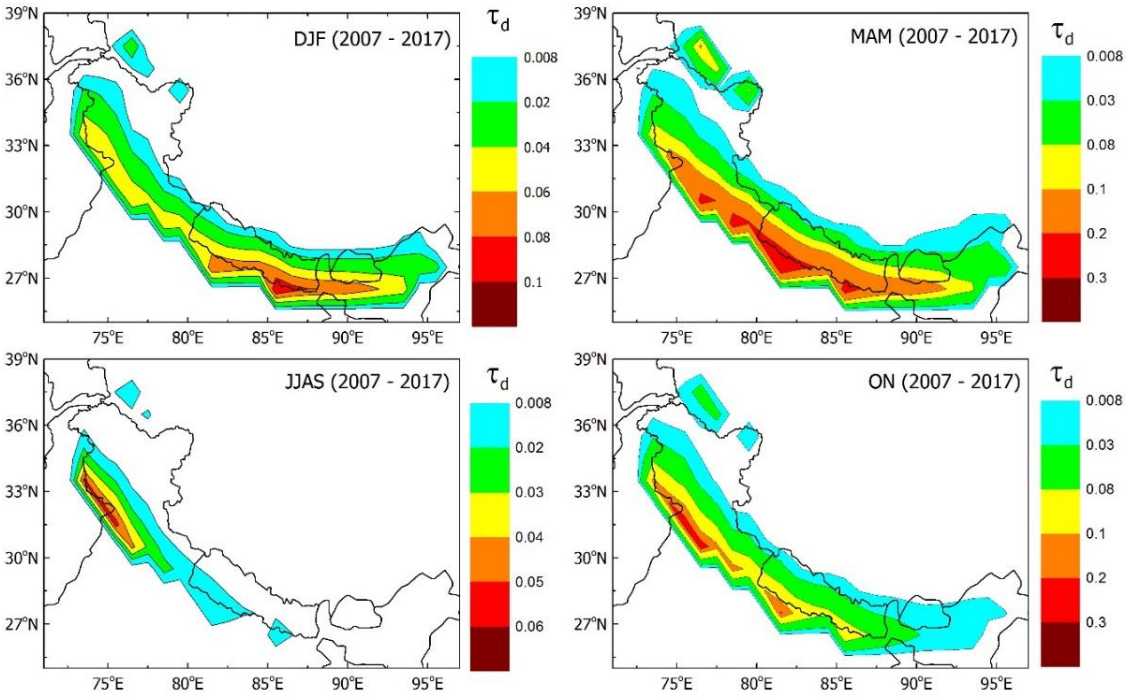


***Figure 5.18*** *- Spatial distribution of average dust optical depth ($\tau_d$) over the Himalayas during DJF, MAM, JJAS and ON of 2006 – 2017.*

During winter, dust loading is higher towards the eastern Himalayas with a mean dust AOD reaching up to 0.1. Snowfall during winter is pre-dominant over the western/central western part of Himalayas that can efficiently remove aerosols present in the atmosphere

over this region (figure 5.5). Dust AOD is highest during pre-monsoon season over most of the Himalayas. Column dust optical depth during pre-monsoon season is found highest over mid-Himalayas implying the role of convectively lifted up mineral dust aerosols from the Indian main land in contributing to the dust loading over the Himalayas. *Manoharan et al., (2014)* has reported enhanced absorption of shortwave radiation by coarse mode particles and their radiative effect over the Gangetic-Himalayan region (mid-Himalayas) based on in situ observations, Dust loading is found to be minimum during summer monsoon period whereas significant dust loading over the southern slopes of Himalayas are observed during post monsoon season with $\tau_d$ reaching up to 0.2. Chemical composition analysis of particulate matter at Nepal Climate Observatory-Pyramid(NCO-P) at 5079 amsl over the central Himalayas, shows significant fraction of mineral dust (50%) to average $PM_{10}$ mass loading *(Decesari et al., 2010).*

Being an absorptive species, dust aerosols produce enhanced radiative effects in the atmospheric column above snow surface and also accelerate snow melting process through its deposition over the snow surface *(Painter et al., 2007).* They exert positive radiative forcing at TOA over highly reflecting surface *(Liao and Seinfeld, 1998).* Dust induced warming is found to have played a significant role in the termination of glacial period *(Overpeck et al., 1996).* Model simulations shows that high dust loading during glacial maximum over tropical regions can have a radiative impact comparable to low glacial $CO_2$ levels *(Harrison et al., 2001)*. On modelling the influence of dust and black carbon deposition on snow surface it was shown that in presence of mineral dust, albedo reduction by BC on snow is reduced *(Dang et al., 2015).* Using snow samples from high altitude stations (5400 to 6400 amsl) from the southern slope of the Himalaya, it is observed that BC and Fe (proxy of dust) concentrations were higher at stations at elevated altitudes and with estimation of albedo changes and radiative forcing calculations it is showed that the snow albedo and radiative forcing effect of dust is considerably greater than BC *(Kaspari et al., 2014).* It is suggested that further observational studies are needed to estimate the contribution of BC and dust to albedo reductions and snow and ice melt *(Kaspari et al., 2014)*. In view of radiative effects, model simulations show that absorptive effects of mineral dust aerosols dominates the radiation interaction, over bright surfaces with surface albedo above a critical magnitude of 0.35 *(Patadia et al., 2009)*. With radiative transfer modelling, *Kaspari et al., (2014)* shows that when dust concentration is high, the impact of BC is negligible and that radiative effect due to dust is considerably greater than BC on snow.

### 5.3.6.3 Dust mass flux deposited over the Himalayas

Snow darkening effect of mineral dust aerosols is still unexplored as quantitative estimate of mineral dust deposition on snow surface over the Himalayas is very limited. Using CALIOP derived profiles of dust extinction coefficient, dust mass flux deposited over the Himalayas is estimated for pre-monsoon season during which dust loading is observed to be the highest (figure 5.17). Dust mass per unit volume ($M_d$) with 'n' particles with a radius 'r' is given by the product of volume, density (ρ) of the particle and number of particles in unit volume as given by

$$M_d = \frac{4}{3}\pi\rho\int r^3 n(r)dr \qquad (5.1)$$

while dust extinction coefficient $\sigma_d$ is given by

$$\sigma_d = \pi\int Q(r)r^2 n(r)dr \qquad (5.2)$$

The quantity

$$\sigma^* = \frac{\sigma_d}{M_d} \qquad (5.3)$$

is defined as the the mass extinction efficiency of dust aerosols and is given by equation (5.3) assuming Q is independent of radius of dust

$$\sigma^* = \frac{Q}{1.33\rho R_{eff}} \qquad (5.4)$$

where

$$R_{eff} = \frac{\int r^3 n(r)dr}{\int r^2 n(r)dr} \qquad (5.5)$$

Assuming Q as 2.2 and ρ as 2.6 g/cm$^3$ as measured during Saharan Dust Experiment (SHADE) using aircraft based measurements *(Haywood et al., 2003)* and $R_{eff}$ as 1.7 μm as retrieved from AERONET measurements, magnitude of σ* would be 0.37 m$^2$/g (Kaufman et al., 2005). Life time ranges from ~ 1- 2 weeks for dust aerosols smaller than 2 μm which facilitate efficient transport of dust with size < 2 μm while only few hours for those greater than 2 μm (Tegen et al., 1996; Miller et al., 2006). Using, Monte Carlo calculations, *Kaufman et al., (2005)* estimates an error of ~ ±15% in the estimated value of σ*. Near surface mass concentration of dust is estimated using CALIOP derived dust extinction coefficient ($\sigma_d$) at range bin close to surface.

Using mass absorption cross-section (σ*) value of 0.37 m$^2$/g in equation (5.3) dust mass concentration close to surface is estimated over the Himalayas. To estimate the deposited

flux of dust, sedimentation through dry deposition and wet scavenging need to be addressed. Dry deposition of aerosols is mainly driven by gravitational settling whereas wet deposition includes scavenging of aerosols that act as cloud condensation nuclei through precipitation (in-cloud) and below cloud scavenging in which falling precipitation wash out aerosols in the column. Dust aerosols with size greater than 20 μm are prone to gravitational settling and their life time is estimated to be of the order of 12 hours *(Ryder et al., 2013*). Wet deposition dominates scavenging for dust aerosols with size less than ~ 5 μm whereas scavenging of aerosols larger than 5 μm are controlled by dry deposition *(Miller et al., 2006; Woodward, 2001; Zender, 2003).* Estimation of scavenging ratios of different chemical species in snow samples collected from north-western Himalayas showed that crustal components are efficiently removed from the atmosphere during snow fall *(Kumar et al., 2016)*. However observations of aerosol size distribution in the atmosphere and snow samples during a dust event and after snow fall event, showed dry deposition clearly dominates for dust aerosols with radii greater than 2.5 μm while wet deposition controls those with radii less than 2.5 μm *(Aoki et al., 2006).* Estimation of dust flux deposited on snow through wet scavenging needs simultaneous measurements of aerosols and precipitation which is out of the scope of the present analysis.

Deposited mass flux of dust through dry deposition is estimated as the product of dust mass concentration and deposition velocity of dust particles and is shown in figure 5.20. Deposition velocity is determined by the size of the particle, resistance offered by eddies, resistance by the quasi-laminar surface layer and canopy resistance. Theoretically, deposition velocity is inversely proportional to the size of the particles *(Seinfeld et al., 1998).* Observations shows that dust particle size distribution is independent of the wind speed at the emission regions (*Reid, Reid et al., 2008)* but during the course of transport, significant fraction of large particles are lost through sedimentation *(Mahowald et al., 2014; Ryder et al., 2013)*. Aircraft based observations of transported mineral dust aerosols over Mediterranean shows that a modal diameter of the number size distribution between 1.3 and 2.0 μm *(Denjean et al., 2016)*. A median effective diameter of 2.5 μm was reported for aged dust during Saharan Mineral Dust Experiment using airborne in-situ measurements *(Weinzierl et al., 2011). Slinn et al., (1978)* estimated the deposition velocity as a function of particle size over water surface using wind tunnel experiment and showed that accumulation mode (0.1 - 1μm) particles have the minimum deposition velocity (0.01 – 0.02 $cms^{-1}$). For dust effective radius from 2 μm to 3 μm, dust deposition velocity varies from ~ 0.08 $cms^{-1}$ to 0.2 $cms^{-1}$ as observed by *Slinn et al., (1978). Zhang et al., (2001)* estimated a much higher dry deposition velocity of an average value of 2.7 $cms^{-1}$ for dust particles at the source region over Tibetan Plateau using observations from cascade

impactor in a two layer deposition model that can be attributed to the larger size of the freshly emitted dust particles over this region. Dry deposition flux is estimated for dust deposition velocity varies from ~ 0.08 $cms^{-1}$ to 0.2 $cms^{-1}$ and the average flux is represented in figure 5.19. Error bar represents the possible variability due to assumed deposition velocity.

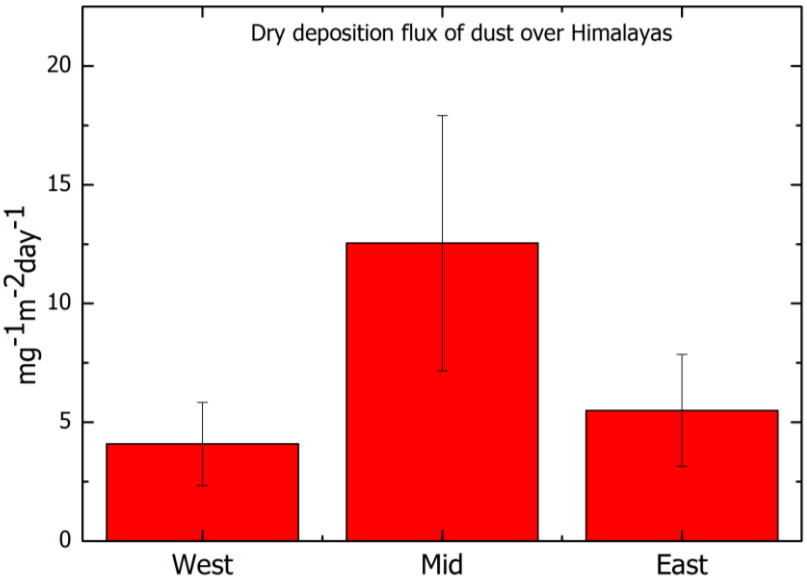


***Figure 5.19*** *- Dust mass flux on the surface due to dry deposition over the Himalayas. Error bar represent the variability in mass flux due to uncertainty in the assumed deposition velocity of dust aerosols.*

### 5.3.7 Radiative implications

Warming induced by the elevated aerosols can enhance to snow melting mechanism through different physical mechanisms. Firstly it can effectively transfer from the atmosphere to the surface as sensible heat flux and promote snow melting, and secondly it can affect conditions favouring snow formation and reduce rate of snowfall on the surface*. Ramana et al., (2004)* carried out observations of aerosol vertical profiles suing micro-pulse lidar and along with direct observations of AOD, SSA, aerosol forcing in the atmosphere is estimated to be 25 $Wm^{-2}$ with a heating rate of about 1 $Kday^{-1}$ within 2 km from the surface. Though AOD values are very low, aerosols over Nepal Climate Observatory-Pyramid (NCO-P) are more absorbing (SSA of 0.6–0.9) and persists throughout the year *(Gobbi et al., 2010).* With numerical experiments, *Lau et al.,(2010)* associates accelerated snow melt with enhanced warming of the atmosphere over the Tibetan Plateau and Himalayas, induced by absorbing aerosols accumulated in the IGP and foothills of Himalayas during this season. The effective transfer of sensible heat flux from the atmosphere to the land set off the snow melting process which is accelerated by an

evaporation–snow–land feedback associated with the increase in atmospheric moisture over the Tibetan Plateau induced by the EHP effect. The warmer atmosphere with more moisture reduces the effective transfer of sensible/latent heat fluxes from the surface to the atmosphere, instead contributes to snow melting which accelerates the process over the Tibetan Plateau and the Himalayas. Analysing satellite observations of aerosol optical depth (MODIS), Aerosol Index (OMI), cloud optical depth (MODIS) and rainfall (TRMM), using empirical orthogonal function analysis, it is observed that over Himalayas, regions of aerosol build-up during the pre-monsoon are collocated with regions of enhanced monsoon rainfall/cloudiness *(Shrestha and Barros, 2010)* which is a supporting information on EHP hypothesis.

Presence of light absorbing particles in the snow reduces snow albedo there by counteracts the dimming effect induced by aerosols. *Flanner et al., (2009)* showed that the warming effect due to snow-darkening by the deposition of absorbing aerosols is almost six folds higher than the cooling at the surface due to direct effect of aerosols. Model simulations shows that, snow-darkening effect due to mineral dust aerosols weakens the Indian monsoon rainfall while the direct radiative forcing strengthens it *(Shi et al., 2018).* To have a more complete understanding on impact of aerosols on cryosphere, it is necessary to address the coupling of radiative balance of atmosphere and snow, which is beyond the scope of this work.

## 5.4 Summary

Seasonal, spatial, and vertical distribution of aerosols are examined over the Himalayas. Overall understanding on the radiative implications of mineral dust aerosols on snow albedo and snow melting is actually hindered by the lack of quantitative estimation of mineral dust using direct experimental observations. Present chapter attempted to characterise mineral dust aerosols, it's spatial, vertical and columnar variations over the Himalayas and estimated the mass flux of dust aerosols deposited over the region through dry deposition. Following are the concluding points

1. Aerosol loading over the Himalayas critically depends on the topography with a drastic decrease in AOD with surface elevation. AOD at high altitude stations decreases up to one order magnitude compared to stations at the foothills.
2. Aerosol loading shows seasonally distinct regional pattern that are associated with the precipitation pattern over the Himalayas. Aerosol loading is observed to be minimum during winter while more than two fold increase is observed during pre-monsoon over mid/eastern Himalayas. During summer monsoon/post monsoon

season aerosol loading is highest over the western Himalayas and lowest over eastern Himalayas.

3. Significant fraction of elevated aerosols is observed over the Himalayas throughout the year. An Average of 50 ± 5% and 48 ± 6% of aerosols in the column is present above 1 km during pre-monsoon and summer monsoon respectively while during winter and post monsoon seasons; contribution of elevated aerosols above 1 km to the columnar loading is 41 ± 8 % and 42 ± 8% respectively.
4. Dust aerosol loading shows regionally and seasonally distinct characteristics over the Himalayas with highest loading over the Mid Himalayas during pre-monsoon season. During this season, the entire Himalayas is significantly influenced by polluted dust where the contribution of polluted dust to the total aerosols over western, mid and eastern Himalayas are 63 %, 67 % and 57 % respectively.

# Chapter 6

# Radiative impacts of elevated aerosols

## 6.1 Introduction

Though absorption of solar and terrestrial radiation by gaseous atmosphere is well understood, effect of aerosols on atmospheric heating rate and its vertical structure is not well addressed. Radiative heating/cooling effects of aerosols are important in the accurate assessment of the impacts of aerosol on climate. Mineral dust and carbonaceous aerosols (black carbon and organic carbon) not only cool the surface by backscattering the solar radiation, they absorb the radiation, and diabatically warm the atmosphere. Globally, there have been several attempts to quantify heating effect of absorbing aerosols in the atmosphere through modelling and using satellite/ground based observations *(Alpert et al., 1998; Quijano et al., 2000; Myhre and Stordal, 2001; Ramanathan et al., 2007; Satheesh et al., 2008*). Significant aerosol forcing is observed on the atmosphere over South Asia during winter under the influence of anthropogenic emission *(Satheesh and Ramanathan, 2000)*. Aerosol system of South Asia is complex due to long-range transport of dust aerosols from West Asia/North-west India as well as spatio-temporal heterogeneity in emission sources and processes like aerosol mixing and aging. Complex and heterogeneous aerosol system over South Asia have significant implications on regional climate and radiation balance. Aerosol-monsoon interaction studies have highlighted the importance of moisture convergence as a result of diabatic heating due to absorbing aerosols *(Lau et al., 2006; Jin et al., 2014; Vinoj et al., 2014; Solmon et al., 2015)*. Mineral dust aerosols have a controlling role in modulating ENSO (El Nino Southern Oscillation), which has further influence on the Indian summer monsoon *(Kim et al., 2016)*. Over Indian landmass, aerosol loading during pre-monsoon season is characterized by higher absorption especially over the Indo-Gangetic plain and western India *(Gautam et al., 2010; Nair et al., 2016)*. Aerosol induced warming has perilous impacts on Himalayan cryosphere by causing enhanced snowmelt and glacier retreat *(Lau et al., 2010; Marcq et al., 2010; Ritesh Gautam et al., 2013; Li et al., 2016)*. Continental outflow from Indian landmass causes significant warming over the atmosphere of oceanic regions of India with high heating rates (up to 1 $Kday^{-1}$) *(Chung et al., 2002; Satheesh, Srinivasan, et al., 2006)*.

Studies on aerosol direct effect on atmospheric heating rate are mostly based on the columnar observations of aerosol loading or near surface observations of aerosol optical

properties. However for the accurate estimation of aerosol radiative effect, it is important to include the vertical distribution of aerosol parameters in the radiative transfer calculations. Direct measurements of vertical profiles of aerosols were spatially and temporally limited before the launch of space-borne lidar. With the advent of space-borne lidar, CALIOP, vertical characterization of aerosols at a globally extended spatial coverage with high resolution became possible. Species wise characterization of aerosol radiative effect is highly uncertain and challenging due to the limited information on the spatial distribution of different aerosol species and their vertical distribution. There are a few studies on mineral dust aerosols based on passive remote sensing from space such as METEOSAT *(Deepshikha et al., 2005)*, OMI *(Prospero et al., 2002)*, and MODIS *(Kaufman et al., 2005*), which are incapable of providing information on the vertical distribution of dust. The present study carry out quantitative analysis of vertical distribution of mineral dust aerosols based on observational datasets from space-borne (CALIOP), ground based (ARFINET) and air-borne (RAWEX) platforms, and estimates aerosol induced vertically resolved heating rate for the first time over the Indian region.

## 6.2 Dataset

Space-borne observations of vertical profiles of aerosol extinction coefficient (CALIOP), ground based columnar observations AOD at ARFINET observatories and aircraft based observations of vertical profiles of aerosol SSA as a part of Regional Warming Experiment (RAWEX) at distinct locations over the Indian landmass are used in Santa Barbara DISORT Atmospheric Radiative Transfer Model (SBDART) *(Ricchiazzi et al., 1998)*, to estimate the vertically resolved aerosol induced heating rate over the Indian region. Details on SBADRT are described in chapter 2, section 2.5.1. CALIOP level 2 version 4.1 observations of back-scattering coefficient and depolarization ratio are used to estimate the vertical profiles of dust extinction coefficient over the study region (Refer to Chapter 2, Section 2.2.1.6). Screening techniques used for CALIOP level 2 dataset and methodology used for the estimation of dust extinction coefficient are explained in chapter 3, section 3.2.

Space-borne air temperature observations are used to study the association of dust aerosols with the tropospheric temperature. MSU-AMSU observations of layer mean temperature of lower troposphere (TLT - Version 4.0) which is provided by the Remote Sensing Systems, are used in the present study *(Mearz and Wentz, 2017)*. The vertical extent TLT data product is from surface to 8 km, but the weighting function (Channel 5 AMSU and Channel 2 MSU) peaks below 5 km altitude and can be used with confidence for the study of lower troposphere temperature. Surface temperature used in the study is the near-surface ensemble median product (Version 4.6) of the Hadley Centre and the Climatic

Research Unit (HadCRUT4) *(Morice et al., 2012)*. Rainfall- dust relationship is investigated using station-based gauge measurements by Indian Meteorological Department (IMD). Details of the datasets used are shown in Table 6.1.

***Table 6.****1 - Details of datasets and models used in the study.*

| Platform | Project/ Model | Parameter | Remarks |
|---|---|---|---|
| **Satellite** | CALIOP | Aerosol Extinction coefficient (vertical) | Level 2 Version 4.1 (2006 – 2017) |
| | MSU-AMSU | Layer mean Temperature (TLT) | Version 4 (monthly) (2006 – 2017) |
| **Ground Based** | ARFINET | Spectral AOD<br>Spectral absorption coefficient<br>Spectral scattering coefficient | (2006 – 2017) |
| | AERONET | AOD | Level2 Version2 (2000 – 2017) |
| | IMD | Rainfall rate | Area weighted (monthly) (2006 – 2017) |
| | HADCRU | Surface air Temperature | Version 4.6 (monthly) (2006 – 2017) |
| **Aircraft based** | RAWEX | Single scattering albedo | 2012 (Nov-Dec)-2013(Apr-May) |
| **Models** | SBDART | Radiation flux | Refer chapter 2 |

This chapter is organized into three sections which are, i) Sensitivity of aerosol vertical distribution to radiative forcing ii) Direct radiative effect due to aerosols over the Indian region, and ii) Long-term trend in mineral dust loading over the Indian region.

## 6.3 Results and Discussion

### 6.3.1 Sensitivity of aerosol vertical distribution to radiative forcing

Radiative effects due to aerosols depend on their columnar loading, physio-chemical properties, vertical distribution, presence of cloud and albedo of the underlying surface albedo *(Haywood and Boucher, 2000)*. In general, radiative transfer calculations make use of column/surface observations and make assumptions on the vertical distribution of aerosols for the estimation of aerosol radiative forcing. Nevertheless vertical distribution of aerosols plays a significant role in assessing the radiative impacts of aerosols especially in the presence of elevated layers at higher altitudes. Estimation of aerosol forcing with realistic profiles of aerosol properties deviates from that using standard vertical profiles,

which are exponentially decreasing with altitude (with typical scale height of 1.5 km) *(Moorthy et al., 2009)*. It has been shown that uncertainty in the vertical distribution can lead to an error of 0.5 $Wm^{-2}$ to the total global aerosol radiative forcing *(Chung et al., 2005)*. There are several studies on the estimation of radiative effect of aerosols based on column/surface observations *(Babu et al., 2007;Niranjan, Sreekanth et al., 2007; Valenzuela et al., 2012)*. Table 6.2 shows the sensitivity of aerosol radiative forcing at TOA (ARF) to AOD (τ), SSA (ω), and Asymmetry parameter (g) using SBDART simulations. Simulations were carried out using $\tau_{550}$=0.1, ω= 0.9, g=0.7 and a surface albedo of 0.04 (ocean surface) with exponentially decreasing standard vertical profile at a solar zenith angle of 60°, which is treated as estimated day-time-mean solar zenith angle in terms of radiation received at TOA *(Coakley and Chylek, 1975)*.

***Table 6.2 -*** *Sensitivity of aerosol radiative forcing (ARF) to columnar aerosol parameters.*

| ($Wm^{-2}$) | $\tau_{550}$ ±0.05 | ω ± 0.05 | g± 0.1 |
|---|---|---|---|
| $ARF_{TOA}$ | ±6 | ±1.3 | ±1.8 |
| $ARF_{SURFACE}$ | ±6.3 | ±3.5 | ±2 |

SBDART uses a standard aerosol vertical distribution which drops off exponentially with a scale height between 1.05 and 1.51 km based on the visibility conditions as shown in figure 6.1.

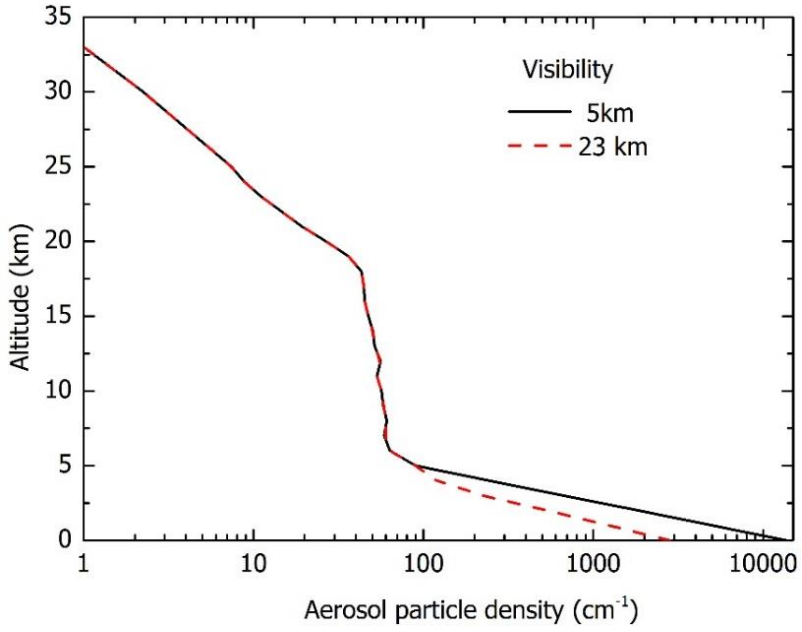


***Figure 6.1 -*** *Vertical profile for aerosols used in SBDART for 23 km (dashed red) and 5 km (solid) visibility.*

Aerosol scale height represents the vertical extent of aerosols in the column. Unlike molecules, aerosol scale height is determined by the columnar loading rather than the

loading at the surface. This is due to the deviation of aerosol vertical distribution from exponentially decreasing pattern and presence of layers aloft. Here aerosol scale height is estimated as the altitude at which AOD reduces to 1/e *(Yu et al., 2010).* Studies on aerosol vertical distribution have shown that radiative effects of absorbing aerosols have stronger dependence on vertical distribution compared to non-absorbing aerosols *(Samset and Myhre, 2011)*. Thus the sensitivity of radiative forcing to vertical distribution in SSA is very important. To carry out sensitivity analysis, an exponentially decreasing aerosol profile is assumed with different aerosol scale heights starting from 0.5 to 6 km as shown in figure 6.2 (a).

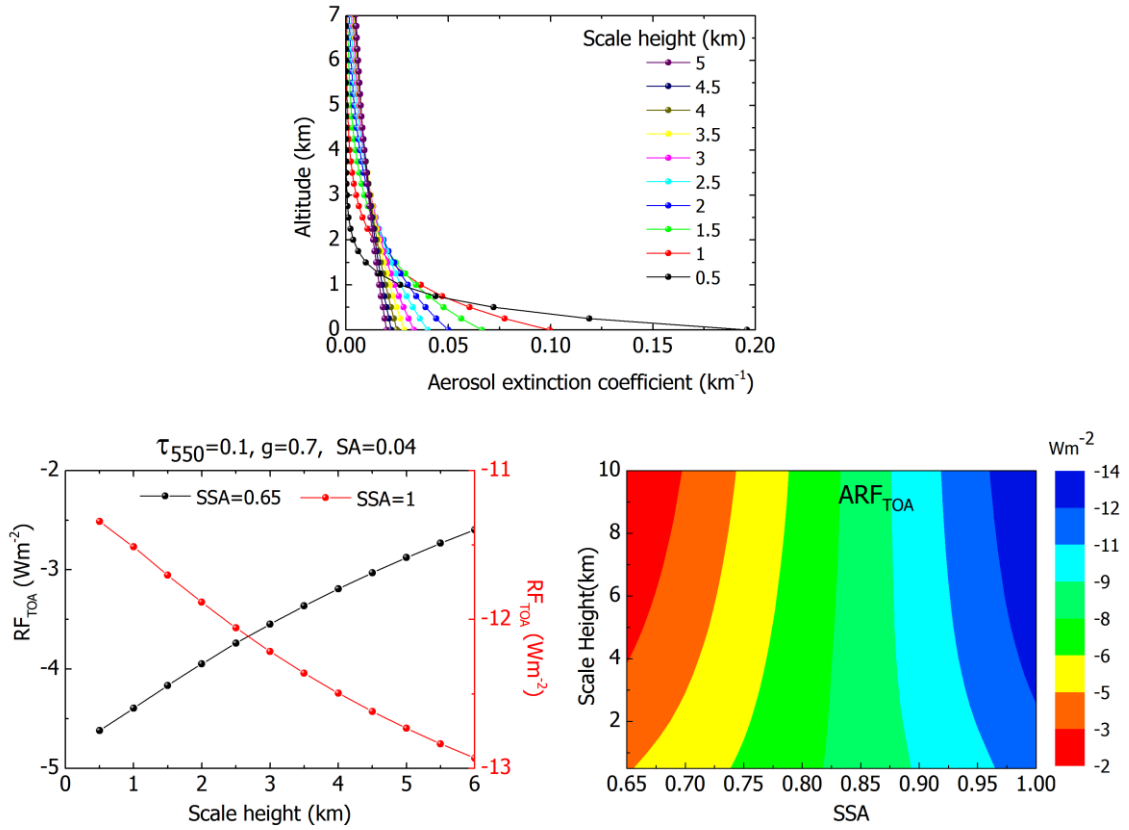


***Figure 6.2*** *- a) Vertical profiles of normalized aerosol concentration with varying scale heights (SH) that are used to simulate the sensitivity of scale height to ARF at TOA b) Variation of ARF at TOA with aerosol scale height with AOD = 0.1, g=0.7 and surface albedo=0.04 at solar zenith angle of 60° for purely scattering (SSA=1) and highly absorbing (SSA=0.65) aerosols c) Sensitivity of ARF at TOA to aerosol scale height as a function of SSA.*

Figure 6.2 (b) shows the sensitivity of radiative forcing at TOA with scale height for g=0.7 and surface albedo=0.04 at solar zenith angle of 60° for purely scattering (SSA=1) and highly absorbing (SSA=0.65) aerosols. As the scale height increases, ARF at TOA ($ARF_{TOA}$) will either increase, or decrease based on the SSA of aerosols present in the column. ARF increases (towards positive) with aerosol scale height for SSA=0.65 (absorbing aerosols),

indicating more absorption of radiation within the atmosphere with scale height. For scattering aerosols (SSA=1), $ARF_{TOA}$ becomes more negative with increasing scale height. i.e., aerosols at higher altitudes scatter back more radiation than when they are close to surface. Thus dependence of $ARF_{TOA}$ on scale height is determined by the single scattering albedo of aerosols in the column. Beyond the critical SSA (SSA>0.82), scattering effects determines dependence of $ARF_{TOA}$ on aerosol vertical distribution and afore critical SSA, it is determined by the absorbing effects (figure 6.2 (c)). These effects are due to the increased availability of radiation for interaction at higher heights due to exponentially decreasing density of atmosphere.

Figure 6.3 shows the sensitivity of ARF at TOA to aerosol scale height as a function of AOD for highly absorbing (SSA =0.65) and purely scattering aerosols (SSA=1). For AOD =1, as scale height changed from 0.5 to 6km, change in ARF is almost 10 $Wm^{-2}$ (for absorbing aerosols) and 13 $Wm^{-2}$ for scattering aerosols.

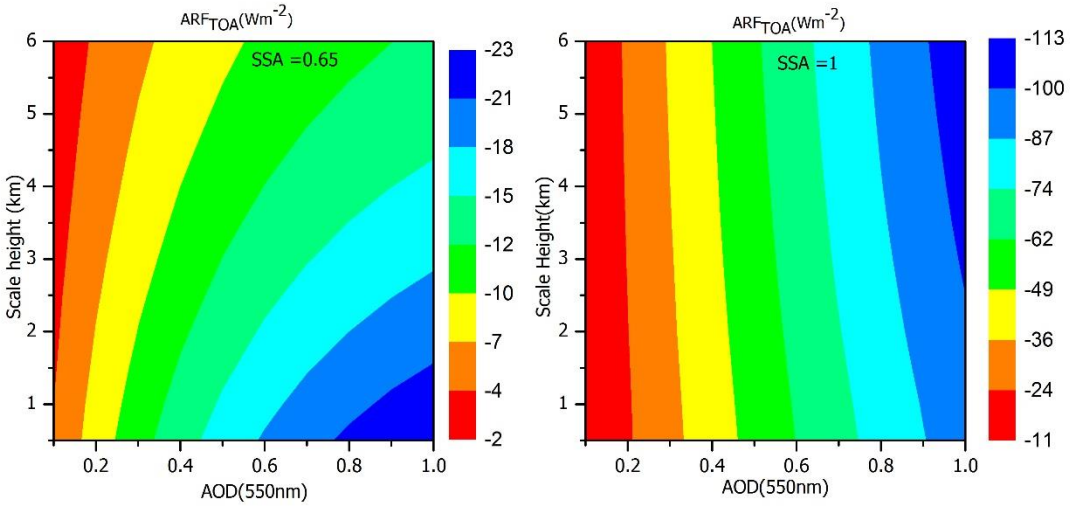


***Figure 6.3*** *- a) Sensitivity of ARF at TOA to aerosol scale height as a function of AOD simulated with SSA= 0.65 and 1, g=0.7 and surface albedo=0.04 at solar zenith angle of 60°.*

It has to be noted that these simulations are carried out with clear sky conditions. In the presence of clouds, aerosol absorptive effects are significantly modulated by their vertical distribution that determine whether the absorbing aerosols are above or below the cloud layers *(Chand et al., 2009; Zarzycki and Bond, 2010; Choi and Chung, 2014).* Aerosol models simulates varying vertical profiles which needs to be unified and validated with observations for better estimates aerosol climate impacts *(Schwarz et al., 2010; Samset and Myhre, 2011).* Inter-comparison study of different global aerosol models shows that the variations in the simulated BC profiles contributes to almost 20 % of the total uncertainty in the BC radiative forcing *(Samset et al., 2013).* Enhanced efforts on observation based

vertical characterization of aerosols are necessary for the validation of models and better estimation of aerosol radiative effects.

### 6.3.2 Aerosol radiative forcing over Indian landmass

Indian region is characterized by high aerosol loading during winter and pre-monsoon seasons. As season changes from winter to pre-monsoon, aerosols are transported to higher altitudes with increasing fraction of mineral dust in total columnar loading (Refer chapter 3, section 3.3.7). Majority of this layer are located above reflective clouds and produce strong warming over the Indian region *(Satheesh et al., 2008)*. Such absorbing layers of aerosols can induce large warming over the Indian region and have effects on the hydrological cycle *(Lau et al., 2006)*. Aerosols at elevated altitudes interact with higher amount of radiation than those located near to the surface. The following section presents the climatological state of aerosol induced heating rate and its vertical variability over the Indian region using multi plat-form observations. Study regions include four distinct geographical regions over the Indian landmass that includes (i) Peninsular India (8°N - 20°N), (ii) northwest India (23°N - 28°N, 69°E - 75°E) which is a dry arid region, (iii) East India (22°N - 28°N, 90°E - 96°E), a densely vegetated region of distinct topography and (iv) a highly polluted Indo-Gangetic Plain, IGP (22°N - 30°N, 76°E - 86°E) (figure 6.4) (Refer chapter 3.3.4).

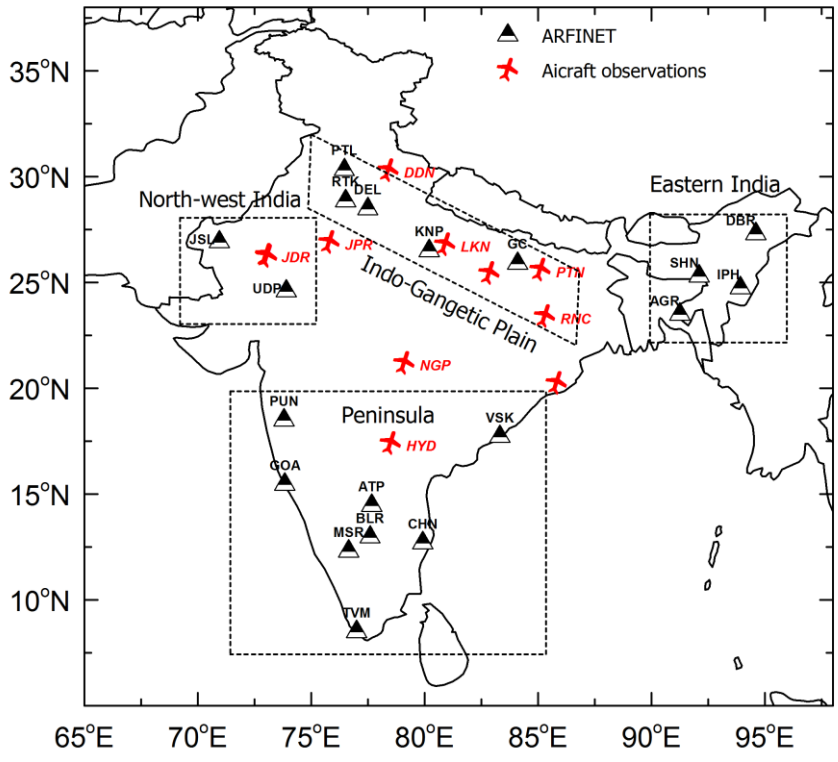


***Figure 6.4*** *- Study regions with locations of ARFINET MWR/sunphotometers and locations of aircraft experiments carried out under RAWEX.*

For the estimation of direct aerosol radiative forcing, spectral variations of AOD, SSA and phase function (or asymmetry parameter) are required. ARFINET AOD data compiled from 20 stations equipped with MWR/sunphotometer were averaged regionally for winter and spring seasons (figure 6.4). Regional mean ARFINET AOD used for the estimation of aerosol radiative forcing are given in table 6.3.

***Table 6.3*** *- Columnar AOD (τ), SSA (ω) and asymmetry parameter (g) at 550nm used in the radiative transfer calculations for estimating heating rate over the study regions.*

| **Region** | **Parameter (Column)** | **Total aerosol (Dust + Non-dust)** | | **Dust aerosol** | |
|---|---|---|---|---|---|
| | | Winter | Pre-monsoon | Winter | Pre-monsoon |
| **PENINSULA** | $\tau_{550\ nm}$ | 0.37 | 0.43 | 0.1 | 0.23 |
| | $SSA_{550nm}$ | 0.88 | 0.79 | 0.93 | 0.93 |
| | $g_{550nm}$ | 0.69 | 0.712 | 0.73 | 0.73 |
| **EAST** | $\tau_{550\ nm}$ | 0.53 | 0.67 | 0.07 | 0.15 |
| | $SSA_{550nm}$ | 0.88 | 0.87 | 0.93 | 0.93 |
| | $g_{550nm}$ | 0.69 | 0.71 | 0.73 | 0.73 |
| **NORTH WEST** | $\tau_{550\ nm}$ | 0.31 | 0.47 | 0.11 | 0.43 |
| | $SSA_{550nm}$ | 0.93 | 0.89 | 0.93 | 0.93 |
| | $g_{550nm}$ | 0.7 | 0.71 | 0.73 | 0.73 |
| **IGP** | $\tau_{550\ nm}$ | 0.57 | 0.5 | 0.12 | 0.35 |
| | $SSA_{550nm}$ | 0.86 | 0.86 | 0.93 | 0.93 |
| | $g_{550nm}$ | 0.7 | 0.71 | 0.73 | 0.73 |

Vertical distribution of aerosol extinction coefficient and SSA are obtained from observations of CALIOP and aircraft experiment under RAWEX respectively. Asymmetry parameter for the estimation of aerosol effect over the study regions is estimated by means of *Hess et al., (1998)* using the aerosol composition simulated by the chemistry transport model GOCART following *Chin et al., (2009)*. Seasonal average value of columnar water vapour was obtained from MODIS (MODIS-Aqua MYD08_M3 Version6) and ozone concentration was obtained from Ozone Mapping Instrument (OMI) measurements (OMDOAO3e Version3) over the years 2006 - 2017. Surface albedo over the study regions is obtained from MODIS - Aqua observations (Level 3, MYD09A1) at seven wavelength bands centered at 0.645, 0.859, 0.469, 0.555, 1.24, 1.64, and 2.13 mm are used. Altitude distribution of aerosol extinction coefficient and SSA used in heating rate estimations are explained in the following sections.

### 6.3.2.1 Altitude distribution of aerosol extinction coefficient

For the estimation of vertical distribution of aerosol heating rate, aerosol vertical distribution is obtained from eleven years (2006 -2017) of CALIOP measurements. Vertical profiles of aerosol extinction coefficient from CALIOP are normalized using regional mean AOD observations under ARFINET (Refer to chapter 3, section 3.3.4). Vertical profiles of normalized aerosol extinction coefficient from CALIOP is vertically interpolated to model's vertical resolution (1 km) and used in the radiative transfer model to represent the vertical distribution of aerosol loading over the study regions and shown in figures 6.5.

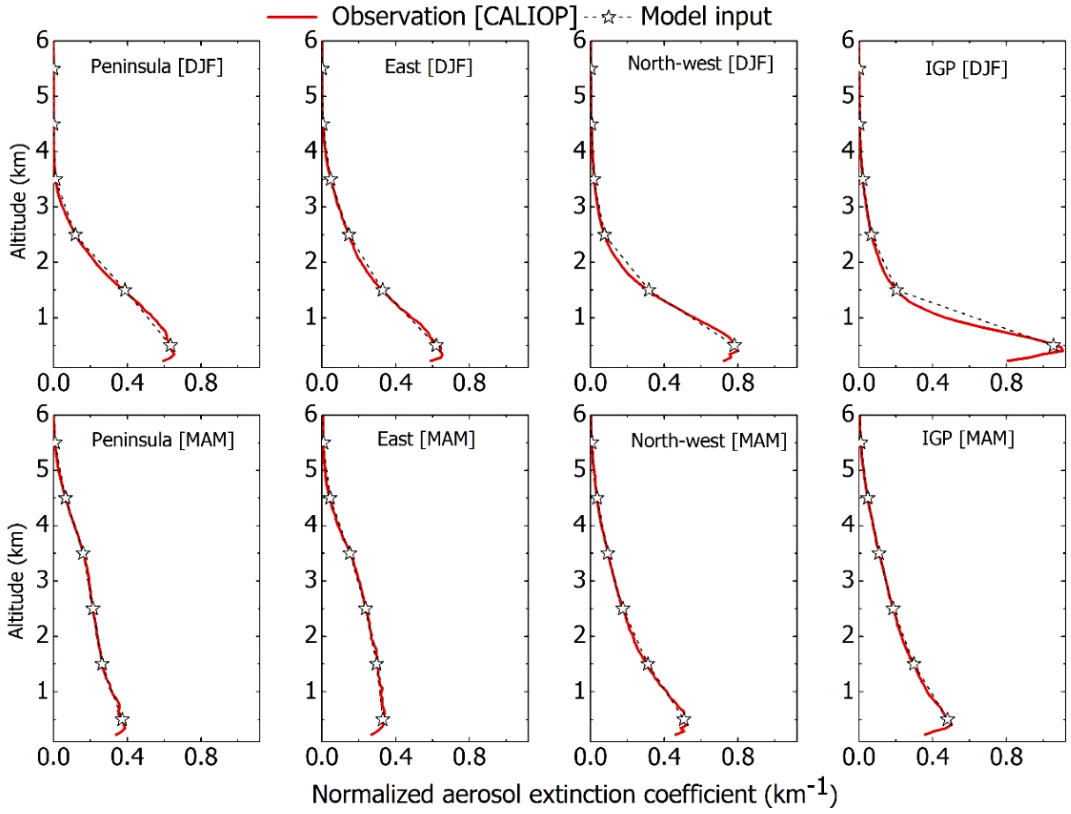


***Figure 6.5 -*** *Profiles of normalized aerosol extinction coefficient from CALIOP along with model input profiles that are interpolated to a vertical resolution of 1 km.*

While aerosols are more confined within PBL during winter season, they are vertically extended up to 6km altitude during pre-monsoon followed by a decrease within PBL. Estimation of aerosol induced heating rate is carried out for these two seasons; winter (December to February) and spring (March to May). During winter Indian region is under the influence of dry airmass rich in continental aerosols while during pre-monsoon north-westerly winds contributes significant amount of mineral dust aerosols to the total loading from the sources over the west of Indian landmass (Refer chapter 3). These contrasting airmass significantly modulates the aerosols properties over the Indian region.

### 6.3.2.2 Altitude distribution of aerosol Single Scattering Albedo

Aircraft measurements of aerosol optical properties were carried out over the study regions during winter (November – December 2012), pre-monsoon/spring (April - May 2013) and just prior to the onset of monsoon (May – June, 2016) under RAWEX. The measurements on-board aircraft includes spectral scattering coefficients (Nephelometer (TSI3653, USA) and spectral absorption coefficients (Aethalometer (model AE33 of Magee Scientific, USA)). In the present study, the altitude profiles of SSA over peninsular India, northwest India, and IGP are derived from these aircraft measurements. Figure 6.6 shows the altitude distribution of SSA used in the radiative transfer model to estimate the vertical distribution of aerosol induced heating rate over the Indian landmass during winter and pre-monsoon seasons.

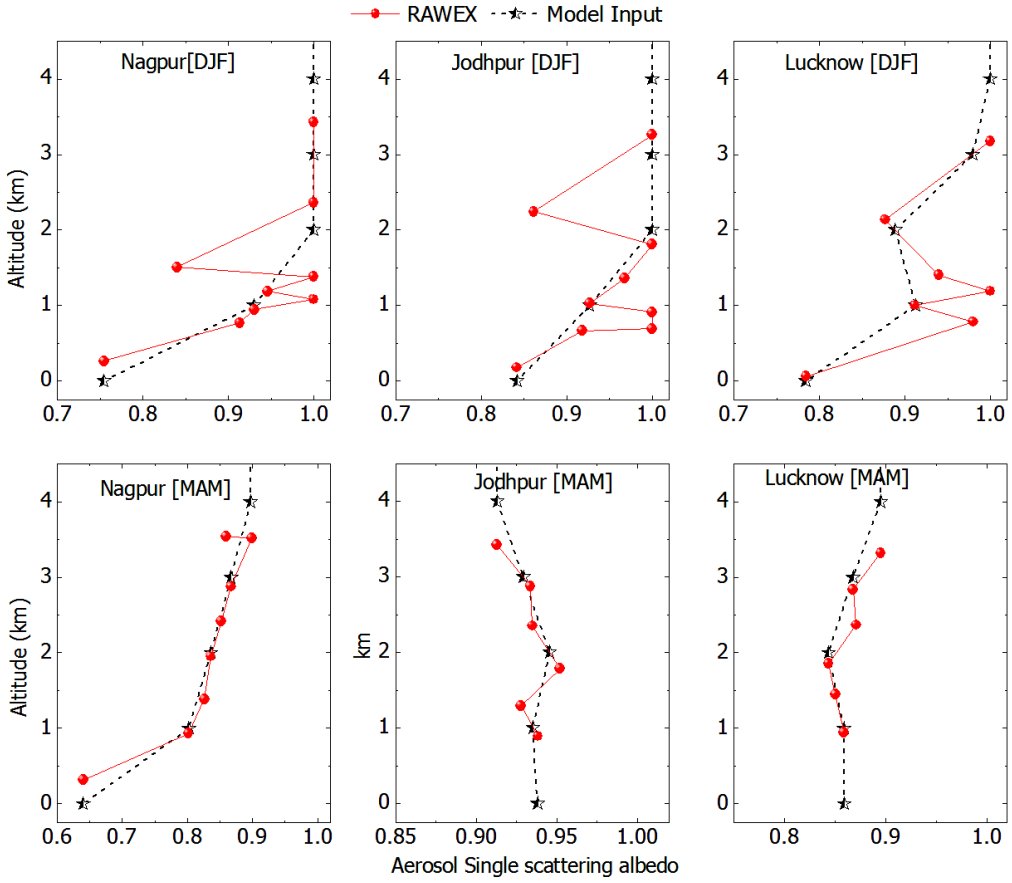


***Figure 6.6*** *- Mean vertical profiles of SSA measured over Nagpur (Peninsula), Jodhpur (North-west India) and Lucknow (IGP) during winter 2012 and pre-monsoon 2013.*

RAWEX observations of vertical distribution of SSA indicate that aerosols within PBL are more absorbing than free tropospheric aerosols during both winter and spring. However in the free troposphere, aerosol absorption significantly enhances as season changes from winter to pre-monsoon *(Babu et al., 2016)*. *Vaishya et al., (2018)* reported regionally dependent aerosol absorption characteristics with a clear west to east gradient in the

vertical distribution of SSA across the northern India. A drastic reduction in SSA values is observed from pre-monsoon to prior to the monsoon onset over IGP which is attributed to the building of absorbing aerosols caused by the reversal of monsoon winds over this region *(Vaishya et al., 2018).*

#### 6.3.2.3 Altitude distribution of aerosol heating rate

Vertical distribution of aerosol extinction coefficient (CALIOP-ARFINET) and SSA (RAWEX) are incorporated in the SBDART model to simulate the fluxes reaching at the top of the atmosphere and surface in the presence and absence of aerosols, and ARF values were estimated at TOA, surface and in the atmosphere (Table 6.4). The sources of uncertainty in the estimated atmospheric forcing includes those due to (i) errors in the measured spectral AOD and (ii) limited dataset on aerosol composition (as given by single scattering albedo) over the study region.

***Table 6.4*** *- ARF estimated at TOA, surface and the atmosphere over the study regions.*

| Region | $ARF_{TOA}$ ($Wm^{-2}$) | | $ARF_{SURFACE}$ ($Wm^{-2}$) | | $ARF_{ATM}$ ($Wm^{-2}$) | |
|---|---|---|---|---|---|---|
| | DJF | MAM | DJF | MAM | DJF | MAM |
| **PENINSULA** | -7 | -2 | -32 | -49 | 25 | 47 |
| **EAST** | -11 | -6 | -37 | -51 | 27 | 45 |
| **NORTH WEST** | -3 | -6 | -24 | -26 | 21 | 20 |
| **IGP** | -7 | -3 | -47 | -44 | 41 | 41 |

Aerosol radiative forcing at TOA ($ARF_{TOA}$) becomes more positive as season changes from winter to pre-monsoon. A twofold increase in atmospheric aerosol forcing ($ARF_{ATM}$) is observed over peninsula and eastern India. Aerosol forcing of the atmosphere ($ARF_{ATM}$) indicates the net radiation absorbed in the atmosphere. Absorption of radiation by aerosols leads to diabatic heating of the atmosphere which is estimated as *(Liou, 1980),*

$$\frac{\partial T}{\partial t} = \frac{g}{C_p}\frac{\Delta F(p)}{\Delta p} \qquad (6.1)$$

where $g$ is the acceleration due to gravity, $C_p$ is the specific heat capacity of the air at constant pressure (1006 $Jkg^{-1}K^{-1}$) , $\Delta F$ is the flux absorbed by the layer (given by $ARF_{ATM}$), $\Delta p$ is the change in atmospheric pressure within the layer (Refer chapter 1 , Section 1.4.2). Heating rate of an aerosol layer is more at higher levels where $\Delta p$ is lower compared to that close to surface. Figure 6.7 shows heating rate due to aerosols over the study regions

of Indian landmass. Aerosol induced heating rate is significantly higher above boundary layer during pre-monsoon while heating was higher within the boundary layer during winter season. Nevertheless, over peninsula, winter time heating within boundary layer was less than that during pre-monsoon. This might be due to the extremely low SSA of ~0.64 within PBL over this region during pre-monsoon which leads to a heating rate of ~2 $Kday^{-1}$. Over peninsular India an atmospheric heating of 1.5 $Kday^{-1}$ is observed under polluted conditions ($\tau$ ~0.45) during winter season *(Babu et al., 2002)*. However a much lower value of nearly 0.8 $Kday^{-1}$ is estimated within PBL over the central India by *Ganguly et al., (2005).* A strong meridional gradient in aerosol heating rate is observed over the Indian region with enhanced warming rate for aerosol layers located above clouds *(Sathessh et al., 2008).*

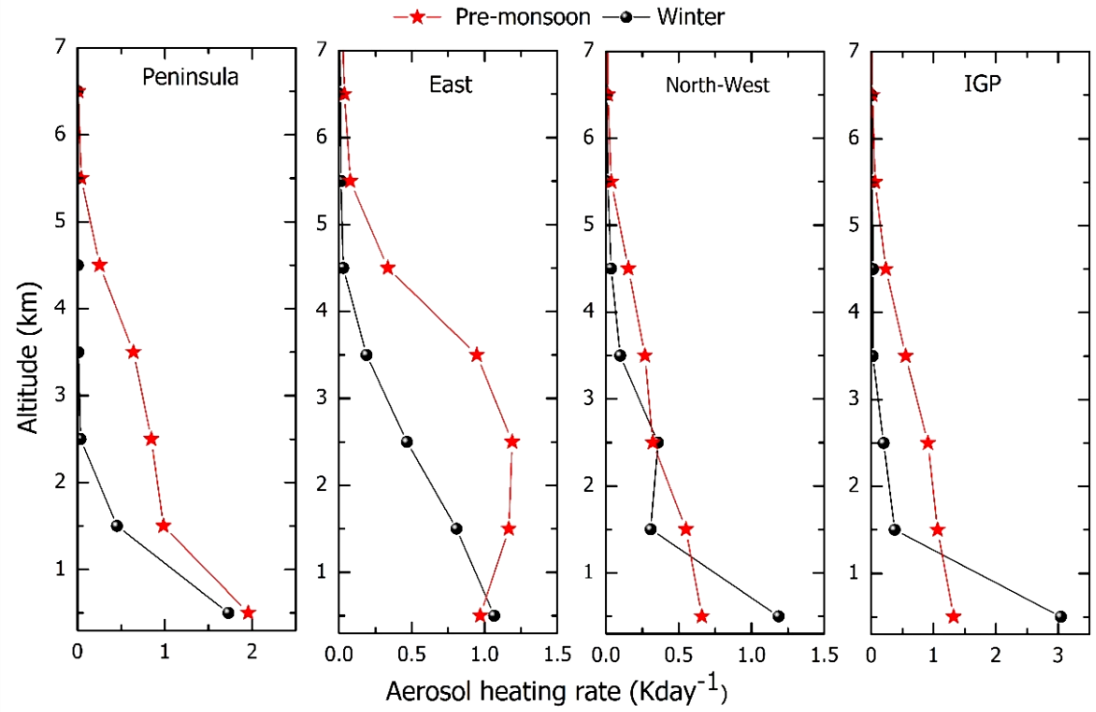


***Figure 6.7****- Vertical profiles of aerosol heating rate over the study regions estimated through radiative transfer simulations using mean vertical distribution from CALIOP, AOD from ARFINET and vertically resolved observations of SSA during RAWEX.*

Over the eastern India significant aerosol heating rate of ~1 $Kday^{-1}$ is observed within PBL as well as free troposphere (up to ~3.5km). Despite of heavy dust loading, pre-monsoon heating over north-west India is comparatively lesser (~0.5 $Kday^{-1}$) owing to the high values of SSA observed for dust aerosols over this region. High aerosol loading over IGP along with an observed low SSA of ~0.79 produce exceptionally high heating rate (~3 $Kday^{-1}$) over this region during winter season. Heating rate of BC at IGP during winter estimated using airborne-measurements showed a highest value of ~2.1 $Kday^{-1}$ at 300 m

altitude *(Tripathi et al., 2007)*. Large heating rates of ~2 $Kday^{-1}$ has been observed over the IGP at 2km altitude using airborne measurements during pre-monsoon and monsoon seasons *(Devi et al., 2011)*. Over IGP and north-west India, $ARF_{ATM}$ is same for both winter and pre-monsoon but vertical distribution of diabatic heating changes considerably from winter to pre-monsoon. The observed heating rates over the Indian region can have significant implications over regional climate and changing precipitation patterns.

#### 6.3.2.4 Heating rate: Dust and Carbonaceous aerosols

Relative contribution of mineral dust and carbonaceous aerosols to the observed aerosol loading on the backdrop of the increasing trend in free-tropospheric temperature is non-existent and needs to be addressed *(Nair et al., 2017)*. In external aerosol mixtures, absorbing aerosols affect radiative effects of scattering aerosols via multiple scattering *(Nair et al., 2014)*. Under the influence of anthropogenic aerosols, radiative effect of dust aerosols largely increases *(Satheesh, Deepshikha, et al., 2006).* The estimate of speciated radiative forcing due to absorbing aerosols such as dust and carbonaceous aerosols is very limited over Indian region due to the lack of accurate information on their vertical distribution. It was reported that the altitude of the dust layer can significantly influence clear sky longwave forcing and cloudy sky shortwave forcing *(Liao and Seinfeld, 1998)*.

For the estimation of dust radiative forcing, dust optical depth obtained at 532 nm and vertical profile of dust extinction coefficient derived using simultaneous observations of aerosol back-scattering coefficient and depolarization ratio from CALIOP are used. Regional mean vertical profiles of dust extinction coefficient are vertically interpolated to model's vertical resolution (1km) and used in the radiative transfer model to represent the vertical distribution of aerosol loading over the study regions and shown in figure 6.8. Single scattering albedo (SSA) value for dust is obtained from the aircraft measurements carried out over the desert regions of north-west India (Jodhpur) during pre-monsoon season (May 2013) as a part of RAWEX project (figure 6.6). An average columnar SSA of 0.93 obtained at 520 nm over these dust dominant regions is very close to the SSA retrieved using AERONET observations at Jaipur *(Nair et al., 2017).* Shape of the particles affect the angular scattering function and the magnitude of SSA. Simulations shows that non-sphericity of dust aerosols can increase the SSA values by ~0.1 over the Indian region *(Srivastava et al., 2017).* Assumption of dust aerosols as spherical particles, can lead to errors, which is of similar magnitude of the errors due to the uncertainty in the refractive index *(Kahnert et al., 2007)*. Hence the asymmetry parameter of dust aerosols are obtained from *Koepke et al., (2015)* that accounts for the nonsphericity of dust aerosols. A table of reported values of dust SSA over Asia is given in table 6.5.

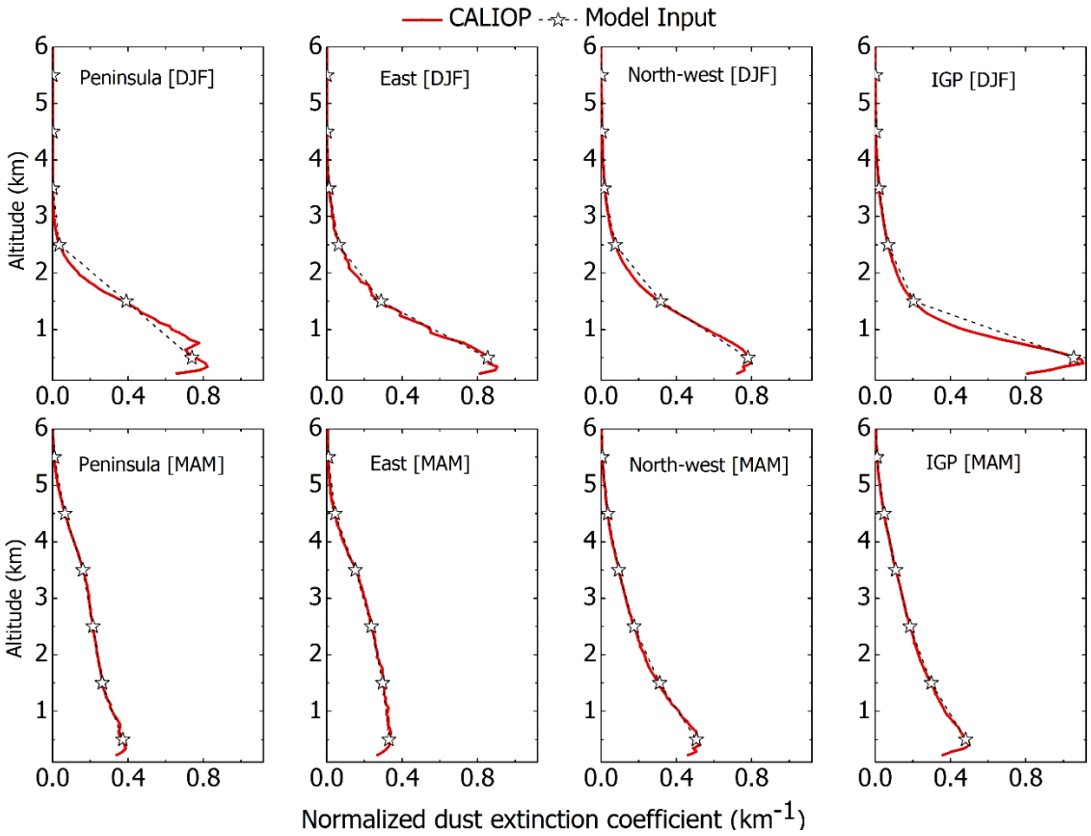


***Figure 6.8*** *- Profiles of normalized dust extinction coefficient as measured by CALIOP along with model input profiles that are interpolated to a vertical resolution of 1 km.*

***Table 6.5 -*** *Reported values of dust SSA.*

| Dust SSA | λ(nm) | Location | Method | Reference |
|---|---|---|---|---|
| **0.92±0.03** | 440 | Bahrain – Persian Gulf | AERONET (Inversion) | Dubovik et al., (2002) |
| **0.95±0.03** | 670 | | | |
| **0.92±0.02** | 440 | Solar village | | |
| **0.96±0.02** | 670 | | | |
| **0.96±0.01** | 550 | Southeast Asia | Aircraft- in situ | Anderson, (2003) |
| **0.89** | 500 | Southeast Asia | Sky radiometer (SKYNET) | Kim et al., (2005) |
| **0.75±0.02** | 500 | North-west China | Surface –in situ | Ge et al., (2010) |
| **0.91- 0.96** | 500 | Deserts of China | Satellite (Inversion) | Lee et al., (2007) |
| **0.935** | 550 | North west India | Aircraft- in situ | Babu et al., (2016) |
| **0.95 ± 0.01** | 405 | South central Asia | Bulk sample entrainment | Moosmller et al., (2012) |
| **0.99± 0.0007** | 870 | (Afghanistan) | | |
| **0.84±0.03** | 550 | North west India | Aircraft –in situ | Vaishya et al., (2018) |

Assuming that the total aerosol absorption is solely due to mineral dust and carbonaceous aerosols, the atmospheric forcing due to carbonaceous aerosols is estimated as the difference between the total and mineral dust forcing and is shown figure 6.9. It shows that atmospheric forcing is mostly induced by carbonaceous species over the Indian region except over north-west India. Dust contribution to the total atmospheric forcing is enhanced during pre-monsoon season from winter season. It is highest over north-west India (83%), which is the major source region of mineral dust over the Indian land mass. Over IGP, dust contributes to ~ 45% to the total atmospheric forcing during this season. Compared to peninsular and eastern India, north-west India and IGP have higher dust forcing in the atmosphere during both the seasons.

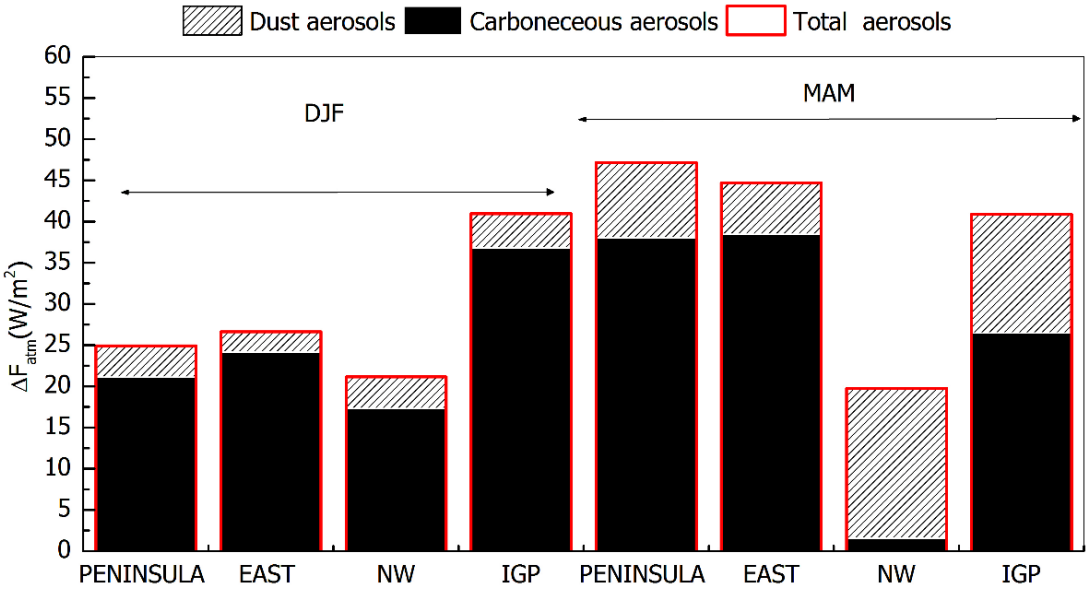


***Figure 6.9*** *- Atmospheric forcing due to dust aerosols and carbonaceous aerosols over the study regions as simulated by SBDART using CALIOP derived mean aerosol vertical profiles, AOD observations of ARFINET and aerosol composition as simulated with GOCART.*

Over Indian region, *Nair et al., (2017)* have carried out species wise estimates of aerosol radiative forcing based on GOCART simulations. Figure 6.10 shows an inter-comparison of percentage contribution of BC and mineral dust to the total aerosol radiative effect within the atmosphere ($DRE_{ATM}$) derived by present study making use of CALIOP observations of vertical profiles of depolarization ratio and RAWEX based SSA measurements, with that derived by *Nair et al., (2017)*. Radiative effect of dust aerosols derived using CALIOP-RAWEX observations are generally lesser than that using GOCART composition by 10 to 20% while CALIOP derived carbonaceous forcing is higher than that derived using GOCART simulations by up to 40%.

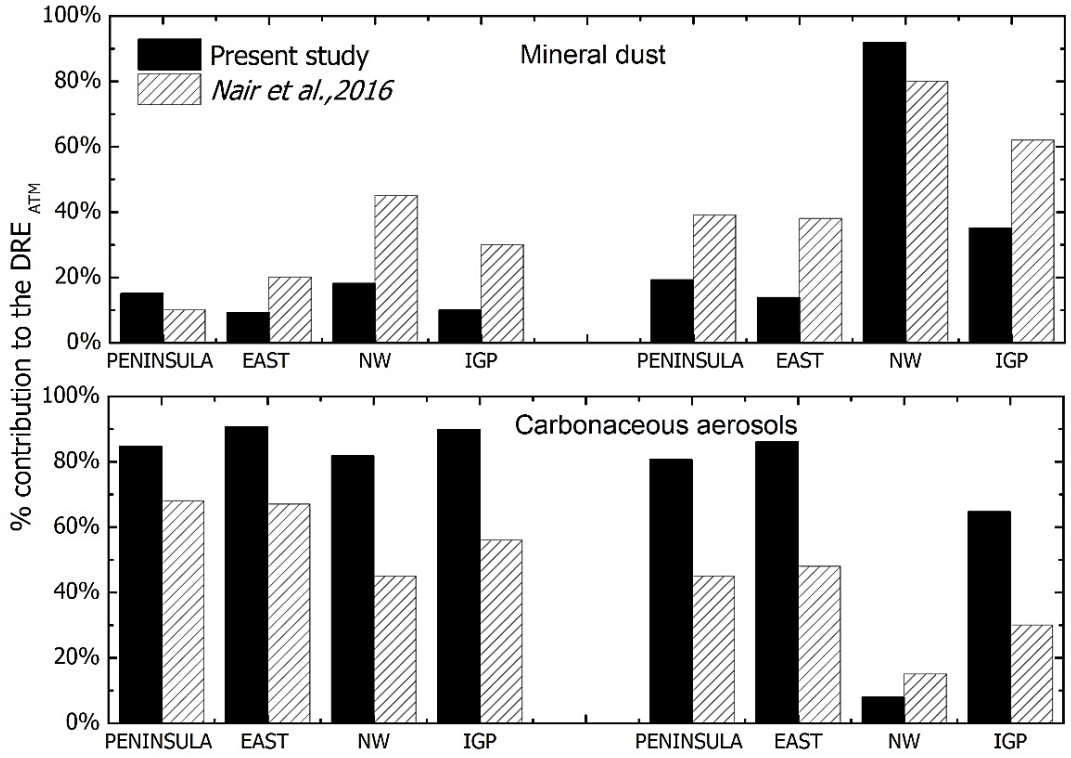


***Figure 6.10*** *- Percentage contribution of CALIOP derived mineral dust/carbonaceous direct radiative effect to the aerosol effect in the atmosphere and inter-comparison with speciated aerosol effect on the atmosphere simulated by GOCART over the study regions.*

Radiative effect of mineral dust aerosols and their heating rate in the atmosphere in both short wave and longwave regime are dependent on vertical distribution of mineral dust, their mineral composition, altitude and optical depth of clouds, and the surface albedo in the estimation of radiative forcing by dust *(Quijano et al., 2000)*. It is found that, with increasing total dust optical depth, dust absorption increases such that this negative radiative effect due to the dust aerosols at TOA becomes positive *(Quijano et al., 2000)*. Reported values of dust induced shortwave forcing at TOA are mostly negative *(Haywood et al., 2001; Heinold et al., 2007; Osborne et al., 2011)* though a few studies have reported a positive dust radiative forcing at TOA *(Quijano et al., 2000; Myhre and Stordal, 2001; Deepshikha et al., 2006;)*. Using in-situ aircraft observations in Saharan dust plume *Otto et al., (2007)* modelled shortwave radiative forcing at TOA over ocean and desert which showed a negative forcing over ocean (-16$Wm^{-2}$) and positive forcing over desert (+37$Wm^{-2}$). Assessment of global dust direct radiative forcing is very uncertain and varies in the range -0.46 $Wm^{-2}$ to 1.64 $Wm^{-2}$ at TOA *(Woodward, 2001; Miller et al., 2004, 2006; Yoshioka et al., 2007).* Vertical profiles of heating rate due to mineral dust and carbonaceous aerosols over distinct regions in India during spring and winter are shown in Figure 6.11.

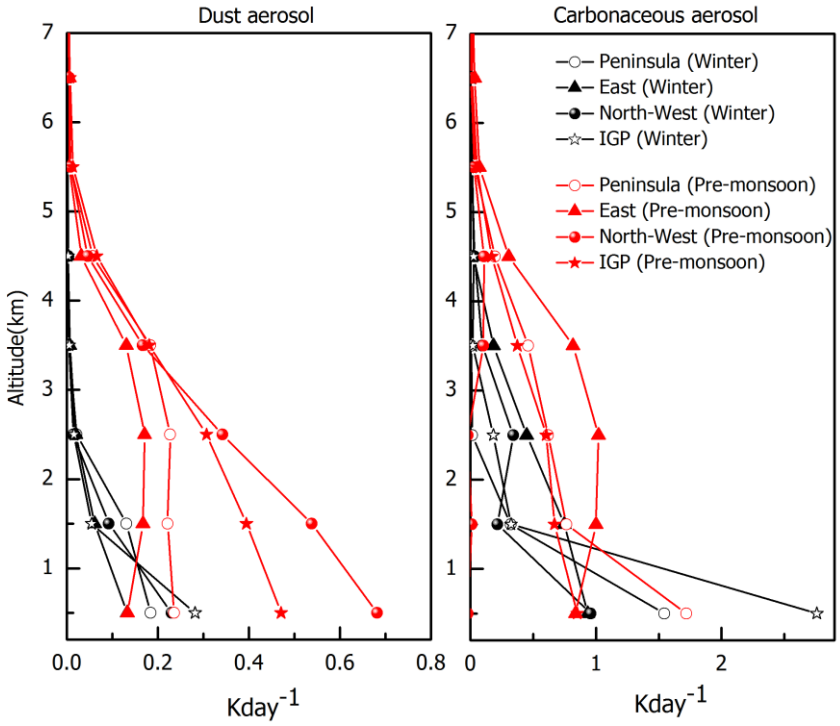


***Figure 6.11-*** *Vertical profile of heating rate due to dust and carbonaceous aerosols over the study regions during winter (black curves) and pre-monsoon (red curves).*

While dust induced heating rates shows a clear transition from winter to pre-monsoon, heating due to carbonaceous aerosols are found equally significant during both the seasons. During pre-monsoon, dust heating rates are prominent near the surface over IGP and North-west India while over Peninsula and eastern India they are prominent above boundary layer than within it. Dust induced heating is observed highest over north-west India with a heating rate of ~0.7 $Kday^{-1}$ at the surface that contributes 100% to the total heating. Significant heating observed over the Eastern India (figure 6.8) is caused by the carbonaceous aerosols (figure 6.11). Carbonaceous heating over IGP and peninsular India is almost comparable during pre-monsoon except for the anomalous carbonaceous heating observed near to surface over Peninsula. High heating rate observed over IGP during winter is mostly contributed by carbonaceous aerosols.

Over the Indian region, *Moorthy et al., (2007)* inferred dust absorption efficiency over the Thar Desert using infra-red remote sensing technique along with ARFINET station observations and estimated dust induced heating rate in the lower atmosphere that varies in the range 0.7 -1.2 $Kday^{-1}$. Unlike the anthropogenic and biomass burning aerosols, the shortwave radiative effects of dust aerosols partly cancel out due to longwave effects, which further depend on the mineral dust properties and atmospheric conditions (drier or clear/cloudy sky). During an intense Saharan dust storm in Mediterranean Sea, longwave forcing compensated 49% of the shortwave forcing at the surface and 77% of

the shortwave warming in the atmosphere *(Di Sarra et al., 2011)*. Estimation of longwave radiative effects of mineral dust aerosols is beyond the scope of the study due to lack of direct observations of dust radiative parameters in the longwave regime. Satellite based flux measurements May be used in future to study the longwave radiative effects of mineral dust over the study regions. Though several simulations of radiative heating rates of mineral dust aerosols were reported evidence based on observations of tropospheric temperature is very scarce over the study region. Over SAL, *Davidi et al., (2012)* used temperature soundings from AIRS, AOD from MODIS along with global data assimilation system to separate dust signal from the meteorological component and derived a dust induced heating of 2 – 4 ˚K within the dust layer. *Gautam et al., (2009)* studied tropospheric warming over Himalayas-Tibetan Plateau using long-term microwave based temperature observations and estimated a warming trend of 2.7 °C during the period 1979–2007 associated with enhanced dust loading over this region. They observed the higher warming trends at elevated altitudes and attribute it to increased absorption by vertically extended dust aerosols. Compared to relatively smaller warming trends over the Indian Ocean, warming trend over the Himalayas is observed to be very high that has implications on the summer monsoon variability over Indian region due to greater land-sea thermal contrast.

### 6.3.3 Long term variation in dust aerosols over South Asia

Several studies have shown the relationship between dust loading over the Middle East and Arabian Sea with Indian summer monsoon *(Jin et al., 2014; Vinoj et al., 2014; Solmon et al., 2015)*. *Vinoj et al., (2014)* shows that dust-induced heating over eastern North Africa and the Arabian Peninsula increases the moisture inflow over to India and modulates Indian summer monsoon over southern and central India. Conversely, *Jin et al., (2014*) proposes that the dust induced elevated heating over the Iranian Plateau May enhance the meridional thermal gradient and intensify the Indian summer monsoon rainfall over Indian subcontinent. However, *Kaskaoutis et al., (2016)* reported that the Caspian Sea – Hindu Kush Index (CasHKI), an indicator of the dust emission and transportation over south west Asia and north Arabian Sea, do not have a significant effect on the Indian summer monsoon. The observational evidence for the link between the elevated aerosols and monsoon rainfall over north India is still inconclusive due to the complex interplay between the aerosol forcing and its feedbacks on meteorology.

The large scale variability of the climate system plays a crucial role in the interannual/decadal variability of dust loading over the source region (eg: West Asia and Thar Desert) and downwind (eg: Indian sub-continent) regions *(Moulin et al., 1997; Kim et al., 2016)*. Sources of dust aerosols show dependence on large scale climate variations and

also influence the regional climate through a feedback process which involves diabatic heating and moisture convergence. This coupled feedback and modification of dust properties during the long-range transport limit the plausibility of attributing the decadal variability of dust loading solely to the meteorological/land surface processes. Using satellite and ground based radiometer data, several authors have reported trends of increased dust activity over west Asia and decreasing dust loading over the Indian region during pre-monsoon season over the last two decades *(Dey and Di Girolamo, 2011; Kaskaoutis et al., 2011; Babu et al., 2013; Pandey et al., 2017)*. The era of ground based and space-borne lidars having polarization capability has enabled the characterization of dust aerosols at global and regional scales *(Liu et al., 2008; Yu, Chin, Bian, et al., 2015)*. In this study, a quantitative analysis of the decadal change in pre-monsoon mineral dust loading in the lower free-troposphere over the Indian region is presented based on the measurements using space-borne lidar and ground-based network of radiometers for the first time. Mean spatial distribution of dust optical depth estimated from the decade long space-borne lidar (CALIPSO) observations over the west Asia and south Asia during spring season is shown in Figure 6.12.

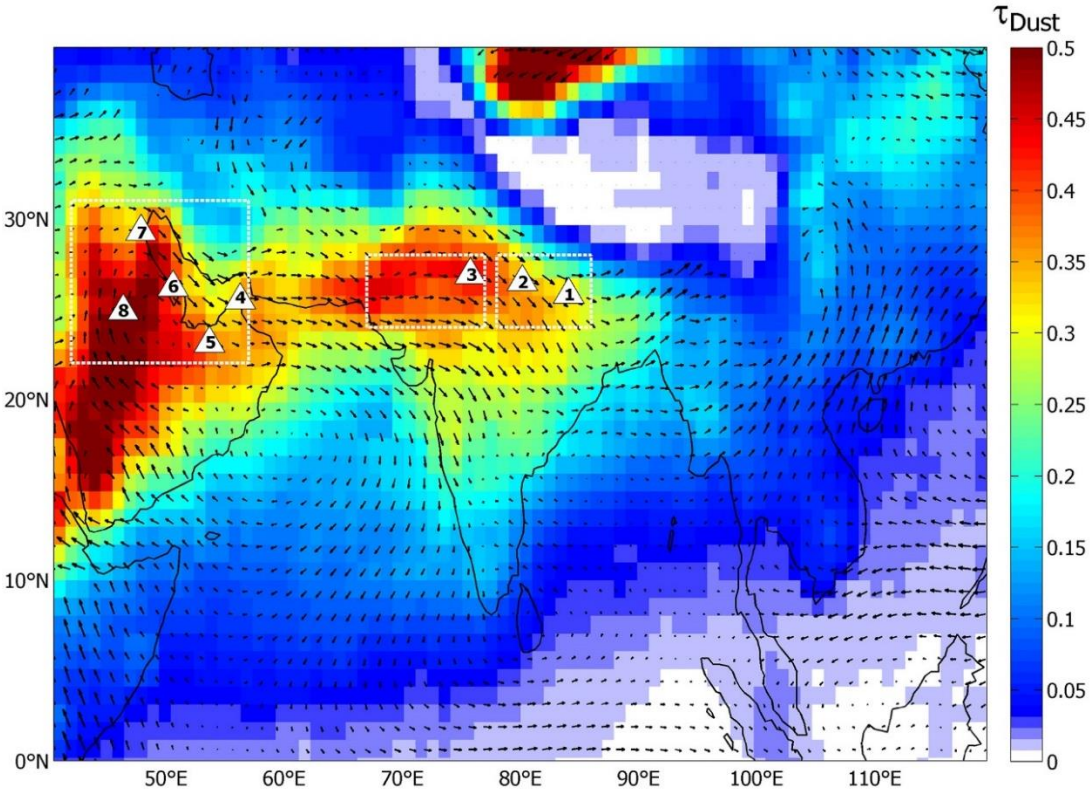


***Figure 6.12*** *- (a) Spatial distribution of dust optical depth over the Indian region during pre-monsoon/spring (MAM) season. Vector winds are at 850 hPa and AERONET radiometer stations (Gandhi College, Kanpur, Jaipur, Solar Village, Dhadnah, Mezaira, Baharain, Kuwait University) are shown in filled star symbols. The three regions representing West Asia, North India and Indo Gangetic Plain are shown in boxes.*

High values (~ 0.5) of dust optical depth is observed over the major source regions like west Asia, Thar and Taklamakan desert while relatively lower values over the downwind regions like Arabian Sea and Indo Gangetic Plain. Analysis is carried out over three distinct geographical regions that include (i) north-west India (24°N - 28°N, 67°E - 76°E) which is a dry arid region over India, (ii) highly polluted Indo-Gangetic Plain (IGP) (24°N - 28°N, 78°E - 86°E) over India and (iii) west Asia (22°N - 31°N, 42°E - 56°E) which is a major dust source region.

The interannual variation of dust aerosol optical depth (dust AOD) derived from CALIOP and coarse mode aerosol optical depth (AOD at 1020 nm) from AERONET stations over IGP, north-west India and west Asia during pre-monsoon season is shown in Figure 6.13.

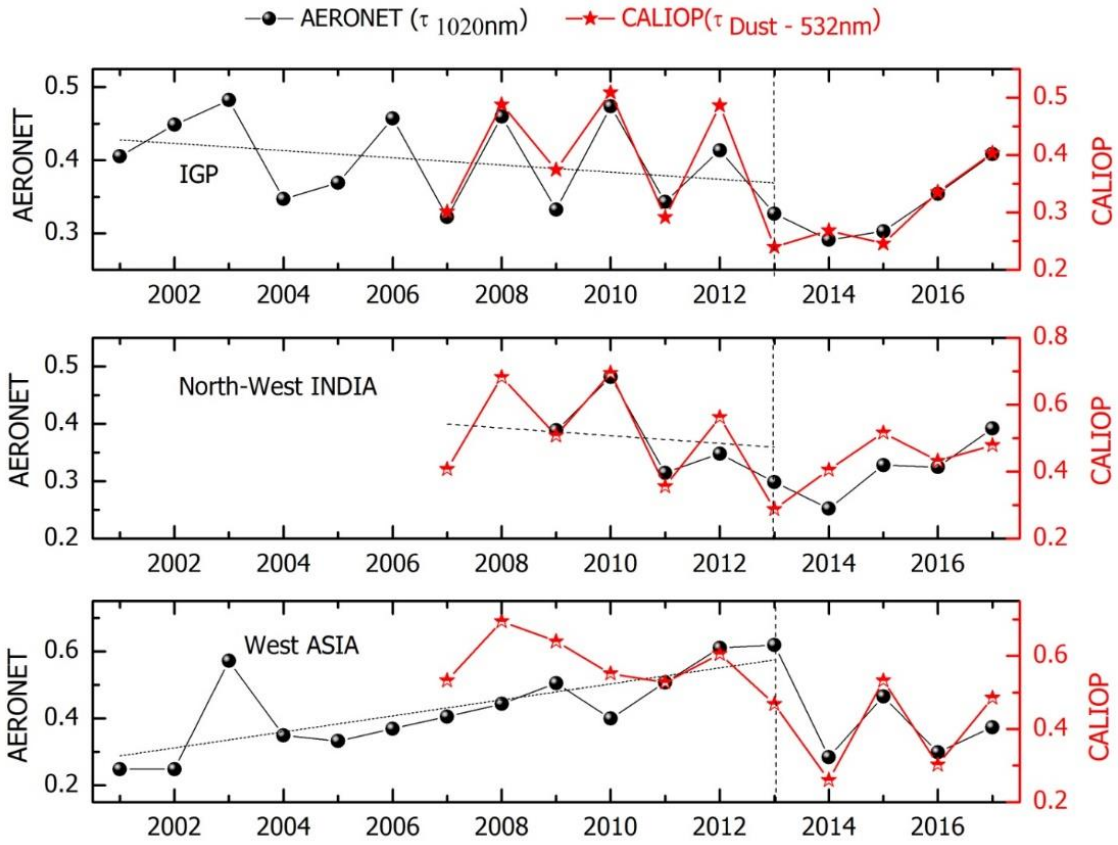


***Figure 6.13*** *- Interannual variation of dust AOD during pre-monsoon season (March - May) retrieved from CALIOP and total coarse mode AOD from AERONET stations, are shown for (a) Indo-Gangetic plain (IGP), (b) North-west India and (c) West Asia. Dashed black lines show linear fits to the data up to 2013 and vertical dashed black lines indicate the end of the slowdown in dust activity.*

The inter-annual variation of pre-monsoon dust AOD over the Indian region shows an oscillatory pattern during 2007 - 2013 with a decreasing trend, which is supported by the long-term variation in coarse mode AOD (mostly contributed by dust) estimated from the

ground based AERONET observations. The increase in pre-monsoon rainfall during the period 2000 to 2015 over the Indian region is reported by *Pandey et al., (2017)* which is attributed to the reason for decreasing trend in dust loading during pre-monsoon over this region. However, a drastic change in the oscillatory pattern of the inter-annual variation in dust AOD is observed after 2013. While dust AOD over the Indian region shows a decreasing trend, and the coarse mode AOD over west Asia showed an increasing trend up to 2013, which also is drastically changed after 2013. The drastic reduction in dust AOD observed over all three study regions after 2013 marks a clear shift in long-term trends that were seen prior to 2013. Linear regression analysis indicates an AOD ($\tau_{1020nm}$) decrease of almost 0.01 $yr^{-1}$ from 2007 to 2013 over north India and 0.005 $yr^{-1}$ over IGP with 95% confidence level following *Weatherhead et al., 1998.* Figure 6.14 shows the anomaly of dust AOD over IGP, north-west India and west Asia during 2007 to 2017 period retrieved from CALIOP measurements.

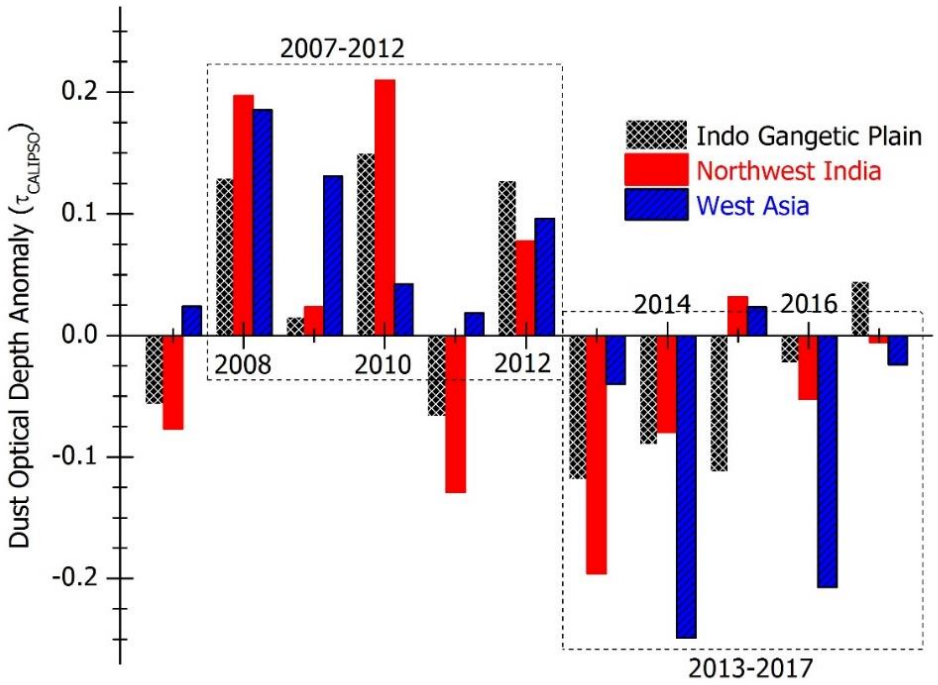


***Figure 6.14*** *- Interannual variations of anomaly of dust optical depth retrieved from CALIOP measurements over Indo-Gangetic Plain, north-west India, and West Asia during pre-monsoon season (March-May).*

It is evident that all the three regions show a clear shift in the pattern of dust AOD between the recent pentad (2013 – 2017) and the previous pentad (2008 -2012). The interannual variations and long-term trends in dust AOD over south Asia is distinctly different to that over West Asia. Within South Asia, interannual variation in dust AOD over IGP and North-west India shows a similar pattern which suggests that dust emission from the Thar Desert

is contributing significantly to the dust loading over IGP. The observed increase in dust AOD over the West Asia during 2000 – 2013 is regarded as a part of decadal oscillation in dust activity, while the inter-annual variations are observed to be linked to the soil conditions and strength of north-westerly Shamal winds *(Notaro et al., 2015; Yu et al., 2015)*. Globally, AOD shows a decrease during the last two decades, while AOD is increasing over south Asia *(Babu et al., 2013)*. The rate of increase is higher during winter and relatively lower and inconspicuous during pre-monsoon *(Babu et al., 2013),* which is partly attributed to the decreasing trend and large interannual variability of the dust aerosols (Figure 6.13) till 2013. Based on the similar methodology, dust loading over the Bay of Bengal showed a decrease during last decade, where dust fraction of the total AOD decreases more steeply than that of dust AOD (Refer chapter 4, Section 4.3.7).

#### 6.3.3.1 Role of wintertime rainfall on the pre-monsoon dust loading

Several studies have attributed the trends in dust loading over India to the recent changes in precipitation pattern during the pre-monsoon *(Pandey et al., 2017)* and previous summer *(Jin and Wang, 2018)* over the region. Rainfall has generally increased during pre-monsoon *(Pandey et al., 2017)* and summer over the western India *(Jin et al., 2018)* simultaneously with decrease in dust loading. However, *(Jin et al., 2018)* attributed the observed decreasing trend in dust loading to the increase in vegetation index associated with the increasing trend in previous year's summer monsoon rainfall. Despite the decreasing trend in dust, on interannual time scale, dust AOD over north-west India is observed to be negatively associated with the rainfall pattern during previous winter rather than the rainfall during the same season (Figure 6.15).

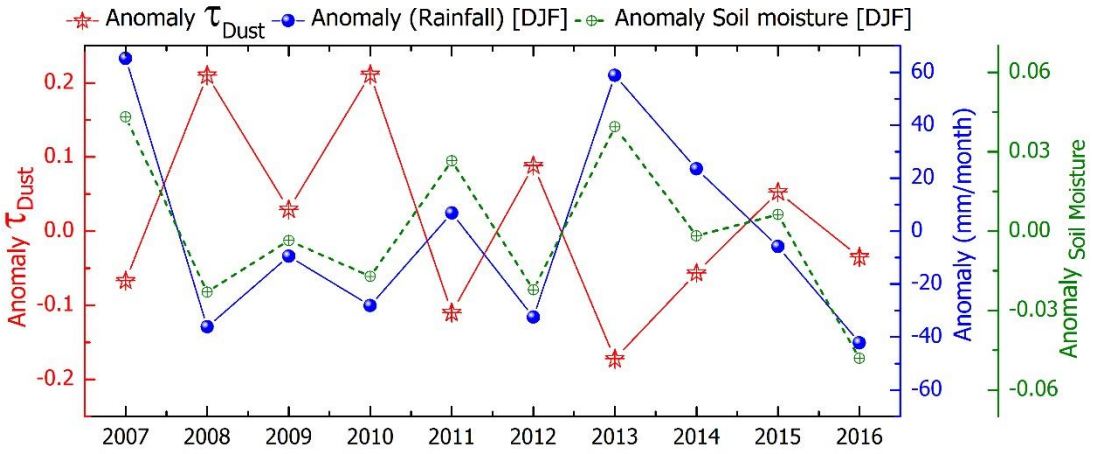


***Figure 6.15*** *- Interannual variation of pre-monsoon dust optical depth anomaly (CALIOP) with rainfall anomaly (IMD) and anomaly in soil moisture (MERRA) during preceding winter months (December - February) over north-west India.*

Correlation coefficient of - 0.72 is observed between the pre-monsoon dust optical depth and preceding winter rainfall over north-west India. Increase in soil moisture and associated changes in vegetation due to increase in winter rains, reduce the dust emission at the source during succeeding pre-monsoon season. However, this systematic pattern in the association also changes after 2013. The complex association of rainfall on dust loading via wet scavenging and reducing the emission flux by increasing the soil moisture needs to be investigated in detail.

#### 6.3.3.2 Dust aerosols and tropospheric temperature

Several studies have highlighted the diabatic heating due to mineral dust over South Asia and its implications on monsoonal circulation, moisture convergence, and rainfall pattern *(Lau et al., 2006; Vinoj et al., 2014; Jin et al., 2014)*. However, the influence of dust aerosols on surface and free tropospheric temperature are inconspicuous on inter-annual time scales. An association of OMI derived aerosol index (AI) with the tropospheric temperature is reported by *(Gautam et al., 2009)* and attributes it to the heating effect of dust aerosols on tropospheric temperature. Direct observations of dust optical depth from CALIPSO (2007 - 2017) allows for quantitative examination of the association between the dust optical depth and the free tropospheric temperature and is shown in Figure 6.16.

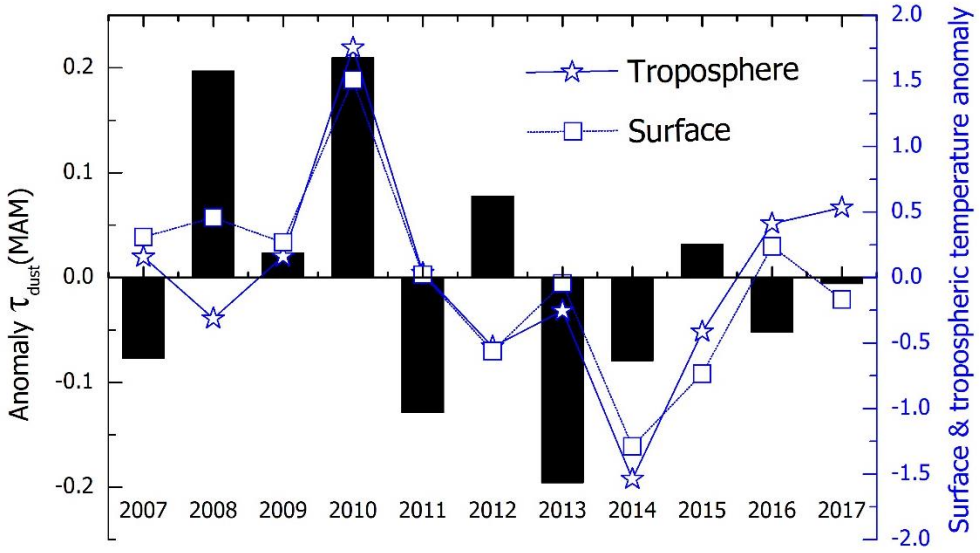


***Figure 6.16*** *- Anomaly of surface (HADCRU) (open Square) and free tropospheric temperature (AMSU-TLT) (open star) with dust optical depth anomaly over north-west India during the pre-monsoon season.*

However, a direct correlation between dust loading and tropospheric temperature is not observed over the study region on an interannual scale. Investigation on the role of meteorological feedback on the dust forcing using regional climate model shows that changing meteorology largely modulates dust outflows and precipitation over South Asia

*(Kaskaoutis et al., 2018)*. Dust activity over the West Asia and North Africa shows distinct decadal oscillations with an increasing trend at the beginning of 21st century, using station based visibility data *(Yu et al., 2015).* The changes in long-term trend in dust loading over India are considered as a signal for regional climate change *(Pandey et al., 2017; Jin et al., 2018).* It should also be noted that the decadal change in dust over the Thar Desert and north India has not investigated in detail, unlike the west Asian counterpart *(Yu et al., 2015).* In the backdrop of the recent (after 2013) shift in dust loading trend over north India, role of climate variability in modulating the dust loading and its relationship with the key variables of the climate system needs to be investigated in detail.

## 6.4 Summary

The chapter presents the radiative effects of aerosols over the Indian region using a synergy of observations from ground based, air-borne and space based platforms. Vertical profiles of the heating rate of absorbing aerosols over the Indian region is estimated by incorporating the observations of vertical distribution of aerosols from the CALIOP and RAWEX aircraft observations, along with ARFINET columnar observations into SBDART (Santa-Barbara Distort Atmospheric Radiation Transfer Model).

Concluding points are as follows

- Role of aerosol vertical distribution in the assessment of aerosol radiative forcing is examined through model simulations. Aerosol radiative forcing at the TOA is dependent on the scale height of aerosols. Aerosol radiative forcing at the TOA become more positive with scale height for absorbing aerosols (SSA=0.65) and more negative with scale height for scattering aerosols (SSA=1).
- Aerosol forcing of the atmosphere shows a twofold increase from winter to pre-monsoon, over peninsular and eastern India. Over IGP and north-west India, $ARF_{ATM}$ is same for both winter and pre-monsoon but vertical distribution of diabatic heating shows significant changes from winter to pre-monsoon.
- Aerosol heating rate is dominant above PBL during pre-monsoon. However, winter time heating rate is observed higher with respect to pre-monsoon, though heating is confined to lower altitudes. Over Peninsular and Eastern regions, heating rate is significantly higher (~1 $Kday^{-1}$) above PBL compared to within PBL during pre-monsoon.
- While dust induced heating rates shows a clear transition from winter to pre-monsoon, heating due to carbonaceous aerosols are found equally significant during both the seasons. Aerosol induced heating rate is exceptionally high over the IGP during winter (~3 $Kday^{-1}$), which is mostly contributed by carbonaceous

aerosols. High values of dust induced heating are observed over north-west India during pre-monsoon with a heating rate of ~0.7 $Kday^{-1}$.

- A distinct shift in trend in dust aerosols is observed during the last decade over the Indian region. The inter-annual variation of pre-monsoon dust AOD over the Indian region shows an oscillatory pattern during 2007 - 2013 with a decreasing trend. The decreasing trend in dust loading over the Indian region has reversed to increasing after the year 2013. Over west Asia, pre-monsoon dust loading showed a clear change in pattern from the year 2013.
- The interannual variability in pre-monsoon dust optical depth over north-west India is found to be associated with the preceding winter time rainfall that alters the soil characteristics over the source regions in the north-west India.
- A direct correlation between dust loading and tropospheric temperature is not observed over the study region on an interannual scale

# Chapter 7

# Summary and conclusion

## 7.1 Summary

Aerosols, especially absorbing aerosols, at elevated altitudes assumes importance because they cause radiative heating of the atmosphere thereby alter the thermal structure of the atmosphere and cloud properties. Radiative effects of aerosols depends on their vertical distribution in the atmosphere. During winter and pre-monsoon seasons, the prevailing meteorology over the Indian region favours the transport of aerosols to the marine regions. This transported aerosols deposit over the oceanic region and influence the marine bio-fertilization of ocean biota that causes alterations in the bio-geo chemical cycle. In addition, over northern region of India, aerosols transported over the Great Himalayas interact with the Himalayan cryosphere through both direct and albedo effect and can affect the snow/glacier cover and the regional hydrological cycle. Realizing the importance of elevated aerosols in determining the radiative effects and climate impact of aerosols, *thesis address the characterization of vertical distribution of aerosols over the Indian land mass, surrounding oceanic regions (the Arabian Sea and the Bay of Bengal) and over the Himalayan region. The radiative effects of elevated aerosols over different regions of India are estimated.*

An overview of the atmospheric aerosols in general and elevated aerosols in particular is given in chapter–1. Besides the basic concepts on aerosol science, this chapter also provides the current understanding on the elevated aerosols and various scientific experiments conducted over different regions to understand its climate impacts.

The details of datasets used, retrieval techniques, and method of analysis are presented in chapter - 2. The major dataset comprises of decade long (2006-2017) observations on the vertical profiles of aerosol back-scatter and particle depolarization by the space-borne lidar, CALIOP on-board CALIPSO. Retrieval of aerosol extinction coefficient from the lidar signal requires assumption of extinction to back-scatter ratio (termed as 'lidar ratio') which depends on the size distribution and composition of aerosols. Lidar ratio of aerosols is estimated over the Indian region using column AOD observations. It is found that lidar ratio used by the CALIOP results in significant underestimation of AOD over the Indian region. Present analysis estimate aerosol extinction coefficient using a combination of

columnar AOD observations (ARFINET/MODIS) and range resolved aerosol backscattering coefficient (CALIOP).

Aerosol system over the South Asia is an external mixture of dust and non-dust aerosols in different proportion, due to seasonally varying distinct outflows of continental and marine origin. Polarization resolved observations of back scattered photons are sensitive to the relative dominance of non-spherical particles and aids in the characterization of mineral dust aerosols owing to their non-spherical morphology. Being an intensive aerosol parameter, particle depolarization ratio is sensitive to mixing processes. Thus by assuming a two-component aerosol system of dust and non-dust, and with a priori information on the dust/non-dust linear depolarization ratio, contribution of dust aerosols to the observed back-scattering coefficient is estimated. Using simultaneous observations of depolarization ratio, aerosol back-scattering coefficient and characteristic dust lidar ratio, dust extinction coefficient is estimated. *The thesis also addresses the quantification of extinction coefficient due to mineral dust aerosols for the first time over the Indian region.*

**Vertical distribution of aerosols over the Indian land mass** is examined in chapter 3 using vertical profiles of aerosol backscattering coefficient from CALIOP coupled with ground based columnar AOD measured at the ARFINET stations using MWR/sunphotometer. Using depolarization observations of CALIOP, contribution of mineral dust to the total system of aerosols is quantified and a three dimensional distribution of dust optical depth is presented over the Indian region. The major findings are following.

- An enhancement in aerosol loading is observed at free tropospheric altitudes during pre-monsoon over the Indian region. As season changes from winter to pre-monsoon, vertical transport of boundary layer aerosols to elevated altitudes causes this enhancement in aerosol loading in the free troposphere and a reduction in aerosols within PBL.
- Vertical spread of aerosols is high during pre-monsoon season and extends up to 4.5 to 5 km, while during winter these aerosols resides within the 3 to 3.5 km (below which 98% of aerosols resides) from the surface.
- Distinct meridional variation in aerosol vertical distribution is observed during the pre-monsoon season over the Indian landmass with minimum vertical extent over the southern latitudes which gradually increase towards northern latitudes.
- Pre-monsoon enhancement in aerosols over the Indian region is associated with high particle depolarization ratio indicating the prominent role of mineral dust

aerosols in the formation of elevated aerosol layer. Mineral dust loading over the Indian region shows a systematic increase from December to May.

Contribution of dust aerosols to the total aerosol optical depth is quantified using CALIOP and ARFINET observations. During the pre-monsoon season, dust fraction is highest over the source regions over the north-western India (90%) and is least over the eastern India (21%) while Indo-Gangetic Plain and Peninsular India are characterized by ~51% and ~67% respectively.

**Vertical distribution of aerosols over the oceanic regions around India** (The Bay of Bengal and the Arabian Sea), is examined using CALIOP observations. Transport of mineral dust aerosols over marine regions and its deposition over oceanic surfaces are very important for the ocean bio-geochemistry. MODIS-AQUA being flown in formation with CALIPSO provides a fairly collocated measurement of AOD with better spatial resolution which helps to improve the accuracy of CALIOP derived aerosol extinction coefficient over the oceanic regions. The major finding are as follows

- Aerosol optical depth is found to be higher during pre-monsoon compared to winter over the Arabian Sea and the Bay of Bengal.
- Distinct seasonal pattern is observed in the vertical structure of both aerosols and dust over the BoB and the Arabian Sea, with a pre-monsoon enhancement in aerosols above MABL. Over BoB, aerosol extinction coefficient near the surface is higher during winter with lower vertical extent while pre-monsoon is characterized by higher aerosol extinction coefficients above MABL. Over AS, aerosol extinction coefficient near the surface is more or less same for both the season but at elevated heights aerosol extinction coefficient is higher during pre-monsoon.
- Vertical distributions of aerosols are distinctly different over the Northern BoB and Southern BoB. Prominent extinction is observed in the altitude range ~1.5 to 4.5 km over the northern BoB during pre-monsoon while aerosol loading linearly decreases above MABL over the southern BoB.
- Enhanced aerosol loading is observed in the altitude range ~1.5 to 4.5 km over the eastern AS similar to that observed over Northern BoB during pre-monsoon. This enhanced aerosol loading at elevated altitudes is attributed to the anti-cyclonic circulation prevailing over the Indian landmass that transports aerosols from the Indian landmass to the northern BoB and south-eastern AS, causing plumes of enhanced AOD over these regions.

- Prominent dust loading is observed over the northern AS with 34 % of the total aerosol loading is constituted by dust aerosols during winter and 62% during pre-monsoon season. Columnar dust fraction over the eastern AS is estimated as 20 % during winter and 37 % during pre-monsoon.
- Significant contribution of dust is observed over the northern BoB during pre-monsoon season where 22% of the total aerosol extinction is contributed by dust aerosols transported from the nearby continental regions. During winter, dust transport is found to be less significant with a fractional contribution of ~10 % - 13 % of the total aerosol optical depth over the Bay of Bengal.
- Dust fraction derived using CALIOP (depolarization technique) and MODIS observations (fine-mode observation based) are compared with that simulated by GOCART over the study regions. MODIS derived dust fraction (fine-mode based) shows an overestimation up to 2 fold compared to CALIOP dust fraction (depolarization based). GOCART simulated dust fraction underestimates the satellite derived dust fractions over the study regions except over northern AS which is a dust dominant region.
- Long term variation (2007- 2017) in AOD shows an increasing trend over the northern Bay of Bengal and eastern part of AS during pre-monsoon. Over northern AS, AOD decreases during the study period. Dust optical depth and dust fraction is showing a decreasing trend over all the study regions indicating the increasing fraction of anthropogenic aerosols over both BoB and AS. Long term trend in dust optical depth derived using both CALIOP (depolarization based) and MODIS (fine-mode based) showed similar results.

Over the Himalayas, aerosols present in the atmosphere causes surface dimming while those deposited over the snow-surface can cause surface warming by lowering the snow-albedo. In the atmosphere, aerosol induced warming assumes significance as the highly reflecting snow surface enhances the radiation absorption by aerosols in the atmosphere leading to atmospheric warming. Passive observations over the Himalayan cryosphere suffer from large uncertainty pertaining to high reflection from the surface. CALIOP provides better estimates of aerosol loading over the Himalayas since it provides active measurements of back-scattered photons from different layers of the atmosphere. **Elevated aerosols over the Himalayas** is examined using CALIOP observations and major findings are as follows

- Aerosol loading over the Himalayas critically depends on the topography with a drastic decrease in AOD with surface elevation. AOD at high altitude stations decreases up to one order magnitude compared to the stations at the foothills.

- Aerosol loading shows seasonally distinct regional pattern that are associated with the precipitation pattern over the Himalayas. Aerosol loading is found to be minimum during winter while more than two fold increase is observed during pre-monsoon over mid/eastern Himalayas. During summer monsoon/post monsoon seasons, aerosol loading is prominent over the western Himalayas compared to mid and eastern Himalayas.
- Significant fraction of elevated aerosols is observed over the Himalayas throughout the year. An Average of 50 ± 5 % and 48 ± 6 % of aerosols in the column is present above 1 km during pre-monsoon and summer monsoon respectively while during winter and post monsoon seasons; contribution of elevated aerosols above 1 km to the columnar loading is 41 ± 8 % and 42 ± 8 % respectively.
- Dust loading shows regionally and seasonally distinct characteristics over the Himalayas with highest loading over the mid Himalayas during pre-monsoon season. During the pre-monsoon, the entire Himalayas is significantly influenced by polluted dust where the contribution of polluted dust to the total aerosols over western, mid and eastern Himalayas are 63 %, 67 % and 57 % respectively.

A synergy of observations from ground based, air-borne and space based platforms are used in the radiative transfer calculations to investigate the **radiative effects of elevated aerosols over the Indian region**. Various aspects of aerosol induced heating in the atmosphere are examined with emphasize on mineral dust aerosols, a well-known absorbing aerosol species. Vertical profiles of the heating rate of aerosols over the Indian region is estimated by incorporating the observations of vertical distribution of aerosols from CALIOP and RAWEX aircraft observations, along with ARFINET columnar observations in Santa-Barbara Distort Atmospheric Radiation Transfer Model (SBDART). Long term trend in mineral dust aerosols over south Asia is investigated using a combination of decade long observations of CALIPSO and AERONET and its implications are discussed. Major findings are as follows

- Role of aerosol vertical distribution in the assessment of aerosol radiative forcing is examined through model simulations. Aerosol radiative forcing at the TOA is found to depend on the scale height of aerosols where TOA forcing become more positive with scale height for absorbing aerosols (SSA=0.65) and more negative with scale height for scattering aerosols (SSA=1).
- Aerosol forcing of the atmosphere shows a twofold increase from winter to pre-monsoon, over peninsular and eastern India. Over IGP and north-west India,

$ARF_{ATM}$ is same for both winter and pre-monsoon but vertical distribution of diabatic heating shows significant changes from winter to pre-monsoon.

- Aerosol heating rate is dominant above PBL during pre-monsoon. However, winter time heating rate is observed higher with respect to pre-monsoon, though heating is confined to lower altitudes. Over peninsular and eastern regions, heating rate is significantly higher (~1 $Kday^{-1}$) above PBL compared to that within PBL during pre-monsoon.
- While dust induced heating rates shows a clear enhancement from winter to pre-monsoon, heating due to carbonaceous aerosols are found to be equally significant during both the seasons. Aerosol induced heating rate is exceptionally high over the IGP during winter (~3 $Kday^{-1}$), which is mostly contributed by carbonaceous aerosols. High values of dust induced heating are observed over north-west India during pre-monsoon with a heating rate of ~0.7 $Kday^{-1}$.
- A distinct shift in trend in dust aerosols is observed during the last decade over the Indian region. The inter-annual variation of pre-monsoon dust AOD over the Indian region shows an oscillatory pattern during 2007 - 2013 with a decreasing trend. The decreasing trend in dust loading over the Indian region has reversed to increasing after the year 2013.
- The interannual variability in pre-monsoon dust optical depth over north-west India is found to be associated with the rainfall during preceding winter, which alters the soil characteristics over the source regions in the north-west India.
- A direct correlation between dust loading and tropospheric temperature anomalies is not observed over the study region on an interannual scale.

In summary, the work presented in this thesis highlight the importance of elevated aerosols over Indian region. The elevated aerosol loading and its vertical extent is found to be significantly high during pre-monsoon season, not only over the Indian mainland but over the oceanic regions around India and Himalayan regions. This enhanced aerosol loading at higher altitudes during the pre-monsoon has a significant contribution from the transported mineral dust. The changes in long term trend in dust loading over India can be considered as a signal for regional climate change. However, it should also be noted that, the decadal change in dust over the Thar Desert and north India has not been investigated in detail, unlike the west Asian counterpart. In the backdrop of the recent shift in the trend in dust loading over north India, role of climate variability in modulating the dust loading and its relationship with the key variables of the climate system needs to be investigated in detail using long term observations and climate modelling.

## 7.2 Scope for Future work

Based on the observations and inferences from the present thesis, following points are emerged for future work

1. **Radiative effects of elevated aerosols in the presence of clouds:** Radiative effects of aerosols in the presence of clouds is significantly different from that during clear sky conditions. Aerosol vertical distribution critically influence the radiative effects of absorbing aerosols in the presence of cloud. Radiative effects of elevated aerosols in cloudy atmosphere is to be addressed using simultaneous observations of aerosol vertical distribution and cloud properties.
2. **Radiative effects of mineral dust aerosols over the Himalayas:** Himalayan cryosphere is mostly under the influence of dust transport from the dessert regions of West Asia. Significant amount of mineral dust aerosols are observed to be deposited over the Himalayas which is significant in the context of snow-albedo feedback and resulting snow melting. On the backdrop of these observations, direct radiative effect and forcing due to snow-albedo feedback of mineral dust aerosols is to be assessed.
3. **Longwave radiative effects of mineral dust aerosols:** While aerosol radiative effects in the short wave regime causes surface cooling, long wave absorption and scattering by aerosols warms the earth-atmosphere system. Neglecting longwave effects of mineral dust aerosols can result in large deviation in the estimation of aerosol radiative effects in climate models *(Satheesh and Lubin, 2003)*. For the precise estimation of radiative effects of mineral dust aerosols on the earth-atmosphere system, their effects on longwave regime is to be quantified. Using satellite based IR flux measurements, longwave radiative effects of mineral dust aerosols is to be addressed over the Indian region.

# Reference


Ackerman, A. S., Toon, O. B., Stevens, D. E., Heymsfield, A. J., Ramanathan, V., & Welton, E. J. (2000). Reduction of tropical cloudiness by soot. *Science*, *288*(5468), 1042–1047. https://doi.org/10.1126/science.288.5468.1042

Ackerman, S. A., Strabala, K. L., Menzel, W. P., Frey, R. A., Moeller, C. C., & Gumley, L. E. (1998). Discriminating clear sky from clouds with MODIS. *Journal of Geophysical Research*, *103*(D24), 32141–32157. https://doi.org/10.1029/1998JD200032

Ackermann, J. (1998). The extinction-to-backscatter ratio of tropospheric aerosol: A numerical study. *Journal of Atmospheric and Oceanic Technology*, *15*(4), 1043–1050.

Albrecht, B. A. (1989). Aerosols, cloud microphysics, and fractional cloudiness. *Science*, *245*(4923), 1227–1230. https://doi.org/10.1126/science.245.4923.1227

Aloysius, M., Mohan, M., Babu, S. S., Nair, V. S., Parameswaran, K., & Moorthy, K. K. (2008). Influence of circulation parameters on the AOD variations over the Bay of Bengal during ICARB. *Journal of Earth System Science*, *117*, 353–360. https://doi.org/10.1007/s12040-008-0038-6

Alpert, P., Kaufman, Y. J., Shay-El, Y., Tanre, D., Da Silva, A., Schubert, S., & Joseph, J. H. (1998). Quantification of dust-forced heating of the lower troposphere. *Nature*, *395*(6700), 367–370. https://doi.org/10.1038/26456

Amiri-Farahani, A., Allen, J. R., Neubauer, D., & Lohmann, U. (2017). Impact of Saharan dust on North Atlantic marine stratocumulus clouds: Importance of the semidirect effect. *Atmospheric Chemistry and Physics*, *17*(10), 6305–6322. https://doi.org/10.5194/acp-17-6305-2017

Amiridis, V., Wandinger, U., Marinou, E., Giannakaki, E., Tsekeri, A., Basart, S., et al. (2013). Optimizing CALIPSO saharan dust retrievals. *Atmospheric Chemistry and Physics*, *13*(23), 12089–12106. https://doi.org/10.5194/acp-13-12089-2013

Anders, A. M., Roe, G. H., Hallet, B., Montgomery, D. R., Finnegan, N. J., & Putkonen, J. (2006). Spatial patterns of precipitation and topography in the Himalaya. In *Special Paper 398: Tectonics, Climate, and Landscape Evolution* (pp. 39–53). https://doi.org/10.1130/2006.2398(03)

Anderson, T. L. (2003). Variability of aerosol optical properties derived from in situ aircraft measurements during ACE-Asia. *Journal of Geophysical Research*, *108*(D23), ACE 15-1-ACE 15-19. https://doi.org/10.1029/2002JD003247

Anderson, T. L., Covert, D. S., Marshall, S. F., Laucks, M. L., Charlson, R. J., Waggoner, A. P., et al. (1996). Performance characteristics of a high-sensitivity, three-wavelength, total scatter/backscatter nephelometer. *Journal of Atmospheric and Oceanic Technology*, *13*(5), 967–986.

Anderson, T. L., Masonis, S. J., Covert, D. S., Charlson, R. J., & Rood, M. J. (2000). In situ measurement of the aerosol extinction-to-backscatter ratio at a polluted continental site. *Journal of Geophysical Research: Atmospheres*, *105*(D22), 26907–26915. https://doi.org/10.1029/2000JD900400

Anderson, T. L., Charlson, R. J., Winker, D. M., Ogren, J. a., & Holmén, K. (2003). Mesoscale Variations of Tropospheric Aerosols. *Journal of the Atmospheric Sciences*, *60*(1), 119–136.

Andersson, S. M., Martinsson, B. G., Vernier, J. P., Friberg, J., Brenninkmeijer, C. A. M., Hermann, M., et al. (2015). Significant radiative impact of volcanic aerosol in the lowermost stratosphere. *Nature Communications*, *6*,, 7692. https://doi.org/10.1038/ncomms8692

Andreae, M. O., & Crutzen, P. J. (1997). Atmospheric aerosols: Biogeochemical sources and role in atmospheric chemistry. *Science*, *276*(5315), 1052–1058. https://doi.org/10.1126/science.276.5315.1052

Ångström, A. (1964). The parameters of atmospheric turbidity. *Tellus*, *16*(1), 64–75. https://doi.org/10.3402/tellusa.v16i1.8885

Ansmann, A., Riebesell, M., & Weitkamp, C. (1990). Measurement of atmospheric aerosol extinction profiles with a Raman lidar. *Optics Letters*, *15*(13), 746. https://doi.org/10.1364/OL.15.000746

Ansmann, A., Riebesell, M., Wandinger, U., Weitkamp, C., Voss, E., Lahmann, W., & Michaelis, W. (1992). Combined raman elastic-backscatter LIDAR for vertical profiling of moisture, aerosol extinction, backscatter, and LIDAR ratio. *Applied Physics B Photophysics and Laser Chemistry*. https://doi.org/10.1007/BF00348608

Ansmann, A., Althausen, D., Wandinger, U., Franke, K., Muller, D., Wagner, F., & Heintzenberg, J. (2000). Vertical profiling of the Indian aerosol plume with six-wavelength lidar during INDOEX: A first case study. *Geophysical Research Letters*, *27*(7), 963–966. https://doi.org/10.1029/1999GL010902

Ansmann, A., Tesche, M., Knippertz, P., Bierwirth, E., Althausen, D., Müller, D., & Schulz, O. (2009). Vertical profiling of convective dust plumes in southern Morocco during SAMUM. *Tellus, Series B: Chemical and Physical Meteorology*, *61*(1), 340–353. https://doi.org/10.1111/j.1600-0889.2008.00384.x

Ansmann, A., Petzold, A., Kandler, K., Tegen, I., Wendisch, M., Müller, D., et al. (2011). Saharan Mineral Dust Experiments SAMUM-1 and SAMUM-2: What have we learned? *Tellus, Series B: Chemical and Physical Meteorology*, *63*(4), 403–429. https://doi.org/10.1111/j.1600-0889.2011.00555.x

Aoki, T., Motoyoshi, H., Kodama, Y., Yasunari, T. J., Sugiura, K., & Kobayashi, H. (2006). Atmospheric Aerosol Deposition on Snow Surfaces and Its Effect on Albedo. *Sola*, *2*(0), 13–16. https://doi.org/10.2151/sola.2006-004

Arnott, W. P., Hamasha, K., Moosmüller, H., Sheridan, P. J., & Ogren, J. A. (2005). Towards aerosol light-absorption measurements with a 7-wavelength aethalometer: Evaluation with a photoacoustic instrument and 3-wavelength nephelometer. *Aerosol Science and Technology*, *39*(1), 17–29. https://doi.org/10.1080/027868290901972

Babu, C. A., & Sivaprasad, P. (2014). Variability and mechanisms of vertical distribution of aerosols over the Indian region. *International Journal of Remote Sensing*, *35*(22), 7691–7705. https://doi.org/10.1080/01431161.2014.975379

Babu, S. S., & Moorthy, K. K. (2002). Aerosol black carbon over a tropical coastal station in India. *Geophysical Research Letters*, *29*(23), 13-1-13–4. https://doi.org/10.1029/2002GL015662

Babu, S. S., Satheesh, S. K., & Moorthy, K. K. (2002). Aerosol radiative forcing due to enhanced black carbon at an urban site in India. *Geophysical Research Letters*, *29*(18), 27-1-27–4. https://doi.org/10.1029/2002GL015826

Babu, S. S., Moorthy, K. K., & Satheesh, S. K. (2004). Aerosol black carbon over Arabian Sea during intermonsoon and summer monsoon seasons. *Geophysical Research Letters*, *31*(6). https://doi.org/ 10.1029/2003GL018716

Babu, S. S., Moorthy, K., Satheesh, S. K. K., Suresh Babu, S., Krishna Moorthy, K., Satheesh, S. K. K., et al. (2007). Temporal heterogeneity in aerosol characteristics and the resulting radiative impacts at a tropical coastal station-Part 2: Direct short wave radiative forcing. *Annales Geophysicae*, *25*(11), 2309–2320. https://doi.org/10.5194/angeo-25-2293-2007

Babu, S. S., Nair, V. S., & Moorthy, K. K. (2008). Seasonal changes in aerosol characteristics over Arabian Sea and their consequence on aerosol short-wave radiative forcing: Results from ARMEX field campaign. *Journal of Atmospheric and Solar-Terrestrial Physics*, *70*(5), 820–834. https://doi.org/10.1016/j.jastp.2007.10.005

Babu, S. S., Moorthy, K. K., Manchanda, R. K., Sinha, P. R., Satheesh, S. K., Vajja, D. P., et al. (2011). Free tropospheric black carbon aerosol measurements using high altitude balloon: Do BC layers build their own homes up in the atmosphere? *Geophysical Research Letters*, *38*(8). https://doi.org/10.1029/2011GL046654

Babu, S. S., Chaubey, J. P., Krishna Moorthy, K., Gogoi, M. M., Kompalli, S. K., Sreekanth, V., et al. (2011). High altitude (~4520 m amsl) measurements of black carbon aerosols over western trans-Himalayas: Seasonal heterogeneity and source apportionment. *Journal of Geophysical Research Atmospheres*, *116*(24). https://doi.org/10.1029/2011JD016722

Babu, S. S., Gogoi, M. M., Kumar, V. H. A. A., Nair, V. S., & Moorthy, K. K. (2012). Radiative properties of Bay of Bengal aerosols: Spatial distinctiveness and source impacts. *Journal of Geophysical Research Atmospheres*, *117*(6). https://doi.org/10.1029/2011JD017355

Babu, S. S., Manoj, M. R., Moorthy, K. K., Gogoi, M. M., Nair, V. S., Kompalli, S. K., et al. (2013). Trends in aerosol optical depth over Indian region: Potential causes and impact indicators. *Journal of Geophysical Research Atmospheres*, *118*(20), 11794–11806. https://doi.org/10.1002/2013JD020507

Babu, S. S., Nair, V. S., Gogoi, M. M., & Krishna Moorthy, K. (2016). Seasonal variation of vertical distribution of aerosol single scattering albedo over Indian sub-continent: RAWEX aircraft observations. *Atmospheric Environment*, *125*, 312–323. https://doi.org/10.1016/j.atmosenv.2015.09.041

Badarinath, K. V. S., Kharol, S. K., Sharma, A. R., & Roy, P. S. (2009). Fog Over Indo-Gangetic Plains—A Study Using Multisatellite Data and Ground Observations. *IEEE Journal of Selected Topics in Applied Earth Observations and Remote Sensing*, *2*(3), 185–195. https://doi.org/10.1109/JSTARS.2009.2019830

Badarinath, K. V. S., Kharol, S. K., Kaskaoutis, D. G., Sharma, A. R., Ramaswamy, V., & Kambezidis, H. D. (2010). Long-range transport of dust aerosols over the Arabian Sea and Indian region — A case study using satellite data and ground-based measurements. *Global and Planetary Change*, *72*(3), 164–181. https://doi.org/10.1016/j.gloplacha.2010.02.003

Banerjee, P., & Prasanna Kumar, S. (2014). Dust-induced episodic phytoplankton blooms in the Arabian Sea during winter monsoon. *Journal of Geophysical Research: Oceans*, *119*(10), 7123–7138. https://doi.org/10.1002/2014JC010304

Barros, A. P., Chiao, S., Lang, T. J., Burbank, D., & Putkonen, J. (2006). From weather to climate—Seasonal and interannual variability of storms and implications for erosion processes in the Himalaya. *Geological Society of America Special Papers*, *398*(02), 17–38. https://doi.org/10.1130/2006.2398(02).

Bartusek, K., Gambling, D. J., & Elford, W. G. (1970). Stratospheric aerosol measurements by optical radar. *Journal of Atmospheric and Terrestrial Physics*, *32*(9), 1535–1544. https://doi.org/10.1016/0021-9169(70)90069-3

Bates, T. S., Huebert, B. J., Gras, J. L., Griffiths, F. B., & Durkee, P. A. (1998). International Global Atmospheric Chemistry (IGAC) Project's First Aerosol Characterization Experiment (ACE 1): Overview. *Journal of Geophysical Research Atmospheres*, *103*(D13), 16297–16318. https://doi.org/10.1029/97JD03741

Beegum, S. N., Moorthy, K. K., Nair, V. S., Babu, S. S., Satheesh, S. K., Vinoj, V., et al. (2008). Characteristics of spectral aerosol optical depths over India during ICARB. *Journal of Earth System Science*, *117*, 303–313. https://doi.org/10.1007/s12040-008-0033-y

Bellouin, N., Boucher, O., Haywood, J., & Reddy, M. S. (2005). Global estimate of aerosol direct radiative forcing from satellite measurements. *Nature*, *438*(7071), 1138–1141. https://doi.org/10.1038/nature04348

Berkoff, T. A., Welton, E. J., Campbell, J. R., Scott, V. S., & Spinhirine, J. D. (2003). Investigation of overlap correction techniques for the micro-pulse lidar network (MPLNET). *IGARSS 2003: IEEE International Geoscience and Remote Sensing Symposium*, *1*(C), 4395–4397. https://doi.org/10.1109/IGARSS.2003.1295527

Bhambri, R., & Bolch, T. (2009). Glacier mapping: A review with special reference to the Indian Himalayas. *Progress in Physical Geography*, *33*(5), 672–704. https://doi.org/10.1177/0309133309348112

Bhat, G. S., Gadgil, S., Hareesh Kumar, P. V., Kalsi, S. R., Madhusoodanan, P., Murty, V. S. N., et al. (2001). BOBMEX: The Bay of Bengal Monsoon experiment. *Bulletin of the American Meteorological Society*, *82*(10), 2217–2243.

Bigg, E. K. (1964). Atmospheric stratification revealed by twilight scattering. *Tellus*, *16*(1), 76–83. https://doi.org/10.3402/tellusa.v16i1.8884

Bolch, T., Kulkarni, a., Kaab, a., Huggel, C., Paul, F., Cogley, J. G., et al. (2012). The State and Fate of Himalayan Glaciers. *Science*, *336*(6079), 310–314. https://doi.org/10.1126/science.1215828

Bollasina, M., Nigam, S., & Lau, K. M. (2008). Absorbing aerosols and summer monsoon evolution over South Asia: An observational portrayal. *Journal of Climate*, *21*(13), 3221–3239. https://doi.org/10.1175/2007JCLI2094.1

Bollasina, M. A., Ming, Y., & Ramaswamy, V. (2011). Anthropogenic aerosols and the weakening of the south asian summer monsoon. *Science*, *334*(6055), 502–505. https://doi.org/10.1126/science.1204994

Bollasina, M. A., Ming, Y., & Ramaswamy, V. (2013). Earlier onset of the Indian monsoon in the late twentieth century: The role of anthropogenic aerosols. *Geophysical Research Letters*, *40*(14), 3715–3720. https://doi.org/10.1002/grl.50719

Bookhagen, B., & Burbank, D. W. (2006). Topography, relief, and TRMM-derived rainfall variations along the Himalaya. *Geophysical Research Letters*, *33*(8). https://doi.org/10.1029/2006GL026037

Bookhagen, B., Thiede, R. C., & Strecker, M. R. (2005). Abnormal monsoon years and their control on erosion and sediment flux in the high, arid northwest Himalaya. *Earth and Planetary Science Letters*, *231*(1–2), 131–146. https://doi.org/10.1016/j.epsl.2004.11.014

Boos, W. R., & Kuang, Z. (2010). Dominant control of the South Asian monsoon by orographic insulation versus plateau heating. *Nature*, *463*(7278), 218–222. https://doi.org/10.1038/ nature08707

Brohan, P., Kennedy, J. J., Harris, I., Tett, S. F. B., & Jones, P. D. (2006). Uncertainty estimates in regional and global observed temperature changes: A new data set from 1850. *Journal of Geophysical Research Atmospheres*, *111*(12). https://doi.org/10.1029/2005JD006548

Browell, E. V, Carter, a F., Shipley, S. T., Allen, R. J., Butler, C. F., Mayo, M. N., et al. (1983). NASA multipurpose airborne DIAL system and measurements of ozone and aerosol profiles. *Applied Optics*, *22*(4), 522–34. https://doi.org/10.1364/AO.22.000522

Brun, J., Shrestha, P., & Barros, A. P. (2011). Mapping aerosol intrusion in Himalayan valleys using the Moderate Resolution Imaging Spectroradiometer (MODIS) and Cloud-Aerosol Lidar and Infrared Pathfinder Satellite Observation (CALIPSO). *Atmospheric Environment*, *45*(35), 6382–6392. https://doi.org/10.1016/j.atmosenv.2011.08.026

Bucci, S., Cagnazzo, C., Cairo, F., Di Liberto, L., & Fierli, F. (2014). Aerosol variability and atmospheric transport in the Himalayan region from CALIOP 2007-2010 observations. *Atmospheric Chemistry and Physics*, *14*(9), 4369–4381. https://doi.org/10.5194/acp-14-4369-2014

Carrico, C. M., Bergin, M. H., Shrestha, A. B., Dibb, J. E., Gomes, L., & Harris, J. M. (2003). The importance of carbon and mineral dust to seasonal aerosol properties in the Nepal Himalaya. *Atmospheric Environment*, *37*(20), 2811–2824. https://doi.org/10.1016/S1352-2310(03)00197-3

Cattrall, C., Reagan, J., Thome, K., & Dubovik, O. (2005). Variability of aerosol and spectral lidar and backscatter and extinction ratios of key aerosol types derived from selected Aerosol Robotic Network locations. *Journal of Geophysical Research D: Atmospheres*, *110*(10), 1–13. https://doi.org/10.1029/2004JD005124

Chagnon, C. W., & Junge, C. E. (1961). the Vertical Distribution of Sub-Micron Particles in the Stratosphere. *Journal of Meteorology*, *18*(6), 746–752.

Chand, D., Wood, R., Anderson, T. L., Satheesh, S. K., & Charlson, R. J. (2009). Satellite-derived direct radiative effect of aerosols dependent on cloud cover. *Nature Geoscience*, *2*(3), 181–184. https://doi.org/10.1038/ngeo437

Charlson, R. J., Schwartz, S. E., Hales, J. M., Cess, R. D., Coakley, J. A., Hansen, J. E., & Hofmann, D. J. (1992). Climate forcing by anthropogenic aerosols. *Science*, *255*(5043), 423–430. https://doi.org/10.1126/science.255.5043.423

Chin, M., Diehl, T., Dubovik, O., Eck, T. F., Holben, B. N., Sinyuk, A., & Streets, D. G. (2009). Light absorption by pollution, dust, and biomass burning aerosols: A global model study and evaluation with AERONET measurements. *Annales Geophysicae*, *27*(9), 3439–3464. https://doi.org/10.5194/angeo-27-3439-2009

Chinnam, N., Dey, S., Tripathi, S. N., & Sharma, M. (2006). Dust events in Kanpur, northern India: Chemical evidence for source and implications to radiative forcing. *Geophysical Research Letters*, *33*(8), 1–4. https://doi.org/10.1029/2005GL025278

Choi, J.-O., & Chung, C. E. (2014). Sensitivity of aerosol direct radiative forcing to aerosol vertical profile. *Tellus B*, *66*(0). https://doi.org/10.3402/tellusb.v66.24376

Choobari, O. A., Zawar-Reza, P., & Sturman, A. (2014). The global distribution of mineral dust and its impacts on the climate system: A review. *Atmospheric Research*, *138*, 152–165. https://doi.org/10.1016/j.atmosres.2013.11.007

Chung, C. E., & Ramanathan, V. (2006). Weakening of north Indian SST gradients and the monsoon rainfall in India and the Sahel. *Journal of Climate*, *19*(10), 2036–2045. https://doi.org/10.1175/JCLI3820.1

Chung, C. E., Ramanathan, V., & Kiehl, J. T. (2002). Effects of the South Asian absorbing haze on the northeast monsoon and surface-air heat exchange. *Journal of Climate*, *15*(17), 2462–2476.

Chung, C. E., Ramanathan, V., Kim, D., & Podgorny, I. A. (2005). Global anthropogenic aerosol direct forcing derived from satellite and ground-based observations. *Journal of Geophysical Research Atmospheres*, *110*(24), 1–17. https://doi.org/10.1029/2005JD006356

Chylek, P., & Wong, J. (1995). Effect of Absorbing Aerosols on Global Radiation Budget. *Geophysical Research Letters*, *22*(8), 929–931. https://doi.org/10.1029/95GL00800

Coakley, J. a., & Chylek, P. (1975). The Two-Stream Approximation in Radiative Transfer: Including the Angle of the Incident Radiation. *Journal of the Atmospheric Sciences*.

Cooke, W. F. (2002). A general circulation model study of the global carbonaceous aerosol distribution. *Journal of Geophysical Research*, *107*(D16), 4279. https://doi.org/10.1029/ 2001JD001274

Copland, L., Sylvestre, T., Bishop, M. P., Shroder, J. F., Seong, Y. B., Owen, L. A., et al. (2011). Expanded and Recently Increased Glacier Surging in the Karakoram. *Arctic, Antarctic, and Alpine Research*, *43*(4), 503–516. https://doi.org/10.1657/1938-4246-43.4.503

Cuesta, J., Edouart, D., Mimouni, M., Flamant, P. H., Loth, C., Gibert, F., et al. (2008). Multiplatform observations of the seasonal evolution of the Saharan atmospheric boundary layer in Tamanrasset, Algeria, in the framework of the African Monsoon Multidisciplinary Analysis field campaign conducted in 2006. *Journal of Geophysical Research Atmospheres*, *113*(23), D00C07. https://doi.org/10.1029/2007JD009417

Cui, Z., Carslaw, K. S., Yin, Y., & Davies, S. (2006). A numerical study of aerosol effects on the dynamics and microphysics of a deep convective cloud in a continental environmental. *Journal of Geophysical Research Atmospheres*, *111*(5). https://doi.org/10.1029/2005JD005981

Dang, C., Brandt, R. E., & Warren, S. G. (2015). Parameterizations for narrowband and broadband albedo of pure snow and snow containing mineral dust and black carbon. *Journal of Geophysical Research*, *120*(11), 5446–5468. https://doi.org/10.1002/2014JD022646

Das, S., Dey, S., Dash, S. K., & Basil, G. (2013). Examining mineral dust transport over the Indian subcontinent using the regional climate model, RegCM4.1. *Atmospheric Research*, *134*, 64–76. https://doi.org/10.1016/j.atmosres.2013.07.019

Davidi, A., Kostinski, A. B., Koren, I., & Lehahn, Y. (2012). Observational bounds on atmospheric heating by aerosol absorption: Radiative signature of transatlantic dust. *Geophysical Research Letters*, *39*(4). https://doi.org/10.1029/2011GL050358

Dawson, K. W., Meskhidze, N., Josset, D., & Gassó, S. (2015). Spaceborne observations of the lidar ratio of marine aerosols. *Atmospheric Chemistry and Physics*, *15*(6), 3241–3255. https://doi.org/ 10.5194/ acp-15-3241-2015

Decesari, S., Facchini, M. C., Carbone, C., Giulianelli, L., Rinaldi, M., Finessi, E., et al. (2010). Chemical composition of PM10 and PM1 at the high-altitude Himalayan station Nepal Climate Observatory-Pyramid (NCO-P) (5079 m a.s.l.). *Atmospheric Chemistry and Physics*, *10*(10), 4583–4596. https://doi.org/10.5194/acp-10-4583-2010

Deepshikha, S., Satheesh, S. K., & Srinivasan, J. (2005). Regional distribution of absorbing efficiency of dust aerosols over India and adjacent continents inferred using satellite remote sensing. *Geophysical Research Letters*, *32*(3), 1–4. https://doi.org/10.1029/2004GL022091

Deepshikha, S., Satheesh, S. K., & Srinivasan, J. (2006). Dust aerosols over India and adjacent continents retrieved using METEOSAT infrared radiance Part I: sources and regional distribution. *Annales Geophysicae*, *24*(1), 37–61. https://doi.org/10.5194/angeo-24-37-2006

Deirmendjian, D. (1969). *Electromagnetic scattering on spherical polydispersions*. Elsevier Publishing Company, New York.

Deluisi, J. J., Furukawa, P. M., Gillette, D. A., Schuster, B. G., Charlson, R. J., Porch, W. M., et al. (1976). Results of a Comprehensive Atmospheric Aerosol-Radiation Experiment in the Southwestern United States Part I: Size Distribution, Extinction Optical Depth and Vertical Profiles of Aerosols Suspended in the Atmosphere. *Journal of Applied Meteorology*, *15*(5), 441–454. https://doi.org/ 10.1175/ 1520-0450(1976)015<0441:ROACAA>2.0.CO;2

DeMott, P. J., Sassen, K., Poellot, M. R., Baumgardner, D., Rogers, D. C., Brooks, S. D., et al. (2003). African dust aerosols as atmospheric ice nuclei. *Geophysical Research Letters*, *30*(14), 26–29. https://doi.org/10.1029/2003GL017410

Denjean, C., Cassola, F., Mazzino, A., Triquet, S., Chevaillier, S., Grand, N., et al. (2016). Size distribution and optical properties of mineral dust aerosols transported in the western Mediterranean. *Atmospheric Chemistry and Physics*, *16*(2), 1081–1104. https://doi.org/10.5194/acp-16-1081-2016

Devara, P. C. S. (1998). Remote sensing of atmospheric aerosols from active and passive optical techniques. *International Journal of Remote Sensing*, *19*(17), 3271–3288.

Devara, P. C. S., & Ernest Raj, P. (1989). Remote sounding of aerosols in the lower atmosphere using a bistatic CW helium-neon lidar. *Journal of Aerosol Science*, *20*(1), 37–44. https://doi.org/10.1016/0021-8502(89)90029-3

Dey, S., & Di Girolamo, L. (2011). A decade of change in aerosol properties over the Indian subcontinent. *Geophysical Research Letters*, *38*(14). https://doi.org/10.1029/2011GL048153

Dimri, A. P., Niyogi, D., Barros, A. P., Ridley, J., Mohanty, U. C., Yasunari, T., & Sikka, D. R. (2015). Western Disturbances: A review. *Reviews of Geophysics*. https://doi.org/10.1002/ 2014RG000460

Douville, H., Chauvin, F., Planton, S., Royer, J. F., Salas-Melia, D., & Tyteca, S. (2002). Sensitivity of the hydrological cycle to increasing amounts of greenhouse gases and aerosols. *Climate Dynamics*, *20*(1), 45–68. https://doi.org/10.1007/s00382-002-0259-3

Draxler, R. R., & Hess, G. D. (1998). An overview of the HYSPLIT4 modelling system for trajectories. *Australian Meteorological Magazine*. https://doi.org/10.1016/j.polymdegradstab.2013.06.004

Dubovik, O., Holben, B., Eck, T. F., Smirnov, A., Kaufman, Y. J., King, M. D., et al. (2002). Variability of Absorption and Optical Properties of Key Aerosol Types Observed in Worldwide Locations. *Journal of the Atmospheric Sciences*, *59*(3), 590–608.

Duchi, R., Cristofanelli, P., Marinoni, A., Bourcier, L., Laj, P., Calzolari, F., et al. (2014). Synoptic-scale dust transport events in the southern Himalaya. *Aeolian Research*, *13*, 51–57. https://doi.org/10.1016/j.aeolia.2014.03.008

Dufresne, J.-L., Gautier, C., Ricchiazzi, P., & Fouquart, Y. (2002). Longwave Scattering Effects of Mineral Aerosols. *Journal of the Atmospheric Sciences*, *59*(12), 1959–1966.

Dumka, U. C., Moorthy, K. K., Pant, P., Hegde, P., Sagar, R., & Pandey, K. (2008). Physical and optical characteristics of atmospheric aerosols during ICARB at Manora Peak, Nainital: A sparsley inhabited, high-altitude location in the Himalayas. *Journal of Earth System Science*, *117*, 399–405. https://doi.org/10.1007/s12040-008-0041-y

Ekman, A. M. L., Wang, C., Ström, J., & Krejci, R. (2006). Explicit Simulation of Aerosol Physics in a Cloud-Resolving Model: Aerosol Transport and Processing in the Free Troposphere. *Journal of the Atmospheric Sciences*, *63*(2), 682–696. https://doi.org/10.1175/JAS3645.1

Elterman, L., Wexler, R., & Chang, D. T. (1969). Features of Tropospheric and Stratospheric Dust. *Applied Optics*, *8*(5), 893. https://doi.org/10.1364/AO.8.000893

Evan, A. T., Dunion, J., Foley, J. A., Heidinger, A. K., & Velden, C. S. (2006). New evidence for a relationship between Atlantic tropical cyclone activity and African dust outbreaks. *Geophysical Research Letters*, *33*(19). https://doi.org/10.1029/2006GL026408

Evan, A. T., Heidinger, A. K., Bennartz, R., Bennington, V., Mahowald, N. M., Corrada-Bravo, H., et al. (2008). Ocean temperature forcing by aerosols across the Atlantic tropical cyclone development region. *Geochemistry, Geophysics, Geosystems*, *9*(5). https://doi.org/10.1029/2007GC001774

Evan, A. T., Vimont, D. J., Heidinger, A. K., Kossin, J. P., & Bennartz, R. (2009). The role of aerosols in the evolution of tropical north atlantic ocean temperature anomalies. *Science*, *324*(5928), 778–781. https://doi.org/10.1126/science.1167404

Fernald, F. G., Herman, B. M., & Reagan, J. A. (1972). Determination of Aerosol Height Distributions by Lidar. *Journal of Applied Meteorology*.

Fiocco, G., & Grams, G. (1969). Optical radar observations of mesospheric aerosols in Norway during the summer 1966. *Journal of Geophysical Research*, *74*(10), 2453–2458. https://doi.org/10.1029/JB074i010p02453

Fiocco, G., & Smullin, L. D. (1963). Detection of scattering layers in the upper atmosphere (60-140 km) by optical radar. *Nature*. https://doi.org/10.1038/1991275a0

Flanner, M. G., Zender, C. S., Hess, P. G., Mahowald, N. M., Painter, T. H., Ramanathan, V., & Rasch, P. J. (2009). Springtime warming and reduced snow cover from carbonaceous particles. *Atmospheric Chemistry and Physics*, *9*(7), 2481–2497. https://doi.org/10.5194/acp-9-2481-2009

Foltz, G. R., & McPhaden, M. J. (2008). Trends in Saharan dust and tropical Atlantic climate during 1980-2006. *Geophysical Research Letters*, *35*(20), 1–5. https://doi.org/10.1029/2008GL035042

Forêt, G., Flamant, C., Cautenet, S., Pelon, J., Minvielle, F., Taghavi, M., & Chazette, P. (2005). The structure of the haze plume over the Indian Ocean during INDOEX: tracer simulations and LIDAR observations. *Atmospheric Chemistry and Physics Discussions*, *5*(3), 3269–3312. https://doi.org/10.5194/acpd-5-3269-2005

Fox, R. J., Grams, G. W., Schuster, B. G., & Weinman, J. A. (1973). Measurements of stratospheric aerosols by airborne laser radar. *Journal of Geophysical Research*, *78*(33), 7789-7801.

Franke, K., Ansmann, A., Müller, D., Althausen, D., Wagner, F., & Scheele, R. (2001). One-year observations of particle lidar ratio over the tropical Indian Ocean with Raman lidar. *Geophysical Research Letters*, *28*(24), 4559–4562. https://doi.org/10.1029/2001GL013671

Freudenthaler, V., Esselborn, M., Wiegner, M., Heese, B., Tesche, M., Ansmann, A., et al. (2009). Depolarization ratio profiling at several wavelengths in pure Saharan dust during SAMUM 2006. *Tellus, Series B: Chemical and Physical Meteorology*, *61*(1), 165–179. https://doi.org/10.1111/j.1600-0889.2008.00396.x

Friedlander, S. K. (1960). Similarity considerations for the particle-size spectrum of a coagulating, sedimenting aerosol. *Journal of Meteorology*, *17*(5), 479–483.

Friedlander, S. K., & Johnstone, H. F. (1957). Deposition of Suspended Particles from Turbulent Gas Streams. *Industrial & Engineering Chemistry*, *49*(7), 1151–1156. https://doi.org/10.1021/ie50571a039

Gadgil, S. (2000). Monsoon - Ocean coupling. *Current Science*.

Gambling, D. J., & Bartusek, K. (1972). Lidar observations of tropospheric aerosols. *Atmospheric Environment (1967)*, *6*(3), 181–190. https://doi.org/10.1016/S0004-6981(72)80146-X

Gautam, R., Hsu, N. C., Kafatos, M., & Tsay, S. C. (2007). Influences of winter haze on fog/low cloud over the Indo-Gangetic plains. *Journal of Geophysical Research Atmospheres*, *112*(5). https://doi.org/10.1029/2005JD007036

Gautam, R., Hsu, N. C., Lau, K. M., & Kafatos, M. (2009). Aerosol and rainfall variability over the Indian monsoon region: Distributions, trends and coupling. *Annales Geophysicae*, *27*(9), 3691–3703. https://doi.org/10.5194/angeo-27-3691-2009

Gautam, R., Hsu, N. C., Lau, K.-M. M., Tsay, S.-C. C., & Kafatos, M. (2009). Enhanced pre-monsoon warming over the Himalayan-Gangetic region from 1979 to 2007. *Geophysical Research Letters*, *36*(7), 1–5. https://doi.org/10.1029/2009GL037641

Gautam, R., Liu, Z., Singh, R. P., & Hsu, N. C. (2009). Two contrasting dust-dominant periods over India observed from MODIS and CALIPSO data. *Geophysical Research Letters*, *36*(6), 1–5. https://doi.org/10.1029/2008GL036967

Gautam, R., Hsu, N. C., & Lau, K. M.-M. (2010). Premonsoon aerosol characterization and radiative effects over the Indo-Gangetic plains: Implications for regional climate warming. *Journal of Geophysical Research Atmospheres*, *115*(D17), D17208. https://doi.org/10.1029/2010JD013819

Gautam, R., Hsu, N. C., Lau, W. K. M., & Yasunari, T. J. (2013). Satellite observations of desert dust-induced Himalayan snow darkening. *Geophysical Research Letters*, *40*(5), 988–993. https://doi.org/10.1002/grl.50226

Ge, J. M., Su, J., Ackerman, T. P., Fu, Q., Huang, J. P., & Shi, J. S. (2010). Dust aerosol optical properties retrieval and radiative forcing over northwestern China during the 2008 China-U.S. joint field experiment. *Journal of Geophysical Research Atmospheres*, *115*(13), 1–11. https://doi.org/10.1029/ 2009JD013263

Giannakaki, E., Van Zyl, P. G., Müller, D., Balis, D., & Komppula, M. (2016). Optical and microphysical characterization of aerosol layers over South Africa by means of multi-wavelength depolarization and Raman lidar measurements. *Atmospheric Chemistry and Physics*, *16*(13), 8109–8123. https://doi.org/10.5194/acp-16-8109-2016

Ginoux, P., Chin, M., Tegen, I., Prospero, J. M., Holben, B., Dubovik, O., & Lin, S. J. (2001). Sources and distributions of dust aerosols simulated with the GOCART model. *Journal of Geophysical Research*, *106*(D17), 20255. https://doi.org/10.1029/2000JD000053

Gobbi, G. P., Barnaba, F., Van Dingenen, R., Putaud, J. P., Mircea, M., & Facchini, M. C. (2003). Lidar and in situ observations of continental and Saharan aerosol: Closure analysis of particles optical and physical properties. *Atmospheric Chemistry and Physics*, *3*(6), 2161–2172. https://doi.org/ 10.5194/ acp-3-2161-2003

Gobbi, G. P., Angelini, F., Bonasoni, P., Verza, G. P., Marinoni, A., & Barnaba, F. (2010). Sunphotometry of the 2006-2007 aerosol optical/radiative properties at the Himalayan Nepal Climate Observatory-Pyramid (5079m asl). *Atmospheric Chemistry and Physics*, *10*(22), 11209–11221. https://doi.org/10.5194/acp-10-11209-2010

Gogoi, M. M., Pathak, B., Moorthy, K. K., Bhuyan, P. K., Babu, S. S., Bhuyan, K., & Kalita, G. (2011). Multi-year investigations of near surface and columnar aerosols over Dibrugarh, northeastern location of India: Heterogeneity in source impacts. *Atmospheric Environment*, *45*(9), 1714–1724. https://doi.org/10.1016/j.atmosenv.2010.12.056

Gogoi, M. M., Moorthy, K. K., Kompalli, S. K., Chaubey, J. P., Babu, S. S., Manoj, M. R., et al. (2014). Physical and optical properties of aerosols in a free tropospheric environment: Results from long-term observations over western trans-Himalayas. *Atmospheric Environment*, *84*, 262–274. https://doi.org/10.1016/j.atmosenv.2013.11.029

Gogoi, M. M., Babu, S. S., Jayachandran, V., Moorthy, K. K., Satheesh, S. K., Naja, M., & Kotamarthi, V. R. (2015). Optical properties and CCN activity of aerosols in a high-altitude Himalayan environment: Results from RAWEX-GVAX. *Journal of Geophysical Research*, *120*(6), 2453–2469. https://doi.org/10.1002/2014JD022966

Gordon, H. R., & Wang, M. (1994). Retrieval of water-leaving radiance and aerosol optical thickness over the oceans with SeaWiFS: a preliminary algorithm. *Applied Optics*, *33*(3), 443. https://doi.org/10.1364/AO.33.000443

Grams, G., & Fiocco, G. (1967). Stratospheric aerosol layer during 1964 and 1965. *Journal of Geophysical Research*, *72*(14), 3523–3542. https://doi.org/10.1029/JZ072i014p03523

Hansen, J., Lacis, A., Ruedy, R., & Sato, M. (1992). Potential climate impact of Mount Pinatubo eruption. *Geophysical Research Letters*, *19*(2), 215–218. https://doi.org/10.1029/91GL02788

Hansen, J., Sato, M., & Ruedy, R. (1997). Radiative forcing and climate response. *Journal of Geophysical Research-Atmospheres*, *102*(D6), 6831–6864. https://doi.org/10.1029/96JD03436

Hansen, J. E., Wang, W. C., & Lacis, A. A. (1978). Mount agung eruption provides test of a global climatic perturbation. *Science*, *199*(4333), 1065–1068. https://doi.org/10.1126/science.199.4333.1065

Hara, Y., Yumimoto, K., Uno, I., Shimizu, A., Sugimoto, N., Liu, Z., & M.Winker, D. (2009). Asian dust outflow in the PBL and free atmosphere retrieved by NASA CALIPSO and an assimilated dust transport model. *Atmospheric Chemistry and Physics*, *9*(4), 1227–1239. https://doi.org/10.5194/acp-9-1227-2009

Harrison, S. P., Kohfeld, K. E., Roelandt, C., & Claquin, T. (2001). The role of dust in climate changes today, at the last glacial maximum and in the future. *Earth-Science Reviews*, *54*(1–3), 43–80. https://doi.org/10.1016/S0012-8252(01)00041-1

Haywood, J., & Boucher, O. (2000). Estimates of the direct and indirect radiative forcing due to tropospheric aerosols: A review. *Reviews of Geophysics*, *38*(4), 513–543. https://doi.org/10.1029/1999RG000078

Haywood, J., Francis, P., Osborne, S., Glew, M., Loeb, N., Highwood, E., et al. (2003). Radiative properties and direct radiative effect of Saharan dust measured by the C-130 aircraft during SHADE: 1. Solar spectrum. *Journal of Geophysical Research: Atmospheres*, *108*(D18), 8577. https://doi.org/10.1029/2002JD002687

Haywood, J. M., Francis, P. N., Glew, M. D., & Taylor, J. P. (2001). Optical properties and direct radiative effect of Saharan dust: A case study of two Saharan dust outbreaks using aircraft data. *Journal of Geophysical Research: Atmospheres*, *106*(D16), 18417–18430. https://doi.org/10.1029/2000JD900319

Haywood, J. M., Allan, R. P., Culverwell, I., Slingo, T., Milton, S., Edwards, J., & Clerbaux, N. (2005). Can desert dust explain the outgoing longwave radiation anomaly over the Sahara during July 2003? *Journal of Geophysical Research D: Atmospheres*, *110*(5), 1–14. https://doi.org/10.1029/2004JD005232

Heese, B., & Wiegner, M. (2008). Vertical aerosol profiles from Raman polarization lidar observations during the dry season AMMA field campaign. *Journal of Geophysical Research Atmospheres*, *113*(23). https://doi.org/10.1029/2007JD009487

Hegde, P., Pant, P., & Bhavani Kumar, Y. (2009). An integrated analysis of lidar observations in association with optical properties of aerosols from a high altitudelocation in central Himalayas. *Atmospheric Science Letters*, *10*(1), 48–57. https://doi.org/10.1002/asl.209

Heinold, B., Helmert, J., Hellmuth, O., Wolke, R., Ansmann, A., Marticorena, B., et al. (2007). Regional modeling of Saharan dust events using LM-MUSCAT: Model description and case studies. *Journal of Geophysical Research Atmospheres*, *112*(11). https://doi.org/10.1029/2006JD007443

Heintzenberg, J., & Welch, R. M. (1982). Retrieval of aerosol size distribution from angular scattering functions: effects of particle composition and shape. *Applied Optics*, *21*(5), 822–30. https://doi.org/10.1364/AO.21.000822

Herman, B. M., Browning, S. R., Herman, B. M., & Browning, S. R. (1975). The Effect of Aerosols on the Earth-Atmosphere Albedo. *Journal of the Atmospheric Sciences*, *32*(7), 1430–1445.

Herman, J. R., & Celarier, E. A. (1997). Earth surface reflectivity climatology at 340–380 nm from TOMS data. *Journal of Geophysical Research*, *102*(D23), 28003. https://doi.org/10.1029/ 97JD02074

Hess, M., Koepke, P., & Schult, I. (1998). Optical Properties of Aerosols and Clouds: The Software Package OPAC. *Bulletin of the American Meteorological Society*, *79*(5), 831–844.

Higdon, N. S., Browell, E. V, Ponsardin, P., Grossmann, B. E., Butler, C. F., Chyba, T. H., et al. (1994). Airborne differential absorption lidar system for measurements of atmospheric water vapor and aerosols. *Applied Optics*, *33*(27), 6422–38. https://doi.org/10.1364/AO.33.006422

Holben, B. N., Eck, T. F., Slutsker, I., Tanré, D., Buis, J. P., Setzer, A., et al. (1998). AERONET - A federated instrument network and data archive for aerosol characterization. *Remote Sensing of Environment*, *66*(1), 1–16. https://doi.org/10.1016/S0034-4257(98)00031-5

Hsu, N. C., Jeong, M. J., Bettenhausen, C., Sayer, A. M., Hansell, R., Seftor, C. S., et al. (2013). Enhanced Deep Blue aerosol retrieval algorithm: The second generation. *Journal of Geophysical Research Atmospheres*, *118*(16), 9296–9315. https://doi.org/10.1002/jgrd.50712

Hu, Y., Winker, D., Vaughan, M., Lin, B., Omar, A., Trepte, C., et al. (2009). CALIPSO/CALIOP cloud phase discrimination algorithm. *Journal of Atmospheric and Oceanic Technology*, *26*(11), 2293–2309.

Huang, J., Minnis, P., Lin, B., Wang, T., Yi, Y., Hu, Y., et al. (2006). Possible influences of Asian dust aerosols on cloud properties and radiative forcing observed from MODIS and CERES. *Geophysical Research Letters*, *33*(6), 4–7. https://doi.org/10.1029/2005GL024724

Huang, J. P., Liu, J. J., Chen, B., & Nasiri, S. L. (2015). Detection of anthropogenic dust using CALIPSO lidar measurements. *Atmospheric Chemistry and Physics*, *15*(20), 11653–11665. https://doi.org/ 10.5194/ acp-15-11653-2015

Huebert, B. J. (2003). An overview of ACE-Asia: Strategies for quantifying the relationships between Asian aerosols and their climatic impacts. *Journal of Geophysical Research*, *108*(D23), 8633. https://doi.org/10.1029/2003JD003550

Huneeus, N., Schulz, M., Balkanski, Y., Griesfeller, J., Prospero, J., Kinne, S., et al. (2011). Global dust model intercomparison in AeroCom phase i. *Atmospheric Chemistry and Physics*, *11*(15), 7781–7816. https://doi.org/10.5194/acp-11-7781-2011

Hunt, W. H., Vaughan, M. A., Powell, K. A., & Weimer, C. (2009). CALIPSO lidar description and performance assessment. *Journal of Atmospheric and Oceanic Technology*, *26*(7), 1214–1228.

Husar, R. B., Prospero, J. M., & Stowe, L. L. (1997). Characterization of tropospheric aerosols over the oceans with the NOAA advanced very high resolution radiometer optical thickness operational product. *Journal of Geophysical Research: Atmospheres*, *102*(D14), 16889–16909. https://doi.org/10.1029/96JD04009

Intergovernmental Panel on Climate Change. (2007). *IPCC Fourth Assessment Report: Climate Change 2007*. *Change* (Vol. 4). http://www.ipcc.ch

Jacobson, M. Z. (2000). A physically-based treatment of elemental carbon optics: Implications for global direct forcing of aerosols. *Geophysical Research Letters*, *27*(2), 217–220. https://doi.org/10.1029/1999GL010968

Jacobson, M. Z. (2001). Strong radiative heating due to the mixing state of black carbon in atmospheric aerosols. *Nature*, *409*(6821), 695–697. https://doi.org/10.1038/35055518

Jai Devi, J., Tripathi, S. N., Gupta, T., Singh, B. N., Gopalakrishnan, V., & Dey, S. (2011). Observation-based 3-D view of aerosol radiative properties over Indian Continental Tropical Convergence Zone: Implications to regional climate. *Tellus, Series B: Chemical and Physical Meteorology*, *63*(5), 971–989. https://doi.org/10.1111/j.1600-0889.2011.00580.x

Jayachandran, V., Nair, V. S., & Babu, S. S. (2018). CCN activation properties at a tropical hill station in Western Ghats during south-west summer monsoon: Vertical heterogeneity. *Atmospheric Research*, *214*, 36–45. https://doi.org/10.1016/j.atmosres.2018.07.018

Jayaraman, A., Ramachandran, S., Acharya, Y. B., & Subbaraya, B. H. (1995). Pinatubo volcanic aerosol layer decay observed at Ahrnedabad (23N), India, using neodymium:yttrium/aluminium/garnet backscatter lidar. *Journal of Geophysical Research*, *100*(D11), 23,209-23,214. https://doi.org/10.1029/ 95JD02195

Jayaraman, A., Lubin, D., Ramachandran, S., Ramanathan, V., Woodbridge, E., Collins, W. D., & Zalpuri, K. S. (1998). Direct observations of aerosol radiative forcing over the tropical Indian Ocean during the January-February 1996 pre-INDOEX cruise. *Journal of Geophysical Research Atmospheres*, *103*(D12), 13827–13836. https://doi.org/10.1029/98JD00559

Ji, Z., Kang, S., Zhang, Q., Cong, Z., Chen, P., & Sillanpää, M. (2016). Investigation of mineral aerosols radiative effects over High Mountain Asia in 1990-2009 using a regional climate model. *Atmospheric Research*, *178–179*, 484–496. https://doi.org/10.1016/j.atmosres.2016.05.003

Jin, Q., & Wang, C. (2018). The greening of Northwest Indian subcontinent and reduction of dust abundance resulting from Indian summer monsoon revival. *Scientific Reports*, *8*(1), 4573. https://doi.org/10.1038/s41598-018-23055-5

Jin, Q., Wei, J., & Yang, Z.-L. (2014). Positive response of Indian summer rainfall to Middle East dust. *Geophys. Res. Lett.*, 2014GL059980+. https://doi.org/10.1002/2014gl059980

Jin, Q., Wei, J., Yang, Z. L., Pu, B., & Huang, J. (2015). Consistent response of Indian summer monsoon to Middle East dust in observations and simulations. *Atmospheric Chemistry and Physics Discussions*, *15*(11), 15571–15619. https://doi.org/10.5194/acpd-15-15571-2015

Jin, Q., Yang, Z. L., & Wei, J. (2016). High sensitivity of Indian summer monsoon to Middle East dust absorptive properties. *Scientific Reports*, *6*, 4–11. https://doi.org/10.1038/srep30690

Johnson, B. T., Shine, K. P., & Forster, P. M. (2004). The semi-direct aerosol effect: Impact of absorbing aerosols on marine stratocumulus. *Quarterly Journal of the Royal Meteorological Society*, *130*, 1407–1422. https://doi.org/10.1256/qj.03.61

Jones, A., Roberts, D. L., & Slingo, A. (1994). A climate model study of indirect radiative forcing by anthropogenic sulphate aerosols. *Nature*, *370*(6489), 450–453. https://doi.org/10.1038/370450a0

Josset, D., Rogers, R., Pelon, J., Hu, Y., Liu, Z., Omar, A., & Zhai, P.-W. (2011). CALIPSO lidar ratio retrieval over the ocean. *Optics Express*, *19*(19), 18696. https://doi.org/10.1364/OE.19.018696

Junge, C. E. (1963). *Air chemistry and radioactivity.* Academic Press, New York.

Junge, C. E., Chagnon, C. W., & Manson, J. E. (1961). Stratospheric aerosols. *Journal of Meteorology*. https://doi.org/10.1175/1520-0469(1961)018

Kacenelenbogen, M., Vaughan, M. A., Redemann, J., Hoff, R. M., Rogers, R. R., Ferrare, R. A., et al. (2011). An accuracy assessment of the CALIOP/CALIPSO version 2/version 3 daytime aerosol extinction product based on a detailed multi-sensor, multi-platform case study. *Atmospheric Chemistry and Physics*, *11*(8), 3981–4000. https://doi.org/10.5194/acp-11-3981-2011

Kahn, R. A., & Gaitley, B. J. (2015). An analysis of global aerosol type as retrieved by MISR. *Journal of Geophysical Research*, *120*(9), 4248–4281. https://doi.org/10.1002/2015JD023322

Kahnert, M., Nousiainen, T., & Räisänen, P. (2007). Mie simulations as an error source in mineral aerosol radiative forcing calculations. *Quarterly Journal of the Royal Meteorological Society*, *133*(623), 299–307.

Kajikawa, Y., Yasunari, T., Yoshida, S., & Fujinami, H. (2012). Advanced Asian summer monsoon onset in recent decades. *Geophysical Research Letters*, *39*(3). https://doi.org/10.1029/2011GL050540

Kalashnikova, O. V., & Sokolik, I. N. (2002). Importance of shapes and compositions of wind-blown dust particles for remote sensing at solar wavelengths. *Geophysical Research Letters*, *29*(10), 38-1-38–4. https://doi.org/10.1029/2002GL014947

Kaskaoutis, D. G., Kharol, S. K., Sinha, P. R., Singh, R. P., Badarinath, K. V. S., Mehdi, W., & Sharma, M. (2011). Contrasting aerosol trends over South Asia during the last decade based on MODIS observations. *Atmospheric Measurement Techniques Discussions*, *4*(4), 5275–5323. https://doi.org/10.5194/amtd-4-5275-2011

Kaskaoutis, D. G., Houssos, E. E., Rashki, A., Francois, P., Legrand, M., Goto, D., et al. (2016). The Caspian Sea–Hindu Kush Index (CasHKI): A regulatory factor for dust activity over southwest Asia. *Global and Planetary Change*, *137*, 10–23. https://doi.org/10.1016/j.gloplacha.2015.12.011

Kaskaoutis, D. G., Houssos, E. E., Solmon, F., Legrand, M., Rashki, A., Dumka, U. C., et al. (2018). Impact of atmospheric circulation types on southwest Asian dust and Indian summer monsoon rainfall. *Atmospheric Research*, *201*, 189–205. https://doi.org/10.1016/j.atmosres.2017.11.002

Kaspari, S., Painter, T. H., Gysel, M., Skiles, S. M., & Schwikowski, M. (2014). Seasonal and elevational variations of black carbon and dust in snow and ice in the Solu-Khumbu, Nepal and estimated radiative forcings. *Atmospheric Chemistry and Physics*, *14*(15), 8089–8103. https://doi.org/ 10.5194/ acp-14-8089-2014

Kato, S., Ackerman, P., Clothiaux, E., Mather, H., Mace, G., Wesely, M. L., et al. (1997). Uncertainties in modeled and measured clear-sky surface shortwave irradiances. *Journal of Geophysical Research*, *102*(D22), 25881–25898. https://doi.org/10.1029/97JD01841

Kaufman, Y. J., & Fraser, R. S. (1997). The effect of smoke particles on clouds and climate forcing. *Science*, *277*(5332), 1636–1639. https://doi.org/10.1126/science.277.5332.1636

Kaufman, Y. J., Tanré, D., Remer, L. A., Vermote, E. F., Chu, A., & Holben, B. N. (1997). Operational remote sensing of tropospheric aerosol over land from EOS moderate resolution imaging spectroradiometer. *Journal of Geophysical Research: Atmospheres*, *102*(D14), 17051–17067. https://doi.org/10.1029/96JD03988

Kaufman, Y. J., Hobbs, P. V., Kirchhoff, V. W. J. H., Artaxo, P., Remer, L. A., Holben, B. N., et al. (1998). Smoke, Clouds, and Radiation-Brazil (SCAR-B) experiment. *Journal of Geophysical Research Atmospheres*, *103*(D24), 31783–31808. https://doi.org/10.1029/98JD02281

Kaufman, Y. J., Koren, I., Remer, L. A., Tanré, D., Ginoux, P., & Fan, S. (2005). Dust transport and deposition observed from the Terra-Moderate Resolution Imaging Spectroradiometer (MODIS) spacecraft over the Atlantic Ocean. *Journal of Geophysical Research D: Atmospheres*, *110*(10), 1–16. https://doi.org/10.1029/2003JD004436

Kaufmann, R. K., Kauppi, H., Mann, M. L., & Stock, J. H. (2011). Reconciling anthropogenic climate change with observed temperature 1998-2008. *Proceedings of the National Academy of Sciences*, *108*(29), 11790–11793. https://doi.org/10.1073/pnas.1102467108

Kedia, S., & Ramachandran, S. (2008). Features of aerosol optical depths over the Bay of Bengal and the Arabian Sea during premonsoon season: Variabilities and antropogenic influence. *Journal of Geophysical Research Atmospheres*, *113*(11), 375–387. https://doi.org/10.1029/2007JD009070

Kim, D. H., Sohn, B. J., Nakajima, T., & Takamura, T. (2005). Aerosol radiative forcing over east Asia determined from ground-based solar radiation measurements. *Journal of Geophysical Research*, *110*(10), 1–17. https://doi.org/10.1029/2004JD004678

Kim, M. H., Kim, S. W., Yoon, S. C., & Omar, A. H. (2013). Comparison of aerosol optical depth between CALIOP and MODIS-Aqua for CALIOP aerosol subtypes over the ocean. *Journal of Geophysical Research Atmospheres*, *118*(23), 13241–13252. https://doi.org/10.1002/2013JD019527

Kim, M. H., Omar, A. H., Vaughan, M. A., Winker, D. M., Trepte, C. R., Hu, Y., et al. (2017). Quantifying the low bias of CALIPSO's column aerosol optical depth due to undetected aerosol layers. *Journal of Geophysical Research*, *122*(2), 1098–1113. https://doi.org/10.1002/2016JD025797

Kim, M. K., Lau, W. K. M., Kim, K. M., Sang, J., Kim, Y. H., & Lee, W. S. (2016). Amplification of ENSO effects on Indian summer monsoon by absorbing aerosols. *Climate Dynamics*, *46*(7–8), 2657–2671. https://doi.org/10.1007/s00382-015-2722-y

Kipling, Z., Stier, P., Johnson, C. E., Mann, G. W., Bellouin, N., Bauer, S. E., et al. (2016). What controls the vertical distribution of aerosol? Relationships between process sensitivity in HadGEM3-UKCA and inter-model variation from AeroCom Phase II. *Atmospheric Chemistry and Physics*, *16*(4), 2221–2241. https://doi.org/10.5194/acp-16-2221-2016

Kittaka, C., Winker, D. M., Vaughan, M. A., Omar, A., & Remer, L. A. (2011). Intercomparison of column aerosol optical depths from CALIPSO and MODIS-Aqua. *Atmospheric Measurement Techniques*, *4*(2), 131–141. https://doi.org/10.5194/amt-4-131-2011

Klett, J. D. (1981). Stable analytical inversion solution for processing lidar returns. *Applied Optics*, *20*(2), 211–220. https://doi.org/10.1364/AO.20.000211

Klett, J. D. (1985). Lidar inversion with variable backscatter/extinction ratios. *Applied Optics*, *24*(11), 1638. https://doi.org/10.1364/AO.24.001638

Koepke, P., Gasteiger, J., & Hess, M. (2015). Technical Note: Optical properties of desert aerosol with non-spherical mineral particles: Data incorporated to OPAC. *Atmospheric Chemistry and Physics*, *15*(10), 5947–5956. https://doi.org/10.5194/acp-15-5947-2015

Koffi, B., Schulz, M., Bréon, F. M., Griesfeller, J., Winker, D., Balkanski, Y., et al. (2012). Application of the CALIOP layer product to evaluate the vertical distribution of aerosols estimated by global models: AeroCom phase i results. *Journal of Geophysical Research Atmospheres*, *117*(10), 1–26. https://doi.org/10.1029/2011JD016858

Koffi, B., Schulz, M., Bréon, F. M., Dentener, F., Steensen, B. M., Griesfeller, J., et al. (2016). Evaluation of the aerosol vertical distribution in global aerosol models through comparison against CALIOP measurements: AeroCom phase II results. *Journal of Geophysical Research*, *121*(12), 7254–7283. https://doi.org/10.1002/2015JD024639

Kompalli, S. K., Suresh Babu, S., Krishna Moorthy, K., Nair, V. S., Gogoi, M. M., & Chaubey, J. P. (2013). Seasonal variation in the spatial distribution of aerosol black carbon over Bay of Bengal: A synthesis of multi-campaign measurements. *Atmospheric Environment*, *64*, 366–373. https://doi.org/ 10.1016/j.atmosenv.2012.09.073

Kompalli, S. K., Suresh Babu, S., Bharatan, L. N., & Krishna Moorthy, K. (2016). Spring-time enhancement in aerosol burden over a high-altitude location in western trans-Himalaya: Results from long-term observations. *Current Science*, *111*(1), 117–131. https://doi.org/10.18520/cs/v111/i1/117-131

Koren, I., Kaufman, Y. J., Remer, L. A., & Martins, J. V. (2004). Measurement of the Effect of Amazon Smoke on Inhibition of Cloud Formation. *Science*, *303*(5662), 1342–1345. https://doi.org/10.1126/science.1089424

Kothawale, D. R., & Rupa Kumar, K. (2005). On the recent changes in surface temperature trends over India. *Geophysical Research Letters*, *32*(18), 1–4. https://doi.org/10.1029/2005GL023528

Kovalev, V. A. (1993). Lidar measurement of the vertical aerosol extinction profiles with range-dependent backscatter-to-extinction ratios. *Applied Optics*, *32*(30), 6053–6065. https://doi.org/10.1364/AO.32.006053

Kowalczyk, G. S., Choquette, C. E., & Gordon, G. E. (1978). Chemical element balances and identification of air pollution sources in Washington, D.C. *Atmospheric Environment (1967)*, *12*(5), 1143–1153. https://doi.org/10.1016/0004-6981(78)90361-X

Krishnamurti, T. N., Jha, B., Prospero, J., Jayaraman, A., & Ramanathan, V. (1998). Aerosol and pollutant transport and their impact on radiative forcing over the tropical Indian Ocean during the January-February 1996 pre-INDOEX cruise. *Tellus, Series B: Chemical and Physical Meteorology*, *50*(5), 521–542. https://doi.org/10.3402/tellusb.v50i5.16235

Krishnamurti, T. N., Chakraborty, A., Martin, A., Lau, W. K., Kim, K. M., Sud, Y., & Walker, G. (2009). Impact of Arabian sea pollution on the bay of Bengal winter monsoon rains. *Journal of Geophysical Research Atmospheres*, *114*(6), 1–22. https://doi.org/10.1029/2008JD010679

Krüger, O., & Graßl, H. (2002). The indirect aerosol effect over Europe. *Geophysical Research Letters*, *29*(19), 31-1-31–4. https://doi.org/10.1029/2001GL014081

Kulkarni, J. R., Maheskumar, R. S., Morwal, S. B., Padma Kumari, B., Konwar, M., Deshpande, C. G., et al. (2012). The cloud aerosol interaction and precipitation enhancement experiment (CAIPEEX): Overview and preliminary results. *Current Science*, *102*(3), 413–425.

Kulkarni, P., Ramachandran, S., Kumar, Y. B., Rao, D. N., & Krishnaiah, M. (2008). Features of upper troposphere and lower stratosphere aerosols observed by lidar over Gadanki, a tropical Indian station. *Journal of Geophysical Research Atmospheres*, *113*(17), D17207. https://doi.org/10.1029/ 2007JD009411

Kumar, A., Sarin, M. M., & Srinivas, B. (2010). Aerosol iron solubility over Bay of Bengal: Role of anthropogenic sources and chemical processing. *Marine Chemistry*, *121*(1–4), 167–175. https://doi.org/10.1016/j.marchem.2010.04.005

Kumar, B., Singh, S., Gupta, G. P., Lone, F. A., & Kulshrestha, U. C. (2016). Long range transport and wet deposition fluxes of major chemical species in snow at Gulmarg in North Western Himalayas (India). *Aerosol and Air Quality Research*, *16*(3), 606–617. https://doi.org/10.4209/aaqr.2015.01.0056

Kumar, K. K., Soman, M. K., & Kumar, K. R. (1995). Seasonal forecasting of Indian summer monsoon rainfall: A review. *Weather*, *50*(12), 449–467.

Kumar, R., Barth, M. C., Madronich, S., Naja, M., Carmichael, G. R., Pfister, G. G., et al. (2014). Effects of dust aerosols on tropospheric chemistry during a typical pre-monsoon season dust storm in northern India. *Atmospheric Chemistry and Physics*, *14*(13), 6813–6834. https://doi.org/10.5194/ acp-14-6813-2014

Kumar, Y. B., Raju, C. N., & Krishnaiah, M. (2006). Indo-Japanese lidar observations of the tropical middle atmosphere during 1998 and 1999. *Advances in Atmospheric Sciences*, *23*(5), 711–725. https://doi.org/10.1007/s00376-006-0711-0

Kummerow, C., Barnes, W., Kozu, T., Shiue, J., & Simpson, J. (1998). The Tropical Rainfall Measuring Mission (TRMM) sensor package. *Journal of Atmospheric and Oceanic Technology*, *15*(3), 809–817.

Kuo-Nan Liou. (1980). *An Introduction to Atmospheric Radiation*. *Academic Press* (Vol. 26). International GeoPhysics SeriesElsevier Science (USA), Academic Press. https://doi.org/10.1017/CBO9781107415324.004

Lacis, A., Hansen, J., & Sato, M. (1992). Climate forcing by stratospheric aerosols. *Geophysical Research Letters*, *19*(15), 1607–1610. https://doi.org/10.1029/92GL01620

Langner, J., Rodhe, H., Crutzen, P. J., & Zimmermann, P. (1992). Anthropogenic influence on the distribution of tropospheric sulphate aerosol. *Nature*, *359*(6397), 712–716. https://doi.org/10.1038/359712a0

Lau, K. M., & Kim, K. M. (2006). Observational relationships between aerosol and Asian monsoon rainfall, and circulation. *Geophysical Research Letters*, *33*(21). https://doi.org/10.1029/2006GL027546

Lau, K. M., Kim, M. K., & Kim, K. M. (2006). Asian summer monsoon anomalies induced by aerosol direct forcing: The role of the Tibetan Plateau. *Climate Dynamics*, *26*(7–8), 855–864. https://doi.org/10.1007/s00382-006-0114-z

Lau, W. K. M., & Kim, K. M. (2010). Fingerprinting the impacts of aerosols on long-term trends of the Indian summer monsoon regional rainfall. *Geophysical Research Letters*, *37*(16). https://doi.org/10.1029/2010GL043255

Lau, W. K. M., Kim, M. K., Kim, K. M., & Lee, W. S. (2010). Enhanced surface warming and accelerated snow melt in the Himalayas and Tibetan Plateau induced by absorbing aerosols. *Environmental Research Letters*, *5*(2), 025204. https://doi.org/10.1088/1748-9326/5/2/025204

Lau, W. K. M., Sang, J., Kim, M. K., Kim, K. M., Koster, R. D., & Yasunari, T. J. (2018). Impacts of Snow Darkening by Deposition of Light-Absorbing Aerosols on Hydroclimate of Eurasia During Boreal Spring and Summer. *Journal of Geophysical Research: Atmospheres*, *123*(16), 8441–8461. https://doi.org/10.1029/2018JD028557

Laurent, B., Tegen, I., Heinold, B., Schepanski, K., Weinzierl, B., & Esselborn, M. (2010). A model study of Saharan dust emissions and distributions during the SAMUM-1 campaign. *Journal of Geophysical Research Atmospheres*, *115*(21). https://doi.org/10.1029/2009JD012995

Lee, K. H., Li, Z., Wong, M. S., Xin, J., Wang, Y., Hao, W. M., & Zhao, F. (2007). Aerosol single scattering albedo estimated across China from a combination of ground and satellite measurements. *Journal of Geophysical Research Atmospheres*, *112*(22), D22S15. https://doi.org/10.1029/ 2007JD009077

Lee, W. S., Bhawar, R. L., Kim, M. K., & Sang, J. (2013). Study of aerosol effect on accelerated snow melting over the Tibetan Plateau during boreal spring. *Atmospheric Environment*, *75*, 113–122. https://doi.org/10.1016/j.atmosenv.2013.04.004

Lelieveld, J. (2001). Pollution from South and Southeast Asia The Indian Ocean Experiment : Widespread Air Pollution from South and Southeast Asia. *Science*, *291*(2001), 1031–1036. https://doi.org/10.1126/science.1057103

Leon, J. F., Chazette, P., Dulac, F., Pelon, J., Flamant, C., Bonazzola, M., et al. (2001). Large-scale advection of continental aerosols during INDOEX. *Journal Of Geophysical Research-Atmospheres*, *106*(D22), 28427–28439. https://doi.org/Doi 10.1029/2001jd900023

Levy, R. C., Mattoo, S., Munchak, L. A., Remer, L. A., Sayer, A. M., Patadia, F., & Hsu, N. C. (2013). The Collection 6 MODIS aerosol products over land and ocean. *Atmospheric Measurement Techniques*, *6*(11), 2989–3034. https://doi.org/10.5194/amt-6-2989-2013

Li, C., Bosch, C., Kang, S., Andersson, A., Chen, P., Zhang, Q., et al. (2016). Sources of black carbon to the Himalayan-Tibetan Plateau glaciers. *Nature Communications*, *7*. https://doi.org/10.1038/ ncomms12574

Li, F., & Ramanathan, V. (2002). Winter to summer monsoon variation of aerosol optical depth over the tropical Indian Ocean. *Journal of Geophysical Research Atmospheres*, *107*(16), 1–13. https://doi.org/10.1029/2001JD000949

Li, Z., Niu, F., Fan, J., Liu, Y., Rosenfeld, D., & Ding, Y. (2011). Long-term impacts of aerosols on the vertical development of clouds and precipitation. *Nature Geoscience*, *4*(12), 888–894. https://doi.org/10.1038/ngeo1313

Liao, H., & Seinfeld, J. H. (1998). Radiative forcing by mineral dust aerosols: Sensitivity to key variables. *Journal of Geophysical Research Atmospheres*, *103*(D24), 31637–31645. https://doi.org/10.1029/1998JD200036

Liou, K. N., Freeman, K. P., & Sasamori, T. (1978). Cloud and aerosol effects on the solar heating rate of the atmosphere. *Tellus*, *30*(1), 62–70. https://doi.org/10.1111/j.2153-3490.1978.tb00818.x

Liu, D., Wang, Z., Liu, Z., Winker, D., & Trepte, C. (2008). A height resolved global view of dust aerosols from the first year CALIPSO lidar measurements. *Journal of Geophysical Research Atmospheres*, *113*(16), 1–15. https://doi.org/10.1029/2007JD009776

Liu, Z., Sugimoto, N., & Murayama, T. (2002). Extinction-to-backscatter ratio of Asian dust observed with high-spectral-resolution lidar and Raman lidar. *Applied Optics*, *41*(15), 2760–2767. https://doi.org/10.1364/AO.41.002760

Liu, Z., Omar, A., Hu, Y., & Vaughan, M. (2005). *CALIOP algorithm theoretical basis document, Part 3: Scene classification algorithms*. *Theoretical Basis Documents*.

Liu, Z., Vaughan, M., Winker, D., Kittaka, C., Getzewich, B., Kuehn, R., et al. (2009). The CALIPSO lidar cloud and aerosol discrimination: Version 2 algorithm and initial assessment of performance. *Journal of Atmospheric and Oceanic Technology*, *26*(7), 1198–1213. https://doi.org/10.1175/2009JTECHA1229.1

Liu, Z., Winker, D., Omar, A., Vaughan, M., Kar, J., Trepte, C., et al. (2015). Evaluation of CALIOP 532 nm aerosol optical depth over opaque water clouds. *Atmospheric Chemistry and Physics*, *15*(3), 1265–1288. https://doi.org/10.5194/acp-15-1265-2015

Lohmann, U., & Feichter, J. (2004). Global indirect aerosol effects: a review. *Atmospheric Chemistry and Physics Discussions*, *4*(6), 7561–7614. https://doi.org/10.5194/acpd-4-7561-2004

Lopes, F. J. S., Landulfo, E., & Vaughan, M. A. (2013). Evaluating CALIPSO's 532 nm lidar ratio selection algorithm using AERONET sun photometers in Brazil. *Atmospheric Measurement Techniques*, *6*(11), 3281–3299. https://doi.org/10.5194/amt-6-3281-2013

Lubin, D., & Vogelmann, A. M. (2006). A climatologically significant aerosol longwave indirect effect in the Arctic. *Nature*, *439*(7075), 453–456. https://doi.org/10.1038/nature04449

Lüthi, Z. L., Škerlak, B., Kim, S. W., Lauer, A., Mues, A., Rupakheti, M., & Kang, S. (2015). Atmospheric brown clouds reach the Tibetan Plateau by crossing the Himalayas. *Atmospheric Chemistry and Physics*, *15*(11), 6007–6021. https://doi.org/10.5194/acp-15-6007-2015

Maher, B. A., Prospero, J. M., Mackie, D., Gaiero, D., Hesse, P. P., & Balkanski, Y. (2010). Global connections between aeolian dust, climate and ocean biogeochemistry at the present day and at the last glacial maximum. *Earth-Science Reviews*. https://doi.org/10.1016/ j.earscirev.2009.12.001

Mahowald, N., Albani, S., Kok, J. F., Engelstaeder, S., Scanza, R., Ward, D. S., & Flanner, M. G. (2014). The size distribution of desert dust aerosols and its impact on the Earth system. *Aeolian Research*, *15*, 53–71. https://doi.org/10.1016/j.aeolia.2013.09.002

Mahowald, N. M., & Luo, C. (2003). A less dusty future? *Geophysical Research Letters*, *30*(17). https://doi.org/10.1029/2003GL017880

Mahowald, N. N. M., & Kiehl, L. M. L. (2003). Mineral aerosol and cloud interactiocns. *Geophysical Research Letters*, *30*(9), 10.109/2002GL016762.

Mamouri, R. E., & Ansmann, A. (2014). Fine and coarse dust separation with polarization lidar. *Atmospheric Measurement Techniques*, *7*(11), 3717–3735.

Mamouri, R. E., Amiridis, V., Papayannis, A., Giannakaki, E., Tsaknakis, G., & Balis, D. S. (2009). Validation of CALIPSO space-borne-derived attenuated backscatter coefficient profiles using a ground-based lidar in Athens, Greece. *Atmospheric Measurement Techniques*, *2*(2), 513–522. https://doi.org/10.5194/amt-2-513-2009

Mamouri, R. E., Ansmann, A., Nisantzi, A., Kokkalis, P., Schwarz, A., & Hadjimitsis, D. (2013). Low Arabian dust extinction-to-backscatter ratio. *Geophysical Research Letters*, *40*(17), 4762–4766. https://doi.org/10.1002/grl.50898

Mani, A., Sreedharan, C. R., & Srinivasan, V. (1965). Measurements of infrared radiative fluxes over India. *Journal of Geophysical Research*, *70*(18), 4529–4536. https://doi.org/10.1029/ JZ070i018p04529

Mani, A., Chacko, O., & Hariharan, S. (1969). A Study of Ångström's turbidity parameters from solar radiation measurements in India. *Tellus*, *21*(6), 829–843. https://doi.org/10.1111/j.2153-3490.1969.tb00489.x

Manoharan, V. S., Kotamarthi, R., Feng, Y., & Cadeddu, M. P. (2014). Increased absorption by coarse aerosol particles over the Gangetic-Himalayan region. *Atmospheric Chemistry and Physics*, *14*(3), 1159–1165. https://doi.org/10.5194/acp-14-1159-2014

Marcq, S., Laj, P., Roger, J. C., Villani, P., Sellegri, K., Bonasoni, P., et al. (2010). Aerosol optical properties and radiative forcing in the high Himalaya based on measurements at the Nepal Climate Observatory-Pyramid site (5079 m a.s.l.). *Atmospheric Chemistry and Physics*, *10*(13), 5859–5872. https://doi.org/10.5194/acp-10-5859-2010

Maring, H. (2003). Vertical distributions of dust and sea-salt aerosols over Puerto Rico during PRIDE measured from a light aircraft. *Journal of Geophysical Research*, *108*(D19), 8587. https://doi.org/10.1029/2002JD002544

Markowicz, K. M., Flatau, P. J., Vogelmann, A. M., Quinn, P. K., & Welton, E. J. (2003). Clear-sky infrared aerosol radiative forcing at the surface and the top of the atmosphere. *Quarterly Journal of the Royal Meteorological Society*, *129*, 2927–2947. https://doi.org/10.1256/ 003590003769682110

Martin, D. W., Hinton, B. B., & Auvine, B. A. (1993). Three years of Rainfall Over the Indian Ocean. *Bulletin of the American Meteorological Society*, *74*(4), 581–590.

Martins, J. V., Artaxo, P., Liousse, C., Reid, J. S., Hobbs, P. V., & Kaufman, Y. J. (1998). Effects of black carbon content, particle size, and mixing on light absorption by aerosols from biomass burning in Brazil. *Journal of Geophysical Research Atmospheres*. https://doi.org/10.1029/98JD02593

Martonchik, J. V., Diner, D. J., Kahn, R. A., Ackerman, T. P., Verstraete, M. M., Pinty, B., & Gordon, H. R. (1998). Techniques for the retrieval of aerosol properties over land and ocean using multiangle imaging. *IEEE Transactions on Geoscience and Remote Sensing*, *36*(4), 1212–1227. https://doi.org/10.1109/36.701027

McGill, M. J., Yorks, J. E., Scott, V. S., Kupchock, A. W., & Selmer, P. A. (2015). The Cloud-Aerosol Transport System (CATS): a technology demonstration on the International Space Station. *Proc.SPIE*, *9612*, 9612-9612–6. https://doi.org/10.1117/12.2190841

McNeil, W. R., & Carsweil, A. l. (1975). Lidar polarization studies of the troposphere. *Applied Optics*, *14*(9), 2158. https://doi.org/10.1364/AO.14.002158

Mie, G. (1908). Beiträge zur Optik trüber Medien, speziell kolloidaler Metallösungen. *Annalen Der Physik*, *330*(3), 377–445. https://doi.org/10.1002/andp.19083300302

Miller, R. L., & Tegen, I. (2010). Climate response to soil dust aerosols. *Journal of Climate*, *11*(12), 3247–3267.

Miller, R. L., Tegen, I., & Perlwitz, J. (2004). Surface radiative forcing by soil dust aerosols and the hydrologic cycle. *Journal of Geophysical Research*, *109*(D4), 1–24. https://doi.org/10.1029/2003JD004085

Miller, R. L., Cakmur, R. V., Perlwitz, J., Geogdzhayev, I. V., Ginoux, P., Koch, D., et al. (2006). Mineral dust aerosols in the NASA Goddard Institute for Space Sciences ModelE atmospheric general circulation model. *Journal of Geophysical Research Atmospheres*, *111*(6). https://doi.org/10.1029/ 2005JD005796

Ming, J., Xiao, C., Cachier, H., Qin, D., Qin, X., Li, Z., & Pu, J. (2009). Black Carbon (BC) in the snow of glaciers in west China and its potential effects on albedos. *Atmospheric Research*, *92*(1), 114–123. https://doi.org/10.1016/j.atmosres.2008.09.007

Ming, Y., & Ramaswamy, V. (2011). A model investigation of Aerosol-Induced changes in tropical circulation. *Journal of Climate*, *24*(19), 5125–5133. https://doi.org/10.1175/2011JCLI4108.1

Mishchenko, M. I., Travis, L. D., & Mackowski, D. W. (1996). T-matrix computations of light scattering by nonspherical particles: A review. *Journal of Quantitative Spectroscopy and Radiative Transfer*. https://doi.org/10.1016/0022-4073(96)00002-7

Mishra, A. K., Koren, I., & Rudich, Y. (2015). Effect of aerosol vertical distribution on aerosol-radiation interaction: A theoretical prospect. *Heliyon*, *1*(2), e00036.

Mishra, M. K., Rajeev, K., Thampi, B. V., & Nair, A. K. M. (2013). *Annual variations of the altitude distribution of aerosols and effect of long-range transport over the southwest Indian Peninsula*. *Atmospheric Environment* (Vol. 81). Elsevier. https://doi.org/10.1016/j.atmosenv.2013.08.066

Moorthy, K. K., & Babu, S. S. (2006). Aerosol black carbon over Bay of Bengal observed from an island location, Port Blair: Temporal features and long-range transport. *Journal of Geophysical Research Atmospheres*, *111*(17), 1–7. https://doi.org/10.1029/2005JD006855

Moorthy, K. K., & Saha, A. (2000). Aerosol study during INDOEX: Observation of enhanced aerosol activity over the Mid Arabian Sea during the northern winter. *Journal of Atmospheric and Solar-Terrestrial Physics*, *62*(1), 65–72. https://doi.org/10.1016/S1364-6826(99)00081-4

Moorthy, K. K., Nair, P. B., & Murthy, B. V. K. (1988). A study of aerosol optical depth at a coastal station, Trivandrum. *Indian J. Radio Space Phys*, *17*, 16–22.

Moorthy, K. K., Murthy, B. V. K., & Nair, P. R. (1993). Sea-Breeze Front Effects on Boundary-Layer Aerosols at a Tropical Coastal Station. *J. Appl. Meteo.*, *32*(7), 1196–1205.

Moorthy, K. K., Babu, S. S., & Satheesh, S. K. (2003). Aerosol spectral optical depths over the Bay of Bengal: Role of transport. *Geophysical Research Letters*, *30*(5). https://doi.org/10.1029/2002GL016520

Moorthy, K. K., Babu, S. S., Sunilkumar, S. V., Gupta, P. K., & Gera, B. S. (2004). Altitude profiles of aerosol BC, derived from aircraft measurements over an inland urban location in India. *Geophysical Research Letters*, *31*(22), 1–4. https://doi.org/10.1029/2004GL021336

Moorthy, K. K., Babu, S. S., & Satheesh, S. K. (2005). Aerosol Characteristics and Radiative Impacts over the Arabian Sea during the Intermonsoon Season: Results from ARMEX Field Campaign. *Journal of the Atmospheric Sciences*, *62*(1), 192–206. https://doi.org/10.1175/JAS-3378.1

Moorthy, K. K., Sunilkumar, S. V., Pillai, P. S., Parameswaran, K., Nair, P. R., Ahmed, Y. N., et al. (2005). Wintertime spatial characteristics of boundary layer aerosols over peninsular India. *Journal of Geophysical Research D: Atmospheres*, *110*(8), 1–11. https://doi.org/10.1029/2004JD005520

Moorthy, K. K., Babu, S. S., Satheesh, S. K., Srinivasan, J., & Dutt, C. B. S. S. (2007). Dust absorption over the "Great Indian Desert" inferred using ground-based and satellite remote sensing. *Journal of Geophysical Research Atmospheres*, *112*(9), 1–10. https://doi.org/10.1029/2006JD007690

Moorthy, K. K., Satheesh, S. K., Babu, S. S., & Dutt, C. B. S. (2008). Integrated Campaign for Aerosols, gases and Radiation Budget (ICARB): An overview. *Journal of Earth System Science*, *117*, 243–262. https://doi.org/10.1007/s12040-008-0029-7

Moorthy, K. K., Nair, V. S., Babu, S. S., & Satheesh, S. K. (2009). Spatial and vertical heterogeneities in aerosol properties over oceanic regions around india: Implications for radiative forcing. *Quarterly Journal of the Royal Meteorological Society*, *135*(645), 2131–2145. https://doi.org/10.1002/qj.525

Moorthy, K. K., Beegum, S. N., Babu, S. S., Smirnov, A., John, S. R., Kumar, K. R., et al. (2010). Optical and physical characteristics of Bay of Bengal aerosols during W-ICARB: Spatial and vertical heterogeneities in the marine atmospheric boundary layer and in the vertical column. *Journal of Geophysical Research Atmospheres*, *115*(24). https://doi.org/10.1029/2010JD014094

Moorthy, K. K., Suresh Babu, S., Manoj, M. R., & Satheesh, S. K. (2013). Buildup of aerosols over the Indian Region. *Geophysical Research Letters*, *40*(5), 1011–1014. https://doi.org/ 10.1002/grl.50165

Moosmller, H., Engelbrecht, J. P., Skiba, M., Frey, G., Chakrabarty, R. K., & Arnott, W. P. (2012). Single scattering albedo of fine mineral dust aerosols controlled by iron concentration. *Journal of Geophysical Research Atmospheres*, *117*(11), 1–10. https://doi.org/10.1029/2011JD016909

Morice, C. P., Kennedy, J. J., Rayner, N. A., & Jones, P. D. (2012). Quantifying uncertainties in global and regional temperature change using an ensemble of observational estimates: The HadCRUT4 data set. *Journal of Geophysical Research Atmospheres*, *117*(8). https://doi.org/10.1029/ 2011JD017187

Moulin, C., Lambert, C. E., Dulac, F., & Dayan, U. (1997). Control of atmospheric export of dust from North Africa by the North Atlantic Oscillation. *Nature*, *387*(6634), 691–694. https://doi.org/ 10.1038/42679

Muller, D., Wagner, F., Althausen, D., Wandinger, U., & Ansmann, A. (2000). Physical properties of the Indian aerosol plume derived from six-wavelength lidar observations on 25 March 1999 of the Indian Ocean Experiment. *Geophysical Research Letters*, *27*(9), 1403–1406. https://doi.org/ 10.1029/1999GL011217

Müller, D., Mattis, I., Wandinger, U., Ansmann, A., Althausen, D., & Stohl, A. (2005). Raman lidar observations of aged Siberian and Canadian forest fire smoke in the free troposphere over Germany in 2003: Microphysical particle characterization. *Journal of Geophysical Research D: Atmospheres*, *110*(17), 75–90. https://doi.org/10.1029/2004JD005756

Müller, D., Ansmann, A., Mattis, I., Tesche, M., Wandinger, U., Althausen, D., & Pisani, G. (2007). Aerosol-type-dependent lidar ratios observed with Raman lidar. *Journal of Geophysical Research Atmospheres*, *112*(16), 1–11. https://doi.org/10.1029/2006JD008292

Müller, D., Lee, K. H., Gasteiger, J., Tesche, M., Weinzierl, B., Kandler, K., et al. (2012). Comparison of optical and microphysical properties of pure Saharan mineral dust observed with AERONET Sun photometer, Raman lidar, and in situ instruments during SAMUM 2006. *Journal of Geophysical Research Atmospheres*, *117*(7). https://doi.org/10.1029/2011JD016825

Murayama, T. (2003). Correction to "An intercomparison of lidar-derived aerosol optical properties with airborne measurements near Tokyo during ACE-Asia." *Journal of Geophysical Research*, *108*(D23), 8005. https://doi.org/10.1029/2003JD004153

Murayama, T., Müller, D., Wada, K., Shimizu, A., Sekiguchi, M., & Tsukamoto, T. (2004). Characterization of Asian dust and Siberian smoke with multi-wavelength Raman lidar over Tokyo, Japan in spring 2003. *Geophysical Research Letters*, *31*(23), 1–5. https://doi.org/ 10.1029/2004GL021105

Myhre, G., & Stordal, F. (2001). Global sensitivity experiments of the radiative forcing due to mineral aerosols. *Journal of Geophysical Research: Atmospheres*, *106*(D16), 18193–18204. https://doi.org/10.1029/2000JD900536

Nair, P. R., George, S. K., Sunilkumar, S. V., Parameswaran, K., Jacob, S., & Abraham, A. (2006). Chemical composition of aerosols over peninsular India during winter. *Atmospheric Environment*, *40*(34), 6477–6493. https://doi.org/10.1016/j.atmosenv.2006.02.031

Nair, V. S., Moorthy, K. K., Alappattu, D. P., Kunhikrishnan, P. K., George, S., Nair, P. R., et al. (2007). Wintertime aerosol characteristics over the Indo-Gangetic Plain (IGP): Impacts of local boundary layer processes and long-range transport. *Journal of Geophysical Research Atmospheres*, *112*(13),. https://doi.org/10.1029/2006JD008099

Nair, V. S., Moorthy, K. K., Babu, S. S., & Satheesh, S. K. (2009). Optical and Physical Properties of Atmospheric Aerosols over the Bay of Bengal during ICARB. *Journal of the Atmospheric Sciences*, *66*(9), 2640–2658. https://doi.org/10.1175/2009JAS3032.1

Nair, V. S., Solmon, F., Giorgi, F., Mariotti, L., Babu, S. S., & Moorthy, K. K. (2012). Simulation of South Asian aerosols for regional climate studies. *Journal of Geophysical Research Atmospheres*, *117*(4). https://doi.org/10.1029/2011JD016711

Nair, V. S., Babu, S. S., Moorthy, K. K., Sharma, A. K., Marinoni, A., & Ajai. (2013). Black carbon aerosols over the Himalayas: Direct and surface albedo forcing. *Tellus, Series B: Chemical and Physical Meteorology*, *65*(1). https://doi.org/10.3402/tellusb.v65i0.19738

Nair, V. S., Moorthy, K. K., & Babu, S. S. (2013). Influence of continental outflow and ocean biogeochemistry on the distribution of fine and ultrafine particles in the marine atmospheric boundary layer over Arabian Sea and Bay of Bengal. *Journal of Geophysical Research Atmospheres*, *118*(13), 7321–7331. https://doi.org/10.1002/jgrd.50541

Nair, V. S., Babu, S. S., Moorthy, K. K., & Prijith, S. S. (2013). Spatial gradients in aerosol-induced atmospheric heating and surface dimming over the oceanic regions around India: Anthropogenic or natural? *Journal of Climate*, *26*(19), 7611–7621. https://doi.org /10.1175/JCLI-D-12-00616.1

Nair, V. S., Suresh Babu, S., Krishna Moorthy, K., & Satheesh, S. K. (2014). Implications of multiple scattering on the assessment of black carbon aerosol radiative forcing. *Journal of Quantitative Spectroscopy and Radiative Transfer*, *148*, 134–140. https://doi.org/10.1016/j.jqsrt.2014.06.018

Nair, V. S., Babu, S. S., Gogoi, M. M., & Moorthy, K. K. (2016). Large-scale enhancement in aerosol absorption in the lower free troposphere over continental India during spring. *Geophysical Research Letters*, *43*(21), 11,453-11,461. https://doi.org/10.1002/2016GL070669

Nair, V. S., Babu, S. S., Manoj, M. R., Moorthy, K. K., & Chin, M. (2017). Direct radiative effects of aerosols over South Asia from observations and modeling. *Climate Dynamics*, *49*(4), 1411–1428. https://doi.org/10.1007/s00382-016-3384-0

Ningombam, S. S., Bagare, S. P., Sinha, N., Singh, R. B., Srivastava, A. K., Larson, E., & Kanawade, V. P. (2014). Characterization of aerosol optical properties over the high-altitude station Hanle, in the trans-Himalayan region. *Atmospheric Research*, *138*, 308–323. https://doi.org/10.1016/j.atmosres.2013.11.025

Niranjan, K., Sreekanth, V., Madhavan, B. L., & Moorthy, K. K. (2007). Aerosol physical properties and radiative forcing at the outflow region from the Indo-Gangetic plains during typical clear and hazy periods of wintertime. *Geophysical Research Letters*, *34*(19), 1–5. https://doi.org/10.1029/2007GL031224

Niranjan, K., Madhavan, B. L., & Sreekanth, V. (2007). Micro pulse lidar observation of high altitude aerosol layers at Visakhapatnam located on the east coast of India. *Geophysical Research Letters*, *34*(3). https://doi.org/10.1029/2006GL028199

Nistor, C. S., & Deaconu, A. (2016). Redesigning the instructional act in Romanian higher education. *Current Science*, *111*(1), 44–51. https://doi.org/10.18520/cs/v111/i1/44-51

Notaro, M., Yu, Y., & Kalashnikova, O. V. (2015). Regime shift in Arabian dust activity, triggered by persistent fertile crescent drought. *Journal of Geophysical Research*, *120*(19), 10229–10249. https://doi.org/10.1002/2015JD023855

Okin, G. S., Mahowald, N., Chadwick, O. A., & Artaxo, P. (2004). Impact of desert dust on the biogeochemistry of phosphorus in terrestrial ecosystems. *Global Biogeochemical Cycles*, *18*(2). https://doi.org/10.1029/2003GB002145

Omar, A. H., Winker, D. M., Vaughan, M. A., Hu, Y., Trepte, C. R., Ferrare, R. A., et al. (2009). The CALIPSO Automated Aerosol Classification and Lidar Ratio Selection Algorithm. *Journal of Atmospheric and Oceanic Technology*, *26*(10), 1994–2014.

Omar, A. H., Winker, D. M., Tackett, J. L., Giles, D. M., Kar, J., Liu, Z., et al. (2013). CALIOP and AERONET aerosol optical depth comparisons: One size fits none. *Journal of Geophysical Research Atmospheres*, *118*(10), 4748–4766. https://doi.org/10.1002/jgrd.50330

Oo, M., & Holz, R. (2011). Improving the CALIOP aerosol optical depth using combined MODIS-CALIOP observations and CALIOP integrated attenuated total color ratio. *Journal of Geophysical Research Atmospheres*, *116*(14), 1–15. https://doi.org/10.1029/2010JD014894

Osborne, S. R., Baran, A. J., Johnson, B. T., Haywood, J. M., Hesse, E., & Newman, S. (2011). Short-wave and long-wave radiative properties of Saharan dust aerosol. *Quarterly Journal of the Royal Meteorological Society*, *137*(658), 1149–1167. https://doi.org/10.1002/qj.771

Otto, S., De Reus, M., Trautmann, T., Thomas, A., Wendisch, M., & Borrmann, S. (2007). Atmospheric radiative effects of an in situ measured Saharan dust plume and the role of large particles. *Atmospheric Chemistry and Physics*, *7*(18), 4887–4903. https://doi.org/10.5194/acp-7-4887-2007

Otto, S., Bierwirth, E., Weinzierl, B., Kandler, K., Esselborn, M., Tesche, M., et al. (2009). Solar radiative effects of a Saharan dust plume observed during SAMUM assuming spheroidal model particles. *Tellus, Series B: Chemical and Physical Meteorology*, *61*(1), 270–296. https://doi.org/10.1111/j.1600-0889.2008.00389.x

Overpeck, J., Rind, D., Lacis, A., & Healy, R. (1996). Possible role of dust-induced regional warming in abrupt climate change during the last glacial period. *Nature*, *384*(6608), 447–449. https://doi.org/10.1038/384447a0

Padmakumari, B., Maheskumar, R. S., Morwal, S. B., Harikishan, G., Konwar, M., Kulkarni, J. R., & Goswami, B. N. (2013). Aircraft observations of elevated pollution layers near the foothills of the Himalayas during CAIPEEX-2009. *Quarterly Journal of the Royal Meteorological Society*, *139*(672), 625–638. https://doi.org/10.1002/qj.1989

Painter, T. H., Barrett, A. P., Landry, C. C., Neff, J. C., Cassidy, M. P., Lawrence, C. R., et al. (2007). Impact of disturbed desert soils on duration of mountain snow cover. *Geophysical Research Letters*, *34*(12), L12502. https://doi.org/10.1029/2007GL030284

Pan, X., Chin, M., Gautam, R., Bian, H., Kim, D., Colarco, P. R., et al. (2015). A multi-model evaluation of aerosols over South Asia: Common problems and possible causes. *Atmospheric Chemistry and Physics*, *15*(10), 5903–5928. https://doi.org/10.5194/acp-15-5903-2015

Pandey, S. K., Vinoj, V., Landu, K., & Babu, S. S. (2017). Declining pre-monsoon dust loading over South Asia: Signature of a changing regional climate. *Scientific Reports*, *7*(1). https://doi.org/10.1038/s41598-017-16338-w

Pant, P., Hegde, P., Dumka, U. C., Sagar, R., Satheesh, S. K., Moorthy, K. K., et al. (2006). Aerosol characteristics at a high-altitude location in central Himalayas: Optical properties and radiative forcing. *Journal of Geophysical Research Atmospheres*, *111*(17), 1–9. https://doi.org/10.1029/2005JD006768

Pappalardo, G., Wandinger, U., Mona, L., Hiebsch, A., Mattis, I., Amodeo, A., et al. (2010). EARLINET correlative measurements for CALIPSO: First intercomparison results. *Journal of Geophysical Research Atmospheres*, *115*(4). https://doi.org/10.1029/2009JD012147

Pappalardo, G., Amodeo, A., Apituley, A., Comeron, A., Freudenthaler, V., Linné, H., et al. (2014). EARLINET: Towards an advanced sustainable European aerosol lidar network. *Atmospheric Measurement Techniques*, *7*(8), 2389–2409. https://doi.org/10.5194/amt-7-2389-2014

Parameswaran, K., Rose, K. O., & Krishna Murthy, B. V. (1984). Aerosol characteristics from bistatic lidar observations. *Journal of Geophysical Research*, *89*(D2), 2541–2552.

Parameswaran, K., Vijayakumar, G., Krishna Murthy, B. V., & Krishna Moorthy, K. (1995). Effect of Wind Speed on Mixing Region Aerosol Concentrations at a Tropical Coastal Station. *Journal of Applied Meteorology*.

Parameswaran, K., Vijayakumar, G., & Krishna Murthy, B. V. (1997). Lidar observations on aerosol mixing height in a tropical coastal environment. *Indian Journal of Radio and Space Physics*, *26*(1), 15–21.

Parameswaran, K., Rajan, R., Vijayakumar, G., Rajeev, K., Krishna, K., Nair, P. R., & Satheesh, S. K. (1998). Seasonal and long term variations of aerosol content in the atmospheric mixing region at a tropical station on the Arabian sea-coast. *Journal of Atmospheric and Solar-Terrestrial Physics*, *60*(1), 17–25.

Parthasarathy, B., Munot, A. A., & Kothawale, D. R. (1995). Monthly and Seasonal Rainfall Series for All-India Homogeneous Regions and Meteorological Subdivisions. *Indian Inst. of Trop. Meteorol.*, 1871 – 1994.

Patadia, F., Yang, E. S., & Christopher, S. A. (2009). Does dust change the clear sky top of atmosphere shortwave flux over high surface reflectance regions? *Geophysical Research Letters*, *36*(15), 1–5. https://doi.org/10.1029/2009GL039092

Patil, N., Dave, P., & Venkataraman, C. (2017). Contrasting influences of aerosols on cloud properties during deficient and abundant monsoon years. *Scientific Reports*, *7*. https://doi.org/10.1038/srep44996

Patterson, E. M., Duckworth, R. M., Wyman, C. M., Powell, E. A., & Gooch, J. W. (1991). Measurements of the optical properties of the smoke emissions from plastics, hydrocarbons, and other urban fuels for nuclear winter studies. *Atmospheric Environment Part A, General Topics*, *25*(11), 2539–2552. https://doi.org/10.1016/0960-1686(91)90171-3

Pelon, J., Flamant, C., Chazette, P., Leon, J. F., Tanre, D., Sicard, M., & Satheesh, S. K. (2002). Characterization of aerosol spatial distribution and optical properties over the Indian Ocean from airborne LIDAR and radiometry during INDOEX'99. *Journal of Geophysical Research Atmospheres*, *107*(19), 1–13. https://doi.org/10.1029/2001JD000402

Penner, J. E., Dong, X., & Chen, Y. (2004). Observational evidence of a change in radiative forcing due to the indirect aerosol effect. *Nature*, *427*(6971), 231–234. https://doi.org/10.1038/nature02234

Pillai, P. S., & Moorthy, K. K. (2001). Aerosol mass-size distributions at a tropical coastal environment: Response to mesoscale and synoptic processes. *Atmospheric Environment*, *35*(24), 4099–4112. https://doi.org/10.1016/S1352-2310(01)00211-4

Powell, K. A., Hostetler, C. A., Liu, Z., Vaughan, M. A., Kuehn, R. E., Hunt, W. H., et al. (2009). Calipso lidar calibration algorithms. Part I: Nighttime 532-nm parallel channel and 532-nm perpendicular channel. *Journal of Atmospheric and Oceanic Technology*, *26*(10), 2015–2033.

Prasanna Kumar, S. (2002). Why is the Bay of Bengal less productive during summer monsoon compared to the Arabian Sea? *Geophysical Research Letters*, *29*(24), 1–17. https://doi.org/10.1029/2002GL016013

Preining, O. (1966). Photophoresis. *Aerosol Science*, 111–135.

Preißler, J., Wagner, F., Pereira, S. N., & Guerrero-Rascado, J. L. (2011). Multi-instrumental observation of an exceptionally strong Saharan dust outbreak over Portugal. *Journal of Geophysical Research Atmospheres*, *116*(24), 1–12. https://doi.org/10.1029/2011JD016527

Prijith, S. S., Aloysius, M., Mohan, M., Beegum, N., & Krishna Moorthy, K. (2012). Role of circulation parameters in long range aerosol transport: Evidence from Winter-ICARB. *Journal of Atmospheric and Solar-Terrestrial Physics*, *77*, 144–151. https://doi.org/10.1016/ j.jastp.2011.12.008

Prospero, J. M. (1979). Mineral and sea salt aerosol concentrations in various ocean regions. *Journal of Geophysical Research*, *84*(C2), 725. https://doi.org/10.1029/JC084iC02p00725

Prospero, J. M., Charlson, R. J., Mohnen, V., Jaenicke, R., Delany, A. C., Moyers, J., et al. (1983). The atmospheric aerosol system: An overview. *Reviews of Geophysics*, *21*(7), 1607–1629. https://doi.org/10.1029/RG021i007p01607

Prospero, J. M., Ginoux, P., Torres, O., Nicholson, S. E., & Gill, T. E. (2002). Environmental characterization of global sources of atmospheric soil dust identified with the Nimbus 7 Total Ozone Mapping Spectrometer (TOMS) absorbing aerosol product. *Reviews of Geophysics*, *40*(1), 1002. https://doi.org/10.1029/2000RG000095

Quijano, A. L., Sokolik, I. N., & Toon, O. B. (2000). Radiative heating rates and direct radiative forcing by mineral dust in cloudy atmospheric conditions. *Journal of Geophysical Research*, *105*(D10), 12207–12219. https://doi.org/10.1029/2000JD900047

Raes, F., Bates, T., McGovern, F., & Van Liedekerke, M. (2000). The 2nd Aerosol Characterization Experiment (ACE-2): General overview and main results. *Tellus, Series B: Chemical and Physical Meteorology*, *52*(2), 111–125. https://doi.org/10.3402/tellusb.v52i2.16088

Raj, P. E., Devara, P. C. S., Maheskumar, R. S., Pandithurai, G., & Dani, K. K. (1997). Lidar measurements of aerosol column content in an urban nocturnal boundary layer. *Atmospheric Research*. https://doi.org/http://dx.doi.org/10.1016/S0169-8095(97)00037-9

Rajeev, K., Ramanathan, V., & Meywerk, J. (2000). Regional aerosol distribution and its long-range transport over the Indian Ocean. *Journal of Geophysical Research*, *105*, 2029. https://doi.org/10.1029/1999JD900414

Rajeev, K., Parameswaran, K., Thampi, B. V., Mishra, M. K., Nair, A. K. M., & Meenu, S. (2010). Altitude distribution of aerosols over Southeast Arabian Sea coast during pre-monsoon season: Elevated layers, long-range transport and atmospheric radiative heating. *Atmospheric Environment*, *44*(21–22), 2597–2604. https://doi.org/10.1016/j.atmosenv.2010.04.014

Ramana, M. V., Ramanathan, V., Podgorny, I. A., Pradhan, B. B., & Shrestha, B. (2004). The direct observations of large aerosol radiative forcing in the Himalayan region. *Geophysical Research Letters*, *31*(5), 0–3. https://doi.org/10.1029/2003GL018824

Ramanathan, V., & Ramana, M. V. (2005). Persistent, widespread, and strongly absorbing haze over the Himalayan foothills and the Indo-Gangetic Plains. *Pure and Applied Geophysics*, *162*(8–9), 1609–1626. https://doi.org/10.1007/s00024-005-2685-8

Ramanathan, V., Crutzen, P. J., Lelieveld, J., Mitra, A. P., Althausen, D., Anderson, J., et al. (2001). Indian Ocean Experiment: An integrated analysis of the climate forcing and effects of the great Indo-Asian haze. *Journal of Geophysical Research Atmospheres*, *106*(D22), 28371–28398. https://doi.org/10.1029/2001JD900133

Ramanathan, V., Chung, C., Kim, D., Bettge, T., Buja, L., Kiehl, J. T., et al. (2005). Atmospheric brown clouds: Impacts on South Asian climate and hydrological cycle. *Proceedings of the National Academy of Sciences*, *102*(15), 5326–5333. https://doi.org/10.1073/pnas.0500656102

Ramanathan, V., Ramana, M. V., Roberts, G., Kim, D., Corrigan, C., Chung, C., & Winker, D. (2007). Warming trends in Asia amplified by brown cloud solar absorption. *Nature*, *448*(7153), 575–578. https://doi.org/10.1038/nature06019

Rasool, S. I., & Schneider, S. H. (1971). Atmospheric carbon dioxide and aerosols: Effects of large increases on global climate. *Science*, *173*(3992), 138–141. https://doi.org/10.1126/science.173.3992.138

Reid, E. A. (2003). Characterization of African dust transported to Puerto Rico by individual particle and size segregated bulk analysis. *Journal of Geophysical Research*, *108*(D19), 8591. https://doi.org/10.1029/2002JD002935

Reid, J. S., Piketh, S. J., Walker, A. L., Burger, R. P., Ross, K. E., Westphal, D. L., et al. (2008). An overview of UAE$^2$ flight operations: Observations of summertime atmospheric thermodynamic and aerosol profiles of the southern Arabian Gulf. *Journal of Geophysical Research Atmospheres*, *113*(14). https://doi.org/10.1029/2007JD009435

Reid, J. S., Reid, E. A., Walker, A., Piketh, S., Cliff, S., Mandoos, A. Al, et al. (2008). Dynamics of southwest Asian dust particle size characteristics with implications for global dust research. *Journal of Geophysical Research Atmospheres*, *113*(14). https://doi.org/10.1029/2007JD009752

Remer, L. A., Kaufman, Y. J., Tanré, D., Mattoo, S., Chu, D. A., Martins, J. V., et al. (2005). The MODIS Aerosol Algorithm, Products, and Validation. *Journal of the Atmospheric Sciences*, *62*(4), 947–973. https://doi.org/10.1175/JAS3385.1

Rezazadeh, M., Irannejad, P., & Shao, Y. (2013). Climatology of the Middle East dust events. *Aeolian Research*, *10*, 103–109. https://doi.org/10.1016/j.aeolia.2013.04.001

Ricchiazzi, P., Yang, S., Gautier, C., & Sowle, D. (1998). SBDART: A Research and Teaching Software Tool for Plane-Parallel Radiative Transfer in the Earth's Atmosphere. *Bulletin of the American Meteorological Society*, *79*(10), 2101–2114.

Rogers, R. R., Hostetler, C. A., Hair, J. W., Ferrare, R. A., Liu, Z., Obland, M. D., et al. (2011). Assessment of the CALIPSO Lidar 532 nm attenuated backscatter calibration using the NASA LaRC airborne High Spectral Resolution Lidar. *Atmospheric Chemistry and Physics*, *11*(3), 1295–1311. https://doi.org/10.5194/acp-11-1295-2011

Rogers, R. R., Vaughan, M. A., Hostetler, C. A., Burton, S. P., Ferrare, R. A., Young, S. A., et al. (2014). Looking through the haze: Evaluating the CALIPSO level 2 aerosol optical depth using airborne high spectral resolution lidar data. *Atmospheric Measurement Techniques*, *7*(12), 4317–4340. https://doi.org/10.5194/amt-7-4317-2014

Rosenfeld, D., Lohmann, U., Raga, G. B., O'Dowd, C. D., Kulmala, M., Fuzzi, S., et al. (2008). Flood or drought: How do aerosols affect precipitation? *Science*, *321*(5894), 1309–1313. https://doi.org/10.1126/science.1160606

Russell, P. B., Viezee, W., Hake, R. D., & Collis, R. T. H. (1976). Lidar observations of the stratospheric aerosol: California, October 1972 to March 1974. *Quarterly Journal of the Royal Meteorological Society*, *102*(433), 675–695. https://doi.org/10.1002/qj.49710243313

Russell, P. B., Hobbs, P. V., & Stowe, L. L. (1999). Aerosol properties and radiative effects in the United States East Coast haze plume: An overview of the tropospheric aerosol radiative forcing observational experiment (TARFOX). *Journal of Geophysical Research Atmospheres*, *104*(D2), 2213–2222. https://doi.org/10.1029/1998JD200028

Ryder, C. L., Highwood, E. J., Lai, T. M., Sodemann, H., & Marsham, J. H. (2013). Impact of atmospheric transport on the evolution of microphysical and optical properties of Saharan dust. *Geophysical Research Letters*, *40*(10), 2433–2438. https://doi.org/10.1002/grl.50482

Sakai, T. (2003). Raman lidar and aircraft measurements of tropospheric aerosol particles during the Asian dust event over central Japan: Case study on 23 April 1996. *Journal of Geophysical Research*, *108*(D12), 4349. https://doi.org/10.1029/2002JD003150

Sakai, T., Shibata, T., Iwasaka, Y., Nagai, T., Nakazato, M., Matsumura, T., et al. (2002). Case study of Raman lidar measurements of Asian dust events in 2000 and 2001 at Nagoya and Tsukuba, Japan. *Atmospheric Environment*, *36*(35), 5479–5489.

Sakai, T., Nagai, T., Zaizen, Y., & Mano, Y. (2010). Backscattering linear depolarization ratio measurements of mineral, sea-salt, and ammonium sulfate particles simulated in a laboratory chamber. *Applied Optics*, *49*(23), 4441. https://doi.org/10.1364/AO.49.004441

Samset, B. H., & Myhre, G. (2011). Vertical dependence of black carbon, sulphate and biomass burning aerosol radiative forcing. *Geophysical Research Letters*, *38*(24). https://doi.org/10.1029/2011GL049697

Samset, B. H., Myhre, G., Schulz, M., Balkanski, Y., Bauer, S., Berntsen, T. K., et al. (2013). Black carbon vertical profiles strongly affect its radiative forcing uncertainty. *Atmospheric Chemistry and Physics*, *13*(5), 2423–2434. https://doi.org/10.5194/acp-13-2423-2013

Samset, B. H., Myhre, G., & Schulz, M. (2014). Upward adjustment needed for aerosol radiative forcing uncertainty. *Nature Climate Change*, *4*(4), 230–232. https://doi.org/10.1038/nclimate2170

Sarangi, C., Tripathi, S. N., Mishra, A. K., Goel, A., & Welton, E. J. (2016). Elevated aerosol layers and their radiative impact over Kanpur during monsoon onset period. *Journal of Geophysical Research*, *121*(13), 7936–7957. https://doi.org/10.1002/2015JD024711

Sarkar, C., Chatterjee, A., Singh, A. K., Ghosh, S. K., & Raha, S. (2015). Characterization of black carbon aerosols over Darjeeling - A high altitude Himalayan station in Eastern India. *Aerosol and Air Quality Research*, *15*(2), 465–478. https://doi.org/10.4209/aaqr.2014.02.0028

Di Sarra, A., Di Biagio, C., Meloni, D., Monteleone, F., Pace, G., Pugnaghi, S., & Sferlazzo, D. (2011). Shortwave and longwave radiative effects of the intense Saharan dust event of 25-26 March 2010 at Lampedusa (Mediterranean Sea). *Journal of Geophysical Research Atmospheres*, *116*(23), https://doi.org/10.1029/2011JD016238

Sassen, K. (1991). The polarization lidar technique for cloud research: A review and current assessment. *Bulletin of the American Meteorological Society*, *72*(12), 1848-1866.

Sassen, K. (2003). Saharan dust storms and indirect aerosol effects on clouds: CRYSTAL-FACE results. *Geophysical Research Letters*, *30*(12), 1–4. https://doi.org/10.1029/2003GL017371

Satheesh, S. K. (2002a). Aerosol radiative forcing over land: effect of surface and cloud reflection. *Annales Geophysicae*, *20*(12), 2105–2109. https://doi.org/10.5194/angeo-20-2105-2002

Satheesh, S. K. (2002b). Radiative forcing by aerosols over Bay of Bengal region. *Geophysical Research Letters*, *29*(22), 2083. https://doi.org/10.1029/2002GL015334

Satheesh, S. K., & Krishna Moorthy, K. (2005). Radiative effects of natural aerosols: A review. *Atmospheric Environment*. https://doi.org/10.1016/j.atmosenv.2004.12.029

Satheesh, S. K., & Lubin, D. (2003). Short wave versus long wave radiative forcing by Indian Ocean aerosols: Role of sea-surface winds. *Geophysical Research Letters*, *30*(13), 10–13. https://doi.org/10.1029/2003GL017499

Satheesh, S. K., & Moorthy, K. K. (1997). Aerosol characteristics over coastal regions of the Arabian Sea. *Tellus, Series B: Chemical and Physical Meteorology*, *49*(4), 417–428. https://doi.org/ 10.3402/ tellusb.v49i4.15979

Satheesh, S. K., & Ramanathan, V. (2000). Large differences in tropical aerosol forcing at the top of the atmosphere and Earth's surface. *Nature*, *405*(6782), 60–63. https://doi.org/10.1038/35011039

Satheesh, S. K., & Srinivasan, J. (2002). Enhanced aerosol loading over Arabian Sea during the pre-monsoon season: Natural or anthropogenic? *Geophysical Research Letters*, *29*(18), 21-1-21–4. https://doi.org/10.1029/2002GL015687

Satheesh, S. K., Ramanathan, V., Holben, B. N., Krishna Moorthy, K., Loeb, N. G., Mating, H., et al. (2002). Chemical, microphysical, and radiative effects of Indian Ocean aerosols. *Journal of Geophysical Research Atmospheres*, *107*(23), AAC 20-1-AAC 20-13. https://doi.org/10.1029/2002JD002463

Satheesh, S. K., Deepshikha, S., Srinivasan, J., & Kaufman, Y. J. (2006). Large dust absorption of infrared radiation over afro-asian regions: Evidence for anthropogenic impact. *IEEE Geoscience and Remote Sensing Letters*, *3*(3), 307–311. https://doi.org/10.1109/LGRS.2006.869988

Satheesh, S. K., Srinivasan, J., & Moorthy, K. K. (2006). Spatial and temporal heterogeneity in aerosol properties and radiative forcing over Bay of Bengal: Sources and role of aerosol transport. *Journal of Geophysical Research Atmospheres*, *111*(8), 1–10. https://doi.org/10.1029/ 2005JD006374

Satheesh, S. K., Vinoj, V., & Moorthy, K. K. (2006). Vertical distribution of aerosols over an urban continental site in India inferred using a micro pulse lidar. *Geophysical Research Letters*, *33*(20), 2–6. https://doi.org/10.1029/2006GL027729

Satheesh, S. K., Krishna Moorthy, K., Suresh Babu, S., Vinoj, V., & Dutt, C. B. S. (2008). Climate implications of large warming by elevated aerosol over India. *Geophysical Research Letters*, *35*(19), 0–5. https://doi.org/10.1029/2008GL034944

Satheesh, S. K., Vinoj, V., Suresh Babu, S., Krishna Moorthy, K., & S. Nair, V. (2009). Vertical distribution of aerosols over the east coast of India inferred from airborne LIDAR measurements. *Annales Geophysicae*, *27*(11), 4157–4169. https://doi.org/10.5194/angeo-27-4157-2009

Satheesh, S. K., Krishna Moorthy, K., Suresh Babu, S., Vinoj, V., Nair, V. S., Naseema Beegum, S., et al. (2009). Vertical structure and horizontal gradients of aerosol extinction coefficients over coastal India inferred from airborne lidar measurements during the integrated campaign for aerosol, gases and radiation budget (ICARB) field campaign. *Journal of Geophysical Research Atmospheres*, *114*(5), 1–11. https://doi.org/10.1029/2008JD011033

Satheesh, S. K., Moorthy, K. K., & Srinivasan, J. (2013). New Directions: Elevated layers of anthropogenic aerosols aggravate stratospheric ozone loss? *Atmospheric Environment*, *79*, 879–882. https://doi.org/10.1016/j.atmosenv.2013.07.052

Schuster, B. G. (1970). Detection of tropospheric and stratospheric aerosol layers by optical radar (Lidar). *Journal of Geophysical Research*, *75*(15), 3123–3132. https://doi.org/10.1029/JC075i015p03123

Schuster, G. L., Vaughan, M., MacDonnell, D., Su, W., Winker, D., Dubovik, O., et al. (2012). Comparison of CALIPSO aerosol optical depth retrievals to AERONET measurements, and a climatology for the lidar ratio of dust. *Atmospheric Chemistry and Physics*, *12*(16), 7431–7452. https://doi.org/10.5194/acp-12-7431-2012

Schwarz, J. P., Spackman, J. R., Gao, R. S., Watts, L. A., Stier, P., Schulz, M., et al. (2010). Global-scale black carbon profiles observed in the remote atmosphere and compared to models. *Geophysical Research Letters*, *37*(18). https://doi.org/10.1029/2010GL044372

Seinfeld, J. H., Pandis, S. N., & Noone, K. (1998). Atmospheric Chemistry and Physics: From Air Pollution to Climate Change. *Physics Today* (Vol. 51). https://doi.org/10.1063/1.882420

Shaik, D. S., Kant, Y., Mitra, D., & Babu, S. S. (2017). Assessment of aerosol characteristics and radiative forcing over northwest himalayan region. *IEEE Journal of Selected Topics in Applied Earth Observations and Remote Sensing*, *10*(12), 5314–5321. https://doi.org/10.1109/JSTARS.2017.2749481

Shao, Y., Klose, M., & Wyrwoll, K. H. (2013). Recent global dust trend and connections to climate forcing. *Journal of Geophysical Research Atmospheres*, *118*(19), 11107–11118. https://doi.org/ 10.1002/jgrd.50836

Shimizu, A., Sugimoto, N., Matsui, I., Arao, K., Uno, I., Murayama, T., et al. (2004). Continuous observations of Asian dust and other aerosols by polarization lidars in China and Japan during ACE-Asia. *Journal of Geophysical Research D: Atmospheres*, *109*(19). https://doi.org/10.1029/2002JD003253

Shin, S., Müller, D., Kim, Y. J., Tatarov, B., Shin, D., Seifert, P., & Noh, Y. M. (2013). The retrieval of the Asian dust depolarization ratio in Korea with the correction of the polarization-dependent transmission. *Asia-Pacific Journal of Atmospheric Sciences*, *49*(1), 19–25. https://doi.org/ 10.1007/s13143-013-0003-4

Shrestha, A. B., P. Wake, C., Dibb, J. E., Mayewski, P. A., Whitlow, S. I., Carmichael, G. R., & Ferm, M. (2000). Seasonal variations in aerosol concentrations and compositions in the Nepal Himalaya. *Atmospheric Environment*, *34*(20), 3349–3363. https://doi.org/10.1016/S1352-2310(99)00366-0

Shrestha, P., & Barros, A. P. (2010). Joint spatial variability of aerosol, clouds and rainfall in the Himalayas from satellite data. *Atmospheric Chemistry and Physics*, *10*(17), 8305–8317. https://doi.org/10.5194/acp-10-8305-2010

Shu, S., & Wu, L. (2009). Analysis of the influence of Saharan air layer on tropical cyclone intensity using AIRS/Aqua data. *Geophysical Research Letters*, *36*(9), L09809. https://doi.org/10.1029/2009GL037634

Singh, P., & Kumar, N. (1997). Effect of orography on precipitation in the western Himalayan region. *Journal of Hydrology*, *199*(1–2), 183–206. https://doi.org/10.1016/S0022-1694(96)03222-2

Slinn, W. G. N., Hasse, L., Hicks, B. B., Hogan, A. W., Lal, D., Liss, P. S., et al. (1978). Some aspects of the transfer of atmospheric trace constituents past the air-sea interface. *Atmospheric Environment (1967)*. https://doi.org/10.1016/0004-6981(78)90163-4

Snider, J. R., & Brenguier, J. L. (2000). Cloud condensation nuclei and cloud droplet measurements during ACE-2. *Tellus, Series B: Chemical and Physical Meteorology*, *52*(2), 828–842. https://doi.org/10.1034/j.1600-0889.2000.00044.x

Sokolik, I. N., & Toon, O. B. (1996). Direct radiative forcing by anthropogenic airborne mineral aerosols. *Nature*, *381*(6584), 681–683. https://doi.org/10.1038/381681a0

Sokolik, I. N., & Toon, O. B. (1997). Regional direct radiative forcing by the airborne mineral aerosols. *Journal of Aerosol Science*. https://doi.org/10.1016/S0021-8502(97)85327-X

Sokolik, I. N., Winker, D. M., Bergametti, G., Gillette, D. a., Carmichael, G., Kaufman, Y. J., et al. (2001). Introduction to special section: Outstanding problems in quantifying the radiative impacts of mineral dust. *Journal of Geophysical Research*, *106*(D16), 18015. https://doi.org/10.1029/2000JD900498

Solmon, F., Nair, V. S., & Mallet, M. (2015). Increasing Arabian dust activity and the Indian summer monsoon. *Atmospheric Chemistry and Physics*, *15*(14), 8051–8064. https://doi.org/10.5194/acp-15-8051-2015

Spinhirne, J. D., Reagan, J. A., & Herman, B. M. (1980). Vertical Distribution of Aerosol Extinction Cross Section and Inference of Aerosol Imaginary Index in the Troposphere by Lidar Technique. *Journal of Applied Meteorology*.

Srinivas, B., & Sarin, M. M. (2012). Atmospheric pathways of phosphorous to the Bay of Bengal: contribution from anthropogenic sources and mineral dust. *Tellus B: Chemical and Physical Meteorology*, *64*(1), 17174. https://doi.org/10.3402/tellusb.v64i0.17174

Srinivas, B., Kumar, a., Sarin, M. M., & Sudheer, a. K. (2011). Impact of continental outflow on chemistry of atmospheric aerosols over tropical Bay of Bengal. *Atmospheric Chemistry and Physics Discussions*, *11*(7), 20667–20711. https://doi.org/10.5194/acpd-11-20667-2011

Srivastava, A. K., Pant, P., Hegde, P., Singh, S., Dumka, U. C., Naja, M., et al. (2011). The influence of a south asian dust storm on aerosol radiative forcing at a high-altitude station in central Himalayas. *International Journal of Remote Sensing*, *32*(22), 7827–7845. https://doi.org/ 10.1080/01431161.2010.531781

Srivastava, P., Dey, S., Srivastava, A. K., Singh, S., Mishra, S. K., & Tiwari, S. (2017). Importance of aerosol non-sphericity in estimating aerosol radiative forcing in Indo-Gangetic Basin. *Science of the Total Environment*, *599–600*, 655–662. https://doi.org/10.1016/j.scitotenv.2017.04.239

Stenchikov, G., Hamilton, K., Stouffer, R. J., Robock, A., Ramaswamy, V., Santer, B., & Graf, H. F. (2006). Arctic Oscillation response to volcanic eruptions in the IPCC AR4 climate models. *Journal of Geophysical Research Atmospheres*, *111*(7). https://doi.org/10.1029/2005JD006286

Stocker, T. F., Qin, D., Plattner, G. K., Tignor, M. M. B., Allen, S. K., Boschung, J., et al. (2013). *Climate change 2013 the physical science basis: Working Group I contribution to the fifth assessment report of the intergovernmental panel on climate change*. *Climate Change 2013 the Physical Science Basis: Working Group I Contribution to the Fifth Assessment Report of the Intergovernmental Panel on Climate Change* (Vol. 9781107057). Cambridge University Press, Cambridge, United Kingdom and New York, NY, USA. https://doi.org/10.1017/ CBO9781107415324

Stone, E. A., Schauer, J. J., Pradhan, B. B., Dangol, P. M., Habib, G., Venkataraman, C., & Ramanathan, V. (2010). Characterization of emissions from South Asian biofuels and application to source apportionment of carbonaceous aerosol in the Himalayas. *Journal of Geophysical Research Atmospheres*, *115*(6), D06301. https://doi.org/10.1029/2009JD011881

Sugimoto, N., & Lee, C. H. (2006). Characteristics of dust aerosols inferred from lidar depolarization measurements at two wavelengths. *Applied Optics*, *45*(28), 7468. https://doi.org/10.1364/ AO.45.007468

Sugimoto, N., & Uno, I. (2009). Observation of Asian dust and air-pollution aerosols using a network of ground-based lidars (ADNet): Realtime data processing for validation/assimilation of chemical transport models. *IOP Conference Series: Earth and Environmental Science*, *7*, 012003. https://doi.org/10.1088/1755-1307/7/1/012003

Sun, D., Lau, K. M., & Kafatos, M. (2008). Contrasting the 2007 and 2005 hurricane seasons: Evidence of possible impacts of Saharan dry air and dust on tropical cyclone activity in the Atlantic basin. *Geophysical Research Letters*, *35*(15). https://doi.org/10.1029/2008GL034529

Swap, R. J., Annegarn, H. J., Suttles, J. T., Haywood, J., Helmlinger, M. C., Hely, C., et al. (2002). The Southern African Regional Science Initiative (SAFARI 2000): Overview of the dry season field campaign. *South African Journal of Science*. https://doi.org/10.1007/s11136-008-9339-0

Takamura, T., Sasano, Y., & Hayasaka, T. (1994). Tropospheric aerosol optical properties derived from lidar, sun photometer, and optical particle counter measurements. *Applied Optics*, *33*(30), 7132–7140. https://doi.org/10.1364/AO.33.007132

Tanré, D. (2003). Measurement and modeling of the Saharan dust radiative impact: Overview of the Saharan Dust Experiment (SHADE). *Journal of Geophysical Research*, *108*(D18), 8574. https://doi.org/10.1029/2002JD003273

Tanré, D., Kaufman, Y. J., Herman, M., & Mattoo, S. (1997). Remote sensing of aerosol properties over oceans using the MODIS/EOS spectral radiances. *Journal of Geophysical Research: Atmospheres*, *102*(D14), 16971–16988. https://doi.org/10.1029/96JD03437

Tegen, I., Lacis, A. A., & Fung, I. (1996). The influence on climate forcing of mineral aerosols from disturbed soils. *Nature*, *380*(6573), 419–422. https://doi.org/10.1038/380419a0

Tesche, M., Ansmann, A., Müller, D., Althausen, D., Engelmann, R., Hu, M., & Zhang, Y. (2007). Particle backscatter, extinction, and lidar ratio profiling with Raman lidar in south and north China. *Applied Optics*, *46*(25), 6302–8. https://doi.org/10.1364/AO.46.006302

Tesche, M., Ansmann, A., Müller, D., Althausen, D., Engelmann, R., Freudenthaler, V., & Groß, S. (2009). Vertically resolved separation of dust and smoke over Cape Verde using multiwavelength Raman and polarization lidars during Saharan Mineral Dust Experiment 2008. *Journal of Geophysical Research Atmospheres*, *114*(13), D13202. https://doi.org/10.1029/2009JD011862

Tesche, M., Gross, S., Ansmann, A., Müller, D., Althausen, D., Freudenthaler, V., & Esselborn, M. (2011). Profiling of Saharan dust and biomass-burning smoke with multiwavelength polarization Raman lidar at Cape Verde. *Tellus, Series B: Chemical and Physical Meteorology*, *63*(4), 649–676. https://doi.org/10.1111/j.1600-0889.2011.00548.x

Tesche, M., Wandinger, U., Ansmann, A., Althausen, D., Müller, D., & Omar, A. H. (2013). Ground-based validation of CALIPSO observations of dust and smoke in the Cape Verde region. *Journal of Geophysical Research Atmospheres*, *118*(7), 2889–2902. https://doi.org/10.1002/jgrd.50248

Textor, C., Schulz, M., Guibert, S., Kinne, S., Balkanski, Y., Bauer, S., et al. (2006). Analysis and quantification of the diversities of aerosol life cycles within AeroCom. *Atmospheric Chemistry and Physics*, *6*(7), 1777–1813. https://doi.org/10.5194/acp-6-1777-2006

Tindale, N. W., & Pease, P. P. (1999). Aerosols over the Arabian Sea: Atmospheric transport pathways and concentrations of dust and sea salt. *Deep-Sea Research Part II: Topical Studies in Oceanography*, *46*(8–9), 1577–1595. https://doi.org/10.1016/S0967-0645(99)00036-3

Torres, O., Tanskanen, A., Veihelmann, B., Ahn, C., Braak, R., Bhartia, P. K., et al. (2007). Aerosols and surface UV products form Ozone Monitoring Instrument observations: An overview. *Journal of Geophysical Research Atmospheres*. https://doi.org/10.1029/2007JD008809

Trenberth, K. E., & Fasullo, J. T. (2013). An apparent hiatus in global warming? *Earth's Future*, *1*(1), 19–32. https://doi.org/10.1002/2013EF000165

Tripathi, S. N., Dey, S., Tare, V., Satheesh, S. K., Lal, S., & Venkataramani, S. (2005). Enhanced layer of black carbon in a north Indian industrial city. *Geophysical Research Letters*, *32*(12), 1–4. https://doi.org/10.1029/2005GL022564

Tripathi, S. N., Tare, V., Chinnam, N., Srivastava, A. K., Dey, S., Agarwal, A., et al. (2006). Measurements of atmospheric parameters during Indian Space Research Organization Geosphere Biosphere Programme Land Campaign II at a typical location in the Ganga basin: 1. Physical and optical properties. *Journal of Geophysical Research Atmospheres*, *111*(23). https://doi.org/10.1029/2006JD007278

Tripathi, S. N., Srivastava, A. K., Dey, S., Satheesh, S. K., & Krishnamoorthy, K. (2007). The vertical profile of atmospheric heating rate of black carbon aerosols at Kanpur in northern India. *Atmospheric Environment*, *41*(32), 6909–6915.

Turco, R. P., Toon, O. B., Ackerman, T. P., Pollack, J. B., & Sagan, C. (1983). Nuclear Winter: Global Consequences of Multple Nuclear Explosions. *Science*, *222*(4630), 1283–1292. https://doi.org/10.1126/science.222.4630.1283

Twomey, S. (1977). The Influence of Pollution on the Shortwave Albedo of Clouds. *Journal of the Atmospheric Sciences*, *34*(7), 1149–1152.

Uno, I., Yumimoto, K., Shimizu, A., Hara, Y., Sugimoto, N., Wang, Z., et al. (2008). 3D structure of Asian dust transport revealed by CALIPSO lidar and a 4DVAR dust model. *Geophysical Research Letters*, *35*(6), 2–8. https://doi.org/10.1029/2007GL032329

Uno, I., Eguchi, K., Yumimoto, K., Takemura, T., Shimizu, A., Uematsu, M., et al. (2009). Asian dust transported one full circuit around theglobe. *Nature Geoscience*, *2*(8), 557–560. https://doi.org/10.1038/ngeo583

Vaishya, A., Babu, S. N. S., Jayachandran, V., Gogoi, M. M., Lakshmi, N. B., Moorthy, K. K., & Satheesh, S. K. (2018). Large contrast in the vertical distribution of aerosol optical properties and radiative effects across the Indo-Gangetic Plain during the SWAAMI–RAWEX campaign. *Atmospheric Chemistry and Physics*, *18*(23), 17669-17685.

Valenzuela, A., Olmo, F. J., Lyamani, H., Antón, M., Quirantes, A., & Alados-Arboledas, L. (2012). Aerosol radiative forcing during African desert dust events (2005-2010) over Southeastern Spain. *Atmospheric Chemistry and Physics*, *12*(21), 10331–10351. https://doi.org/10.5194/acp-12-10331-2012

Vaughan, M. A., Powell, K. A., Kuehn, R. E., Young, S. A., Winker, D. M., Hostetler, C. A., et al. (2009). Fully automated detection of cloud and aerosol layers in the CALIPSO lidar measurements. *Journal of Atmospheric and Oceanic Technology*, *26*(10), 2034–2050.

Vernier, J. P., Thomason, L. W., & Kar, J. (2011). CALIPSO detection of an Asian tropopause aerosol layer. *Geophysical Research Letters*, *38*(7), 1–6. https://doi.org/10.1029/2010GL046614

Veselovskii, I., Goloub, P., Podvin, T., Bovchaliuk, V., Derimian, Y., Augustin, P., et al. (2016). Retrieval of optical and physical properties of African dust from multiwavelength Raman lidar measurements during the SHADOW campaign in Senegal. *Atmospheric Chemistry and Physics*, *16*(11), 7013–7028. https://doi.org/10.5194/acp-16-7013-2016

Vinoj, V. (2004). Radiative forcing by aerosols over the Bay of Bengal region derived from shipborne, island-based, and satellite (Moderate-Resolution Imaging Spectroradiometer) observations. *Journal of Geophysical Research*, *109*(D5), D05203. https://doi.org/10.1029/2003JD004329

Vinoj, V., & Satheesh, S. K. (2003). Measurements of aerosol optical depth over Arabian Sea during summer monsoon season. *Geophysical Research Letters*, *30*(5). https://doi.org/10.1029/2002GL016664

Vinoj, V., Rasch, P. J., Wang, H., Yoon, J. H., Ma, P. L., Landu, K., & Singh, B. (2014). Short-term modulation of Indian summer monsoon rainfall by West Asian dust. *Nature Geoscience*, *7*(April), 308–313. https://doi.org/10.1038/ngeo2107

Wandinger, U., Tesche, M., Seifert, P., Ansmann, A., Müller, D., & Althausen, D. (2010). Size matters: Influence of multiple scattering on CALIPSO light-extinction profiling in desert dust. *Geophysical Research Letters*, *37*(10). https://doi.org/10.1029/2010GL042815

Weatherhead, E. C., Reinsel, G. C., Tiao, G. C., Meng, X. L., Choi, D., Cheang, W. K., et al. (1998). Factors affecting the detection of trends: Statistical considerations and applications to environmental data. *Journal of Geophysical Research Atmospheres*, *103*(D14), 17149–17161. https://doi.org/10.1029/98JD00995

Weinzierl, B., Petzold, A., Esselborn, M., Wirth, M., Rasp, K., Kandler, K., et al. (2009). Airborne measurements of dust layer properties, particle size distribution and mixing state of Saharan dust during SAMUM 2006. *Tellus, Series B: Chemical and Physical Meteorology*, *61*(1), 96–117. https://doi.org/10.1111/j.1600-0889.2008.00392.x

Weinzierl, B., Sauer, D., Esselborn, M., Petzold, A., Veira, A., Rose, M., et al. (2011). Microphysical and optical properties of dust and tropical biomass burning aerosol layers in the Cape Verde region-an overview of the airborne in situ and lidar measurements during SAMUM-2. *Tellus, Series B: Chemical and Physical Meteorology*, *63*(4), 589–618. https://doi.org/10.1111/j.1600-0889.2011.00566.x

Welton, E. J., Voss, K. J., Quinn, P. K., Flatau, P. J., Markowicz, K., Campbell, J. R., et al. (2002). Measurements of aerosol vertical profiles and optical properties during INDOEX 1999 using micropulse lidars. *Journal of Geophysical Research Atmospheres*, *107*(19), 1–20. https://doi.org/10.1029/2000JD000038

Wilcox, E. M. (2010). Stratocumulus cloud thickening beneath layers of absorbing smoke aerosol. *Atmospheric Chemistry and Physics*, *10*(23), 11769–11777. https://doi.org/10.5194/acp-10-11769-2010

Winker, D. M., Couch, R. H., & Mccormick, M. P. (1996). An overview of LITE: NASA's lidar in-space technology experiment. *Proceedings of the IEEE*, *84*(2), 164–180. https://doi.org/10.1109/5.482227

Winker, D. M., & Pelon, J. (2003). The CALIPSO mission. *IGARSS 2003. 2003 IEEE International Geoscience and Remote Sensing Symposium. Proceedings)*, 1329–1331. https://doi.org/10.1109/IGARSS.2003.1294098

Winker, D., Vaughan, M., & Hunt, B. (2006). The CALIPSO mission and initial results from CALIOP. *Lidar Remote Sensing for Environmental Monitoring VII*, *6409*, 8–15. https://doi.org/10.1117/12.698003

Winker, D. M., Hunt, W. H., & McGill, M. J. (2007). Initial performance assessment of CALIOP. *Geophysical Research Letters*, *34*(19), 1–5. https://doi.org/10.1029/2007GL030135

Winker, D. M., Vaughan, M. A., Omar, A., Hu, Y., Powell, K. A., Liu, Z., et al. (2009). Overview of the CALIPSO mission and CALIOP data processing algorithms. *Journal of Atmospheric and Oceanic Technology*, *26*(11), 2310–2323. https://doi.org/10.1175/2009JTECHA1281.1

Winker, D. M., Pelon, J., Coakley, J. A., Ackerman, S. A., Charlson, R. J., Colarco, P. R., et al. (2010). The Calipso Mission: A Global 3D View of Aerosols and Clouds. *Bulletin of the American Meteorological Society*, *91*(9), 1211–1229. https://doi.org/10.1175/2010BAMS3009.1

Woodward, S. (2001). Modeling the atmospheric life cycle and radiative impact of mineral dust in the Hadley Centre climate model. *Journal of Geophysical Research*, *106*(D16), 18155. https://doi.org/10.1029/ 2000JD900795

Wu, C., Lin, Z., Liu, X., Li, Y., Lu, Z., & Wu, M. (2018). Can Climate Models Reproduce the Decadal Change of Dust Aerosol in East Asia? *Geophysical Research Letters*, *45*(18), 9953–9962. https://doi.org/10.1029/2018GL079376

Wu, Y., Cordero, L., Gross, B., Moshary, F., & Ahmed, S. (2012). Smoke plume optical properties and transport observed by a multi-wavelength lidar, sunphotometer and satellite. *Atmospheric Environment*, *63*, 32–42. https://doi.org/10.1016/j.atmosenv.2012.09.016

Wu, Y., de Graaf, M., & Menenti, M. (2017). The impact of aerosol vertical distribution on aerosol optical depth retrieval using CALIPSO and MODIS data: Case study over dust and smoke regions. *Journal of Geophysical Research: Atmospheres*, *122*(16), 8801–8815. https://doi.org/10.1002/2016JD026355

Xia, X., & Zong, X. (2009). Shortwave versus longwave direct radiative forcing by Taklimakan dust aerosols. *Geophysical Research Letters*, *36*(7), 1–5. https://doi.org/10.1029/2009GL037237

Xie, C., Nishizawa, T., Sugimoto, N., Matsui, I., & Wang, Z. (2008). Characteristics of aerosol optical properties in pollution and Asian dust episodes over Beijing, China. *Applied Optics*, *47*(27), 4945–4951. https://doi.org/10.1364/AO.47.004945

Yang, E. S., Gupta, P., & Christopher, S. A. (2009). Net radiative effect of dust aerosols from satellite measurements over Sahara. *Geophysical Research Letters*, *36*(18). https://doi.org/10.1029/2009GL039801

Yoshioka, M., Mahowald, N. M., Conley, A. J., Collins, W. D., Fillmore, D. W., Zender, C. S., & Coleman, D. B. (2007). Impact of desert dust radiative forcing on sahel precipitation: Relative importance of dust compared to sea surface temperature variations, vegetation changes, and greenhouse gas warming. *Journal of Climate*, *20*(8), 1445–1467. https://doi.org/10.1175/JCLI4056.1

Young, S. A. (1995). Analysis of lidar backscatter profiles in optically thin clouds. *Applied Optics*, *34*(30), 7019–7031. https://doi.org/10.1364/AO.34.007019

Young, S. A., & Vaughan, M. A. (2009). The Retrieval of Profiles of Particulate Extinction from Cloud-Aerosol Lidar Infrared Pathfinder Satellite Observations (CALIPSO) Data: Algorithm Description. *Journal of Atmospheric and Oceanic Technology*, *26*(6), 1105–1119.

Young, S. A., Vaughan, M. A., Kuehn, R. E., & Winker, D. M. (2013). The retrieval of profiles of particulate extinction from Cloud-Aerosol Lidar and Infrared Pathfinder Satellite Observations (CALIPSO) data: Uncertainty and error sensitivity analyses. *Journal of Atmospheric and Oceanic Technology*, *30*(3), 395–428.

Yu, H., Chin, M., Remer, L. A., Kleidman, R. G., Bellouin, N., Bian, H., & Diehl, T. (2009). Variability of marine aerosol fine-mode fraction and estimates of anthropogenic aerosol component over cloud-free oceans from the Moderate Resolution Imaging Spectroradiometer (MODIS). *Journal of Geophysical Research Atmospheres*, *114*(10). https://doi.org/10.1029/2008JD010648

Yu, H., Chin, M., Winker, D. M., Omar, A. H., Liu, Z., Kittaka, C., & Diehl, T. (2010). Global view of aerosol vertical distributions from CALIPSO lidar measurements and GOCART simulations: Regional and seasonal variations. *Journal of Geophysical Research Atmospheres*, *115*(4). https://doi.org/10.1029/ 2009JD013364

Yu, H., Chin, M., Bian, H., Yuan, T., Prospero, J. M., Omar, A. H., et al. (2015). Quantification of trans-Atlantic dust transport from seven-year (2007-2013) record of CALIPSO lidar measurements. *Remote Sensing of Environment*, *159*, 232–249. https://doi.org/10.1016/j.rse.2014.12.010

Yu, H., Chin, M., Yuan, T., Bian, H., Remer, L. A., Prospero, J. M., et al. (2015). The fertilizing role of African dust in the Amazon rainforest: A first multiyear assessment based on data from Cloud-Aerosol Lidar and Infrared Pathfinder Satellite Observations. *Geophysical Research Letters*, *42*(6), 1984–1991. https://doi.org/10.1002/2015GL063040

Yu, Y., Notaro, M., Liu, Z., Wang, F., Alkolibi, F., Fadda, E., & Bakhrjy, F. (2015). Climatic controls on the interannual to decadal variability in Saudi Arabian dust activity: Toward the development of a seasonal dust prediction model. *Journal of Geophysical Research*, *120*(5), 1739–1758. https://doi.org/10.1002/2014JD022611

Zarzycki, C. M., & Bond, T. C. (2010). How much can the vertical distribution of black carbon affect its global direct radiative forcing? *Geophysical Research Letters*, *37*(20). https://doi.org/10.1029/2010GL044555

Zender, C. S. (2003). Mineral Dust Entrainment and Deposition (DEAD) model: Description and 1990s dust climatology. *Journal of Geophysical Research*, *108*(D14), 4416. https://doi.org/10.1029/2002JD002775

Zhang, J., & Christopher, S. A. (2003). Longwave radiative forcing of Saharan dust aerosols estimated from MODIS, MISR, and CERES observations on Terra. *Geophysical Research Letters*, *30*(23), https://doi.org/10.1029/2003GL018479

Zhang, J., & Reid, J. S. (2006). MODIS aerosol product analysis for data assimilation: Assessment of over-ocean level 2 aerosol optical thickness retrievals. *Journal of Geophysical Research Atmospheres*, *111*(22). https://doi.org/10.1029/2005JD006898

Zhang, Q., Quan, J., Tie, X., Huang, M., & Ma, X. (2011). Impact of aerosol particles on cloud formation: Aircraft measurements in China. *Atmospheric Environment*, *45*(3), 665–672. https://doi.org/10.1016/ j.atmosenv.2010.10.025

Zhang, X. Y., Arimoto, R., Cao, J. J., An, Z. S., & Wang, D. (2001). Atmospheric dust aerosol over the Tibetan Plateau. *Journal of Geophysical Research Atmospheres*, *106*(D16), 18471–18476. https://doi.org/10.1029/2000JD900672